

# The Role of Biological Water in Biomimetic Cell Membrane Dynamics and Molecular Interactions

M.Sc. Madhurima Chattopadhyay

Supervisor: Dr. hab. Eng. Łukasz Piątkowski, Prof. PUT



Poznan University of Technology  
Faculty of Materials Engineering and Technical Physics  
Institute of Physics  
June 2023

A thesis submitted in partial fulfillment of the requirements for the degree of  
Doctor of Philosophy





Dedicated to  
My beloved parents  
and my doctoral supervisor, Lukasz Piatkowski



"মহাবিশ্বে মহাকাশে মহাকাল-মাঝে  
আমি মানব একাকী ভ্রমি বিশ্বয়ে, ভ্রমি বিশ্বয়ে।।"

Among the infinite worlds of the infinite universes, imbibed in infinite time,  
I, a finite human, wander alone with curious eyes of wonder.

(Translated from a Bengali song by Rabindranath Tagore).



# Contents

<b>Abstract</b>	<b>IV</b>
<b>List of abbreviations</b>	<b>IX</b>
<b>1 Introduction</b>	<b>1</b>
1.1 Preface . . . . .	1
1.2 Motivation . . . . .	2
1.3 Outline . . . . .	3
 <b>Part I: Theoretical background</b>	 <b>5</b>
<b>2 Lipid bilayers - cell membranes to biomimetic membrane systems</b>	<b>6</b>
2.1 Lipids . . . . .	6
2.2 Cell membrane . . . . .	8
2.3 Biomimetic cell membranes . . . . .	9
2.3.1 Thermodynamics of model membrane systems . . . . .	9
2.3.2 Supported lipid bilayers (SLBs) . . . . .	10
2.3.3 Giant Unilamellar Vesicles (GUVs) . . . . .	11
2.3.4 Bead Supported Lipid Bilayer (BSLB) . . . . .	12
2.3.5 Giant Plasma Membrane Vesicles (GPMVs) . . . . .	12
<b>3 Lipid-water interplay</b>	<b>14</b>
3.1 Biological water . . . . .	14
3.2 Water hydrating lipids . . . . .	15
3.3 Dehydration of lipid membranes . . . . .	17
3.3.1 Dehydration events in biological systems . . . . .	17
3.3.2 Dehydration of biomimetic membranes . . . . .	18
<b>4 Lipid diffusion</b>	<b>20</b>
4.1 Lateral diffusion of lipids in membranes . . . . .	20
4.2 Mechanisms of lipid diffusion . . . . .	22
<b>5 Fluorescence techniques to study lipid diffusion</b>	<b>24</b>
5.1 Fluorescence microscopy . . . . .	24
5.1.1 Fluorescence . . . . .	24
5.1.2 Confocal microscopy . . . . .	26
5.2 Fluorescence recovery after photobleaching (FRAP) . . . . .	28
5.3 Fluorescence correlation spectroscopy (FCS) . . . . .	31
5.4 Single particle tracking (SPT) . . . . .	33

5.5	Comparison of FRAP, FCS and SPT . . . . .	34
<b>6</b>	<b>Fluorescent probes: seeing the invisible</b>	<b>35</b>
6.1	Phase-specific probes . . . . .	35
6.2	Environment-sensitive probes . . . . .	37
 <b>Part II: The effect of membrane hydration on lipid diffusion and inter-lipid interactions</b>		 <b>39</b>
<b>7</b>	<b>Hydration layer of few water molecules control lipid mobility in biomimetic cell membranes</b>	<b>40</b>
<b>8</b>	<b>Sensing hydration of biomimetic cell membranes</b>	<b>64</b>
<b>9</b>	<b>Cooperativity between sodium ions and water molecules facilitates lipid mobility in model cell membranes</b>	<b>78</b>
<b>10</b>	<b>Phospholipids undergo anomalous sub-diffusion at reduced hydration conditions in model membranes</b>	<b>95</b>
10.1	Abstract . . . . .	95
10.2	Introduction . . . . .	95
10.3	Experimental section . . . . .	97
10.3.1	Materials . . . . .	97
10.3.2	SLB preparation . . . . .	97
10.3.3	Preparation of SLBs with lower hydration conditions . . . . .	98
10.3.4	Point and scanning FCS data acquisition and analysis . . . . .	98
10.4	Results . . . . .	99
10.4.1	Point FCS measurements . . . . .	100
10.4.2	Scanning FCS measurements . . . . .	103
10.5	Discussion . . . . .	105
10.6	Conclusion . . . . .	108
<b>11</b>	<b>Conclusions and outlook</b>	<b>109</b>
11.1	Conclusions . . . . .	109
11.2	Outlook . . . . .	110
 <b>Bibliography</b>		 <b>111</b>
<b>12</b>	<b>Scientific achievements</b>	<b>130</b>
12.1	Publications . . . . .	130
12.1.1	Articles . . . . .	130
12.1.2	Conference papers . . . . .	130
12.2	Patent applications . . . . .	131
12.3	Participation in conferences . . . . .	131
12.4	Participation in courses . . . . .	133
12.5	Research internships . . . . .	133
12.6	Grants . . . . .	134
12.7	Awards and distinctions . . . . .	134
12.8	Scientific outreach . . . . .	135

---

Acknowledgements	136
Declarations of co-authors	139





# Abstract

Biological membranes are self-assembled bilayer structures composed of a large variety of lipids and embedded with proteins. They act as a dynamic barrier separating intra- and extra-cellular matrices and encapsulate various subcellular organelles. The self-assembly of the lipid membranes is a consequence of the amphiphilic nature of the lipids and the tendency to avoid hydrophobic interactions between water and the hydrophobic tails of lipids. At the same time, polar headgroups of the lipids are stabilized by a hydration shell. Hence, not only the lipid-lipid and lipid-protein interactions, but also interactions between lipids and water molecules hydrating the membrane play a significant role in determining the structure, organization, and dynamics of the membrane and its constituents. Intriguingly, the membrane does not always experience abundant hydration conditions - many biochemical processes, such as cell fusion, viral entry, fertilization, neurotransmission, or adsorption of macromolecules, are associated with the local and transient dehydration of the membrane. Lipid diffusion is an elementary process in the cellular membrane that actively and continuously contributes to the reorganization of the membrane constituents, maintenance of lipid homeostasis, signal transduction, cell signalling, and transport. It is therefore crucial to understand how the hydration of the membrane influences the dynamics of the lipids and the organization of the membrane. However, investigations of the effect of local hydration on the structure and, in particular, on the diffusivity of membrane components have so far been hindered by the challenges in preparing desiccation-tolerant membranes. In this doctoral thesis, I addressed the lipid dynamics at varying hydration conditions by developing a method of preserving the intact structure of membranes over multiple dehydration and rehydration cycles. Using fluorescence microscopy and fluorescence recovery after photobleaching (FRAP) technique, I demonstrated that the hydration shell around the lipid headgroup facilitates lateral diffusion of lipids acting as an aqueous lubricant. The diffusion coefficient ( $D$ ) of lipids decreases steadily with the decrease in relative humidity (RH) of membranes environment from  $\sim 90\%$  to  $\sim 50\%$ , whereas below  $\sim 50\%$  RH, lipid mobility remains almost constant, indicating a key role played by the water molecules desorbed from the hydration shell around lipid headgroup. From fully hydrated to dehydrated membranes ( $\sim 0\%$  RH), approximately a six-fold decrease in  $D$  value is observed. Moreover, the change in  $D$  values of lipids is completely reversible and repeatable with the change in the hydration states of the membrane, and it is sensitive to only a few water molecules per lipid. Based on this significant dependence and the high sensitivity, I proposed lipid diffusion as a hydration-sensing tool to investigate local hydration heterogeneities in lipid membranes. Next, I extended the research to lipid-water-ion interplay in the context of lipid diffusion, as ions are vital constituents of the lipid-water interface, and modulate the hydration structure of the lipids. I discovered that  $\text{Na}^+$  and  $\text{K}^+$  ions support lipid mobility after the partial membrane dehydration by strengthening the hydration shell around the PC lipid headgroups. In contrast,  $\text{Ca}^{2+}$  and  $\text{Mg}^{2+}$  ions are unable to show this effect. Finally, I focused on elucidating the nature of the diffusion of lipids at varying hydration conditions. Using fluorescence correlation spectroscopy (FCS), I showed that the lateral diffusion of lipids transforms into anomalous sub-diffusion in the absence of the membrane's external hydration layer, in contrast to free diffusion taking place in fully hydrated membranes. Overall, the studies presented in this thesis shine light on the importance of the hydration layer around the lipid headgroups and lipid-water-ion

interactions in defining the lateral diffusion of lipids in biomimetic membranes and provide new insights into the molecular interactions during lipid de/rehydration processes. Thus, the research possesses important implications in the fields of membrane biology, biophysics and physical chemistry.

# Streszczenie

Błony biologiczne są samoorganizującymi się dwuwarstwowymi strukturami złożonymi z wielu różnych lipidów oraz z osadzonych w nich białek. Pełnią one funkcję dynamicznej bariery oddzielającej matrycę wewnątrz- i zewnątrzkomórkowe i okalającej różne organelle wewnątrz-komórkowe. Samoorganizacja błon lipidowych jest konsekwencją amfifilowej natury lipidów i tendencji do unikania oddziaływań hydrofobowych między wodą a hydrofobowymi ogonami lipidów. Jednocześnie polarne główki lipidów są stabilizowane przez powłokę hydratacyjną. W związku z tym nie tylko interakcje lipid-lipid i lipid-białko, ale także oddziaływania między lipidami i cząsteczkami wody uwadniają błonę odgrywając znaczącą rolę w definiowaniu struktury, organizacji i dynamiki błony i jej składników. Co ciekawe, błona nie zawsze doświadcza warunków obfitego nawodnienia - wiele procesów biochemicznych, takich jak fuzja komórek, wnikanie wirusów, zapłodnienie, neurotransmisja lub adsorpcja makrocząsteczek, wiąże się z lokalnym i przejściowym odwodnieniem błony. Dyfuzja lipidów jest podstawowym procesem w błonie komórkowej, który aktywnie i stale przyczynia się do reorganizacji składników błony, utrzymania homeostazy lipidów, transdukcji sygnałów, sygnalizacji komórkowej i transportu. Dlatego też kluczowe jest zrozumienie, w jaki sposób uwodnienie błony wpływa na dynamikę lipidów i organizację błony. Jednak badania wpływu lokalnego uwodnienia błony na jej strukturę, a w szczególności na dyfuzyjność składników błony, były dotychczas utrudnione przez wyzwania związane z przygotowaniem błon odpornych na osuszanie. W niniejszej pracy doktorskiej przedstawiłam swoje badania nad dynamiką lipidów w różnych warunkach hydratacji poprzez opracowanie metody pozwalającej na zachowania nienaruszonej struktury błony lipidowej wystawionej na wiele cykli odwodnienia i rehydratacji. Wykorzystując mikroskopię fluorescencyjną i technikę odzyskiwania fluorescencji po fotowysbieleniu (z ang. FRAP - fluorescence recovery after photobleaching), wykazałam, że powłoka hydratacyjna wokół główek lipidów ułatwia dyfuzję lateralną lipidów, działając jako wodny 'smar'. Współczynnik dyfuzji ( $D$ ) lipidów stale maleje wraz ze spadkiem wilgotności względnej (RH) środowiska błony z  $\sim 90\%$  RH do  $\sim 50\%$  RH, podczas gdy poniżej  $50\%$  RH mobilność lipidów pozostaje prawie stała, co wskazuje na kluczową rolę odgrywaną przez cząsteczki wody desorbowane z otoczki hydratacyjnej wokół główek lipidów. Dla odwodnionej błony ( $\sim 0\%$  RH) obserwuje się około sześciokrotny spadek wartości  $D$  w stosunku do w pełni uwodnionej błony. Co więcej, zmiana wartości  $D$  lipidów jest całkowicie odwracalna i powtarzalna wraz ze zmianą stanu uwodnienia błony i co ważne, jest ona wrażliwa na zmiany uwodnienia błony rzędu kilku cząsteczek wody przypadających na lipid. Opierając się na tej silnej zależności i wysokiej czułości, zaproponowaliśmy pomiar dyfuzji lipidów jako narzędzie do określania hydratacji w celu badania lokalnych heterogeniczności nawodnienia błon lipidowych. Następnie rozszerzyłam badania na interakcje lipid-woda-jon w kontekście dyfuzji lipidów, ponieważ jony są istotnymi składnikami interfejsu lipid-woda i modulują strukturę hydratacji lipidów. Odkryłam, że jony  $\text{Na}^+$  i  $\text{K}^+$  wspierają mobilność lipidów po częściowej dehydratacji błony poprzez wzmocnienie powłoki hydratacyjnej wokół główek lipidowych PC. Natomiast jony  $\text{Ca}^{2+}$  i  $\text{Mg}^{2+}$  nie wykazują tego efektu. Wreszcie, skupiłam się na wyjaśnieniu dokładnej natury mechanizmu dyfuzji lipidów w różnych warunkach nawodnienia błony. Wykorzystując spektroskopię korelacji fluorescencji (z ang. FCS - fluorescence correlation spectroscopy), wykazałam, że lateralna dyfuzja lipidów przekształca się w anomalną subdyfuzję w przypadku braku zewnętrznej warstwy hydratacyjnej błony, w przeciwieństwie

do swobodnej dyfuzji zachodzącej w całkowicie uwodnionej błonie. Reasumując, badania przedstawione w niniejszej rozprawie rzucają światło na znaczenie warstwy hydratacyjnej wokół główek lipidów i interakcji lipid-woda-jon w definiowaniu lateralnej dyfuzji lipidów w biomimetycznych błonach oraz zapewniają nowe spojrzenie na interakcje molekularne podczas procesów odwadniania/nawadniania błon lipidowych. Badania te mają zatem istotne implikacje w dziedzinie biologii błon, biofizyki i chemii fizycznej.

# Funding

The research presented in this thesis was funded by:

**FIRST TEAM, Foundation for Polish Science,**  
*HYDRA – Elucidating the role of hydration heterogeneity and hydrophobic mismatch in biomimetic cell membranes organization*, grant number: POIR.04.04.00-00-5D32/18-00, principal investigator: dr hab. eng. Łukasz Piątkowski (prof. PUT)



**EMBO Installation Grant, European Molecular Biology Organization,**  
*Biological water: the role of hydration in cell membrane organization*, grant number: IG 4147, principal investigator: dr hab. eng. Łukasz Piątkowski (prof. PUT)



**EMBO Scientific Exchange Grant, European Molecular Biology Organization,** grant number: 9439,  
*Elucidating the interplay between biological water and nanoscale lipid dynamics in cellular membranes*, principal investigator: M.Sc. Madhurima Chattopadhyay





# List of abbreviations

<b>D</b>	Diffusion coefficient
<b>H-bond</b>	Hydrogen bond
<b>RH</b>	Relative humidity
<b>DNA</b>	Deoxyribonucleic acid
<b>CMC</b>	Critical micelle concentration
<b>IUPAC</b>	International Union of Pure and Applied Chemists
<b>IUBMB</b>	International Union of Biochemistry and Molecular Biology
<b>DOPC</b>	1,2-Dioleoyl-sn-glycero-3-phosphocholine
<b>POPC</b>	1-palmitoyl-2-oleoylphosphatidylcholine
<b>DOPE</b>	1,2-dioleoyl-sn-glycero-3-phosphoethanolamine
<b>DPPE</b>	1,2-Dipalmitoyl-sn-glycero-3-phosphorylethanolamine
<b>PC</b>	Phosphatidylcholine
<b>PE</b>	Phosphatidylethanolamine
<b>PS</b>	Phosphatidylserine
<b>PG</b>	Phosphatidylglycerol
<b>PI</b>	Phosphatidylinositol
<b>SM</b>	Sphingomyelin
<b>T<sub>m</sub></b>	Transition temperature
<b>L<sub>o</sub></b>	Liquid ordered
<b>L<sub>d</sub></b>	Liquid disordered
<b>SLB</b>	Supported lipid bilayer
<b>SUV</b>	Small unilamellar vesicle
<b>LUV</b>	Large unilamellar vesicle
<b>SALB</b>	Solvent assisted lipid bilayer
<b>AFM</b>	Atomic force microscopy
<b>STM</b>	Scanning tunneling microscopy

<b>GUV</b>	Giant unilamellar vesicles
<b>BSLB</b>	Bead supported lipid bilayer
<b>GPMV</b>	Giant plasma membrane vesicle
<b>IR</b>	Infrared
<b>SFG</b>	Sum frequency generation
<b>NMR</b>	Nuclear magnetic resonance
<b>EPR</b>	Electron spin resonance
<b>SANS</b>	Small angle neutron scattering
<b>LEA</b>	Late embryogenesis abundance
<b>MSD</b>	Mean square displacement
<b>NA</b>	Numerical aperture
<b>TIRF</b>	Total Internal Reflection Fluorescence
<b>STED</b>	Stimulated emission depletion
<b>STORM</b>	Stochastic Optical Reconstruction Microscopy
<b>PALM</b>	Photoactivated localization microscopy
<b>SMLM</b>	Single molecule localization microscopy
<b>MF</b>	Mobile fraction
<b>FRAP</b>	Fluorescence recovery after photobleaching
<b>FCS</b>	Fluorescence correlation spectroscopy
<b>STED</b>	Stimulated emission depletion
<b>SPT</b>	Single particle tracking
<b>s-FCS</b>	Scanning FCS
<b>FCCS</b>	Fluorescence cross-correlation spectroscopy
<b>GFP</b>	Green fluorescent protein
<b>NBD</b>	4-nitrobenz-2-oxa-1,3-diazole
<b>Rh</b>	Rhodamine
<b>PEG</b>	Polyethylene glycol
<b>E<sub>a</sub></b>	Activation energy of diffusion
<b>JACS</b>	Journal of the American Chemical Society



**HEPES** 4-(2-hydroxyethyl)-1-piperazineethanesulfonic acid

**ASR** Abberior STAR RED

**GM1** Monosialotetrahexosylganglioside



# Chapter 1

## Introduction

### 1.1 Preface

Cellular membranes are chemically highly heterogeneous structures, whose components work in a concerted manner, facilitating a broad range of important cellular functions. The organization of the cell membrane and the assembly of membrane constituents into various micro and nanostructures are strongly related to the intricate combination of hydrophilic and hydrophobic interactions of the polar and nonpolar parts of the lipids with the hydrating water. Since defects in membrane organization may translate into dysregulation of membrane activity, it is crucial to understand the interactions of membrane components with their hydration layer. The hydration layer, i.e. the water molecules at the lipid-water interface of the cellular membrane are comparatively more ordered than the ones in bulk water. The charge and the H-bonding ability of the lipid headgroup greatly influence the orientation and diffusion of the hydration layer around the lipid headgroups[1, 2, 3]. Such less mobile and ordered water layer in the close vicinity of biomolecules, the so-called “biological water”, is known to modulate inter- and intra-molecular interactions of biomolecules in many ways. For example, the water molecules present around the DNA double helix mediate the interactions of any other molecule coming to bind to DNA by H-bonding[4]. Moreover, the hydrophobic base-pairing of the DNA double helix structure is strengthened in the presence of water molecules around the DNA[5]. The importance of the biological water around lipids is no exception. For instance, it is believed that the water molecules around the lipid headgroup decrease the inter-lipid electrostatic repulsions between the adjacent lipid headgroups[6, 7]. Therefore, a solid impact of this biological water layer at the lipid-water interface could be anticipated on various properties of the membrane, such as structural organization or lipid diffusion. Lateral diffusion of lipids plays a key role in maintaining membrane homeostasis and cell-cell communication. Hence, understanding lipid diffusion at various physiological conditions is of utmost importance. Various spectroscopy studies and molecular dynamics simulation studies have confirmed that the diffusion of bound water molecules at the lipid-water interface becomes restricted due to interaction with lipid headgroups[1, 8, 9, 10]. Moreover, the mobility of functional groups, such as carbonyl, at the lipid headgroup region also depends on the H-bonding with the surrounding water molecules[11]. At lower hydration conditions longer residence time of water molecules at the polar hydrated carbonyl functional groups leads to lower orientational mobility of those moiety of lipids[12, 13]. Water has been mentioned as “lubricant” in lipid bilayer[2]. Transition temperature ( $T_m$ ) of lipids was also shown to decrease at lower hydration conditions[14, 15]. Furthermore, dehydration causes decrease in the area per lipid and consequently an increase in membrane thickness and order parameter[13]. Previous studies have pointed toward the possibility of hampered lateral diffusion in the absence of sufficient water at the lipid-water interface[16]. All these make a strong ground to investigate how the lipid hydration layer modulates lipid diffusion. To explore how the water molecules at the lipid-water interface affect lipid mobility, the water layer has

to be perturbed. As lipid bilayers curl up to form vesicles and aggregates during dehydration, preparation of desiccation-tolerant membranes has been very challenging. This has hindered experimental investigation on the activity and dynamics of dehydrated membranes. In this thesis, I report my doctoral work on developing a protocol for preparing membranes with a well-defined hydration properties and addressing the lipid dynamics in phase-separated biomimetic membranes at varying hydration conditions.

## 1.2 Motivation

Water is an irreplaceable element of life that pervades both the outer and inner layers of the lipid membrane in biological systems. At first glance dehydrated lipid membrane may not sound like a physiological condition. But if we dig deeper into the molecular basis of various biochemical reactions, local dehydration of membranes is not only possible, but also essential for many biological processes. As the self-assembled structure of the bilayer originates from the hydrophobic and hydrophilic interactions of the lipids with water, removal of the water molecules is required to break the bilayer structure of lipids. Such scenario takes place during fusion of two lipid membranes, where the bilayer structure of lipids has to be disturbed to initiate fusion and then restored once the fusion event is complete. Therefore, at the initial stage of the membrane fusion, water molecules have to be moved away from the lipid headgroup region for the hydrophobic chains from two different bilayers to interact and finally merge (the so-called hemifusion). Such membrane fusion is at the heart of many fundamental biological processes – fertilization, neurotransmission, viral entry, to mention a few. Moreover, a local temporary dehydration of the membrane occurs in some other processes, such as absorption of a macromolecules. Additionally, many living organisms survive at severe dehydration stress. This unique ability is known as anhydrobiosis[17, 18, 19]. In such conditions also membranes are exposed to low hydration conditions. To understand the mechanisms behind these biological processes involving membrane dehydration, it is necessary to explore lipids behavior at low hydration conditions. The lipid diffusion studies at reduced water availability conditions may reveal the importance of membrane fluidity/rigidity during cellular fusion depending on the chemical mechanism of the fusion process. On one hand, it can be anticipated that a minimum fluidity/diffusion of lipids is an essential factor during fusion as initiating a defect in the bilayer is required for the fusion to take place[20]. On the other hand, various membrane protein complexes take part in regulating the fusion process, where slowing down of lipid diffusion may facilitate the local increase in local concentration of the key proteins at the active zone to form the essential complexes. All these speculations are yet to be verified, and the first step would be to understand how water molecules at the lipid-water interface influence lipid diffusion. Furthermore, not only water alone, but the presence of various ions in the intra- and extra-cellular matrices also has to be considered in this regard, as it has important implications in defining the hydration structure at the interface[21]. Thus, in this thesis I have started a journey with the foremost steps to answer these key questions of membrane dehydration-related phenomena by investigating the hydration dependence of lipid mobility. During the course of my doctoral study, the path was also extended to understanding the lipid-water-ion interplay and nature of lipid diffusion at perturbed hydration conditions. Further investigations in this topic still await realization, the outlook of which is discussed at the end of this thesis.

## 1.3 Outline

In this doctoral dissertation, I present the molecular-level details of the interplay between the hydration layer of membrane lipids and their dynamical properties in the membrane. This thesis is based on three, original, peer-reviewed research articles and one chapter showcasing a draft manuscript to be published in the nearest future, all supplemented with an extensive discussion on the theoretical background of the performed scientific investigations. Starting with a general introduction to the topic, the thesis is arranged in two parts: Part I (Chapters 2-6) - theoretical background and experimental methods – where readers will be introduced to the concept of biomimetic cell membranes and their interactions with water. An extensive discussion on the lateral diffusion of lipids in model membranes, including fluorescence techniques and probes to study lipid diffusion is also presented. Part II (Chapters 7-10) - the second part comprises of the following three, peer-reviewed scientific articles, published in journals indexed in Journal Citation Reports (JCR), Scopus and Scimago Journal & Country Rank (SJR) databases:

- **Madhurima Chattopadhyay\***, Emilia Krok, Hanna Orlikowska, Petra Schwille, Henri G. Franquelim and Lukasz Piatkowski\*, *Hydration layer of only few molecules controls lipid mobility in biomimetic membranes*, **Journal of the American Chemical Society**, 2021, volume 143, issue 36, page 14551-14562, **IF: 16.383**
- **Madhurima Chattopadhyay\*#**, Hanna Orlikowska#, Emilia Krok and Lukasz Piatkowski\*, *Sensing hydration of biomimetic cell membranes*, **Biosensors**, 2021, volume 11, issue 7, page 241, **IF: 5.743**
- **Madhurima Chattopadhyay\***, Emilia Krok, Hanna Orlikowska-Rzeznik and Lukasz Piatkowski\*, *Cooperativity between sodium ions and water molecules facilitates lipid mobility in model cell membranes*, **Chemical Science**, 2023, issue 14, page 4002-4011, **IF 9.969**

A short summary of each of these articles is included in the thesis and the full-length published versions of the articles and their supplementary information is attached in the respective chapters. Moreover, in an additional chapter, an unpublished research manuscript is included.

In publication 1 (chapter 7), I reported a successful protocol for preparing stable, desiccation-tolerant, phase-separated artificial membranes with well-defined hydration properties using a humidity control setup, co-designed and constructed by me. Furthermore, in the same article, exploiting this novel dehydration method, I showed the dependence of the lateral diffusion of lipids in phase-separated, supported lipid bilayers (SLBs) on the lipid hydration state and explained its molecular basis.

Next, in publication 2 (chapter 8), I investigated the dependence of lipid mobility in single-component (single phase) SLBs. Moreover, knowing the hydration dependence of lipid mobility, a novel method of hydration sensing in biomembranes based on the measurements of diffusion coefficient of lipids was proposed.

In the next publication 3 (chapter 9), I have extended my lipid-water interaction studies to lipid-water-ion interactions as ions are an important part of the membrane-water interface in biological systems. I have investigated the role of four biologically relevant ions (sodium, potassium, magnesium and calcium ions) in shaping lipid mobility at full and reduced hydration conditions.

In the next chapter (chapter 10), I explored the nature of the lateral diffusion of lipids in SLBs at low water availability conditions and compared it with fully hydrated conditions. This work will be submitted to a peer-reviewed journal in the nearest future.

Finally, the conclusions and outlook of the topic are discussed at the end.

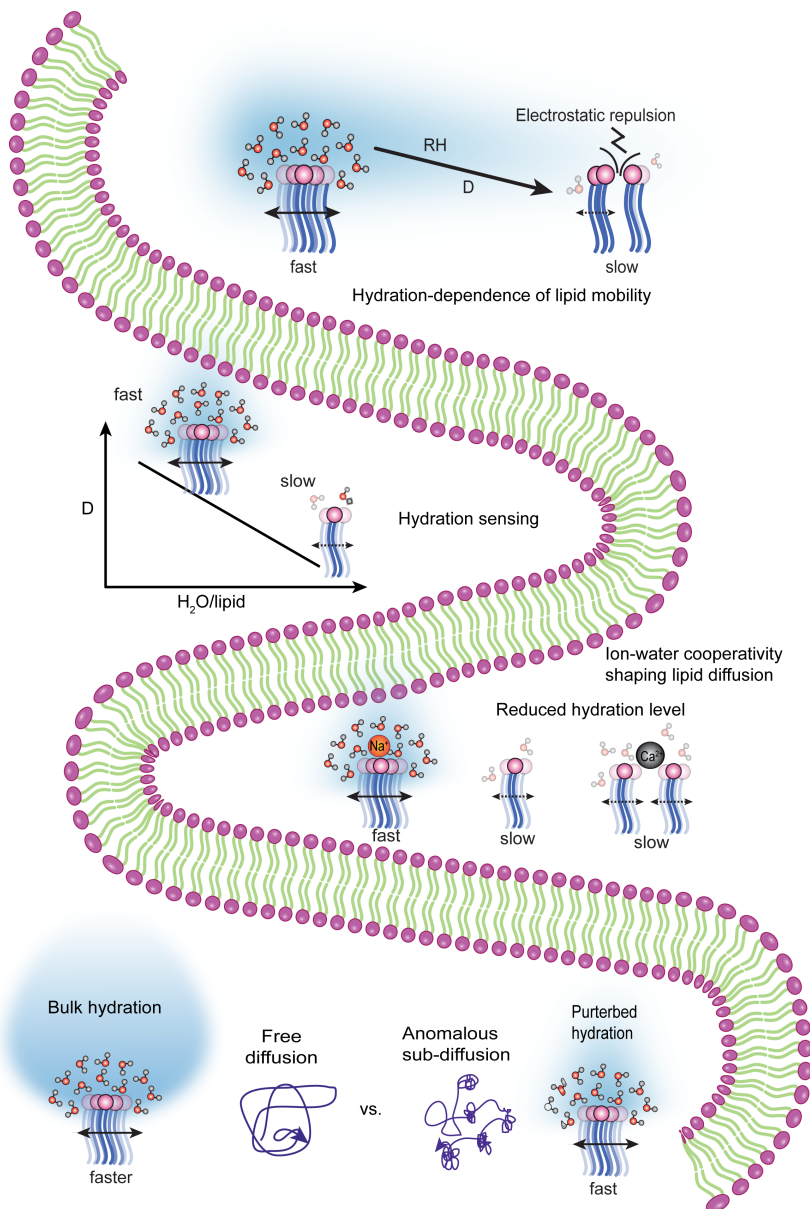


Figure 1.1: Thesis at a glance: the whole journey starting with understanding of lipid diffusion as a function of hydration and thereafter extending the study to hydration sensing approach, investigating lipid-ion-water interplay and finally addressing the nature of lipid diffusion in membranes at different hydration states.

# Part I: Theoretical background





# Chapter 2

## Lipid bilayers - cell membranes to biomimetic membrane systems

### 2.1 Lipids

Lipids comprise a class of compounds, that are amphiphilic in nature, having a small hydrophilic headgroup and long hydrophobic hydrocarbon tails. As it is said, “like dissolves like” - the headgroup region, either charged or zwitterionic, is polar and hence stays solvated in polar water molecules. On the other hand, the acyl chain tails are nonpolar and tend to remain unexposed to water. This binary interaction of lipid molecules with water drives them into a specific pattern of self-assembled structures. As in the case of any amphiphilic molecules, lipids dispersed on water form a monolayer with their headgroups encapsulated in water and fatty acid chains exposed to air at the air-water interphase (Figure 2.1A). Above a certain concentration of lipids, the so-called critical micelle concentration (CMC), when the air-water interphase is saturated, the lipids form spherical micelle structures with the headgroups pointing outside and the hydrophobic tails hidden inside the micelle. In biological systems, such micelle structures are called lipid droplets. (Figure 2.1B). However,

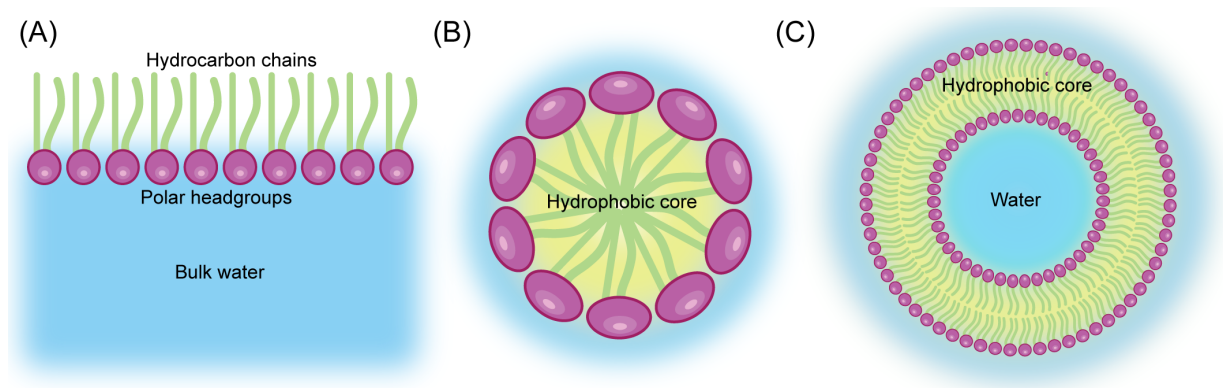


Figure 2.1: (A) Lipid monolayer on water surface, (B) Micelle structure of lipids, (C) Liposome structure of lipids.

at even higher concentrations, lipids form liposomes, which are single or multilamellar spherical structures, where lipids are arranged in bilayer structures with the headgroups exposed to water and acyl chains forming a hydrophobic core (Figure 2.1C). Nature has made a proper use of this beautiful self-assembled system by choosing it to form the cellular boundary – the cell membrane, a semi-permeable encapsulation allowing selective transport of particles in and out of the cell.

Lipids found in biological systems are structurally highly diverse due to the wide variety of headgroups and fatty acid chain structures. For easier understanding, apart from the generally accepted International Union of Pure and Applied Chemists and the International Union of Biochemistry and Molecular Biology (IUPAC-IUBMB) Commission on

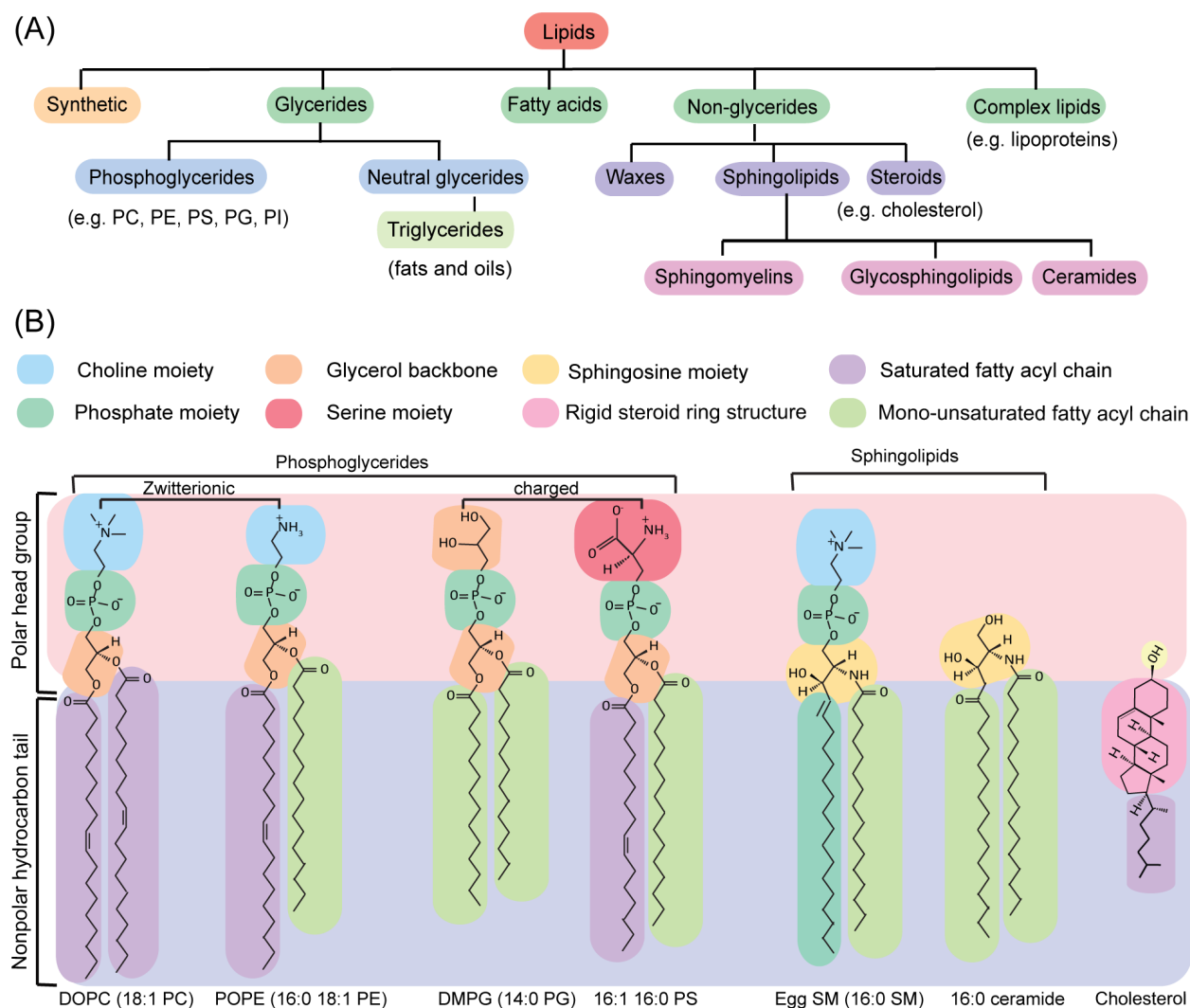


Figure 2.2: (A) An arbitrary classification of different types of lipids, (B) Chemical structures of selected, commonly used lipids in biomimetic membrane systems.

Biochemical Nomenclature, another systematic nomenclature system for lipids according to their headgroup structure, hydrophobic chain length and saturation, cis/trans, R/S conformations proposed by LIPID MAPS is followed[22, 23]. The basic rule in this nomenclature is to name lipids in the following format – (no. of carbon atoms: no. of double bonds) in the hydrocarbon chain followed by a short name of the lipid headgroup structure. For example, 1,2-Dioleoyl-sn-glycero-3-phosphocholine (DOPC) lipid can be termed as 18:1 PC as it has 18 carbons and 1 double bond in each hydrocarbon chain, and the headgroup is PC i.e. phosphocholine. If a lipid has two different types of hydrocarbon chains, such as, 1-palmitoyl-2-oleoylphosphatidylcholine (POPC) having one unsaturated 16-carbon acyl chain and the other acyl chain with 18 carbon atoms and one double bond, it is then termed as 16:0 18:1 PC (Figure 2.2B). Moreover, specific rules are maintained to specify stereochemistry and the cis/trans forms of the lipids.

The vast variety of the lipids present in the biological membranes can be classified in few groups according to their chemical structure. A rough classification of various types of natural and synthetic lipids is demonstrated in Figure 2.2A. However, it should be noted that here I mention only few most common classes of lipids, highlighting those that are

the most relevant to the studies carried out in this thesis. The most abundant membrane lipids are phospholipids[24], which have a polar headgroup with a phosphate group and two hydrocarbon tails. These tails are mainly fatty acid chains of varying lengths (typically ranging from 14-24 carbon atoms)[24]. Lipids with one saturated and one unsaturated tail are very common in biological membranes[24, 25]. Moreover, the hydrocarbon chains can be saturated or unsaturated. Generally, in biological membranes, the unsaturated hydrocarbon tails contain one or more *cis* double bonds resulting in a kink in their structure due to the planar nature of the double bond. The presence of unsaturation has important implications as it affects the packing of the lipids in the bilayer, which will be discussed later.

One common class of phospholipids is phosphoglycerides having a glycerol backbone attached to the phosphate group. Their long fatty acid chains are connected to the two adjacent carbons of the glycerol backbones by ester bonds. The third carbon of the glycerol is linked to the phosphate group, which again is connected to one of a few other functional groups, such as choline, serine, ethanolamine, glycerol – resulting in diverse groups of various phospholipids, namely, phosphatidylcholines (PC), Phosphatidylserines (PS), Phosphatidylethanolamines (PE), Phosphatidylglycerols (PG) etc. (Figure 2.2B).

Another class of phospholipids are sphingolipids, where the phosphate group and the fatty acid chains are interlinked by a sphingosine moiety instead of glycerol. The most common sphingolipid is sphingomyelin (SM), where one fatty acid chain is attached to the amino group of sphingosine moiety and the phosphocholine group is connected to the terminal hydroxyl group (Figure 2.2B).

Besides phospholipids, glycolipids are also important constituents of biological membranes. Their structure is similar to sphingolipids, but with phosphate head groups replaced by sugars. Another crucial membrane constituent molecule is cholesterol, which has a sterol structure – a rigid ring structure along with a polar hydroxyl group (figure 2.2B). All these phospholipids:PC, PS, PE, SM and cholesterol together form the major mass of the cell membrane[24].

## 2.2 Cell membrane

Cell, the fundamental unit of life, is largely composed of four groups of macromolecules – nucleic acids, proteins, carbohydrates and lipids - the main building blocks of life. The functioning of the cells is governed by the arrangements and interactions of these macromolecules, actively facilitating life-supporting biochemical reactions inside and outside the cell. The cellular machinery and the extracellular matrix are separated by a self-assembled thin bilayer (or two in case of some bacterial membranes) of lipids – the cell membrane. In some cases, however, for example in gram negative bacteria, membranous barrier around nucleus, mitochondria or in chloroplast, the envelopes are made of two stacked lipid bilayers[26]. The cell membrane not only acts as a semipermeable barrier encapsulating the cell and other organelles, but also plays a crucial role in cell signaling, membrane trafficking, and selective transport of biologically important molecules across the membrane[27]. Moreover, the membrane shelters various transmembrane proteins that catalyze vital reactions involving molecules inside and outside the cells[28]. Thus, clearly, the importance of understanding the structure and dynamics of biomembranes, which serve functions much beyond simple compartmentalization of cells, cannot be overstated. Lipids are the main building blocks of biological membranes. As discussed above, to minimize the exposure of the hydrophobic tails to aqueous environments around the cell membranes,

they self-assemble into a bilayer structure. Around five decades ago, to explain the structure and organization of cell membranes, the famous “fluid mosaic model” by Singer and Nicolson proposed the structure of plasma membrane to be a homogeneous lipid bilayer embedded with proteins, arranged in an amphipathic structure, where the polar groups are protruding on the edge of the membrane towards the aqueous phase and the nonpolar parts are buried inside the hydrophobic core of the membrane[29]. However, later extensive experimental studies revealed that cell membranes are structurally and chemically highly heterogeneous. A single cell membrane may contain hundreds of lipid species. The complex architecture of the biological membranes emerges both from the wide variety of lipids, in terms of their head group structure and hydrophobic chain length and saturation as well as their intricate organization. Numerous studies suggested the presence of dynamic, highly packed and viscous nanodomains, often termed as “lipid rafts”, enriched with saturated sphingolipids and cholesterol[30, 31, 32]. The selective incorporation of various membrane proteins into these rafts is believed to play an important role in membrane trafficking and cell signalling[30]. Due to the nanoscopic and transient nature of the rafts (and the high complexity of biomembranes) they can hardly be detected in native plasma membranes by conventional light microscopy, rising considerable controversy about their existence[33, 34]. Additionally, the interaction of the membrane lipids with the cell cytoskeleton further complicates the system to explore. Thus it became extremely necessary to design simpler systems that resemble the chemical and structural environment of biomembranes to systematically investigate various properties of the membrane from a physical point of view.

### 2.3 Biomimetic cell membranes

“Everything should be made as simple as possible, but not simpler.”

—Albert Einstein

Given the intricate, diverse molecular interactions and structural complexity that transpire plasma membranes, biomimetic model membrane systems are especially appealing choice for biophysicists for controlled exploration of many physicochemical properties of the membrane. Model membrane systems can be supported or floating, planar or spherical lipid bilayer systems, where biologically abundant lipids, such as various phospholipids, sphingolipids, cholesterol, or other lipids are mixed at a tunable ratio, with optional incorporation of membrane proteins, to create an artificial lipid bilayer to mimic the biological membrane in a simplistic way.

#### 2.3.1 Thermodynamics of model membrane systems

To mimic the heterogeneity of biomembranes, model membrane systems are often prepared using saturated and unsaturated lipids along with cholesterol. Depending on the chemical structure of the lipids, such as hydrocarbon chain length, chain saturation, head group and charge, each lipid has a transition temperature ( $T_m$ ), below which they form highly ordered and viscous gel phase with elongated, straightened hydrophobic tails, whereas above  $T_m$ , they form more fluid liquid crystalline phase with disordered hydrocarbon chains. Due to compact packing of the hydrocarbon chains, saturated lipids have higher  $T_m$  than that of unsaturated lipids. At room temperature, saturated lipids stay in gel phase

whereas unsaturated lipids remain in highly fluid liquid disordered state. Cholesterol acts as a buffer regulating the fluidity of the lipid phases - with the addition of cholesterol, the order of the gel phase decreases, whereas the fluid phase order increases[35]. When saturated and unsaturated lipids of similar hydrocarbon chain length are mixed at room temperature, the difference in their  $T_m$  results in differences in their structural packing and fluidity. Moreover, a height mismatch is present between the highly ordered and longer saturated lipids and shorter, fluid unsaturated lipids. This height mismatch brings part of the hydrocarbon chain of the longer saturated lipids in contact with water at the lipid-water interface, leading to the exposed hydrocarbon chain-water interactions - the so-called "hydrophobic mismatch". Thus, this unfavourable interactions, between the saturated and unsaturated lipids induce a phase separation between highly ordered liquid-ordered ( $L_o$ ) phase with preferential partitioning of cholesterol and more fluid liquid-disordered ( $L_d$ ) phase. Presence of lipid rafts in the highly heterogeneous cell membranes, are thought to be result of such phase separation. To understand its nature and properties, the phase separation has been extensively studied in different types of model membrane systems. The most important and commonly used model membrane systems will be discussed below.

### 2.3.2 Supported lipid bilayers (SLBs)

Supported lipid bilayers (SLBs) are flat lipid bilayers formed on top of a smooth and hydrophilic solid substrate such as mica, glass or silica, with a very thin ( $\sim 1$  nm, though still debated) water layer between the membrane and the substrate (Figure 2.3A). At the beginning SLBs were prepared by sequential transfer of two monolayers from air-water interface to a solid substrate[36]. Afterwards vesicle deposition method became very popular, where small unilamellar vesicles (SUVs) or large unilamellar vesicles (LUVs) are deposited on the surface to burst and form bilayer (Figure 2.3B). The electrostatic interactions between the substrate with the lipid headgroups play a vital role in the process of adsorption and rapturing of the vesicles on the substrate[37]. Positively charged lipids spontaneously burst on the negatively charged substrate like mica and silica, whereas metal ions, in particular  $Ca^{2+}$  mediate these interactions promoting adsorption and rapturing of the vesicles on the substrate in case of zwitter-ionic and negatively charged lipids[38]. Another common method of SLB preparation is the solvent-assisted lipid bilayer (SALB) formation technique, where the lipid mixture dissolved in organic solvent is deposited on the surface followed by the solvent exchange to aqueous buffer to form lipid bilayers[39]. Apart from these, various other methods such as spin coating, lipid wetting, bicelle adsorption are used to prepare SLBs[40, 41, 42, 43].

SLBs are widely accepted as biomimetic model membrane systems for studying various physicochemical properties of the membrane, such as phase-separation, lipid diffusion, fluidity and mechanical strength, lipid protein interactions, to mention a few[44, 45, 46, 47, 48, 49, 50]. Moreover, SLBs are also an attractive platform for biosensing and biotechnological applications for their easy preparation and handling procedures[51, 52]. SLBs being constrained to a solid support, not only have been investigated by various optical microscopies, but also high-resolution surface probing techniques like atomic force microscopy (AFM), scanning tunneling microscopy (STM) and tunneling electron microscopy (TEM)[46, 53, 54, 55]. On the other hand, the interactions with the substrate may affect or alter certain properties of the lipid bilayer, such as the diffusion of membrane constituents. To get rid of the lipid-substrate interactions, often free standing bilayers are used, where the lipid membrane remains hanging in free air/buffer while supported on the sides. This

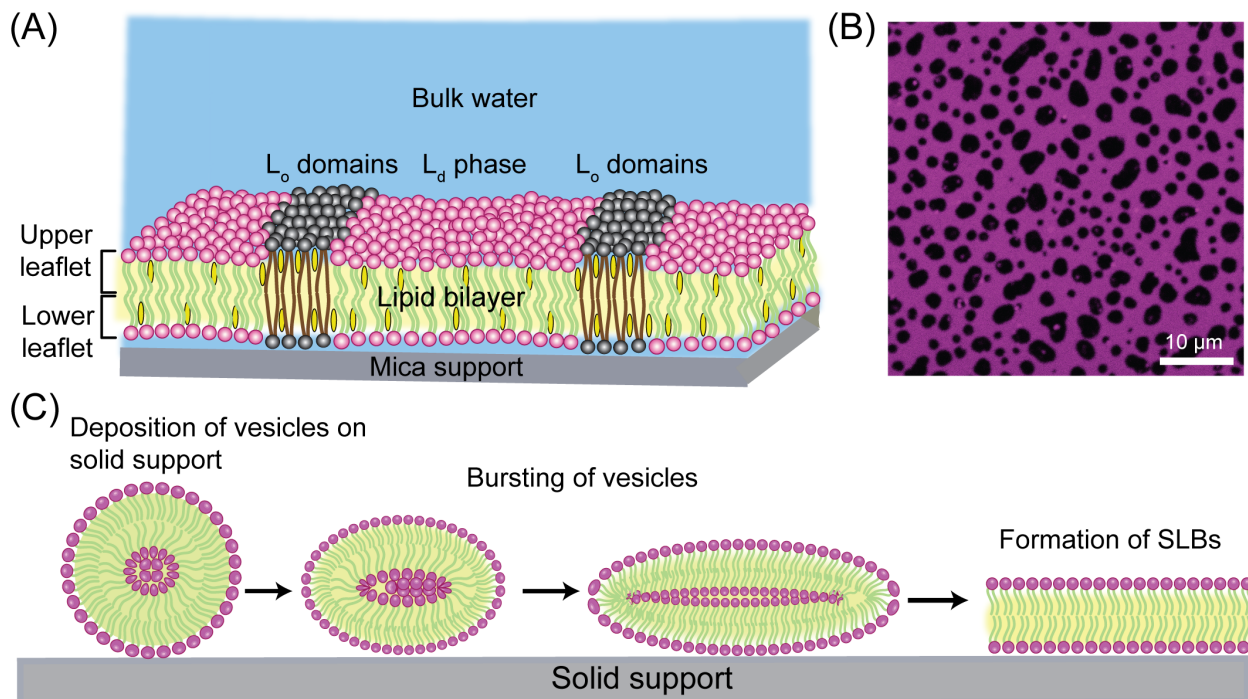


Figure 2.3: (A) Schematic representation of phase-separated SLB, (B) Representative confocal image of a phase-separated SLB, (C) Cartoon representation of formation on SLB by vesicle deposition method.

configuration allows to obtain similar environmental conditions at both leaflet interfaces. However, such bilayers are very unstable, and it is very tricky to vary the environmental conditions (such as ionic strength of the buffer). Unlike in case of free standing bilayer, the physical conditions of the membrane can be easily varied when using SLBs. Thus, to overcome the major drawback of SLBs, that is the lower leaflet-substrate interactions, scientists have introduced some solutions, such as the use of polymer cushion between the substrate and the bilayer in order to increase the hydration layer therein or creating the bilayer on top of a porous substrate to obtain free-standing membrane like behavior along with the benefits of a flat SLB[56, 57, 58]. Overall, the SLBs can be very well-regulated and form a convenient biomimetic membrane system of a desired composition to study the membrane structure, phase-separation, lipid diffusion and other physical properties, and to explore the effects of changing the external environment. In order to understand the role of biological water in lipid diffusion, SLBs have been chosen for the research works described in this thesis for their suitability to our dehydration procedure.

### 2.3.3 Giant Unilamellar Vesicles (GUVs)

In aqueous solution, due to the amphiphilic character, lipids self-assemble into spherical bilayer/multilayer structures (liposomes), exposing the hydrophilic head groups towards aqueous phase and hydrophobic tails remain buried inside the core of the bilayer. These liposomes can be of varying size, and often multilamellar. Subjected to an electric field, the liposomes may vesiculate into very large unilamellar vesicles with a diameter  $>1 \mu\text{m}$ , termed as Giant unilamellar vesicles (GUVs)[59]. The method of preparation of GUVs with alternating current is called electroformation, where the lipid mixture of the desired



composition in organic solvent is put on platinum electrodes, and the organic solvent is evaporated, followed by supplying AC current for certain time while dipping them into an aqueous buffer[59]. The size of the vesicles produced in this method is much larger than the SUVs or LUVs prepared by sonication or extrusion through polycarbonate membrane of specific pore size. GUVs are routinely used as model membrane systems as the bilayer in GUVs mimic the shape and the size of the native cell membranes, making them a perfect choice for studying the effect of membrane curvature, fluidity, phase separation, cell-cell fusion, lipid diffusion or protein-lipid interactions[60, 61, 62, 63]. Moreover, by tuning the composition of GUVs membrane heterogeneity can be introduced and investigated[64].

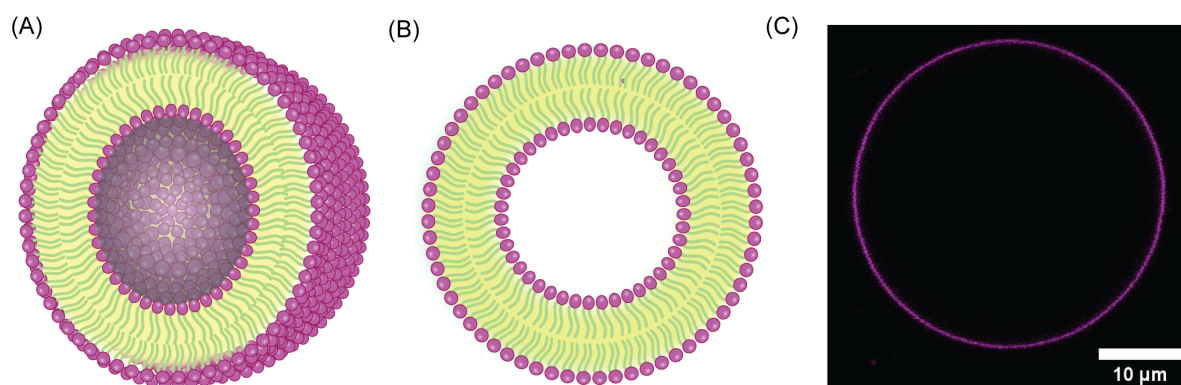


Figure 2.4: Cartoon representation of (A) three dimensional view of a half cut GUV, (B) an equitorial cross-section of a GUV; (C) Fluorescence image of an equitorial cut of a single phase GUV (image acquisition Emilia Krok).

### 2.3.4 Bead Supported Lipid Bilayer (BSLB)

Another type of model membrane system is bead supported lipid bilayer (BSLB), where the lipid bilayer is attached around silica bead of a few microns in diameter. In this case, both the advantages of GUVs and SLBs are combined to obtain cell-like curvature, shape and size like in GUVs and higher stability and support like in case of SLBs. BSLBs are preferred platform for various biological studies, such as, protein-lipid interactions, T-cell-antigen presenting cells interactions, mimicking the cellular interactions with virus particles, macrophages or membrane fusion as the curvature is often a crucial factor for various biological processes[65, 66, 67, 68].

### 2.3.5 Giant Plasma Membrane Vesicles (GPMVs)

Giant plasma membrane vesicles (GPMVs) or blebs are vesicles filled with cytoplasm derived directly from plasma membrane by chemically induced vesiculation[69]. Hence GPMVs are an excellent model membrane system where the complexity and protein diversity of the parent plasma membrane are fully retained[70]. Today they are used commonly to investigate phase separation, lipid/protein interaction, diffusion or cellular fusion [60, 70, 71, 62]. Moreover, GPMVs are also used for lipidomics studies of cell membranes

and employed as a carrier in drug delivery systems[70, 72, 73, 74, 75]. Recent discovery of the phase separation in GPMVs directly obtained from live cells have indicated positively towards the validity of the raft hypothesis[70]. However, it should be noted that though GMPVs represent the native plasma membrane complexity and lipid/protein composition more than any other model membrane system, it does not completely imitate the structure of its parent cell membrane. After inducing vesiculation by chemical reagents, asymmetry of lipid membrane is largely lost. In addition, GPMVs are in equilibrium, whereas cellular membranes are a dynamic, non-equilibrium systems with constant changes in composition by membrane trafficking and cellular transport.

Overall, to summarize, all the model membrane systems have their own benefits and drawbacks. SLBs, GUVs, BSLBs and free standing bilayers allow to tune lipid composition, which is advantageous for lipid composition related studies of biophysical properties, such as phase separation, membrane curvature, fluidity, rigidity etc. In contrast, GPMVs are more appropriate for investigation of biological processes due to their high chemical resemblance of membrane composition to native plasma membranes. SLBs having a solid support, are better choice for their stability and suitability for force microscopy experiments and as biotechnological platforms. But they lack the cellular membrane curvature. In addition, the solid support often influences the lower leaflet lipids through lipid-substrate interactions. On the other hand, GUVs do not have these problems and possess cell membrane like curvature and allow membrane permeability studies, but GUVs are not as stable as SLBs or BSLBs. Thus all these biomimetic systems are complementary to each other. They offer the highest benefits when chosen suitably depending on the experimental techniques to be used and posed the research questions. However, it should be noted, that although I outlined few widely used biomimetic membrane systems, there are many other types of systems, such as black lipid membranes, or tethered lipid membranes, and membrane scientists are constantly exploring the possibility of new biomimetic membrane systems and modifying the existing systems to obtain the best-suited model for their research questions.



# Chapter 3

## Lipid-water interplay

### 3.1 Biological water

Water is an inseparable part of any living system – as it says in a Bengali proverb, “another name for water is life”. Water has many unique functions in living organisms. It acts as a solvent to dissolve various biomolecules and ions, a transporter of biological substances (such as blood, food, excretory substances), a lubricant in bone joints and pleural cavity containing the lungs, an essential reactant in fundamental reactions of life e.g. photosynthesis or temperature control, to mention a few. Apart from these roles at the macroscale, the presence of water, also at a molecular level, shapes the molecular interactions essential for protein folding, aggregation and stabilization, functioning of DNA, and self-assembly of membranes[76, 77, 78, 79]. The thin layer of water, directly interacting with the biomolecules is commonly termed as ‘biological water’ and it exhibits distinctive properties compared to bulk water in terms of rotational and translational mobility, orientation and H-bond strength[3, 80]. Two types of biological water molecules in the vicinity of the biomolecules can be distinguished – first, the water molecules trapped inside a macromolecule, such as, protein or DNA loop, and second, the water molecules adsorbed at the surface of biomolecules. The first type is comparatively less labile (higher residence time) than the second category[76]. Various spectroscopic techniques like infrared (IR) spectroscopy, sum frequency generation (SFG) spectroscopy, transient absorption and dielectric spectroscopy, nuclear magnetic resonance (NMR), and neutron scattering studies have shown detectable changes in the dynamics and structural organization of the interfacial water molecules compared to bulk water[8, 10, 80, 81]. The hydration shell of biomolecules may contain water molecules of varying order, both less fluid and more ordered water molecules as well as comparatively more fluid and more disordered ones[76]. The electrostatic interactions that dominate in the biological water are controlled by Debye screening length, which is less than 1 nm in physiological ionic strength of 150 mM[80]. However, recent MD simulation studies reported the presence of bound and unbound water layers around the phosphocholine headgroups of phospholipids, whose dynamics, structural properties and hydrogen bonds are affected up to a distance of 2.4 nm[3]. The water molecules being polar in nature participate in dipole-dipole and ion-dipole interactions. The most prevalent interaction for water is through the formed H-bonds – water molecules can act as both H-bond donors and acceptors. With all these interactions with the polar moieties of biomolecules, water molecules become less labile at the interface. Additionally, the hydration layer also induce electrostatic screening between charged moieties at the interface. Thus it is evident that water around the biomolecules is not merely a structureless aqueous solvent but its implications modulating the molecular interactions in the vicinity of proteins, lipids and other biomolecules are highly important to consider.

## 3.2 Water hydrating lipids

As the amphiphilic lipid molecules are naturally engineered to form self-assembled structures upon exposure to water, the interaction of lipids with water plays a pivotal role in determining their structural organization, dynamics and other biophysical properties of these self-assemblies, i.e. the lipid membranes. A lipid bilayer submerged in water comprises three distinct parts. In the outer part, surrounding the bilayer exists the bulk water region and in the inner part, the core of the bilayer reside the hydrophobic acyl chains. In between these two parts, there is the lipid-water interface region where the water molecules interact with the functional groups of the lipid headgroups. As discussed above, the thin hydration layer of water hydrating the polar headgroup of lipids behaves differently than the bulk water. Various experimental and MD simulation studies have confirmed the altered orientation and restricted mobility of the water molecules bound to the membrane[6, 82, 83]. The water molecules in the close vicinity ( $\leq 30$  Å) of the polar head group possess an ordered structure of their dipole moments with respect to the bilayer normal and this effect varies with the functional groups at the interface[6, 82, 84, 85]. Moreover, the H-bonds formed by the water molecules at the lipid-water interface and the confinement of the water molecules in between the lipid headgroups makes their diffusion far from free diffusion[86]. The rotational and translational diffusion of water molecules at the extended H-bond network of lipid oxygen slow down and the closer they are from the lipid functional groups, less mobile they are[83, 87]. Presence of two types of water molecules was reported – water molecules tightly bound to the phosphate and/or carbonyl oxygens of lipids (bound hydration) and less tightly bound water molecules that can be displaced by osmosis (unbound hydration layer)[6, 9, 10]. However, lipid-water interactions at the interface not only alter the behavior of the biological water layer but also, in return, modulate the properties of the membrane itself. The orientation, fluidity, dipole potential of the lipid headgroups are known to be significantly affected by the presence of the hydration layer[6]. The depth of penetration of the water molecules into the interface region depends on the lipid types and their phases[6, 82, 88]. Moreover, the hydration of the lipid headgroup also influences the area per lipid[89]. Previous X-ray and neutron scattering studies as well as spectroscopic investigations have claimed that in general around 6-20 water molecules per lipid form the hydration layer[6, 10, 90]. However, the exact nature/structure of the hydration shell around the lipid headgroup is highly dependent on the chemical structure of the lipid, in particular the headgroup region. The membrane hydration is also affected by the hydrocarbon tails, or in other words, its phase, due to differences in the packing. Apart from the lipid structure, the presence of other membrane components, such as cholesterol or ions also dramatically affects the hydration structure of the lipids.

### The effect of lipid headgroups

As it is the polar headgroup region of the lipids that directly interacts with the interfacial water, the hydration structure of the lipids is largely determined by the type and character of the lipid headgroup. The major component of mammalian membranes - PC lipids are zwitterionic in nature with a positively charged choline group and a negatively charged phosphate group. Being only H-bond acceptor, PC can not form inter-lipid H-bonds, but it can form 2-4 H-bonds with water molecules through the carbonyl and phosphate oxygens. Both in PC and SM, the choline group being incapable of forming

H-bonds, a water clathrate cage structure containing around 6-8 water molecules per lipid is formed around the phosphocholine moiety. Due to the absence of direct H-bonds with the choline group, the water clathrate cage is not a rigid structure, but rather a dynamic and comparatively fluid (than H-bonded water molecules) water shell assembled by weak van der Waals interactions. However, nearly 60% of these clathrate water molecules remain simultaneously H-bonded to the phosphate and/or carbonyl carbon of the same or neighboring lipids[82]. Together with the 2-4 H-bonded strongly bound water molecules at the phosphate and carbonyl groups and the 6-8 water molecules forming the clathrate structure, overall 10-12 water molecules form the primary hydration shell of PC and SM at fully hydrated conditions[6, 82, 83, 91, 92, 87]. In contrast, PE, PS, PG lipids have different hydration layer structure, that involves water molecules bound with direct H-bonds to the headgroup moieties. Moreover, being both H-bond donor and acceptor, they form inter-lipid H-bonds, decreasing the overall number of lipid-water H-bonds and water molecules (6-7 water molecules per PE or PG) in their solvation shell[93].

## The effect of acyl chains

In parallel to the headgroup structure, hydrophobic chains of the lipids also affect their hydration structure. Though the hydrocarbon tails are not in contact with water, they influence the lipid hydration by controlling the molecular packing of the bilayer. Systematic studies on the effect of lipids' chain saturation showed that the number of H-bonded water molecules per lipid is higher for unsaturated PC than saturated PC and that the number of water bridges between adjacent PCs are lower in case of unsaturated lipids[94]. These results are a consequence of lower area per lipid in case of saturated lipids with relatively more compact packing compared to unsaturated lipids. The nature of double bonds (cis or trans) does not affect the hydration structure[94], but the position of the double bond was found to affect the hydration of lipid headgroups. MD simulation studies involving variation of the double bond position along the hydrophobic chain for lipids with specific headgroup, showed that lipids with the double bond linking C9 and C10 carbon, possess the highest number of H-bonded water molecules and highest area per lipid[95, 96]. It is interesting to note that in biologically prevalent unsaturated lipids, the double bonds are mostly present at C9-C10 position.

## The effect of cholesterol

Cholesterol is an important constituent of mammalian plasma membranes, and it affects membrane properties such as structural organization, phase separation, fluidity or area per lipid. Hydration of lipid headgroups is also influenced by the presence of cholesterol molecules, which reside in between the lipids with their rigid ring structure aligned along the hydrophobic tails and the hydrophilic hydroxy group close to the polar headgroup of lipids. The hydroxy group of cholesterol makes H-bond with the carbonyl group of glyceride lipids and to the amine moiety in SM[97]. MD simulation results showed that the water molecules around the lipid headgroups becomes less ordered and more bulk-like in the presence of cholesterol[98]. Using electron spin resonance (EPR) and NMR techniques, the surface water diffusivity was reported to increase upon the addition of cholesterol to DPPC membranes[99, 100]. Presence of cholesterol induces replacement of the water H-bond bridges between adjacent lipids by lipid-solvent H-bonds leading to an increase of water diffusivity[99]. In contrast, the translational dynamics of water molecules

in membrane interior becomes slower with increase in cholesterol concentration[100].

## The effect of ions

Ions are an integral part of the aqueous solution around biological membrane. Presence of ions significantly alters the hydration structure of the lipid headgroups, depending on the charge distribution of the lipid headgroup and the charge, size and hydration energy of the ions[82].  $\text{Na}^+$  ions penetrate into the carbonyl region in the PC head group, whereas  $\text{Cl}^-$  ions mostly reside in the bulk water phase[101, 102]. But in the gel phase due to tight packing of lipids  $\text{Na}^+$  ions do not penetrate deep in between the lipid headgroups[103].  $\text{Ca}^{2+}$  has high affinity to bind to lipid oxygens (carbonyl and phosphate) resulting in its complexation with more than one lipid. SFG, small angle neutron scattering (SANS), IR spectroscopy studies as well as MD simulation results reported partial dehydration of the lipid head group region caused by the presence of various ions for example,  $\text{Ca}^{2+}$ ,  $\text{Cu}^{2+}$  or  $\text{Zn}^{2+}$  ions[101, 104, 105, 106, 107, 108].

In summary, the hydration properties of lipid headgroups result from numerous factors ranging from chemical structure of the lipids, their physical phase, order, packing or guest molecules present in the membrane. It is to be emphasized that all these parameters are deeply interlinked and act together to shape the overall hydration structure of lipids in biomembranes. Perturbing one factor may have indirect effect on the other parameters. Although the basic influencing parameters are known, the lipid hydration properties in complex systems like plasma membrane are still unclear. Therefore, for an in-depth understanding of the hydration properties of the membrane, it is important to investigate lipid membranes of different chemical and structural properties, at different environmental and compositional conditions as one could expect markedly different lipid hydration properties in different cases.

## 3.3 Dehydration of lipid membranes

As discussed above, hydration of lipids is of immense importance that influences membrane structure, dynamics and interactions of lipids and ions. Water is an essential part of our life supporting machinery. Dehydration may cause serious oxidative stress and cell death in living systems[109, 110]. But there are several examples in nature (discussed below) where dehydration takes place in living systems.

### 3.3.1 Dehydration events in biological systems

One of the most common examples of dehydration in living systems is “anhydrobiosis” – life without water. This is a unique capability that certain microorganisms have developed to survive in very harsh environmental conditions. In this state of life all the metabolic processes almost cease temporarily, and the organisms go to an inactive state of life. But as the hydration conditions improve, their metabolism revives again. Tardigrades, nematodes, bdelloid rotifer, yeasts, various bacteria, seeds, pollens and anhydrobiotic plants are capable of anhydrobiosis[17, 18, 111]. Extensive investigation has been performed to understand the desiccation tolerance mechanism of these microorganisms. The most prevalent survival mechanism of anhydrobiosis is production of trehalose, a nonreducing disaccharide of glucose, which interacts with the polar lipid headgroups by H-bonding with the hydroxy groups of the carbohydrates, and thus stabilizing the membrane while replacing

the hydration layer[112, 113]. The transition temperature of dry DPPC lipid was found to be similar to fully hydrated DPPC in the presence of trehalose, whereas it was 30 K higher without trehalose[112]. Trehalose was also found to protect the cell membrane in *Saccharomyces cerevisiae* at dehydrated conditions[114]. In contrast, bdelloid rotifers do not produce trehalose, but survive dehydration in another way – in dehydrated condition, they contract their body into “tuns” and reduce their volume allowing slow water evaporation[18, 115]. Additionally, late embryogenesis abundance (LEA) proteins prevent damaging protein aggregation during water stress in pollens, seeds, and plants that help them stay in dehydrated dormant state for a long time[116].

Apart from these anhydrobiotic organisms, local transient dehydration also occurs in advanced eukaryotic and prokaryotic cellular systems. Various biological processes, such as cell fusion, neurotransmission, viral entry or fertilization involve merging of two lipid bilayers[61, 71, 117, 118] (Figure 3.1). In such cases an intermediate stalk (a neck-like connection between two fusing membranes) formation (Figure 3.1B) occurs where the hydrocarbon chains from two different bilayer come in contact. For this, a hydration barrier has to be overcome to remove water molecules around the lipid headgroups at the fusing zone in order to get the hydrophobic tails from the two lipid bilayers to interact, finally leading to membranes fusion[118]. Moreover, in endoplasmic reticulum (ER), Golgi apparatus lipid membranes are closely interleaved with each other creating water depleted environment. To understand the exact mechanisms of such biological phenomena, it is important to investigate behavior of lipid membranes at lower hydration conditions.

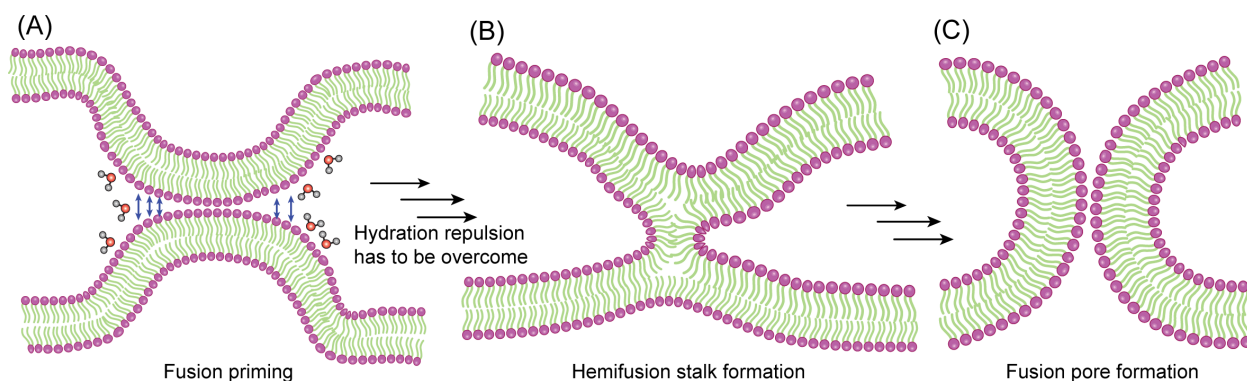


Figure 3.1: Local and transient dehydration occurs during the merging of two lipid membranes. The main intermediate steps during such process: A) Two bilayers come in close contact, B) Hemifusion stalk formation occurs after removing water molecules away from the merging spot, C) Initial pore formation occurs leading to complete fusion.

### 3.3.2 Dehydration of biomimetic membranes

To investigate the lipid behavior in membranes at low water availability conditions and to understand the precise mechanisms underlying the above mentioned biological processes, it is crucial to obtain intact lipid bilayers equilibrated to lower hydration levels. Moreover, lipid bilayers are also used as an excellent biosensor platform and biocompatible coating materials[119, 120, 121]. Creating air-stable membranes would make their usage and handling much simpler and effective. However, keeping the lipid membrane structure intact is experimentally challenging due to the rapturing, delamination and vesiculation

of the membrane in the absence of water. Naturally, GUVs burst in the absence of water as the pressure of the aqueous medium inside the vesicle becomes higher than outside when water is removed. Hence GUVs are not fit for dehydration studies. SLBs, having a solid support underneath, are a more suitable platform for dehydration studies. However, structural preservation of SLBs was also found to be non-trivial. In a solid supported membrane, when the macroscopic water layer dries, the perimeter of the water droplet slowly contracts and the water front moves through the surface. During this drying process, an interfacial force acts at the air-water interface of the bilayer at the perimeter of the water droplet, that peels off the membrane from the support[122]. Preservation of lipid bilayer in lower hydration conditions has been attempted in a number of ways targeting to overcome the destructive air-water interfacial force. The general idea was to increase rigidity of the bilayer - either by strengthening the bilayer-solid support interactions by chemical modification of the lipids, or by including a protective layer on top of the membrane. Air-stable SLBs were formed by enhancing the attractive interactions between solid support and bilayer by using tethered cholesteryl-PEG group, zirconium phosphate,  $\gamma$ -aminopropylsaline or negatively charged poly(dimethylsiloxane)[123, 124, 125, 126]. Additionally, desiccation-tolerant SLBs have also been achieved by chemical cross-linking of the two leaflets of the bilayer, polymerized bis-diene lipids and attaching polymers to the lipid headgroups[123, 127, 128, 129]. Besides these chemical modifications, another parallel approach for creating air-stable membrane was introducing physical confinement on the SLB to dissipate the air-water interfacial peeling force[122]. Moreover, motivated by the trehalose-producing anhydrobiotic organisms, addition of proteins, enzymes, disaccharides onto the membrane was also successfully employed for obtaining stable, dehydrated lipid membranes[120, 122, 130, 131]. Apart from all these dehydration attempts on SLBs, few experimental investigations have been carried out on lipid monolayers and multilayers at varying hydration conditions to understand various physical parameters, such as, the water and lipid headgroup dynamics, phase transition temperature or the order parameter of lipids[10, 15, 16, 90]. However, though using all the above mentioned techniques air-stable SLBs could be obtained, their native properties were strongly altered by the chemical or physical modification. Moreover, in case of the lipid multilayers, the exact hydration level in between the distinct lipid layers was not well-defined. Hence, a long-desired method of creating dehydration resistant lipid membrane with a well-controlled hydration properties has been still lacking. I have resolved this challenging task by developing a novel method for controlling lipid bilayer hydration state without the use of chemical or physical modifications, which is discussed in chapter 7.

# Chapter 4

## Lipid diffusion

### 4.1 Lateral diffusion of lipids in membranes

Biological membrane is a two-dimensional liquid, in which individual lipid molecules can exchange their places with their neighbours freely within the same leaflet. This gives rise to a constant lateral diffusion (Figure 4.1) of lipids within the lipid membrane. Moreover, nuclear and electron spin measuring techniques, such as NMR, and EPR spectroscopy showed that the lipid molecules also rotate and that the hydrocarbon chains wag individually in space (flexion) (Figure 4.1). The exchange of lipids from the inner to the outer leaflet of the lipid bilayer and vice versa is very rare as it involves transiting of the polar headgroup of the lipid through the hydrophobic core of the lipid bilayer costing high energy. But it is established that a constant compositional asymmetry is maintained in the plasma membranes. PS and PE lipids are abundant in the inner leaflet of the membrane, whereas PC lipids are mostly located in the outer leaflet[132]. But during apoptosis (cell death), PS lipids appear on the outer leaflet to serve as a signalling system to attract the macrophages[133]. The purpose of the assisted flip-flop movement of lipids is served by various proteins like flippase, floppase and scramblase.

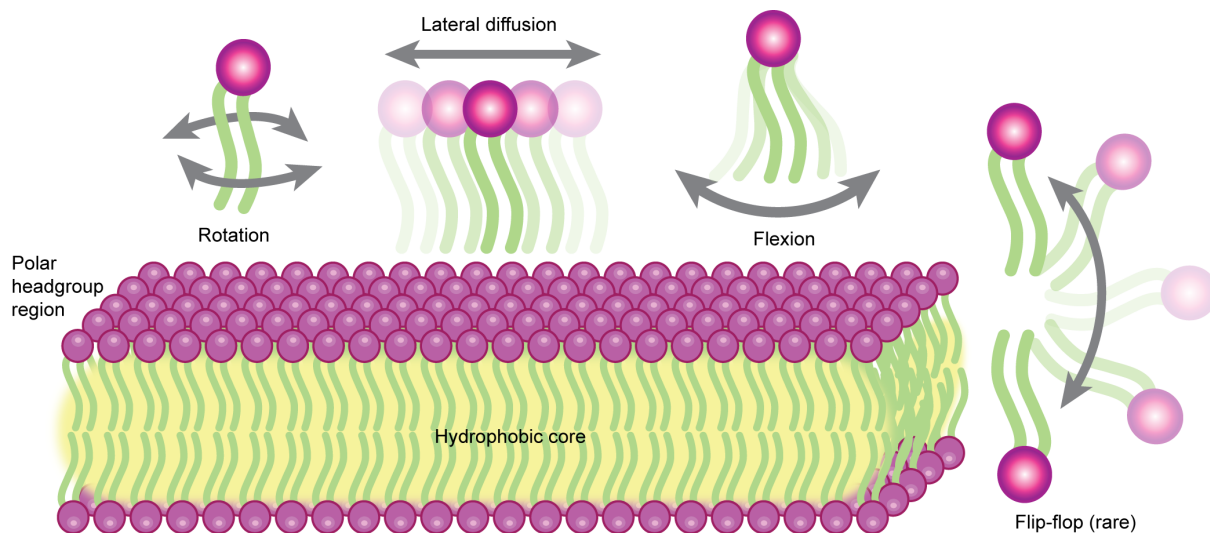


Figure 4.1: Schematic representation of different types of lipid diffusion in a lipid bilayer.

It is well known that the diffusion of lipids in biological membranes is a key physical process that facilitates cellular signalling, membrane trafficking, and transport as well as maintains homeostasis of the membrane[134, 135]. Hence comes the importance and significance of investigating the lipid dynamics in membranes. As discussed above, the lateral diffusion of lipids is the most prevalent diffusion type in lipid membranes and also plays a

significant role in terms of the biological activity of lipids. This encouraged scientists to study the lateral diffusion of lipids in various cell membranes and model membrane systems using various dedicated fluorescence microscopy techniques (see Chapter 5). Theoretically, molecular diffusion of a spherical particle in a three dimensional liquid can be calculated by the well known Stokes-Einstein equation:

$$D = \frac{TK_B}{6\pi\eta r} \quad (4.1)$$

where  $D$  is the diffusion coefficient,  $K_B$  is the Boltzmann constant,  $\eta$  is the dynamic viscosity and  $r$  is the hydrodynamic radius of the spherical diffusing particle. Shaffman and Delbrook extended this model for a cylindrical object moving laterally and rotating around the  $z$  axis in a two dimensional fluid (such as lipid bilayer membrane) in their hydrodynamic model for Brownian motion, where the translational (i.e. lateral for two dimensional fluid) diffusion was quantified by[136]:

$$D = \frac{K_B T}{4\pi h \eta_m} \left( \ln \left( \frac{h \eta_m}{R \eta_f} \right) - \gamma \right) \quad (4.2)$$

where  $\eta_m$  is the membrane viscosity,  $h$  is membrane thickness,  $\eta_f$  is the viscosity of the surrounding bulk fluid,  $R$  is the hydrodynamic radius of the diffusing lipid/protein, and  $\gamma$  is the Euler constant. It has been demonstrated in biomimetic membrane studies that the lipid mobility in the membrane depends on various physical parameters, ranging from the structural parameters (such as the chemical composition of lipids, molecular mass, aggregation, lipid-protein and lipid-lipid interactions) of the membrane itself to external environmental parameters (e.g. temperature, viscosity, surface pressure)[137]. The fluidity of the membrane is an important parameter that highly influences the lateral diffusion of lipids – higher the fluidity of the membrane, higher is the lateral diffusion of lipids therein. The fluidity is determined by both the temperature and chemical structure of lipids. Lipids, above their  $T_m$ , behave like a fluid and below  $T_m$  change their state to a two-dimension rigid crystalline or gel phase. The  $T_m$  mostly depends on the efficiency of packing of the hydrophobic tails of the lipids. The shorter the chain length, the less pronounced is their mutual interaction and packing, leading to lower  $T_m$ . Moreover, the presence of unsaturation in the acyl chain of the lipids also induces a “kink” in the lipid tail structure originating from the different bond angles of the planar  $SP^2$  hybridized unsaturated carbons. This structural deformity inhibits regular packing of the lipids making them more fluid and decreasing the  $T_m$ . Thus plasma membranes of various fishes living in cold water tend to contain high amounts of mono and polyunsaturated fatty acids that help to maintain the fluidity of their plasma membrane at lower environmental temperatures. Cholesterol content in the lipid membrane also greatly influences membrane’s fluidity. For the  $L_o$  phase increase in cholesterol disrupts the tight packing of lipids leading to an increase in fluidity and lipid mobility. In contrast, presence of cholesterol decreases lipid diffusion in the  $L_d$  phase by interacting with the hydrophobic tails and making this phase less fluid. Moreover, lipid diffusion is greatly affected by the inter-lipid interactions and the interactions with neighboring proteins[138, 139, 140]. Ions often bind with more than one lipid at the same time, forming ion-lipids complexes, which altogether move slower than indeividual lipids[102, 141, 142]. Macroscopic phase separation in model membranes and nanoscopic domains/lipid rafts within the membrane also hinder the diffusion of individual lipid molecules[143].

The dependence of lipid diffusion on the above physicochemical parameters can also be explained by the probability of a lipid molecule to diffuse at a particular time. According



to the theory of free volume analysis by Almeida et al., at each diffusion step in a bilayer a lipid molecule must possess certain activation energy of diffusion ( $E_a$ ) and a minimum free area to move into[144]. The probability of fulfilling these two criteria together controls if diffusion takes place or not. When immobile obstructions are introduced into the membrane, the  $D$  value of lipids decreases because of lower probability of finding free area to move into[145]. Similar situation occurs in case of highly packed membranes – free area to move into is also scarce. Moreover, for a particular lipid bilayer, as the area is fixed, the diffusion is associated with continuous density fluctuations that occur without any change in the total energy contained in the membrane. On the other hand, the activation energy of lipid diffusion depends on various molecular interactions in the membrane, such as intra- and inter-lipid interactions, lipid-protein interactions, interactions of lipids with the surrounding hydration layer and ions. At higher temperature, lipid mobility also increases as more lipids possess energy higher than the  $E_a$  required for the diffusion step to occur.

## 4.2 Mechanisms of lipid diffusion

Comparing the lipid mobility in biological and biomimetic systems, it was found that the lateral diffusion of lipids in plasma membranes is 2-100 times slower than in model membrane systems[146, 147, 148]. The presence of nanodomains, interactions with cytoskeleton and membrane-associated proteins, extensive compositional complexity and compartmentalization in plasma membranes, all act as obstructions and hinder the spontaneous diffusion of lipids[149, 150, 151]. Generally, in the absence of any obstruction, lipids undergo free diffusion (Brownian motion), where they move within the two dimensional lipid membrane in a random and chaotic manner with the mean square displacement (MSD) proportional with time. But, due to the membrane heterogeneity and complexity often the free diffusion of lipids is converted to anomalous diffusion, having the MSD proportional to  $t^\alpha$ , with  $\alpha$  being the anomaly parameter[152, 153]. The main criterium of anomalous diffusion is the time-dependence of the MSD – when  $\alpha > 1$ , i.e. MSD increases with time, then it is called anomalous super-diffusion and when  $\alpha < 1$ , i.e. MSD decreases with time, then it is termed as anomalous sub-diffusion. In biomembranes, apart from free diffusion, anomalous sub-diffusion is commonly observed. There are a variety of underlying mechanisms or types of anomalous sub-diffusion, such as hop diffusion, transient immobilization or domain incorporation. The underlying diffusion types can be distinguished based on the dependence of the  $D$  values on the diameter of the observation spot during the diffusion measurement. These experiments have become possible with the advent of super-resolution microscopy and single molecule tracking techniques[154, 155]. For free diffusion, the  $D$  values are completely independent of the observation spot size (Figure 4.2). On the other hand, for hindered diffusion, at bigger observation spot (diffraction-limited), the measured diffusion coefficient is an average of  $D$  values at hindered sites and free sites. As the observation spot decreases the occasional slowing down of the diffusion in the obstruction sites becomes prominent. According to the picket-fence model, the actin-based cytoskeleton acts as fences and anchored transmembrane proteins as pickets compartmentalizing the plasma membrane. Lipids and proteins embedded in the membranes collide with these ‘picket and fence’ and they temporarily confine in a 30-700 nm sized compartments with occasional intercompartment diffusion, which is termed as hop diffusion[147, 156]. Another type of mechanism of hindered diffusion is transient immobilization or trapped diffusion, where a lipid molecule becomes temporarily immobilized/trapped due to transient interaction with certain membrane components, such as cholesterol mediated molecular complexes of <20

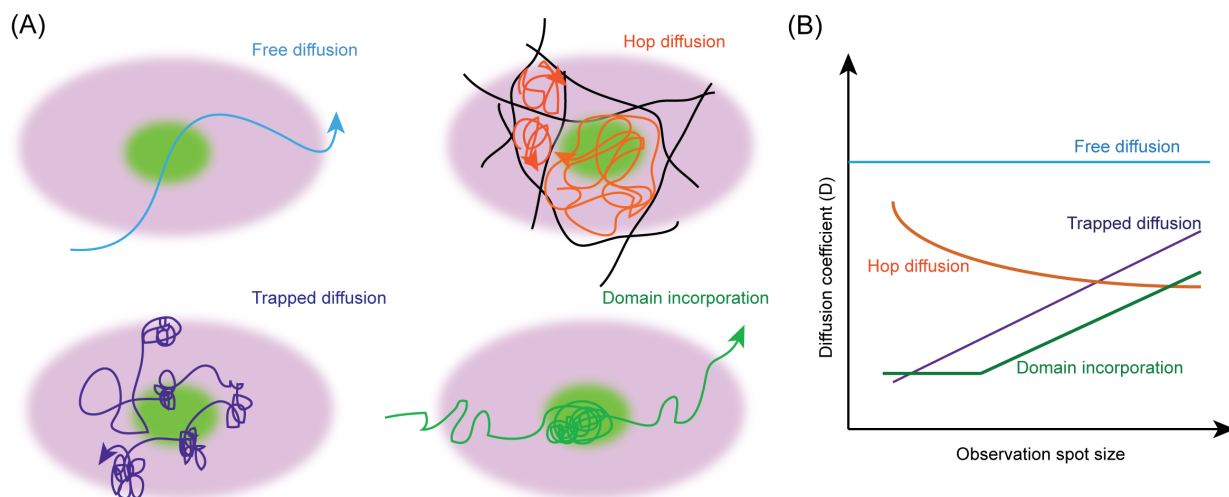


Figure 4.2: (A) Various diffusion patterns of membrane constituents. The pink area represents the membrane surface and the green spot represents the observation spot illuminated with laser. (B) Difference in the trend of changes of lipid diffusion coefficient values as a function of observation spot size, differentiating various diffusion patterns.

nm size[157]. It was reported that phospholipids undergo free diffusion with a constant  $D$ , or hop diffusion where  $D$  increases with smaller observation spot size[158, 159, 160], while sphingolipids and glycolipids exhibit transient immobilization where  $D$  drops with decreasing observation spot size (Figure 4.2)[157, 161, 162]. On the other hand, GPI-anchored proteins undergo domain-like diffusion[163]. Being able to differentiate between the different diffusion modes of various membrane constituents is very crucial to understand their bioactivity. In particular, because lipids take part in cellular signalling pathways, the interactions with various membrane-associated proteins and interaction timescales could provide important indications about signalling processes. Many membrane proteins contain specific binding sites for specific lipids, and such lipid bindings play an important role in the bioactivity of those proteins[163]. For example, HIV-1 glycoprotein gp41 contains cholesterol binding motif that controls their lateral sorting and oligomerization[164]. Similarly, the transmembrane domain of the COPI machinery protein contains dedicated binding site for single sphingolipid species which regulates the equilibrium between inactive monomeric form and the active oligomeric form of the protein[165]. Hence it is very important to investigate the diffusion of lipids along with their specific diffusion modes in biomembranes. The next chapter describes the various fluorescence microscopy techniques to probe lipid diffusion.

# Chapter 5

## Fluorescence techniques to study lipid diffusion

### 5.1 Fluorescence microscopy

“Progress in science depends on new techniques, new discoveries and new ideas, probably in that order.”

-Sydney Brenner (Nobel Prize in Physiology and Medicine, 2002)

Microscopy reveals a whole new world in front of our eyes allowing to generate magnified images of tiny objects not visible to the naked human eyes. According to the published literature, the first compound microscope (with two lens system) was designed by the Dutch spectacle maker Zacharias Janssen in the late sixteen century. But the mentions and descriptions of “Sukshmjeevanu” (molecular life forms invisible to the naked eye) – microorganisms and leaf cells can be found in the ancient Indian Vedic literature, written thousands of years BC, indicating the prolonged history of microscopy in human civilization[166, 167]. The whole concept of microscopy and microorganisms became famous in the mid-seventeenth century when independently, two fellows of the Royal Society, Antoni Van Leeuwenhoek observed microscopic organisms, red blood cells and sperm cells and Robert Hooke published his book *Micrographia* containing “physiological description of minute bodies”[168]. Then for almost two centuries the microscope designs remained more or less similar until the late nineteenth century when the invention of advanced apochromatic objectives by Hans Abbe paved the road towards high-resolution imaging. Then gradually the emergence of modern microscopy started leading to the development of a bunch of microscopy techniques – wide field microscopy, confocal microscopy, total internal reflection (TIRF) microscopy, two-photon microscopy, photo-activated localization microscopy (PALM), stochastic optical reconstruction microscopy (STORM), stimulated emission depletion (STED) microscopy, optogenetics, that revolutionized research in biological as well as material sciences. From the abundance of different microscopy approaches used in modern research, in this thesis, I include an overview of a few of them that have been exploited in my doctoral research.

#### 5.1.1 Fluorescence

When light and matter interact, various photophysical and/or photochemical processes may take place. When a molecule absorbs light energy, it reaches a higher energy level, from where it can either go back to the ground energy state by typically a combination of radiative and non-radiative decay (photophysical process) or the activated molecule may undergo some chemical reaction (photochemical process). When light falls on molecules, they can absorb photons and go from one electronic energy state to an excited electronic energy state of the same spin multiplicity (singlet). This process is followed by non-radiative

decay (vibrational relaxation) and may be followed by a radiative decay from the lowest electronic excited state (Figure 5.1). This radiative decay is called fluorescence and these molecules with high probability of having such radiative emission are called fluorescent molecules. Fluorescence is a photophysical process, typically occurring in the time scales of  $10^{-7} - 10^{-10}$  s. This absorption of the external energy in form of light (photons) by the molecule is called the excitation and the radiative decay associated with the molecules dropping down from the higher electronic energy state to lower one is called the fluorescence emission. Fluorescence emission is always red-shifted i.e. the wavelengths of the emitted fluorescence light are higher than the excitation wavelength due to the vibrational relaxation happening before and after the radiative fluorescence emission. Though the radiative transition from singlet to triplet state is quantum mechanically forbidden, molecules can sometimes go to the triplet state from singlet state by non-radiative process (inter-system crossing), and then come back to a ground state radiatively (phosphorescence) or non-radiatively (external conversion) (Figure 5.1).

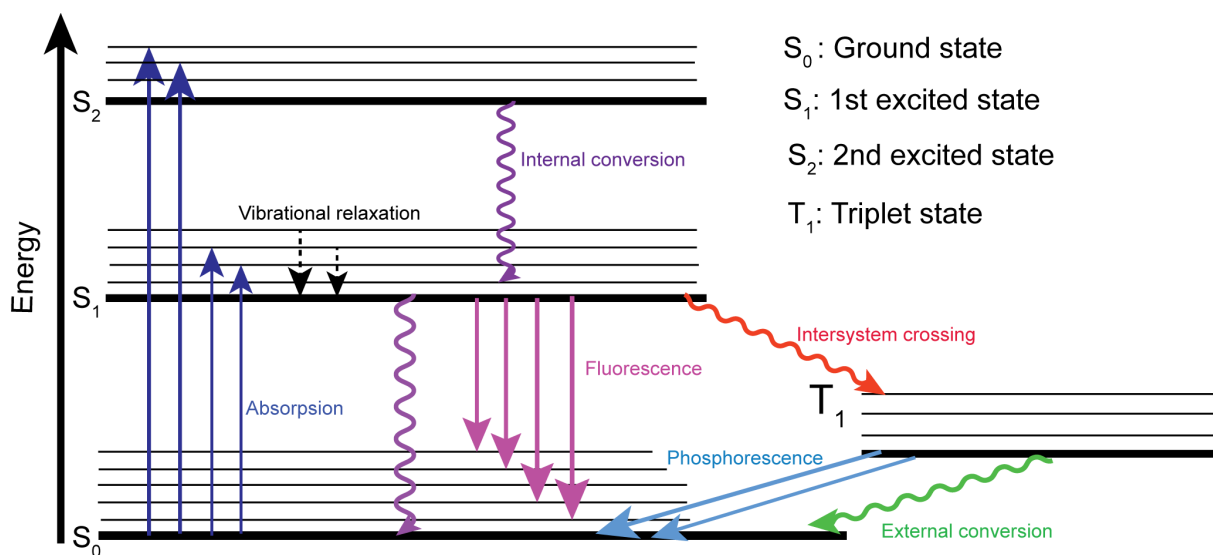


Figure 5.1: Jablonski diagram depicting various photophysical processes.

Molecules with delocalized electrons, such as aromatic molecules show fluorescence. The higher the delocalization of electrons with more aromatic rings and their substitutions, higher is the probability/intensity of fluorescence. Unlike rotational and vibrational spectra, which are only absorption spectra, both absorption and emission spectra are obtained in case of fluorescence. Fluorescence is radiative emission from higher electronic energy level to ground electronic energy level. Difference in electronic energy levels is much higher than rotational and vibration energy levels, and hence the energy emitted can not be dissipated within the short lifetime of excited electronic states by only non-radiative decay, leading to radiative emission i.e. fluorescence. The electronic excitation and emission spectra are band spectra with high broadening as the electronic transitions are accompanied by various rotational and vibrational transitions. Moreover, various inter- and intra-molecular interactions and energy-time uncertainty contribute to spectral broadening.

The first documented observation of fluorescence was a blue color light from a wood infusion, by Spanish physician and botanist Nikolas Monardes though it was not scientifically understood then[169]. Physicist Sir George Gabriel Stokes first coined the term “fluorescence” and clearly identified the phenomenon when he placed quinine under ultraviolet

radiation in 1852[169]. After more than half a century, fluorescence staining for biological samples became possible. Later after the commercialization of microscopes by Hans Abbe and Carl Zeiss, fluorescence detection was introduced in microscopy by August Koehler and Oscar Heimstaedt[170]. The discovery of green fluorescent protein with its incorporation in cellular organelles and the advent of confocal microscopy brought a new era of fluorescence microscopy, that is still widely used for visualization and diffusion analysis of biological systems. Importantly, fluorescence microscopy is still being intensively developed, mainly in terms of sensitivity and spatial resolution (super-resolution techniques).

### 5.1.2 Confocal microscopy

Fluorescence microscopy is a special class of optical microscopy, where fluorescent sample is illuminated with a specific fluorescence excitation wavelength and the emitted fluorescence signal from the sample is detected to obtain the magnified image of the sample. Wide-field microscopy is the simplest form of fluorescence microscopy, in which the entire sample is equally illuminated. But in this case, the reflected light or fluorescence emitted from below and above the focal plane reach the detector acting as background noise and blur the image formed by the light from the desired focal plane. To overcome this drawback, Marvin Minsky patented his idea of rejecting all the out-of-focus light by using pinhole apertures in the illumination and detecting path of the light, making it “confocal”. Moreover, the pointed illuminating light source scanned in X and Y directions on the sample allows to obtain intensity information point by point to build up the whole image[171, 172]. This improved version of fluorescence microscopy is called confocal microscopy, which is one of the most widely used light microscopy techniques applied in today’s molecular biology and cell dynamics research. Thanks to its ability to filter out all of the out-of-focus light, confocal microscopes can generate images not only with high spatial resolution, but also it is a very efficient tool for optical sectioning of deep tissues for the 3D reconstruction of images. Thus, the fundamental difference between conventional wide-field microscopy and confocal microscopy lies in the point illumination of the sample and the pinhole aperture used in the detection. Apart from eliminating the out-of-focus light, closing the pinhole to its minimum also improves the resolution of the images. In light microscopy, the resolution, i.e. the minimum separation between two adjacent points at which they can be distinguished, is termed as diffraction limit. When light passes through an object, a diffraction pattern with a central high intensity spot surrounded by circular alternating dark and bright fringes with diminishing intensity, called Airy disk, is formed. The resolution is determined by the Rayleigh criterium, which says that two adjacent points can be distinguished if the central bright peak of one point’s Airy pattern coincides with the first dark fringe of the neighboring point’s Airy pattern. The minimum detectable distance between the two neighboring points is then defined as,

$$d = \frac{0.61\lambda}{n\sin\theta} = \frac{0.61\lambda}{NA} \quad (5.1)$$

where,  $\lambda$  is the wavelength of the illuminating light,  $\theta$  is the half-angle subtended at the specimen by the pupil of the lens, NA is the numerical aperture of the objective, n is the refractive index medium between the objective and the specimen.

Depending on what is considered to be resolvable points, the minimum detectable distance can also be calculated by Abbe and Sparrow criteria. Abbe demonstrated resolution limit using a fine and periodic grid structure, that forms a diffraction pattern while illuminated by parallel light. The undeviated, 0<sup>th</sup> order light does not contain any information

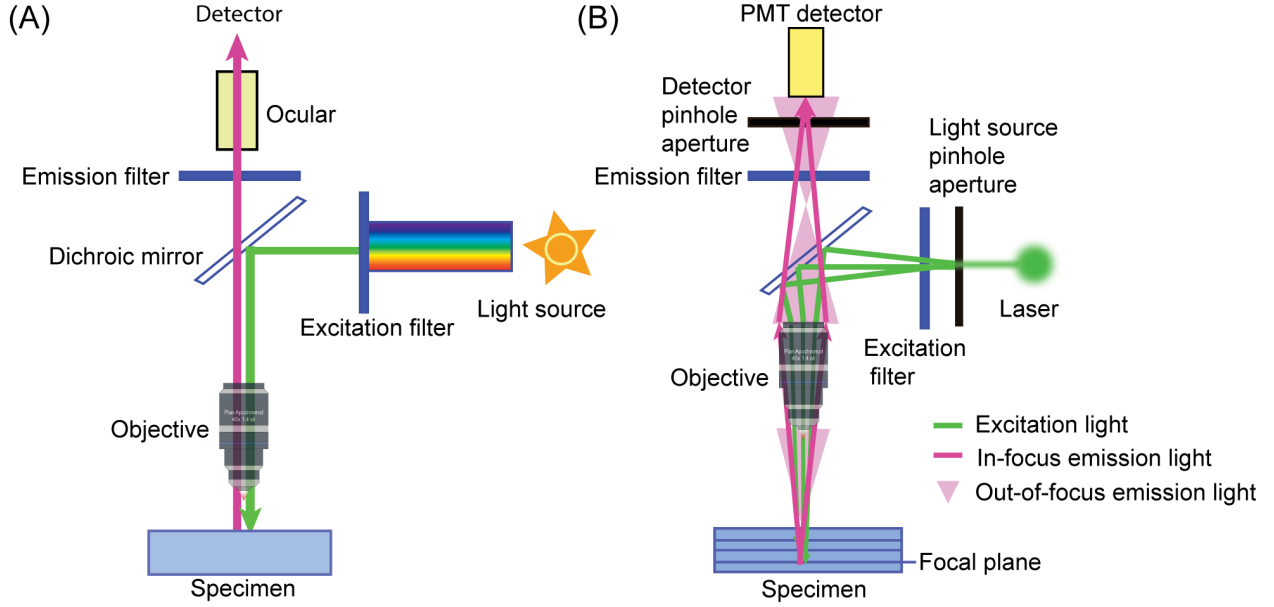


Figure 5.2: Schematic representation of a wide-field (A) and confocal (B) fluorescence microscopy system.

from the sample. At least the first order diffraction is required to form an image. The optical resolution depends on the NA, which is defined by the angle at which the first order is diffracted by the sample. The higher is the NA, the higher order of light can be captured by lens, leading to improved resolution. According to Abbe criterion of optical resolution, the resolution limit is reached when two neighbouring structures become indistinguishable, and the grid of periodic structures generate an image with equal intensity. In that case, lateral resolution  $R_{\text{lateral}}$  and axial resolution  $R_{\text{axial}}$  are:

$$R_{\text{lateral}} = \frac{0.5\lambda}{\text{NA}} \quad (5.2)$$

and

$$R_{\text{axial}} = \frac{2\lambda}{(\text{NA})^2} \quad (5.3)$$

On the other hand, Sparrow criterium of resolution limit largely resembles the Raleigh criterium, with some modification. Sparrow resolution limit is met when the central part of the two Airy patterns of two adjacent points are at a distance where there is no dip in intensity between their maxima, rather there is a constant intensity maintained across this region. According to Sparrow criterium of resolution[154],

$$d = \frac{0.47\lambda}{\text{NA}} \quad (5.4)$$

Using oil immersion, for the common high NA objectives, around 1.45 NA is reached (with few exceptions such as for “ZEISS  $\alpha$  Plan-Apochromat 100 $\times$  / 1.57 Oil-HI DIC Corr objective” NA is 1.57). Consequently, considering light of wavelength 550 nm, theoretically, according to Abbe criterium, resolution can be reached down to around 180 nm laterally and 520 nm axially. However, experimentally this is not always achieved. In practice, pinhole can not be made as small as the laser’s focal spot size. Moreover, various optical

aberrations introduced by the objective lenses, such as chromatic aberration and/or spherical aberration, reduce the lateral resolution[173]. However, despite using the pinhole, the axial resolution can not go down as low as the lateral resolution, causing the 3D reconstruction of images to blur in the Z direction. This is a major technical problem in live cell or tissue imaging, where improved microscopy strategies like light sheet microscopy or total internal reflection fluorescence (TIRF) microscopy are being used. Many other variants of fluorescent microscopy, including two-photon microscopy and various super-resolution approaches, such as stimulated emission depletion microscopy (STED), stochastic optical reconstruction microscopy (STORM), photoactivated localization microscopy (PALM), single molecule localization microscopy (SMLM) are also used for precise, high resolution imaging of biological samples.

Since the axial dimension of lipid membranes is much lower ( $\sim 4$  nm) compared to the typical axial resolution of  $\sim 0.6$   $\mu\text{m}$ , it can be regarded as 2D, and therefore, the axial resolution constraint in confocal microscopy is not a major problem in imaging of biomimetic membrane systems. Hence, confocal imaging, in particular, is used as one of the most suitable tools for studying lipid membrane systems. In my doctoral research showcased in this thesis, all imaging and diffusion studies were performed using fluorescence confocal microscopy.

## 5.2 Fluorescence recovery after photobleaching (FRAP)

Fluorescence recovery after photobleaching (FRAP) or fluorescence photobleaching recovery (FPR) is a standard and powerful technique to study diffusion of fluorescent molecules in two dimensional systems. With the advent of confocal microscopy, FRAP became a readily available quantitative method that have been widely used for investigating lipid and protein diffusion in biomimetic as well as cellular membrane systems. The basic principle of FRAP is based on the irreversible photobleaching of fluorescent molecules within a well-defined area and the observation of diffusion-induced fluorescence intensity recovery in this area (Figure 5.3A-B). One small area of the sample is photobleached with high power and short laser illumination causing an immediate drop in fluorescence intensity in this area. Then the fluorescence intensity of the bleached area is monitored over time as other unbleached fluorescent molecules diffuse into the spot, while the bleached ones move out due to their natural diffusion. Thus an intensity trace of the bleached area over time is obtained, which reflects the dynamics of the fluorophores. This intensity trace is then fitted to an appropriate mathematical model of diffusion to get the diffusion coefficient ( $D$ ) values (Figure 5.3C). When all the fluorophores are mobile, after a certain time the intensity in the bleached spot should reach the intensity value equal to that before the bleaching event. The difference in fluorescence intensity between the initial (before bleaching) and final time points (theoretically after infinite time, and practically when no significant change in the fluorescence signal is observed) indicates the fraction of molecules that are immobile. The mobile fraction ( $MF$ ) of the molecules is defined as

$$MF = \frac{I_i - I_0}{I_\infty - I_0} \quad (5.5)$$

where  $I_i$  is the initial intensity of the bleached spot before photobleaching,  $I_0$  is the intensity immediately after bleaching and  $I_\infty$  is the intensity of that spot after infinite time. And the immobile fraction of molecules is  $(1 - MF)$ . In practice, even in model membrane



systems, there is always some immobile fraction observed, though the reason is not always clear.

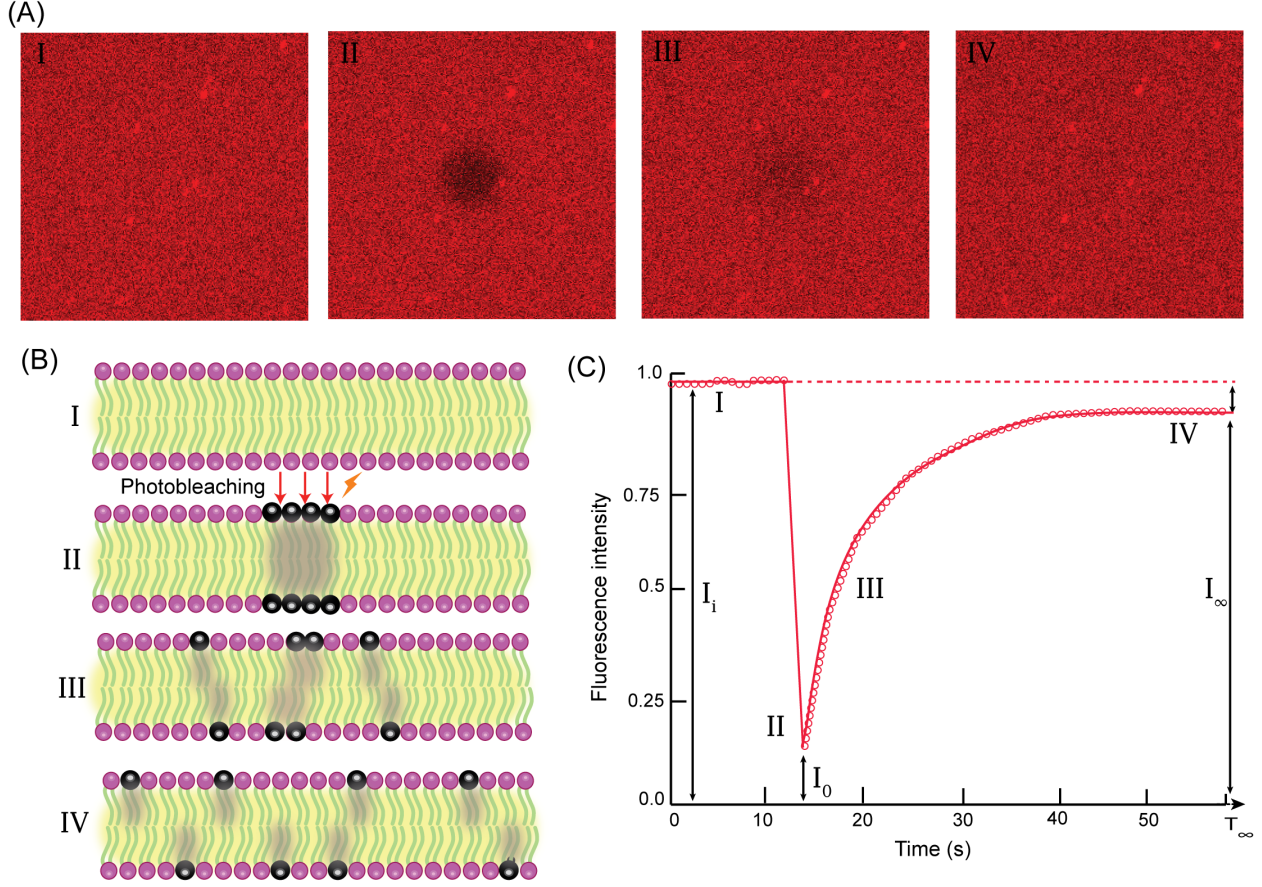


Figure 5.3: (A) Fluorescence images of a single component SLB before photobleaching (I), immediately after photobleaching (II), few seconds after photobleaching (III) and after fluorescence recovery (IV), (B) A schematic representation of lipid molecules in a bilayer diffusing during FRAP experiments, (C) A typical FRAP trace.

While the concept and instrumentation for FRAP is relatively simple, the theoretical calculations and mathematical models to analyze FRAP data are complicated. Commonly, the mathematical fitting of the FRAP intensity trace is performed assuming Brownian diffusion model developed by Soumpasis[174]:

$$f(t) = e^{-\frac{2\tau_D}{t}} \left[ J_0 \left( \frac{2\tau_D}{t} \right) + J_1 \left( \frac{2\tau_D}{t} \right) \right] \quad (5.6)$$

where,

$J_0$  = Bessel function of 0<sup>th</sup> order,

$J_1$  = Bessel function of 1<sup>st</sup> order, and

$$\tau_D = \frac{\omega^2}{4D} \quad (5.7)$$

where  $\tau_D$  is the diffusion time and  $\omega$  is the radius of the circular bleached spot. The above fitting formula is modified to  $F(t) = A + Bf(t)$ , to consider the immobile fraction and



the incomplete bleaching of the bleached area, where  $A$  is the amplitude of the recovery function ( $I_{\infty}-I_0$  in Figure 5.3C) and  $B$  is the fluorescence intensity remaining right after the bleaching event ( $I_0$  in Figure 5.3C).

To get a reliable output from the fitting of the FRAP image series, certain image acquisition conditions are highly required to be maintained, such as:

- The frame acquisition time and frame interval have to be as short as possible, at least before the half recovery period to get as many as data points so that the fitting procedure is reliable. This is especially crucial for fast diffusion processes.
- Fast imaging should be prioritized with image resolution. Hence averaging should be avoided and small area imaging is recommended.
- At least 3-10 pre-bleaching images should be obtained to get reliable pre-bleaching intensity.
- The bleaching should be as instantaneous – as quick as possible to avoid bleached molecules to go out or non-bleached molecules to come in the bleached spot during bleaching timeframe.
- The laser power should be kept as low as possible to avoid overall bleaching during image acquisition.
- The FRAP series should be long enough for the FRAP trace to reach a plateau at its highest fluorescence intensity after recovery.
- The fitting model depends on the shape of the bleached spot, hence the shape of the bleached spot should be chosen accordingly.

In spite of using low laser power, overall photobleaching during imaging of FRAP series often influences the intensity trace, especially for slow moving particles. To get rid of this issue, photobleaching correction is performed on the raw FRAP trace by dividing it with the reference intensity trace integrated from all other part of the image frame except the photobleached area, over the entire measurement time. FRAP has been widely used not only for diffusion studies, but also to understand binding and aggregation of molecules[175, 176]. Moreover, with complex FRAP analysis two component lateral diffusion and anomalous sub-diffusion have also been identified[144, 177, 178]. FRAP experiments can give information about the mobility for relatively slow diffusing molecules in comparison to other fluorescence based diffusion analysis techniques, down to  $0.05\text{-}0.1\text{ }\mu\text{m}^2/\text{s}$  though for such a slow dynamics the analysis becomes challenging[179]. Diffusion models in FRAP experiments are based on two-dimensional diffusion approximation. Hence, FRAP is not a suitable technique for measuring diffusion in three dimensional volume. Moreover, the high laser power used for photobleaching may cause phototoxicity in live cells. In spite of these limitations, due to its simple instrumental requirements FRAP is one of the most commonly used techniques for studying lipid/protein dynamics in live cells and model membrane systems. SLB being a two dimensional system, FRAP is perfectly suited for diffusion studies therein. In my doctoral research most of the lipid diffusion measurements were performed using FRAP.

Another technique, that closely resembles FRAP conceptually is fluorescence loss in photobleaching (FLIP). This technique provides qualitative diffusion information revealing about diffusional compartmentalization in live cells[180]. In this technique, one part of the

cell is photobleached iteratively, and the fluorescence intensity drop in other locations is monitored to understand if there is a diffusional exchange of the molecule of interest in between these regions.

### 5.3 Fluorescence correlation spectroscopy (FCS)

Fluorescence correlation spectroscopy (FCS) is a highly efficient and versatile tool to provide information on molecular dynamics in both two dimensional and three dimensional systems. It is being routinely employed to tackle a diverse spectrum of research questions - determining diffusion coefficients, concentration, chemical rate constants, binding, aggregation and molecular brightness[181, 182]. FCS technique was invented in the 1970s, when two groups in Cornell University (USA) and Karolinska Institutet (Sweden) separately developed fluorescence fluctuation approach to study chemical kinetics of untwisting of DNA and rotational diffusion of fluorescent molecules in viscous solvents, respectively[182, 183, 184].

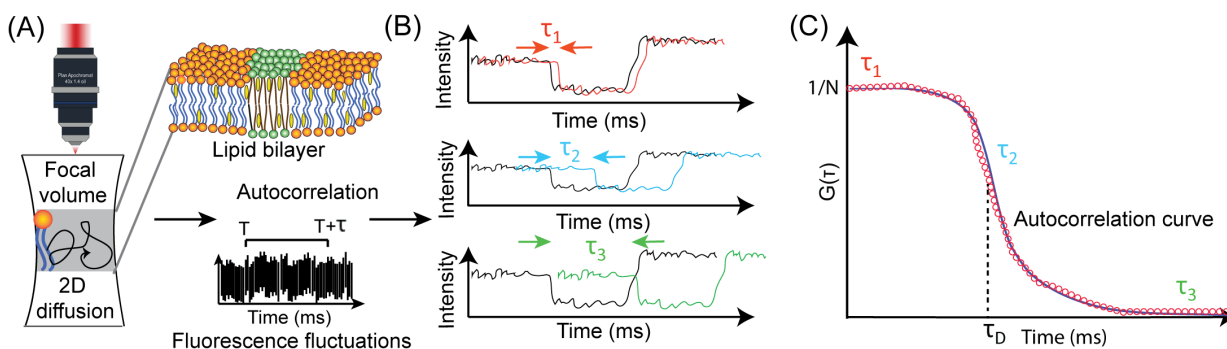


Figure 5.4: Schematic diagram of the fluorescence correlation spectroscopy. (A) Recording fluorescence fluctuations over time by monitoring fluorescence intensity at the focal volume in a lipid bilayer sample. (B) Concept of the autocorrelation of fluorescence intensity over time depicting high correlation at a smaller time gap ( $\tau_1$ ) and medium and no correlation at medium ( $\tau_2$ ) and large ( $\tau_3$ ) time gap, respectively. (C) A typical FCS curve.

The basic concept of FCS is based on the autocorrelation of the fluorescence fluctuations over time to obtain kinetic as well as thermodynamic properties of the fluorescent molecules in either equilibrium or nonequilibrium steady state (Figure 5.4). If a sub-volume of the steady state system is monitored, the diffusing fluorescent particles diffuse in and out of the monitored volume, or in case of a reaction, the concentration of the reactants/intermediates/products fluctuates around their equilibrium values. In either case, though the overall concentration of the molecules is constant over large, theoretically infinite, time scale, the local fluctuation of concentration occurs due to the Brownian motion of the diffusing particles and the reaction being a Poisson process (constant probability of happening in space and time)[182]. But these fluctuations in concentration, reflected in fluctuations of fluorescence intensity, being stochastic in nature, can not provide information on diffusion coefficient by itself. But, according to the Onsager regression hypothesis, the rate of dissipation of these fluctuations is the same as the macroscopic dynamic processes[182, 185]. Thus, it is possible to apply the concept of a statistical analysis of the fluctuations data by calculating its autocorrelation over the evolved time, as penned down by Elliot Elson, one of the pioneers of FCS[182]. The output autocorrelation curves

(FCS curves) provide a measure of the self-similarity of the fluorescence trace with time lags, over the entire measurement time. At small time lags ( $\tau_1$ ), the fluorescence signal is very similar to itself and as the time lag increases ( $\tau_2$  and  $\tau_3$ ), the similarity between the fluorescence signal and the lagged version of itself decreases (Figure 5.4B). The general equation for the fluctuation autocorrelation function ( $G(\tau)$ ) is:

$$G(\tau) = \frac{\langle \delta F(t) \cdot \delta F(t + \tau) \rangle}{\langle F(t) \rangle^2} = \frac{\langle \delta F(0) \cdot \delta F(\tau) \rangle}{\langle F(t) \rangle^2} \quad (5.8)$$

where,  $\delta F(t)$  is the fluctuation of fluorescence intensity ( $F(t)$ ) from the average fluorescence intensity value  $\langle F(t) \rangle$ , given by  $\delta F(t) = F(t) - \langle F(t) \rangle$ . The symbol  $\langle \dots \rangle$  denotes averaging over an infinitesimally long period of time (temporal average) and  $\tau$  is the lag time. In the 2<sup>nd</sup> equality, the stationary system is alternatively described as the average over many, randomly selected lag times  $\tau$  (ensemble average). The denominator is used for the normalization purpose in both cases.

During the FCS measurement, a small sub-volume of the sample is illuminated by a laser beam, and the fluorescence intensity from this particular spot is recorded over time and then the trace is autocorrelated using the above correlation function, generating an experimental FCS curve. The obtained FCS curve is then fitted with appropriate physical models, which provide information regarding various basic physical parameters of the system, such as diffusion coefficient, concentration or molecular brightness. The time dependence of  $G(\tau)$  reveals the dynamic characteristics of the system. On the other hand, the correlation function at  $\tau = 0$ ,  $G(0)$  is a thermodynamic property and it provides information on the concentration and molecular brightness of the diffusing particles. At such condition,

$$G(0) = \frac{\langle (\delta F)^2 \rangle}{\langle F \rangle^2} \quad (5.9)$$

where  $\langle (\delta F)^2 \rangle$  and  $\langle F \rangle^2$  can be replaced by  $\langle (\delta N)^2 \rangle$  and  $\langle N \rangle^2$  as fluorescence intensity is directly proportional to the no. of fluorescent particles ( $N$ ), when the intensity is normalized. According to Poisson statistics for random processes, the variance of  $N$ ,  $\langle (\delta N)^2 \rangle = \langle N \rangle$ . Thus,

$$G(0) = \frac{\langle (\delta F)^2 \rangle}{\langle F \rangle^2} = \frac{\langle N \rangle}{\langle N \rangle^2} = \frac{1}{\langle N \rangle} \quad (5.10)$$

implying that the amplitude of the FCS curve is numerically reciprocal of the average concentration of diffusing fluorescent particles in the system. Similarly, molecular brightness,  $\eta = \frac{F(t)}{\langle N \rangle}$  can also be obtained as  $G(0) \cdot F(t)$ .

Experimentally, FCS requires a delicate experimental set-up with a very sensitive, photon-counting detector. A mandatory calibration of the confocal volume, by measuring the diffusion time of a standard dye in aqueous solution is performed prior to a specific experiment. Moreover, by precisely adjusting the correction collar of the objective, correction for the difference in the refractive indices of the sample, coverslip and imaging medium is done. Additionally, the pinhole is minutely adjusted to achieve the highest photon counts from the focal plane. Furthermore, the following experimental measures should be taken to obtain reliable FCS curves:

- The fluorescent dye concentration should be chosen delicately, typically within the range of  $>100$  pM to  $<1$   $\mu$ M. When the dye concentration is too high, the relative fluctuations are very low resulting in low FCS curve amplitude. On the other hand, in case of too low concentration, the noise starts to dominate over fluorescence fluctuations.

- The laser power should be chosen carefully to reduce photobleaching of the dye, but also to maintain sufficient fluorescence signals.
- For 2D samples, such as lipid bilayers, it is very important to keep the sample in the focal plane of the objective lens for attaining maximum fluorescence intensity.
- The measuring time has to be sufficiently long for correlation, but too long illumination may cause photobleaching.
- Highly photostable fluorescent dyes are required for FCS measurements.

Photobleaching of the fluorophore is a serious problem in FCS measurements. Moreover, FCS fails to provide reliable results for slowly moving particles ( $<1 \mu\text{m}^2/\text{s}$ ). In spite of these limitations FCS has been proven to be a very useful technique for diffusion analysis due to its sensitivity both in single molecules as well as ensemble averaged measurements. FCS is also capable of providing distinct information about rotational and translational dynamics as well as triplet state transitions of the particle of interest. Free diffusion and anomalous diffusion can also be well-distinguished by this method[186, 187, 188].

Different variations of the conventional FCS are available that stretch the boundary of tremendous capabilities of FCS, such as scanning FCS (s-FCS), fluorescence cross correlation spectroscopy (FCCS), FCS combined with stimulated emission depletion microscopy (STED-FCS) or spot variation FCS. S-FCS is performed by collecting fluorescence fluctuation data from a selected line on the sample systematically, many times and generating a correlation carpet containing FCS curves for each pixel of the line. This technique has been used to distinguish free diffusion from hindered diffusion[189]. FCCS is performed by generating cross-correlation between fluorescence fluctuations from two different dyes, and thus it can detect the interactions between two distinct diffusing particles labeled with different dyes, for example, protein-protein or protein-lipid interactions[190]. STED-FCS is a super-resolution microscopy technique coupled with FCS, where the focal spot size can be controlled, and diffusion can be measured at varying volumes of the sample, revealing the diffusion mechanism by analysing the dependence of the D value on the observation spot size (or volume)[154].

## 5.4 Single particle tracking (SPT)

Although FRAP and FCS are the most common fluorescence-based techniques to probe lateral diffusion of lipids, the lateral resolution in both of these methods (with an exception of FCS combined with super-resolution techniques, e.g. STED-FCS) is limited by the diffraction barrier of the confocal microscopy and an average of many molecular diffusion events is used to acquire the diffusion information. These two limitations can be overcome by single particle tracking (SPT), where the movement of a single, isolated, diffusing particle is tracked over time. The particle/molecule of interest is typically tagged with a fluorescent bead, gold nanoparticle or a quantum dot and its motion is recorded over time as a trajectory, analyzed by calculating the MSD, and finally fitted with a suitable theoretical model[179]. Various studies of lipid diffusion using SPT technique have proved that lipid diffusion should not be considered as free diffusion in plasma membranes – the interactions with the cytoskeleton often makes its movement restricted[152, 155]. Moreover, studies using SPT revealed that lipids and transmembrane proteins undergo hop diffusion and/or confined diffusion in cellular membranes[158].

## 5.5 Comparison of FRAP, FCS and SPT

All the above-discussed techniques are broadly used to study lipid diffusion in both model membranes and biological membrane systems, though all of them have some advantages and disadvantages.

In terms of optimal dye concentration, FRAP, FCS and SPT fall in different regimes. For FRAP higher concentration (0.1 – 0.5  $\mu\text{M}$ ) of the fluorophore compared to FCS is required – around 100 fluorophores in 1  $\mu\text{m}^2$  is optimal for FRAP measurements[179]. The quality of FRAP traces i.e. signal to noise ratio increases with dye concentration. In contrast, for FCS optimal dye concentration is commonly within 1-100 nM range and increase in concentration deteriorates the FCS curves by lowering the initial amplitude of the autocorrelation trace. For SPT single molecule level concentration is used (typical concentrations on the order of  $10^{-10}$  M).

These techniques also differ in temporal resolution scale. FCS has higher temporal resolution than FRAP allowing it to probe very fast dynamics, but it is not the most appropriate technique for slow diffusion ( $<1 \mu\text{m}^2/\text{s}$ ) as photobleaching hampers the quality of the FCS curves in this case. On the other hand FRAP is a better approach for measuring diffusion of slower particles. SPT can measure both slow and fast diffusing particles but attaching a relatively big probe to the diffusing molecule can interfere with the native diffusion time of the particle of interest.

The applicability of these fluorescence techniques varies for different sample systems. FRAP is suitable for two-dimensional samples, such as supported lipid bilayers, while FCS and SPT can be used to study both two-dimensional and three-dimensional systems.

In addition to the diffusion coefficient values, these techniques are complementary in obtaining various other supplementary information about the system under study. For example, FRAP can provide information on the mobile and immobile fraction of the molecules. From FCS and SPT measurements this information can not be obtained. In contrast, FCS and SPT can clearly point out the potential presence and nature of anomalous diffusion, which FRAP method can not detect precisely.

Thus overall all these three fluorescence techniques for measuring lipid diffusion are complementary to each other and should be chosen carefully according to the specificity of the system and the posed research question.



# Chapter 6

## Fluorescent probes: seeing the invisible

The development of fluorescence imaging and diffusion-sensitive techniques is not only based on the technical development of the microscopy setups, but also on the development of proper fluorescent dyes to probe specific molecules/organelles in cellular systems. The advantages of sophisticated fluorescence imaging methods would go in vain without the availability of suitable fluorescent labels selectively going to the desired organelles or binding to membrane components. After the discovery of the green fluorescent protein (GFP) in 1962 by Osamu Shimomura, it took three decades more to realize the huge potential of fluorescent dyes in biological research until Martin Chalfie demonstrated that GFP can be functionally encoded in the gene of the eukaryotic and prokaryotic cells [191, 192]. Since then GFP and its variants have been widely used to visualize the native localization of various proteins in the biological systems. But it could not be of much help elucidating lipid diffusion due to its comparatively large size, which influences the lipid dynamics itself. Hence, various synthetic, organic fluorescent dyes chemically conjugated with lipids are used to probe the diffusion of lipids in model membrane systems as well as in cell membranes. Moreover in the last decade direct and selective labeling of specific lipids *in vivo* was reported and used to image lipid membranes and visualise transport in the cells using click chemistry[193, 194, 195]. In this chapter I briefly discuss the various fluorescent probes commonly used to understand the structural organization and the lateral diffusion of lipids in cellular membranes. The membrane binding fluorescent probes can be classified into two major categories: phase specific probes and environment sensitive probes.

### 6.1 Phase-specific probes

Phase specific fluorescent probes are most commonly lipid analogs covalently linked to a synthetic, organic dye. Depending on the hydrophobic tail saturation (which determines lipid packing) of the lipid analog, and the structure of the dye, it may specifically partition into different lipid phases, for example, the  $L_o$  or  $L_d$  phase. A number of systematic studies investigating the correlation of phase specific binding of lipid probes with their chemical structures have concluded that majority of these probes preferentially partition to the  $L_d$  phase, with only a very few exceptions[196, 197, 198, 199]. Saturated lipids in  $L_o$  or gel phase, because of their tight packing, generally prohibit insertion of saturated lipids attached to big organic dye molecules. For example, NBD-DOPE preferentially partitions to  $L_d$  phase since the lipid analog (DOPE) has two unsaturated hydrophobic chains, which fit well within the fluid  $L_d$  phase[197]. But, NBD-DPPE, in spite of having saturated tails, was reported to still preferentially partition into the  $L_d$  phase in GUVs due to highly ordered structure and tight packing of the  $L_o$  phase[197]. Similarly, both Rh-DOPE and Rh-DPPE prefer to bind into the  $L_d$  phase[197]. Both headgroup and acyl chain labeled SM (saturated lipid) analogs were shown to partition more into the  $L_d$  phase in GUVs[199]. To overcome the problem of specific labeling of the  $L_o$  phase, dyes are often connected with the saturated lipid analog via a hydrophilic spacer polymer chain polyethylene glycol

(PEG), which keeps the organic dye molecule protruding out of the highly packed  $L_o$  phase without perturbing the tail packing when the lipid analog embeds into the  $L_o$  phase. Thus, DSPE-KK114 partitions more into the  $L_d$  phase, whereas DSPE-PEG-KK114 binds more specifically to the  $L_d$  phase in model membrane systems[186].

Apart from phospholipid and sphingolipid labeling, various dyes are also attached to cholesterol to visualize the lipids *in vitro* and *in vivo*[197]. It is generally accepted that cholesterol preferentially partitions into the  $L_o$  phase. But it should be noted that partitioning of the fluorescently labeled cholesterol is highly dependent on the attached fluorophore – TopFluor-cholesterol binds more to the  $L_o$  phase[199], whereas NBD-cholesterol prefers to partition into the  $L_d$  phase[197]. More polar character of NBD compared to BODIPY (TopFluor) inhibits the natural cholesterol insertion into the  $L_o$  phase.

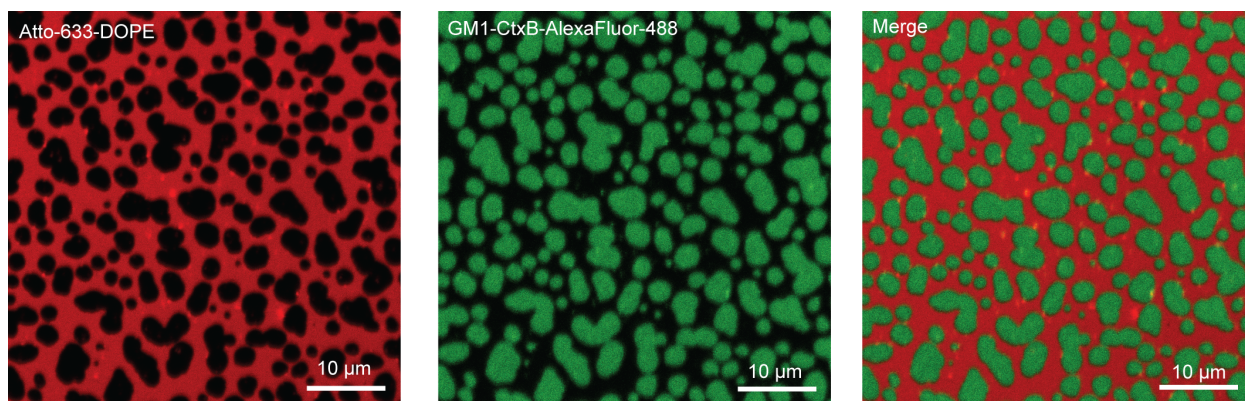


Figure 6.1: Fluorescence image of an exemplary SLB showing Atto-633-DOPE partitioning into the  $L_d$  phase and GM1-CTxB-AlexaFluor-488 dye into the  $L_o$  phase.

Apart from lipid analogs, fluorescently labeled, specific proteins that attach selectively to a particular lipid component present in the membrane are also used to label particular membrane phases. One common example is fluorescently labeled Cholera Toxin subunit B (CTxB), that selectively binds to monosialotetrahexosylganglioside (GM1 ganglioside) pentamer and altogether partitions into the  $L_o$  phase in the membrane[200]. Another common approach is to use the specific binding ability of antibodies for selective labeling of specific membrane components. Fluorescent antibodies that bind specifically to cholesterol are used to localize cholesterol rich regions in membranes [196].

The biggest advantage of such synthetic fluorescent lipid analogues is that they leave us with a large variety of organic dyes that can be conjugated to various lipids. The fluorescence properties of these dyes generally result from the extended conjugation in the aromatic ring structure. By modifying the conjugating functional groups of these dyes, it is possible to adjust their photophysical properties, most notably their excitation and emission wavelengths, for example Atto dyes are produced with different excitation and emission wavelengths resulting from suitable chemical modifications, such as Atto-390, Atto-465, Atto-488, Atto-495, Atto-633, Abberior STAR Red, Abberior STAR green. Moreover, structural modification also helps in achieving beneficial optical properties such as high quantum yield or improved photostability for these dyes. The dyes can be attached either to the head group of the lipids or to their acyl chains. Mostly polar dyes are linked to the lipid head groups and nonpolar hydrophobic dyes are conjugated to the acyl chains, with some exceptions – for instance, non-polar dye NBD is often attached to the ethanolamine (PE) or serine (PS) phospholipid headgroups. For their wide versatility and



phase-specificity the discussed dyes are inevitable for imaging of lipid membranes.

## 6.2 Environment-sensitive probes

The second category of fluorescent labels used to study lipid membranes are phase sensitive or environment sensitive probes that undergo a change in their fluorescence properties, such as intensity and/or emission spectrum in response to a change in their microscopic environment. Unlike phase-specific dyes, these “smart dyes” can efficiently penetrate into both  $L_o$  and  $L_d$  phase of lipid membrane, and are capable of reporting on the physical properties of the membrane, such as fluidity, viscosity, hydration and order by sensing their molecular environment[201, 202]. The main molecular mechanism of such sensing ability results from various excited-state phenomena, such as conformational change, charge transfer, proton transfer or non-covalent interactions with the surroundings, for example, H-bonding, dipole-dipole or van der Waals interactions[202]. The most common solvatochromic environment-sensitive dyes show red shift of their single emission band in more polar environment resulting from the enhanced dipolar relaxation in the excited state[12]. Upon electronic excitation, due to excited state intra-molecular charge transfer the dipole moment increases, resulting in an enhanced dipolar relaxation of surrounding molecules[12, 202]. The enhanced dipolar reorientation consumes energy from the excited state of the dye, causing red shift of the emission spectrum. Laurdan, prodan, Nile red are a few examples of environment sensitive dyes that fall into this category. As their spectral maxima shift with the change of solvent’s polarity, they are also called solvatochromic probes. The most common environment-sensitive probe Laurdan was first synthesized by Gregorio Weber in 1979 to study dipolar relaxation and later Tiziana Parasassi employed it for distinguishing the different membrane phases[203, 204, 205]. Laurdan and its derivatives (C-Laurdan, Prodan, and other analogs) partition into both  $L_o$  and  $L_d$  phases but their emission spectra become more red-shifted in the  $L_d$  phase compared to the  $L_o$  phase as some energy is consumed for the reorientation of the polar moieties and their hydration structure in more polar and fluid  $L_d$  phase. The emission maximum of Laurdan in the  $L_d$  phase is centered around 460 nm, whereas for the  $L_o$  phase it is centered at around 430 nm (Figure 6.2)[12]. To mathematically express the extent of the emission peak shift in  $L_o$  and  $L_d$  phase, an indicative parameter called generalized polarization (GP) is calculated as:

$$GP = \frac{(I_{Lo} - I_{Ld})}{(I_{Lo} + I_{Ld})} \quad (6.1)$$

where  $I_{Lo}$  and  $I_{Ld}$  denote the fluorescence intensities at two specific wavelengths or wavelength ranges close to the peaks in  $L_o$  (typically 430 nm) and  $L_d$  (typically 460 nm) phase, respectively.

Another common environment sensitive dye is di-4-ANEPPDHQ, which can sense electrical properties of the membrane such as membrane potential. In this case the dielectric constant of the solvent determines the shift of the fluorescence spectrum, which results from the complex relaxation kinetics involving multiple processes[201]. Di-4-ANEPPDHQ can also detect changes in cholesterol concentration better than Laurdan, which means it can indicate fluidity properties of the membrane more accurately[134, 201]. Moreover, recent study demonstrated new environment-sensitive fluorophores to successfully sense various other biophysically relevant parameters of the local lipid environment, such as degree of lipid saturation, double bond position and configuration (cis vs. trans), phospholipid head-group and cholesterol content in a precise manner, depending on the depth of insertion of

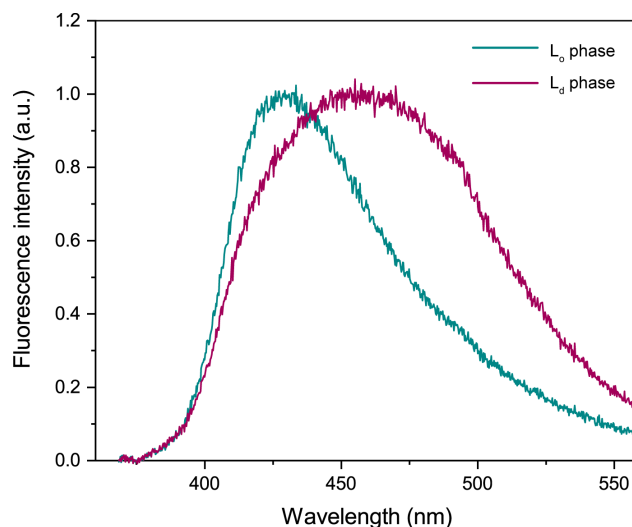


Figure 6.2: Laurdan fluorescence emission spectra acquired from the  $L_d$  phase and from the  $L_o$  phase (data acquisition: Hanna Orlikowska-Rzeźnik).

these dyes into the membrane[206]. Thus overall the environment sensitive probes form an extremely powerful tool for the biophysical mapping of the membrane properties.

The fluorescent membrane probes are an inseparable part of modern fluorescence microscopy of both biological and biomimetic membrane systems. Still an intensive development of fluorescent probes in terms of their stability and/or quantum yield continues. With the recent presentation of the MINFLUX and MINSTED nanoscopy techniques, the maximum optical resolution of the fluorophores has been reached (1-3 nm)[207, 208, 209, 210]. As Stefan Hell, the 2014 Nobel laureate in chemistry claims, the development in fluorescence microscopy now lies only in designing more sophisticated fluorophores for the visualization of cellular systems[211].

## Part II: The effect of membrane hydration on lipid diffusion and inter-lipid interactions



# Chapter 7

## Hydration layer of few water molecules control lipid mobility in biomimetic cell membranes

The main goal of my doctoral research was to understand the effect of the hydration layer in the vicinity of lipid headgroups on the lateral diffusion of lipids and their molecular interactions. To investigate the role of the interfacial water on lipid dynamics, gradual perturbation of the water layer is required, while keeping the membrane structure intact. In publication 1, I proposed a novel method of preservation of SLBs at lower hydration conditions without any external, chemical or physical modifications. In

order to prepare membranes with a well-controlled hydration state, I designed and constructed a humidity control setup that allows for the preparation of nitrogen gas of desired relative humidity (from completely dry  $N_2$  gas with 0% RH to  $N_2$  with >90% RH) and precise control of its flow over a biomimetic cell membrane. Upon removal of bulk water, in which the membrane is submerged, I could immediately purge  $N_2$  gas with the desired RH over the sample and gradually vary it (2-3% RH per minute) to successfully prepare stable, desiccation-tolerant, phase-separated biomimetic cell membranes. This approach readily allowed me to investigate the structural and dynamical properties of lipid membranes in different hydration states. Using fluorescence recovery after photobleaching (FRAP) technique, I addressed hydration-dependent diffusivity of membrane components embedded in phase-separated, supported lipid bilayers. I determined the diffusion coefficient ( $D$ ) of membrane constituents at different hydration conditions and found that  $D$  decreases sharply in the range of 90-50% RH. At RH below 50% the mobility remains almost constant at a very low level. Intriguingly, upon rehydration  $D$  follows the same trend and nearly regains its initial value. At full hydration, around 10-12 water molecules are present in the first hydration shell of PC lipids, among which around 6 water molecules form hydrogen bonds with phosphate and carbonyl oxygen. The choline group is not involved in the formation of hydrogen bonds. Instead, a clathrate cage structure containing 6.4 water molecules surrounds the phosphocholine moiety. I established that the sharp decrease of  $D$  is related to the breaking of the clathrate cage structure around the phosphocholine moi-

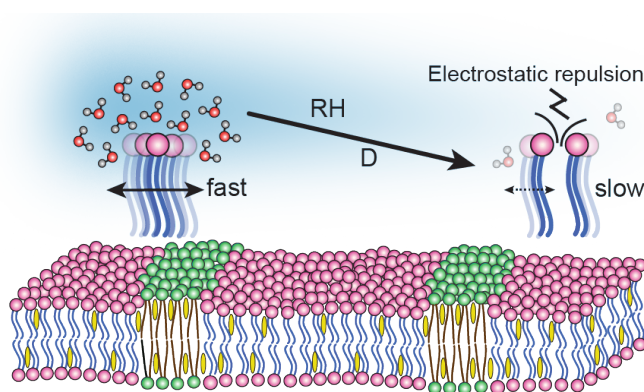


Figure 7.1: A schematic diagram summarizing the main findings of Publication 1.

ety. At lower membrane hydration levels only those water molecules are left, which form very strong hydrogen bonds with the lipids phosphate and carbonyl moieties. These water molecules clearly are not involved in modulating the lateral diffusion of lipids. To unravel the details of the physical mechanism of the hydration-dependence of lateral mobility of lipids, I performed temperature variation experiments. These experiments allowed me to determine the activation energy of diffusion ( $E_a$ ), which revealed that ( $E_a$ ) for dehydrated membranes is approximately two times higher than that of fully hydrated membranes. This can be explained by considering the fact that water molecules in the first hydration shell around the lipid headgroup screen the electrostatic repulsion between the adjacent lipid head groups. Consequently, in the absence of these shielding water molecules, the repulsive interactions between lipids become more prominent, which in turn increases the activation energy of diffusion. The details of this work can be found in the research article, and the associated supplementary information, published in the prestigious Journal of the American Chemical Society (JACS) and attached below. I am the first and corresponding author in this publication (publication 1). The significance of this work has been further corroborated by the fact that our illustration was chosen to decorate the front cover of the JACS issue.

## Hydration Layer of Only a Few Molecules Controls Lipid Mobility in Biomimetic Membranes

Madhurima Chattopadhyay,\* Emilia Krok, Hanna Orlowska, Petra Schwill, Henri G. Franquelim, and Lukasz Piatkowski\*

Cite This: *J. Am. Chem. Soc.* 2021, 143, 14551–14562

Read Online

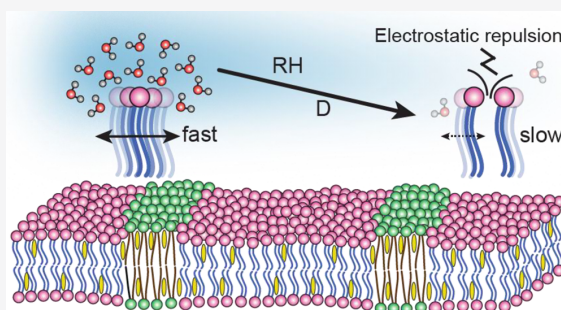
ACCESS |

Metrics &amp; More

Article Recommendations

Supporting Information

**ABSTRACT:** Self-assembly of biomembranes results from the intricate interactions between water and the lipids' hydrophilic head groups. Therefore, the lipid–water interplay strongly contributes to modulating membrane architecture, lipid diffusion, and chemical activity. Here, we introduce a new method of obtaining dehydrated, phase-separated, supported lipid bilayers (SLBs) solely by controlling the decrease of their environment's relative humidity. This facilitates the study of the structure and dynamics of SLBs over a wide range of hydration states. We show that the lipid domain structure of phase-separated SLBs is largely insensitive to the presence of the hydration layer. In stark contrast, lipid mobility is drastically affected by dehydration, showing a 6-fold decrease in lateral diffusion. At the same time, the diffusion activation energy increases approximately 2-fold for the dehydrated membrane. The obtained results, correlated with the hydration structure of a lipid molecule, revealed that about six to seven water molecules directly hydrating the phosphocholine moiety play a pivotal role in modulating lipid diffusion. These findings could provide deeper insights into the fundamental reactions where local dehydration occurs, for instance during cell–cell fusion, and help us better understand the survivability of anhydrobiotic organisms. Finally, the strong dependence of lipid mobility on the number of hydrating water molecules opens up an application potential for SLBs as very precise, nanoscale hydration sensors.



## INTRODUCTION

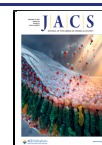
Biological cell membranes are dynamic barriers composed of a large variety of lipids and embedded with various proteins. Due to the complex miscellaneous molecular interactions occurring in cellular membranes, lipid model systems are particularly attractive alternatives for the controlled investigation of various physicochemical processes affecting the membrane architecture and dynamical properties. In this regard, self-assembling supported lipid bilayers (SLBs) have been well accepted as one of the most suitable model membrane systems, due to their analogous physical and structural properties to those of biomembranes and their easy preparation and handling methods.<sup>1</sup> Consequently, SLBs have been exploited to investigate membrane architecture and properties such as domain formation,<sup>2,3</sup> lateral diffusion or ion transport,<sup>4,5</sup> and biological processes at the cellular and molecular levels, such as protein–membrane interactions,<sup>6</sup> ligand–receptor interactions, cellular signaling,<sup>7,8</sup> or cell adhesion.<sup>9,10</sup>

Various types of chemical and physical interactions determine the complex properties, architecture, and activity of the membrane. Membrane intricacy results not only from the interactions between membrane constituents, such as lipid–lipid and lipid–protein interactions, but also from the

hydrophobic mismatch that arises from the interplay with water hydrating the membrane. In fact, hydrophobic mismatch is considered to be one of the key physicochemical mechanisms that regulate membrane organization and promotes nanoscopic and microscopic separation of liquid ordered ( $L_o$ ) and liquid disordered ( $L_d$ ) phases. It also determines the position and orientation of transmembrane proteins in both model and living cell membranes.<sup>6</sup> The thin layer of water that directly hydrates the membrane, commonly referred to as biological water,<sup>11,12</sup> has been proven to actively participate in the biological functioning of DNA.<sup>13</sup> Moreover, biological water is inherently connected with the process of protein folding,<sup>14</sup> aggregation,<sup>15,16</sup> and stabilization of the structure even in extreme thermodynamic conditions.<sup>17</sup> Numerous experiments aimed at understanding the properties of biological water, using nuclear magnetic resonance,<sup>18</sup> X-ray

Received: April 28, 2021

Published: August 3, 2021



and neutron scattering,<sup>19,20</sup> infrared spectroscopy,<sup>21</sup> sum frequency generation,<sup>22,23</sup> and molecular dynamics simulations,<sup>24–27</sup> among others, showed that water molecules form a network structure, being bound by hydrogen bonds and weak van der Waals interactions around the polar head group, the so-called clathrate hydration structure.<sup>24</sup> Moreover, water molecules present in the direct or indirect hydration shell around the head group region exhibit markedly different properties from those of bulk water.<sup>28–30</sup>

Water is unambiguously essential for maintaining biological activities in living systems. But, in fact, nature shows various phenomena of anhydrobiosis (“life without water”) in which the cell membrane not only survives harsh dehydration but also regains full activity upon rehydration. The most common method allowing dehydration is an increased production of carbohydrates (mostly trehalose) in organisms such as tardigrades,<sup>31–34</sup> nematodes,<sup>35</sup> and yeasts.<sup>36,37</sup> The water-replacement hypothesis states that trehalose stabilizes the head groups and enables maintaining the spacing between the fatty acyl chains.<sup>38</sup> On the other hand, *Bdelloid rotifers* base their survival mechanism on the contraction of the body, which reduces the surface exposed to the environment and allows slow evaporation.<sup>39,40</sup> High desiccation resistance in seeds, pollens, and anhydrobiotic plants is associated with the production of LEA (late embryogenesis abundant) proteins that are responsible for ion sequestration, protection of membranes, and renaturation of proteins that unfolded due to the lack of water.<sup>41</sup>

Importantly, it should be noted that local, temporary dehydration of the cell membranes also occurs continuously in our bodies during, for example, adsorption of biomacromolecules or cell–cell fusion events. A prerequisite for membrane fusion is establishing close contact between the outer leaflets of lipid bilayers such that the thin layer of water molecules is expelled (the clathrate hydration structure is disturbed) and finally overcoming the energy barrier, commonly referred to as “hydration force”, present mainly due to the repulsive forces between lipid bilayers.<sup>42,43</sup>

Last but not least, various studies of the electrical, mechanical, and physicochemical properties of planar lipid bilayers have revealed that these platforms have huge application potential from a technological standpoint as biosensors and biocoatings.<sup>44,45</sup> These bioapplications require SLBs to be exposed to changes of external conditions such as temperature during preservation, reagent addition, and, importantly, humidity.

Hence, understanding the interplay between the hydration layers and the cell membrane is of utmost importance, both in unraveling mechanisms behind membrane organization and activity and in the frameworks of biotechnology and bioengineering. Unfortunately, the ability to investigate the intimate interactions between the membrane and the biological water has so far been hindered by the lack of appropriate experimental approaches for the preparation and study of lipid membranes in a controlled hydration state. In particular, keeping the membrane structure intact under decreased hydration conditions is challenging.<sup>24,26</sup> So far, several approaches to protect the membrane from rupturing and vesiculation have been utilized: modification of lipid head groups in order to strengthen the SLB–mica attractive interactions,<sup>46–49</sup> cross-linking the lipid bilayer,<sup>50,51</sup> attaching polymers to the head group of lipids,<sup>46,52</sup> and adding biomolecules such as proteins, disaccharides, or en-

zymes.<sup>45,51,53–55</sup> These approaches, however, inevitably alter the intrinsic properties of the SLBs. Moreover, the exact hydration state of the membrane is unknown. Consequently, a method for preparing and stabilizing the membrane under varying, well-controlled hydration conditions without the use of additional stabilizing agents or chemical modification is needed.

Here, we present an unprecedented way to obtain phase-separated, stable SLBs with a well-controlled hydration state without interfering with membrane composition, which enables the investigation of bilayer structure and dynamics under arbitrary hydration conditions. Using a combination of fluorescence microscopy imaging and fluorescence recovery after photobleaching (FRAP) experiments, we report interesting observations of the structural and dynamical changes taking place. We show that the structure of SLBs can be preserved under dry conditions by a controlled drying process with a slow and sequential reduction in relative humidity of the membrane environment. Such an approach revealed that the lateral diffusion dynamics of the liquid disordered phase is significantly reduced with dehydration. Importantly, the membrane can undergo multiple de- and rehydration cycles always reviving its native dynamics. We also show that the diffusion activation energy for lipids in a dehydrated membrane is much higher than for fully hydrated SLBs. Finally, we provide molecular-level insights into how and which water molecules around lipids play a key role in regulating lipid dynamics in the membrane.

## EXPERIMENTAL SECTION

**Materials.** 1,2-Dimyristoleoyl-*sn*-glycero-3-phosphocholine (14:1 PC), egg yolk sphingomyelin (SM), 23-(dipyrrometheneboron difluoride)-24-norcholesterol (TopFluor cholesterol), and cholesterol were purchased from Avanti Polar Lipids, Alabaster, AL, USA. Monosialoganglioside (GM1) from bovine brain and 1,2-dioleoyl-*sn*-glycero-3-phosphoethanolamine labeled with Atto 633 (DOPE-Atto 633), 4-(2-hydroxyethyl)piperazine-1-ethanesulfonic acid (HEPES) sodium salt, sodium chloride (NaCl), 1,2-dioleoyl-*sn*-glycero-3-phosphoethanolamine-*N*-(7-nitro-2-(1,3-benzoxadiazol-4-yl)-ammonium salt (18:1 NBD PE), sodium dithionite, and chloroform (HPLC grade) were purchased from Merck KGaA, Darmstadt, Germany. Alexa Fluor 488 conjugated with cholera toxin B subunit (CTxB 488) and Alexa Fluor 594 conjugated with cholera toxin B subunit (CTxB 594) were obtained from Molecular Probes, Life Technologies, Grand Island, NY, USA. All the materials were used without further purification.

**Vesicle Preparation.** The SLB was prepared by the vesicle deposition method following a formerly established protocol<sup>56</sup> with suitable modification. In order to form multilamellar vesicles (MLVs), 14:1 PC, SM, and cholesterol in chloroform solution were mixed at a molar ratio 1:1:1 with the addition of 0.1 mol % of GM1 and 0.1 mol % of DOPE-Atto-633 to form a 10 mM solution of the lipids. The lipid mixture was dried under nitrogen gas, leaving a thin film of lipids deposited on the bottom of the vial, followed by desiccation under vacuum for at least 2 h. The lipids were resuspended in buffer solution (10 mM HEPES and 150 mM NaCl, pH adjusted to 7.4) and exposed to a few cycles of heating on the hot plate at 60 °C and vortexing. The lipid suspension containing MLVs was aliquoted into sterilized glass vials and diluted 10 times (final concentration of lipids 1 mM) using buffer solution. Aliquots were stored at –20 °C for further use.

**SLB Preparation.** Aliquots containing MLVs of the desired composition were bath-sonicated for 10 min at maximum power to generate small unilamellar vesicles (SUVs). Freshly cleaved mica was glued to a coverslip by UV-activated glue (Norland 68), and the top layer of mica was removed right before the deposition to keep the surface properties of freshly cleaved mica intact during deposition. A



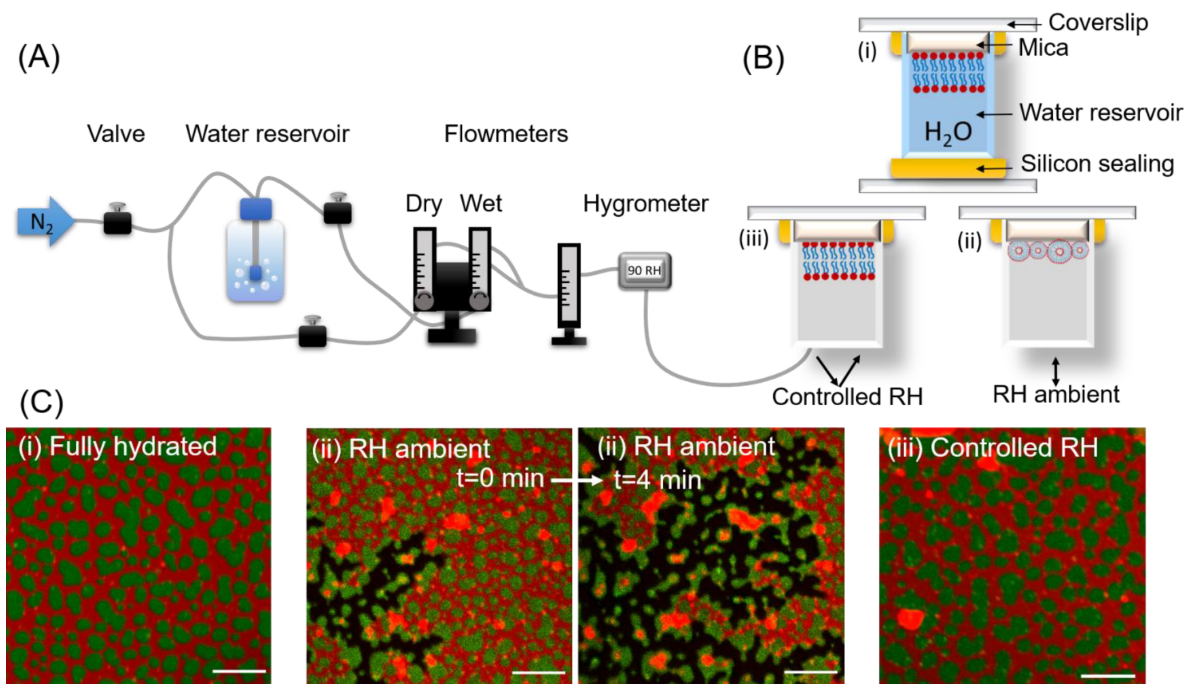


**Figure 1.** (A) Schematic representation of the home-built humidity-controlling setup. (B) Cartoon depiction of the three types of SLBs studied here: (i) fully hydrated with bulk water, (ii) exposed to the ambient humidity, where the lipid membrane curls up, forming vesicles and aggregates, (iii) exposed to atmosphere with well-controlled humidity, which at complete dehydration resembles the fully hydrated membrane. (C) Fluorescence images of the representative SLBs exhibiting phase separation into L<sub>q</sub> (labeled with Atto-633-DOPE, shown in red) and L<sub>o</sub> (labeled with CTxB-Alexa488, shown in green) domains in different hydration conditions indicated in panel B. The two middle panels show progressive rupturing and delamination of the SLB abruptly exposed to ambient RH. Upon dehydration the lipid membrane detaches from the solid support, leaving areas of bare mica (black). The curled-up membrane forms big clusters composed of both phases, which are visible as orange and yellow aggregates. Scale bar corresponds to 10  $\mu$ m.

half-cut Eppendorf tube was placed on the top of the coverslip and sealed with silicone. A 100  $\mu$ L amount of SUV solution was deposited on top of mica followed by the addition of 2  $\mu$ L of 0.1 M CaCl<sub>2</sub> solution and 9  $\mu$ L of 0.01 mM CTxB dissolved in buffer solution, all at room temperature. The SLB was allowed to settle for 30 s, and then 400  $\mu$ L of buffer solution (10 mM HEPES and 150 mM NaCl, pH adjusted to 7.4) was added and the sample was incubated for 30 min. The bilayer was rinsed 10 times with 2 mL of buffer solution to wash out excess unfused vesicles. The Eppendorf tube reservoir was fully filled with buffer solution, closed with a glass coverslip, and sealed with silicone to prepare a fully hydrated sample containing bulk water.

**Preparation of SLBs at Different Hydration Levels.** In our work, two distinct methods were implemented for drying the SLBs. (a) The bulk water was pipetted out and the sample was left open to dry and equilibrate to atmospheric humidity ( $\sim$ 30% RH) at room temperature, and (b) after removal of bulk water by micropipet the sample was equilibrated in an atmosphere of different relative humidity (RH%). An atmosphere of different relative humidity was created inside the open half-cut Eppendorf tube by purging nitrogen gas of a specific relative humidity using a home-built control unit (see Figure 1A). The setup consisted of three flow meters, three manual valves, a reservoir with water, and an electronic hygrometer with 0–95% RH range and 1% precision. The relative humidity of nitrogen gas was adjusted and maintained by mixing a suitable amount of wet (saturated with water vapor, 90% RH) N<sub>2</sub> and dry (2–3% RH) N<sub>2</sub> gas. The electronic hygrometer was used to monitor the final relative humidity and temperature of the N<sub>2</sub> gas being purged toward the sample. To study the SLB structure and dynamics at different relative humidity, the silicone seal of the sample was cut, water was pipetted out completely, and purging of wet nitrogen gas of 90% RH was started immediately toward the SLB. The RH was decreased (and

subsequently increased) in steps of  $\sim$ 20% at a rate of 2–3% RH per minute. Next, the SLB was equilibrated at a given RH for about 10 min before FRAP measurements were performed. The relative humidity of wet nitrogen gas was decreased gradually from 90% ( $62 \times 10^{19}$  water molecules/min) to approximately 70% ( $48 \times 10^{19}$  water molecules/min), 50% ( $34 \times 10^{19}$  water molecules/min), and 30% ( $20 \times 10^{19}$  water molecules/min), and finally dry nitrogen (around 2–3% RH) was purged to the SLB. Similarly, rehydration of the dried SLB was done by purging wet nitrogen gas with increasing relative humidity and finally resealing the half-cut Eppendorf tube filled with water.

**Fluorescence Microscopy and FRAP.** Laser-scanning confocal imaging and FRAP experiments were performed on SLBs using an upright Zeiss LSM 710 (Carl Zeiss, Jena, Germany) microscope with a 40 $\times$  1.3 NA oil immersion objective. Lasers of wavelengths 488 and 633 nm were used for excitation of Alexa Fluor 488 and Atto-633-DOPE, respectively. In the case of 3-fold labeling with TopFluor cholesterol, CTxB-Alexa Fluor-594, and Atto-633-DOPE, lasers of 488, 543, and 633 nm were applied accordingly. Laser power was adjusted during imaging to avoid excessive photobleaching of the sample. A small circular spot of 10  $\mu$ m diameter was bleached, and the area of the bleached spots was kept constant for all FRAP experiments. Diffusion coefficients were calculated by fitting the fluorescence recovery curve considering free Brownian lateral diffusion of lipid molecules in the membrane using the modified Soumpasis formula:<sup>37</sup>  $F(t) = b + a \times f(t)$ , where  $a$  is the amplitude of the recovery function,  $b$  is the remaining fluorescence after bleaching, and  $f(t)$  is the Soumpasis function. Fitting was done for data normalized with respect to the reference intensity signal of the whole image excluding the bleached spot. A complete dehydration and rehydration cycle was performed for three samples, and FRAP

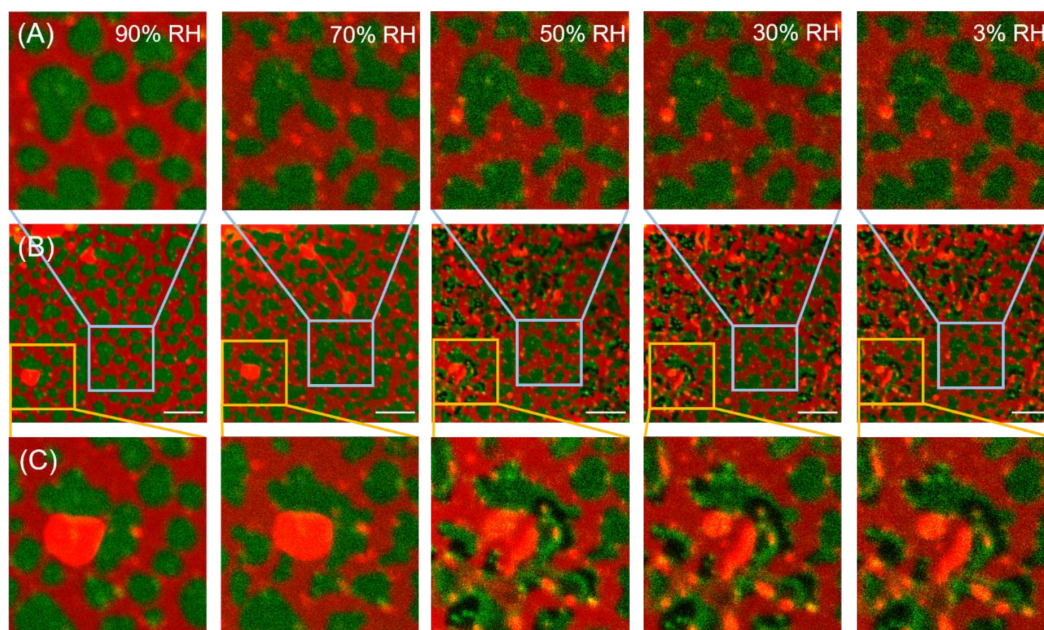


**Figure 2.** Consecutive fluorescence images of the same area of SLB exposed to 90%, 70%, 50%, 30%, and 3% RH. Top row (A) and bottom row (C) show the zoomed-in region indicated by the blue and yellow rectangles in images in the middle row (B), respectively. Equilibration time for each hydration condition and between consecutive images was  $\sim 30$  min. The  $L_d$  phase is labeled with Atto-633-DOPE (red), and the  $L_o$  phase is labeled with CTxB-Alexa488 (green). Scale bar corresponds to  $10 \mu\text{m}$ .

experiments were performed in at least five different spots at a particular relative humidity for each sample. Diffusion coefficients were averaged over a range of RH at which particular traces were measured.

**Temperature Dependence Experiments.** Variation of  $D(T)$  was examined for two hydrated and two dehydrated samples in the temperature range  $25 \pm 1$  to  $45 \pm 1$  °C. A resistive tape was attached to the sample reservoir tube for heating, and a thermocouple was placed inside the reservoir tube for continuous monitoring of sample temperature. Activation energies for the two samples were calculated using the Arrhenius equation:  $\ln D = \ln A - E_a/RT$  where  $D$  is the diffusion coefficient,  $A$  is the pre-exponential factor (assumed to be temperature independent in this range),  $R$  is the universal gas constant, and  $T$  is the temperature in Kelvin scale. For Arrhenius plots, weighted linear regression of  $\ln D$  values was presented. The confidence bounds generated by the fitting of FRAP traces were considered as error bars for  $D$  and their reciprocals to be the weights.

## RESULTS

**Structure.** In this study, the changes in the membrane structure at different hydration conditions have been examined by fluorescence imaging. In the experiments we considered three levels of membrane hydration, described in detail in the Experimental Section and schematically depicted in Figure 1B: (i) fully hydrated SLB, where the membrane is submerged in bulk water, (ii) SLB for which most of the bulk water was pipetted out and the sample was left open to equilibrate to room humidity ( $\sim 30\%$  RH), and (iii) SLB for which bulk water was removed to the highest extent and the sample was immediately exposed to a  $N_2$  atmosphere with  $\sim 90\%$  RH.

Fully hydrated SLBs, marked as (i) in Figure 1B,C, exhibit homogeneously distributed domains of liquid-ordered ( $L_o$ ) phase with an average area of  $1.77 \pm 0.29 \mu\text{m}^2$ . The domain size, distribution, and shape are typical of  $L_d/L_o$  phase-separated SLBs prepared in such conditions, in full agreement

with previous reports.<sup>58</sup> SLBs are far from static; over time they slowly merge with each other to form bigger domains. Over the course of  $\sim 24$  h the average domain size increases by up to 40%.

The SLB (marked as (ii) in Figure 1B,C) for which most of the bulk water was removed and the surface was exposed to open air of low RH ( $\sim 30\%$ ) initially exhibits an identical structure to the fully hydrated sample. Compared to fully hydrated SLBs, here we observed an increase in vesicle-like aggregated structures, mainly composed of  $L_d$  phase residing on the surface of the SLB. However, as spontaneous drying proceeds, the remnant bulk water layer shrinks, causing the drop-like macroscopic water layer wavefront to pass over the membrane surface. The local changes of surface tension induce delamination of the membrane from the mica support (the two middle panels in Figure 1C). Intriguingly, in most cases, the  $L_d$  phase detaches from mica first, while  $L_o$  domains remain attached to mica (extended time series is shown in Figure S1 and in Movie M1). Shortly after, over the course of a few minutes, also  $L_o$  domains shrink and form curled-up vesicle-like structures mixed with the  $L_d$  phase lipids. Delamination of the membrane ceases as soon as the residual bulk water is evaporated. However, it should be noted that even when the process of dehydration is conducted in a rapid manner, in several areas confined by mica terraces the SLB structure remains unperturbed (Figure S2). This mechanism of membrane preservation in the presence of mica terraces as mechanical supports is explained in more details in the Discussion section.

Markedly different behavior was observed when the SLB was exposed to a  $N_2$  atmosphere with a high RH of  $\sim 90\%$ , directly after bulk water removal. The SLB kept under a continuous flow of a  $N_2$  atmosphere with high RH (denoted as (iii) in

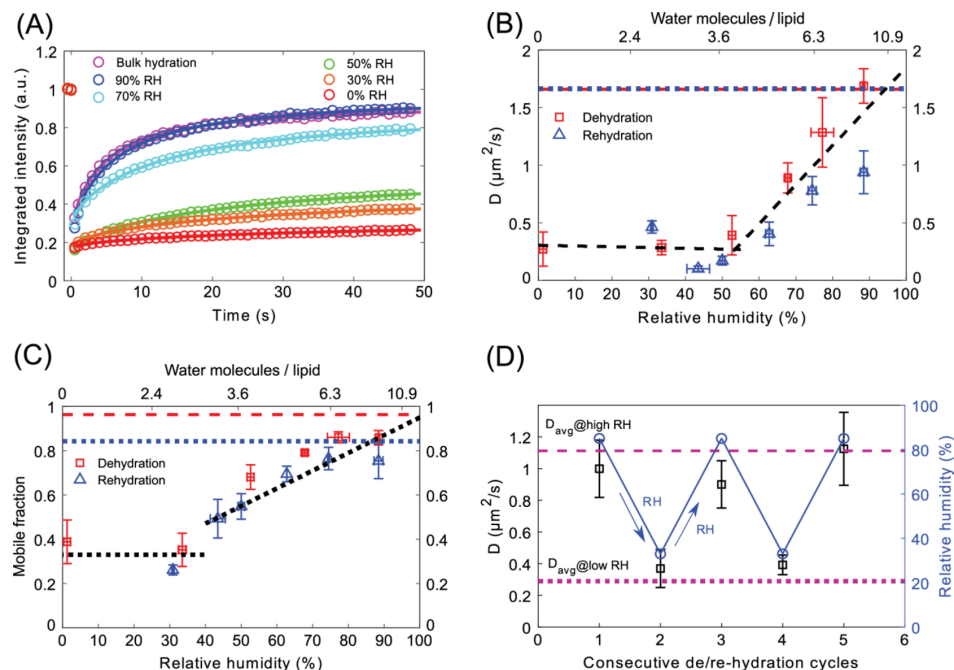


**Figure 3.** (A) FRAP traces of fully hydrated SLB and SLB equilibrated to 90%, 70%, 50%, 30%, and 0% relative humidity. (B) Diffusion coefficient for the  $L_d$  phase for SLBs at different relative humidity during dehydration (red squares) and rehydration (blue triangles). The data points correspond to the diffusion coefficient averaged from at least 5 FRAP traces from each of the 3 samples at a particular RH. The two black dashed lines are separate linear regressions of the data points at  $>55\%$  RH and at  $<55\%$  RH. The red dashed and blue dotted lines correspond to diffusion coefficient for a fully (bulk) hydrated SLB (averaged over three different samples) before dehydration and after rehydration, respectively. (C) Mobile fractions extracted from the fits of the modified Soumpasis formula (see Experimental Section) to the FRAP traces during dehydration (red squares) and rehydration (blue triangles). The black dotted lines are guides to the eye highlighting the data changes similar to those in panel B. The red dashed and blue dotted lines correspond to mobile fractions for a fully hydrated SLB (averaged over three different samples) before dehydration and after rehydration, respectively. (D) Diffusion coefficient (black squares) averaged over 5–7 FRAP traces at each hydration level during consecutive dehydration and rehydration (87%  $\leftrightarrow$  33% RH) cycles (blue circles). Purple dashed and dotted lines correspond to the average diffusion coefficient for all the measured FRAP traces for SLBs kept at high (85–90% RH) and low (30–35% RH) relative humidity, respectively.

Figure 1B,C) qualitatively closely resembles a fully hydrated SLB. Minor delamination was observed solely on the perimeter of the sample, close to the mica edges. This curling up of the membrane occurs during the time required to remove bulk water and expose the membrane to an atmosphere of high RH. These events are likely responsible for the increased number of vesicles and aggregates at the top of the membrane (Figure 2A–C). The aggregates that appear due to bulk water removal are initially mobile and float while the residual water evaporates. Once the sample equilibrates with an atmosphere of high RH (70–80% RH), the aggregates become stagnant. No change in the structure or quality of the SLB kept in such conditions was observed over the course of a few hours. No significant change in the quality of the membrane structure was noticed, although the perimeter of domains became increasingly jagged with further, gradual decrease of the RH down to about 50%.

At around 50% relative humidity, the appearance of seemingly hole-like dark spots within  $L_o$  domains (labeled with CTxB-Alexa 488) is observed at several locations on confocal microscopy images. In the range of 50% through 30% to nearly 0% RH, the membrane structure does not change significantly except for the appearance of dark spots in  $L_o$  domains in a few more locations. Noticeably, the formation of these hole-like dark spots is limited to a few areas, while an

unperturbed and continuous phase-separated membrane structure can be observed over the prevalent sample area even at a relative humidity close to 0%. Evidently, by means of a slow, well-controlled, and gradual ( $\sim 2$ –3% RH/min; for details see the Experimental Section) decrease of membrane hydration, an air-stable membrane can be formed without the addition of external stabilizing agents. Additional confocal images of the sample as a function of hydration are shown in Supporting Information Figure S3. On lowering the hydration below 50% RH, the big aggregates (ranging from 5 to 25  $\mu\text{m}^2$ ), located at the top of the membrane, break into smaller ones.

It should be noted that the membrane equilibrated at different hydration states is stable for up to a few hours. Intriguingly, the process of dehydration is fully reversible; that is, the dehydrated membrane can be rehydrated back to the state compliant with high RH and further to full hydration by addition of bulk water (Figure S4). Upon rehydration, the darker spots within  $L_o$  domains become homogeneously bright again and the domains regain their former (rounder) shapes at around 70–85% RH. Images of SLBs at different RH during rehydration are shown in Figure S3.

**Dynamics.** Next, we examined whether the hydration state of the membrane affects the mobility of the lipids by performing FRAP experiments on membranes equilibrated at different hydration conditions. The mobility of lipids



constituting the membrane depends on the composition of the SLB.<sup>59</sup> The measured single-component fully hydrated membrane of 14:1 PC shows a higher diffusion coefficient ( $2.93 \pm 0.44 \mu\text{m}^2/\text{s}$ ) than the  $L_d$  phase of our, phase-separated SLB ( $\sim 1.7 \mu\text{m}^2/\text{s}$ ), which is consistent with the previous reports.<sup>60</sup>

FRAP traces obtained for the phase-separated SLBs in different hydration states are shown in Figure 3A. Evidently, with lowering hydration of the membrane, the mobility of the  $L_d$  phase decreases significantly. At a fully hydrated condition, i.e., before removal of bulk buffer solution, the  $L_d$  phase lipids showed the highest mobility of  $1.66 \pm 0.22 \mu\text{m}^2/\text{s}$ . After the withdrawal of bulk water and being equilibrated to  $\sim 90\%$  RH, the mobility remained unaltered. With a further decrease in hydration level, the diffusion coefficient ( $D$ ) of lipids has been observed to decrease prominently (Figure 3B). The average  $D$  decreases over 6 times during dehydration from  $1.69 \pm 0.29 \mu\text{m}^2/\text{s}$  for  $87 \pm 2\%$  RH to  $0.27 \pm 0.29 \mu\text{m}^2/\text{s}$  at  $3 \pm 2\%$  RH. A steady decrease in the mobility of lipids is observed from full hydration to around 50% RH. Below 50% RH, the mobility of  $L_d$  lipids remains almost constant. The fluorescence recovery for fully hydrated membranes and membranes equilibrated with high RH% ( $\sim 90\%$ ) reaches  $93 \pm 3\%$  of the initial fluorescence intensity. At a relative humidity less than 85% the fluorescence does not recover up to the initial intensity, and in the case of RH lower than 50%, fluorescence recovery is significantly lower and amounts to less than 50% of the initial fluorescence intensity. The extracted mobile fraction, defined as the amplitude of the fitted recovery function normalized to the total bleach depth ( $\frac{a}{(1-b)}$ ), as a function of (de)hydration state of the membrane, is shown in Figure 3C.

Interestingly, during rehydration of the SLB, by increasing the relative humidity level gradually from 0% to 90%, the mobility of lipids increased accordingly and was strongly correlated with the diffusion coefficient observed during dehydration of the membrane (Figure 3B).

The extracted mobile fraction during the rehydration process also closely resembles that observed during dehydration for each specific hydration state. Upon a full dehydration/rehydration cycle, both the average  $D$  value and mobile fraction reach their initial values. Taking all the data into account, we observed two regimes. In the range of 50–90% RH,  $D$  exhibits significant changes with hydration. On the other hand, below 50% RH,  $D$  is nearly independent of the hydration of the membrane. The linear regressions performed on the data points in these two ranges show a clear turnover point at about 50% RH. A similar trend is observed for the mobile fraction: a significant decrease above 50% RH and little dependence in the hydration range below 50% RH.

Consecutive cycles of drying and rehydrating the SLB in the range of 87% to 33% RH were performed three times on the same sample while at each hydration state recording FRAP traces from a minimum of six spots. The sample was equilibrated for 10 min at a particular RH%. Remarkably, once bulk water is completely removed, the membrane exhibits very good stability in terms of structure and full reversibility of its dynamics. Keeping the membrane in such conditions allows strong modulation of the mobility by a factor of nearly 4:  $\sim 0.3 \mu\text{m}^2/\text{s}$  vs  $\sim 1.2 \mu\text{m}^2/\text{s}$  (see Figure 3D).

In accordance with previous reports the diffusion rates of  $L_o$  and  $L_d$  phases are significantly different:  $1.66 \pm 0.22 \mu\text{m}^2/\text{s}$  for  $L_d$  and  $0.1 \pm 0.01 \mu\text{m}^2/\text{s}$  for  $L_o$ . While qualitatively it appears

that the diffusion coefficient decreases for the  $L_o$  phase when lowering a membrane's hydration, it is very difficult to quantify this change in a reliable manner for two reasons: (a) the diffusion coefficient is already very low at full hydration, as it corresponds to the diffusion of the GM1-CTxB-AlexaFluor complex, where one CTxB molecule binds to 1–5 units of GM1,<sup>61</sup> leading to the diffusion of few lipids at the same time, and (b) the signal-to-noise ratio of the signal is quite low due to the much lower (4–8 times) fluorescence quantum efficiency of the CTxB label at low hydration conditions (see Figure S8). However, to still address the mobility of the  $L_o$  phase under different hydration conditions, we used an alternative fluorescent label (TopFluor cholesterol), which participates in both  $L_o$  and  $L_d$  phases with a roughly 80:20 ratio, respectively.<sup>62</sup> To this end, we prepared membranes with only the  $L_o$  phase, composed of cholesterol and SM at a molar ratio of 1:1. The obtained FRAP traces and extracted diffusion coefficients are presented in Figure S5. We observed that the mobility of the  $L_o$  phase decreases with the lowering of the membrane hydration, following the same trend as for the  $L_d$  phase. It can be concluded that although the absolute values of the diffusion coefficient for the more dynamic  $L_d$  phase and the less mobile  $L_o$  phase are different, the response of both phases to the hydration changes is similar.

## DISCUSSION

**Structure.** The multicomponent SLBs composed of 14:1 PC, SM, and cholesterol exhibit substantial structural changes with abrupt dehydration, but remain largely intact at lower hydration conditions when subjected to a well-controlled, gradual decrease in hydration level.

After bulk dehydration, the membrane is covered with a remnant, thin layer of water that desorbs over time. Exposing the membrane to the ambient RH causes the residual water to evaporate rapidly, causing fast shrinking of the water layer and inducing delamination and curling up of the membrane followed by lipid aggregation (see Figure 1C, Figure S1, and Movie M1). This is due to the domination of the air–water interfacial force over the attractive forces between the mica substrate and the proximal leaflet of the SLB.<sup>45</sup> Detachment and curling up of the  $L_d$  phase prior to the  $L_o$  phase during drying can be explained by differences in mechanical properties of the two phases. The  $L_o$  phase is stiffer (higher bending modulus and area expansion modulus) than the  $L_d$  phase,<sup>63</sup> which results in lower steric forces and stronger interaction with the substrate. The observed stronger interaction of the  $L_o$  phase with mica than the  $L_d$  phase is consistent with the stronger adhesive interactions observed for DSPC gel phase domains, reported in previous research.<sup>64</sup> It should be noted that the probability of survival of SLBs during rapid drying is increased by the presence of intrinsic defects of the support, such as mica terraces and/or cleaving defects (see Figure S2). The defects obstruct the drying water, decreasing the local water–air tension and protecting the membrane from delamination. This observation is in accordance with the previous report on preparation of an air-stable membrane by generating an obstacle network made of peripheral enzyme phospholipase  $A_2$  as physical confinement, where the presence of defects affects the local surface tension and stops the water–air from propagation, leaving the membrane intact.<sup>45</sup>

In contrast, for the SLB exposed and equilibrated to high relative humidity ( $\sim 90\%$ ) the overall membrane structure remains largely unaffected, except for the deposition of a few

aggregates on top of the bilayer (see Figure 2). Upon decreasing the relative humidity further in the range of 90–55%, we observed no significant changes to the structure of the membrane: the SLB still exhibits homogeneously distributed  $L_o$  domains in an  $L_d$  matrix. With decreasing hydration, however, the perimeter of the  $L_o$  domains becomes increasingly jagged (see Figure 2A). The ragged outlines of the  $L_o$  domains are mostly evident in the AFM topography image acquired on a membrane equilibrated to 30% RH (see Figure S6). AFM studies of fully hydrated SLBs of analogous composition showed round  $L_o$  domains with a smooth perimeter.<sup>65</sup> Moreover, the thickness difference between the  $L_d$  and  $L_o$  phases for a dehydrated SLB is nearly 3 times lower ( $\sim 0.6$  nm, see Figure S6) compared to the thickness mismatch for a fully hydrated SLB with the same composition ( $\sim 1.56 \pm 0.13$  nm).<sup>65</sup> Clearly, lowering the hydration of the membrane leads to a decrease in the hydrophobic mismatch between the  $L_d$  and  $L_o$  phases and consequently of the line tension.

At lower hydration conditions (<50% RH), dark spots in some of the  $L_o$  domains appear (see Figure 2C), where fluorescence of the labeled GM1-CTxB complex is not detected. At the same time, parts of these  $L_o$  domains exhibit locally higher fluorescence intensity. Detailed analysis of the fluorescence images reveals the nature of the dark spots within the  $L_o$  domains. The shape (outline) of the domains before the appearance of the dark spots (RH > 50%), with the dark spots present (RH < 50%), and after the disappearance of the dark spots (upon rehydration) remains the same (see Figure S7). If the dark spots were due to the formation of holes within the membrane, one would expect that upon rehydration the shape would randomly change; that is, the holes would be filled randomly by the  $L_d$  and/or  $L_o$  phase. Instead, we observe that the  $L_o$  domains maintain their original shape and regain a fluorescence distribution as before the dehydration.

Next, we analyzed the fluorescence intensity of selected  $L_o$  domains containing the dark spots as a function of hydration. The total integrated fluorescence intensity of an  $L_o$  domain before, during, and after filing the dark spots remains the same and is only affected by the overall photobleaching of the dye (see Figure S8). Thus, the dark spots do not result from the local bleaching of the CTxB label, but rather from the local redistribution/aggregation of the GM1-CTxB complexes.

More detailed insights and the proof for the aggregation of the CTxB within  $L_o$  domains comes from fluorescence images with the 3-fold labeling. We kept the labeling of the  $L_d$  and  $L_o$  phases (DOPE-Atto and GM1-CTxB, respectively), but we added fluorescently labeled cholesterol (TopFluor), which should partition in both  $L_d$  and  $L_o$  phases (see Figure S9). As expected, for domains that exhibit a homogeneous distribution of CTxB within the  $L_o$  domain, we observe homogeneous colocalization of CTxB and labeled cholesterol within the  $L_o$  phase. For domains that exhibit aggregation of CTxB, we still observe the homogeneous distribution of the labeled cholesterol. This unambiguously proves that the local appearance of dark areas within the  $L_o$  phases is solely related to CTxB aggregation and not to structural changes of the membrane. While the exact reason behind the CTxB aggregation remains elusive, it should be noted that it is mainly observed where aggregates of other membrane constituents on top of the membrane are present. We also note that at about 50% RH, aggregates on top of the membrane break into smaller pieces, likely taking up the energetically more favorable structure at the anhydrous

conditions. Intriguingly, when increasing the hydration state of the membrane, the homogeneous fluorescence signal within the  $L_o$  domains is recovered, indicating that the distribution of the GM1-CTxB complexes becomes homogeneous (Figure S3).

It is evident that the dehydration process itself, when carried out in a controlled manner, does not affect the structure of the SLB. Such preserved membrane structure-wise remains insensitive to dehydration and rehydration cycles. This conclusion is consistent with the recent molecular dynamics simulations study, which for a strongly dehydrated lipid bilayer reported the presence of four bridging water molecules per lipid (discussed in detail later). These strongly H-bonded water molecules at the interior of the membrane (bound to a carbonyl and/or phosphate group) contribute strongly to the structural and mechanical integrity of the membrane.<sup>66</sup>

**Dynamics.** With a decrease in hydration level, the mobility of  $L_d$  lipids decreases. As evident from Figure 3B, we find that the diffusion coefficient decreases between the fully hydrated sample and the fully dehydrated sample by over a factor of 6 (from 1.69 to 0.27  $\mu\text{m}^2/\text{s}$ ), which confirms a major role of water in lipid dynamics.

Upon removal of bulk water when the SLB is equilibrated to a humid environment (90% RH), the diffusion coefficient remains unchanged and the fluorescence intensity recovers to a similar extent after photobleaching, as in the case of fully hydrated SLB (Figure 3C). This implies that the fluidity of  $L_d$  lipids remains unhindered in the absence of bulk water and that water molecules present per lipid at 90% RH are sufficient for the lipids to retain their native (read in full hydration) mobility. This is understandable, as at high RH membrane constituents can coordinate as many water molecules as it is energetically most favorable, likely completely filling their direct hydration shell. The biggest changes to the diffusion coefficient are observed with lowering the RH down to about 50%. Further lowering of RH brings little change to the diffusion coefficient.

So far we assumed that the measured lipid mobility reflects the entire bilayer, that is both the upper and lower leaflet. However, the literature is inconsistent as to whether the lipids in the upper and lower leaflet of a bilayer exhibit similar diffusional dynamics. Hetzer et al. showed that for bilayers on silica beads the diffusion coefficient of lipids in the upper monolayer is roughly 2 times higher than for lipids in the lower monolayer.<sup>67</sup> On the other hand, studies by Zhang and Granick<sup>68</sup> showed that regardless of whether the DLPC bilayers were deposited on quartz or on a polymer cushion,  $D$  was the same for the outer and inner leaflet within the experimental uncertainty. To address this issue, we redesigned the experiment and used DOPE coupled with NBD dye, which undergoes irreversible fluorescence quenching upon addition of sodium dithionite,<sup>69</sup> allowing the detection of lipids from only the lower leaflet. Addition of sodium dithionite to the fully hydrated membrane indeed leads to a 2-fold decrease in mean fluorescence intensity of the membrane, indicating that the upper leaflet is quenched and the fluorescence signal only comes from the lower leaflet (Figure S10A). The diffusion coefficient (Figure S10B) and extracted mobile fractions (Figure S10C) are nearly identical before and after quenching, revealing that for the used, fully hydrated membrane diffusional dynamics of the upper and lower leaflet are very much alike. The diffusion coefficient for the half-quenched bilayer shows a strong decrease with dehydration of the

membrane (see Figure S11B). The measured roughly 5-fold decrease in  $D$  is very similar to the  $\sim 6$ -fold decrease of  $D$  with dehydration in the case of FRAP acquired for both leaflets, giving a clear indication that the two leaflets respond very similarly to the dehydration. Hence in what follows we assume similar mobility and hydration properties of lipids in the upper and lower leaflet. However, we note here that the fluorescence signal intensity during dehydration process shows a significant increase (Figure S11A). This originates from an increase in the fluorescence quantum yield of NBD dye at lower hydration conditions.<sup>70,71</sup>

In order to understand the changes in the diffusion coefficient under varying hydration conditions, we need to consider the hydration structure of individual lipid molecules. Phosphatidylcholine (PC) molecules are zwitterionic lipids containing a positively charged choline ( $(\text{CH}_3)_3\text{N}^+\text{CH}_2\text{CH}_2\text{OH}$ ) moiety and a negatively charged phosphate ( $\text{PO}_4^{3-}$ ) group. Three distinct regions have been identified (Figure 4) within PC, where water molecules are

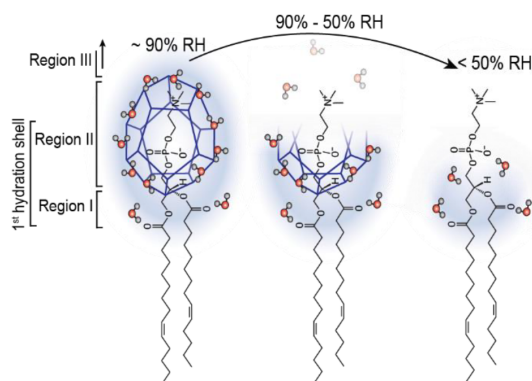


**Figure 4.** Schematic description of stepwise detachment of water molecules from the three regions of a 14:1 PC lipid during a controlled dehydration process.

bound either by weak van der Waals interactions or by H-bonds.<sup>72</sup> Region I corresponds to the interior water molecules, buried deeper in the membrane and forming H-bonds with carbonyl oxygens of the glycerol region. Region II refers to water molecules forming a cage-like (clathrate) structure around the whole phosphocholine group. Finally, the consecutive hydration shells/bulk water around the head group belong to region III.<sup>25</sup> Molecular dynamics (MD) simulations of a PC bilayer revealed that there are 10–12 water molecules in the first hydration shell, and among these, up to three water molecules remain tightly attached to lipids (in the glycerol and/or phosphate region), even after drastic drying.<sup>24</sup> Another MD simulation by Gierula et al. showed that nonesterified oxygen atoms of the phosphate group form about four H-bonds and the two carbonyl oxygen atoms form about one H-bond each;<sup>26</sup> thus approximately six H-bonded water molecules per PC are present in the first hydration shell (regions I and II). The choline group cannot form a H-bond with water molecules; instead it remains surrounded by a clathrate hydrate containing  $\sim 6.4$  water molecules,<sup>26</sup> held via weak electrostatic and van der Waals interactions.

The experimental studies using X-ray diffraction (XRD) and infrared spectroscopy also showed that upon bulk water dehydration of stacked lipid bilayers and equilibration of the

system at  $\sim 95\%$  RH there are around 11 to 12 water molecules per lipid, confirming quantitatively the structure of the first solvation shell around the lipid group.<sup>21,73</sup> Both theoretical and experimental studies are thus consistent as to the number of water molecules ( $\sim 12$ ) per PC lipid in the first solvation shell. The same experimental works determined that a further decrease in RH ( $95\% \rightarrow 75\% \rightarrow 50\% \rightarrow 25\%$ ) of the environment of bilayer stacks leads to a lowering of the hydration of lipids to approximately 10.9, 6.3, 3.6, and 2.4 water molecules per lipid (averaged from the two experimental works), respectively. Naturally, the desorption of water molecules should occur according to their H-bonding energies. Previous studies reported that H-bonds between the water molecule and the phosphate group are stronger than water–carbonyl group H-bonds, while both of these H-bonds are stronger than interwater molecule H-bonds.<sup>72</sup> Therefore, water molecules loosely bound with weak van der Waals interactions, as well as bound to other water molecules, will detach first, followed by a detachment of water molecules bound through the strongest H-bonds to phosphate and/or carbonyl moieties. This is in accordance with the molecular dynamics simulation results, which showed that, upon dehydration, water–water hydrogen bonds break, while the lipid–water bridging hydrogen bonds persist.<sup>66,74</sup>

Supplementing our experimental observations with the considerations above, a clear picture of the interplay between the water and the lipid membrane emerges (Figure 4). Upon withdrawal of bulk water and equilibration of the SLB with high RH, outer solvation shells are removed and only the first, direct solvation shell containing around 12 water molecules per lipid remains. Under these conditions, the diffusion coefficient of the  $L_d$  phase remains unaffected. Clearly, the water molecules beyond the first hydration shell are not involved in the mobility regulation of the lipids in SLBs. When decreasing the RH down to  $\sim 50\%$ , a sharp and continuous drop in the mobility of  $L_d$  phase lipids occurs. In this regime, each lipid loses six to seven water molecules. This implies that the clathrate structure breaks apart because at  $50\%$  RH only about four water molecules are left, which is insufficient to form a stable cage around the phosphate moiety. In the regime below  $50\%$  RH the lipid mobility hardly changes. Apparently, the remnant two to four water molecules tightly attached to phosphate and, in particular, carbonyl oxygen atoms do not affect lipid mobility. Interestingly, both molecular dynamics simulations and experimental works revealed that the diffusional and orientational mobility of the strongly bound water molecules is diminished at low hydration states.<sup>21,74</sup> These findings strongly correlate with our current observation of the very low mobility of lipids at low hydrations. It is evident that out of the water molecules within the first solvation shell, those forming the clathrate structure are mostly involved in facilitating the lateral diffusion of the lipids in SLBs.

After establishing which water molecules contribute to the regulation of the lateral mobility of lipids, the question arises of why and how these water molecules affect the mobility of lipids. For each diffusion step, a lipid molecule needs to possess energy higher than the activation energy of diffusion ( $E_a$ ) and to have sufficient free volume in the vicinity.<sup>75</sup> Free volume in our SLBs could decrease if small perforations (or nanoholes) were formed in the bilayer in a dehydrated condition. However, fluorescence images and AFM topography images (Figure S6), revealing a flawless and uniform  $L_d$  phase in



dehydrated SLBs, nullify this scenario. Therefore, the activation energy factor must dominate here.

Water molecules forming the clathrate screen the repulsive Coulombic interactions between adjacent lipid head groups.<sup>24,76</sup> Consequently, in the absence of this shielding water cage, the repulsive interactions between adjacent head groups become more prominent, increasing the activation energy for diffusion. In other words, for dehydrated SLB, a lower population of lipids possesses sufficient energy to overcome the diffusion activation energy barrier. Consequently, the probability for a lipid molecule to overcome the activation energy barrier at a particular time decreases, leading to an overall decrease in diffusion coefficient and mobile fraction. We confirmed this by measuring the activation energy for diffusion for fully hydrated and dehydrated (~30% RH) SLBs. Figure 5A depicts representative Arrhenius plots for hydrated and dehydrated SLBs.  $E_a$  for fully hydrated bilayers averaged over four data sets (two SLBs, increasing and decreasing temperature for each SLB) amounts to  $23 \pm 4$  kJ

mol<sup>-1</sup>, which is consistent with the previous reports.<sup>77</sup>  $E_a$  for a dehydrated membrane, averaged over four data sets, is approximately twice as high and amounts to  $47 \pm 17$  kJ mol<sup>-1</sup>. An increase of  $E_a$  for a dehydrated lipid monolayer has been qualitatively predicted earlier based on theoretical considerations.<sup>78</sup> The higher standard deviation of  $E_a$  for the dehydrated sample results from higher uncertainty in fitting the very slow fluorescence recovery in the FRAP data. Evidently, decreasing hydration of the SLB leads to a noticeable increase in activation energy for the  $L_d$  phase.

Importantly, the significant increase in  $E_a$  for diffusion with dehydration explains the observed decrease in mobile fraction during dehydration. As  $E_a$  increases, the population of molecules having enough energy to overcome the barrier at a particular time decreases (Figure 5C), which is reflected in the slower recovery of FRAP traces and lower mobile fraction. In this case, an increase in mobile fraction should be observed with increasing the temperature, as more energy is delivered to the lipids. For a fully hydrated sample, the mobile fraction is already greater than ~95% and there is very little or no room for it to increase further. In the case of the dehydrated SLB, the mobile fraction indeed tends to increase at higher temperatures (Figure 5B).

Altogether, the observed slowing down of the diffusion with an increase in diffusion activation energy suggests that the SLB quasi-gellifies (stiffens) upon dehydration, in particular upon the removal of the clathrate water molecules. This is in agreement with previous studies, which indeed suggested that dehydration leads to an increase in the main phase transition temperature of lipids,<sup>79,80</sup> indicating fluid-to-gel-like transition at lower hydration conditions.

Finally, we note that with rehydration the former mobility of lipids is restored. The variation of diffusion coefficient with hydration state for a few dehydration and rehydration cycles demonstrates that the mobility of lipids strongly depends on the availability of the water molecules per lipid, and the diffusion coefficient is instantaneously responsive toward water content. It is also evident that, for the intact membrane that survived the dehydration process, losing or gaining mobility of lipids due to change in hydration is completely reversible and repeatable.

## CONCLUSIONS

We successfully prepared desiccation-tolerant, phase-separated lipid bilayers without mechanical or chemical alterations. While a rapid reduction in water content causes irreversible damage to the SLB structure, a gradual and controlled dehydration process allows the preparation of stable SLBs even in the complete absence of water. Dried SLBs can be brought back to full hydration without affecting their integrity and reused as functional membranes after rehydration. Thus, storage and handling of such desiccation-tolerant SLBs become much easier for bioengineering applications such as biocoatings.

We carefully addressed the structural and dynamical properties of SLBs across a wide spectrum of hydration states. While structurally, SLBs showed little sensitivity to the hydration state of the SLB, we observed a 6-fold decrease in lateral diffusion coefficient for the lipids forming an  $L_d$  phase with lowering hydration of the SLB. Importantly, we correlated the observed changes of the diffusion coefficient with the lipid hydration structure and established that these are six to seven water molecules hydrating the phosphocholine head group and forming a cage-like structure that acts as a lubricant for the

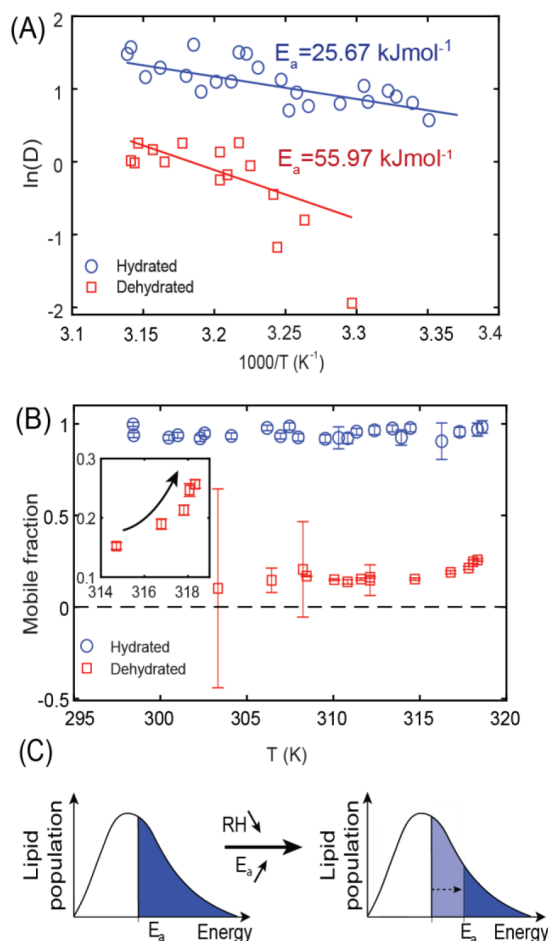


**Figure 5.** (A) Arrhenius plots for one representative fully hydrated (blue circles) and dehydrated (red squares) SLB. (B) Temperature dependence of the mobile fraction extracted from the data shown in panel A. (C) Schematic representation of the relation between the diffusion activation energy and the lipid mobile fraction in the dehydration experiment.

diffusion and modulates the lateral mobility of disordered phase in the SLBs. We demonstrate that the observed slowing down of the diffusion is directly related to an increase in activation energy for diffusion at lowered hydration conditions. Together with the unpredicted overall structural stability, these findings point toward quasi-gellification of the SLB with lowering its hydration. Intriguingly, the native dynamics of the fully hydrated SLB is recovered with rehydration. Consequently, the dried SLB with unperturbed membrane structure and dramatically reduced mobility can be considered as a less active form of the membrane, which can be compared with the dormant stage of organisms exhibiting anhydrobiosis. Local “anhydrobiosis” occurs also in our organisms during for instance cell–cell interactions or during binding of large biomacromolecules, when the water molecules are expelled from the interaction site. It is thus conceivable that the observed slowing down in SLB dynamics also occurs locally and leads to stiffening and stabilization of the membrane, potentially stabilizing transient molecular interactions.

Our studies on the interplay between the membrane and its hydration open up a range of exciting experiments that could certainly provide new molecular-level insights into effects such as hydrophobic mismatch, line tension, or the properties of the interphase boundaries of the membrane structural complexes.

Finally, a clear relation between the diffusion coefficient and the number of water molecules hydrating the membrane could be utilized for biosensing applications to monitor the local hydration state of biomimetic systems. This idea further gains in impact when the hydration sensing is done on a single-molecule/probe level using, for example, fluorescence correlation spectroscopy or single-particle tracking techniques. Our findings thus hold a huge application potential from both biological and technological viewpoints.

## ■ ASSOCIATED CONTENT

### SI Supporting Information

The Supporting Information is available free of charge at <https://pubs.acs.org/doi/10.1021/jacs.1c04314>.

Supplementary Figures S1–S11 (PDF)

Supplementary Movie 1 (MP4)

## ■ AUTHOR INFORMATION

### Corresponding Authors

**Madhurima Chattopadhyay** – Faculty of Materials Engineering and Technical Physics, Poznan University of Technology, 60-965 Poznan, Poland; [orcid.org/0000-0001-8900-163X](https://orcid.org/0000-0001-8900-163X); Email: [madhurima.chattopadhyay@put.poznan.pl](mailto:madhurima.chattopadhyay@put.poznan.pl)

**Lukasz Piatkowski** – Faculty of Materials Engineering and Technical Physics, Poznan University of Technology, 60-965 Poznan, Poland; [orcid.org/0000-0002-1226-2257](https://orcid.org/0000-0002-1226-2257); Email: [lukasz.j.piatkowski@put.poznan.pl](mailto:lukasz.j.piatkowski@put.poznan.pl)

### Authors

**Emilia Krok** – Faculty of Materials Engineering and Technical Physics, Poznan University of Technology, 60-965 Poznan, Poland; [orcid.org/0000-0002-4637-2729](https://orcid.org/0000-0002-4637-2729)

**Hanna Orlikowska** – Faculty of Materials Engineering and Technical Physics, Poznan University of Technology, 60-965 Poznan, Poland; [orcid.org/0000-0003-0697-4781](https://orcid.org/0000-0003-0697-4781)

**Petra Schulle** – Department of Cellular and Molecular Biophysics, Max Planck Institute of Biochemistry, 82152 Martinsried, Germany; [orcid.org/0000-0002-6106-4847](https://orcid.org/0000-0002-6106-4847)

**Henri G. Franquelim** – Department of Cellular and Molecular Biophysics, Max Planck Institute of Biochemistry, 82152 Martinsried, Germany; [orcid.org/0000-0001-6229-4276](https://orcid.org/0000-0001-6229-4276)

Complete contact information is available at:  
<https://pubs.acs.org/10.1021/jacs.1c04314>

### Notes

The authors declare no competing financial interest.

## ■ ACKNOWLEDGMENTS

The authors acknowledge the financial support from the EMBO Installation Grant (IG 4147) and from the Ministry of Science and Higher Education of Poland in the year 2021 under Project No. 0512/SBAD/2120. L.P. acknowledges the financial support from the First TEAM Grant No. POIR.04.04.00-00-SD32/18-00, provided by the Foundation for Polish Science (FNP). This work was financed from the budget funds allocated for science in the years 2019–2023 as a research project under the “Diamond Grant” program (Decision No. 0042/DIA/2019/48). The authors thank MSc. Marek Weiss and Prof. Arkadiusz Ptak for their assistance in acquiring AFM images. P.S. and H.G.F. acknowledge the financial support from the Max Planck Society.

## ■ REFERENCES

- (1) Sackmann, E. Supported Membranes: Scientific and Practical Applications. *Science* **1996**, *271* (5245), 43–48.
- (2) Crane, J. M.; Tamm, L. K. *Fluorescence Microscopy to Study Domains in Supported Lipid Bilayers*; Humana Press, 2007; Vol. 400, pp 481–488.
- (3) London, E. Insights into Lipid Raft Structure and Formation from Experiments in Model Membranes. *Curr. Opin. Struct. Biol.* **2002**, *12* (4), 480–486.
- (4) Vallejo, A. E.; Gervasi, C. A. Impedance Analysis of Ion Transport through Gramicidin Channels in Supported Lipid Bilayers. *Bioelectrochemistry* **2002**, *57* (1), 1–7.
- (5) Picas, L.; Rico, F.; Scheuring, S. Direct Measurement of the Mechanical Properties of Lipid Phases in Supported Bilayers. *Biophys. J.* **2012**, *102* (1), L01–L03.
- (6) Lee, A. G. How Lipids Affect the Activities of Integral Membrane Proteins. *Biochim. Biophys. Acta, Biomembr.* **2004**, *1666* (1–2), 62–87.
- (7) Céspedes, P. F.; Beckers, D.; Dustin, M. L.; Sezgin, E. Model Membrane Systems to Reconstitute Immune Cell Signaling. *FEBS J.* **2021**, *288*, 1070.
- (8) Pautot, S.; Lee, H.; Isacoff, E. Y.; Groves, J. T. Neuronal Synapse Interaction Reconstituted Between Live Cells and Supported Lipid Bilayers. *Nat. Chem. Biol.* **2005**, *1* (5), 283–289.
- (9) Castellana, E. T.; Cremer, P. S. Solid Supported Lipid Bilayers: From Biophysical Studies to Sensor Design. *Surf. Sci. Rep.* **2006**, *61* (10), 429–444.
- (10) Perez, T. D.; Nelson, W. J.; Boxer, S. G.; Kam, L. E-Cadherin Tethered to Micropatterned Supported Lipid Bilayers as a Model for Cell Adhesion. *Langmuir* **2005**, *21* (25), 11963–11968.
- (11) Jungwirth, P. Biological Water or Rather Water in Biology? *J. Phys. Chem. Lett.* **2015**, *6* (13), 2449–2451.
- (12) Fausto, M.; Calero, C.; Franzese, G. Redefining the Concept of Hydration Water near Soft Interfaces. *Biointerphases* **2021**, *16* (2), No. 020801.
- (13) Zhong, D.; Pal, S. K.; Zewail, A. H. Biological Water: A Critique. *Chem. Phys. Lett.* **2011**, *503* (1–3), 1–11.



- (14) Bianco, V.; Franzese, G. Contribution of Water to Pressure and Cold Denaturation of Proteins. *Phys. Rev. Lett.* **2015**, *115* (10), 1–5.
- (15) Bianco, V.; Franzese, G.; Coluzza, I. Silico Evidence That Protein Unfolding Is a Precursor of Protein Aggregation. *ChemPhysChem* **2020**, *21* (5), 377–384.
- (16) March, D.; Bianco, V.; Franzese, G. Protein Unfolding and Aggregation near a Hydrophobic Interface. *Polymers (Basel, Switz.)* **2021**, *13* (1), 1–14.
- (17) Bianco, V.; Franzese, G.; Dellago, C.; Coluzza, I. Role of Water in the Selection of Stable Proteins at Ambient and Extreme Thermodynamic Conditions. *Phys. Rev. X* **2017**, *7* (2), 1–15.
- (18) Roberts, M. F.; Redfield, A. G.; Mohanty, U. Phospholipid Reorientation at the Lipid/Water Interface Measured by High Resolution 31P Field Cycling NMR Spectroscopy. *Biophys. J.* **2009**, *97* (1), 132–141.
- (19) Alsop, R. J.; Maria Schober, R.; Rheinstädter, M. C. Swelling of Phospholipid Membranes by Divalent Metal Ions Depends on the Location of the Ions in the Bilayers. *Soft Matter* **2016**, *12* (32), 6737–6748.
- (20) Lautner, L.; Pluhackova, K.; Barth, N. K. H.; Seydel, T.; Lohstroh, W.; Böckmann, R. A.; Unruh, T. Dynamic Processes in Biological Membrane Mimics Revealed by Quasielastic Neutron Scattering. *Chem. Phys. Lipids* **2017**, *206*, 28–42.
- (21) Piatkowski, L.; De Heij, J.; Bakker, H. J. Probing the Distribution of Water Molecules Hydrating Lipid Membranes with Ultrafast Förster Vibrational Energy Transfer. *J. Phys. Chem. B* **2013**, *117* (5), 1367–1377.
- (22) Livingstone, R. A.; Zhang, Z.; Piatkowski, L.; Bakker, H. J.; Hunger, J.; Bonn, M.; Backus, E. H. G. Water in Contact with a Cationic Lipid Exhibits Bulklike Vibrational Dynamics. *J. Phys. Chem. B* **2016**, *120* (38), 10069–10078.
- (23) Chen, X.; Hua, W.; Huang, Z.; Allen, H. C. Interfacial Water Structure Associated with Phospholipid Membranes Studied by Phase-Sensitive Vibrational Sum Frequency Generation Spectroscopy. *J. Am. Chem. Soc.* **2010**, *132* (32), 11336–11342.
- (24) Disalvo, E. A.; Lairion, F.; Martini, F.; Tymczyszyn, E.; Frias, M.; Almalek, H.; Gordillo, G. J. Structural and Functional Properties of Hydration and Confined Water in Membrane Interfaces. *Biochim. Biophys. Acta, Biomembr.* **2008**, *1778* (12), 2655–2670.
- (25) Lopez, C. F.; Nielsen, S. O.; Klein, M. L.; Moore, P. B. Hydrogen Bonding Structure and Dynamics of Water at the Dimyristoylphosphatidylcholine Lipid Bilayer Surface from a Molecular Dynamics Simulation. *J. Phys. Chem. B* **2004**, *108* (21), 6603–6610.
- (26) Pasenkiewicz-Gierula, M.; Baczynski, K.; Markiewicz, M.; Murzyn, K. Computer Modelling Studies of the Bilayer/Water Interface. *Biochim. Biophys. Acta, Biomembr.* **2016**, *1858* (10), 2305–2321.
- (27) Alper, H. E.; Bassolino-Klimas, D.; Stouch, T. R. The Limiting Behavior of Water Hydrating a Phospholipid Monolayer: A Computer Simulation Study. *J. Chem. Phys.* **1993**, *99* (7), 5547–5559.
- (28) Bagchi, B. *Water in Biological and Chemical Processes: From Structure and Dynamics to Function*; Cambridge University Press, 2011; pp 1–364.
- (29) Martelli, F.; Ko, H. Y.; Borralo, C. C.; Franzese, G. Structural Properties of Water Confined by Phospholipid Membranes. *Front. Phys.* **2018**, *13* (1), 1–8.
- (30) Martelli, F.; Crain, J.; Franzese, G. Network Topology in Water Nanoconfined between Phospholipid Membranes. *ACS Nano* **2020**, *14* (7), 8616–8623.
- (31) Hengherr, S.; Heyer, A. G.; Köhler, H. R.; Schill, R. O. Trehalose and Anhydrobiosis in Tardigrades - Evidence for Divergence in Responses to Dehydration. *FEBS J.* **2008**, *275* (2), 281–288.
- (32) Wright, J. C. Cryptobiosis 300 Years on from van Leuwenhoek: What Have We Learned about Tardigrades? *Zool. Anz.* **2001**, *240* (3–4), 563–582.
- (33) Crowe, J. H.; Crowe, L. M.; Chapman, D. Preservation of Membranes in Anhydrobiotic Organisms: The Role of Trehalose. *Science* **1984**, *223* (4637), 701–703.
- (34) Richaud, M.; Le Goff, E.; Cazevielle, C.; Ono, F.; Mori, Y.; Saini, N. L.; Cuq, P.; Baghdiguian, S.; Godefroy, N.; Galas, S. Ultrastructural Analysis of the Dehydrated Tardigrade *Hypsibius Exemplantis* Unveils an Anhydrobiotic-Specific Architecture. *Sci. Rep.* **2020**, *10*, 1.
- (35) Madin, K. A. C.; Crowe, J. H. Anhydrobiosis in Nematodes: Carbohydrate and Lipid Metabolism during Dehydration. *J. Exp. Zool.* **1975**, *193* (3), 335–342.
- (36) Eleutheria, E. C. A.; de Araujo, P. S.; Panek, A. D. Role of the Trehalose Carrier in Dehydration Resistance of *Saccharomyces Cerevisiae*. *Biochim. Biophys. Acta, Gen. Subj.* **1993**, *1156* (3), 263–266.
- (37) Rapoport, A. *Anhydrobiosis and Dehydration of Yeasts*; Springer: Cham, 2017; pp 87–116.
- (38) Golovina, E. A.; Golovin, A.; Hoekstra, F. A.; Faller, R. Water Replacement Hypothesis in Atomic Details: Effect of Trehalose on the Structure of Single Dehydrated POPC Bilayers. *Langmuir* **2010**, *26* (13), 11118–11126.
- (39) Marotta, R.; Leasi, F.; Uggetti, A.; Ricci, C.; Melone, G. Dry and Survive: Morphological Changes during Anhydrobiosis in a Bdelloid Rotifer. *J. Struct. Biol.* **2010**, *171* (1), 11–17.
- (40) Lapinski, J.; Tunnacliffe, A. Anhydrobiosis without Trehalose in Bdelloid Rotifers. *FEBS Lett.* **2003**, *553* (3), 387–390.
- (41) Goyal, K.; Walton, L. J.; Tunnacliffe, A. LEA Proteins Prevent Protein Aggregation Due to Water Stress. *Biochem. J.* **2005**, *388* (1), 151–157.
- (42) Wilschut, J.; Hoekstra, D. Membrane Fusion: Lipid Vesicles as a Model System. *Chem. Phys. Lipids* **1986**, *40* (2–4), 145–166.
- (43) Aeffner, S.; Reusch, T.; Weinhausen, B.; Salditt, T. Energetics of Stalk Intermediates in Membrane Fusion Are Controlled by Lipid Composition. *Proc. Natl. Acad. Sci. U. S. A.* **2012**, *109* (25), 9678.
- (44) Holden, M. A.; Jung, S. Y.; Yang, T.; Castellana, E. T.; Cremer, P. S. Creating Fluid and Air-Stable Solid Supported Lipid Bilayers. *J. Am. Chem. Soc.* **2004**, *126* (21), 6512–6513.
- (45) Han, C. T.; Chao, L. Creating Air-Stable Supported Lipid Bilayers by Physical Confinement Induced by Phospholipase A2. *ACS Appl. Mater. Interfaces* **2014**, *6* (9), 6378–6383.
- (46) Deng, Y.; Wang, Y.; Holtz, B.; Li, J.; Traaseth, N.; Veglia, G.; Stottrup, B. J.; Elde, R.; Pei, D. Fluidic and Air-Stable Supported Lipid Bilayer and Cell-Mimicking Microarrays. *J. Am. Chem. Soc.* **2008**, *130* (12), 6267–6271.
- (47) Oberts, B. P.; Blanchard, G. J. Formation of Air-Stable Supported Lipid Monolayers and Bilayers. *Langmuir* **2009**, *25* (11), 2962–2970.
- (48) Fabre, R. M.; Talham, D. R. Stable Supported Lipid Bilayers on Zirconium Phosphonate Surfaces. *Langmuir* **2009**, *25* (9), 12644–12652.
- (49) Fang, Y.; Frutos, A. G.; Lahiri, J. Membrane Protein Microarrays. *J. Am. Chem. Soc.* **2002**, *124* (11), 2394–2395.
- (50) Conboy, J. C.; Liu, S.; O'Brien, D. F.; Saavedra, S. S. Planar Supported Bilayer Polymers Formed from Bis-Diene Lipids by Langmuir - Blodgett Deposition and UV Irradiation. *Biomacromolecules* **2003**, *4*, 841–849.
- (51) Halter, M.; Nogata, Y.; Dannenberger, O.; Sasaki, T.; Vogel, V. Engineered Lipids That Cross-Link the Inner and Outer Leaflets of Lipid Bilayers. *Langmuir* **2004**, *20* (14), 2416–2423.
- (52) Albertorio, F.; Diaz, A. J.; Yang, T.; Chapa, V. A.; Kataoka, S.; Castellana, E. T.; Cremer, P. S. Fluid and Air-Stable Lipopolymer Membranes for Biosensor Applications. *Langmuir* **2005**, *21* (16), 7476–7482.
- (53) Oliver, A. E.; Kendall, E. L.; Howland, M. C.; Sanii, B.; Shreve, A. P.; Parikh, A. N. Protecting, Patterning, and Scaffolding Supported Lipid Membranes Using Carbohydrate Glasses. *Lab Chip* **2008**, *8* (6), 892–897.
- (54) Dong, Y.; Phillips, K. S.; Cheng, Q. Immunosensing of Staphylococcus Enterotoxin B (SEB) in Milk with PDMS Micro-

fluidic Systems Using Reinforced Supported Bilayer Membranes (r-SBMs). *Lab Chip* **2006**, 6 (5), 675–681.

(55) Chiantia, S.; Kahya, N.; Schwille, P. Dehydration Damage of Domain-Exhibiting Supported Bilayers: An AFM Study on the Protective Effects of Disaccharides and Other Stabilizing Substances. *Langmuir* **2005**, 21 (14), 6317–6323.

(56) Matysik, A.; Kraut, R. S. Preparation of Mica Supported Lipid Bilayers for High Resolution Optical Microscopy Imaging. *J. Visualized Exp.* **2014**, No. 88, 52054.

(57) Soumpasis, D. M. Theoretical Analysis of Fluorescence Photobleaching Recovery Experiments. *Biophys. J.* **1983**, 41 (1), 95–97.

(58) Mangiarotti, A.; Wilke, N. Electrostatic Interactions at the Microscale Modulate Dynamics and Distribution of Lipids in Bilayers. *Soft Matter* **2017**, 13 (3), 686–694.

(59) Murase, K.; Fujiwara, T.; Umemura, Y.; Suzuki, K.; Iino, R.; Yamashita, H.; Saito, M.; Murakoshi, H.; Ritchie, K.; Kusumi, A. Ultrafine Membrane Compartments for Molecular Diffusion as Revealed by Single Molecule Techniques. *Biophys. J.* **2004**, 86 (6), 4075–4093.

(60) Ries, J.; Chiantia, S.; Schwille, P. Accurate Determination of Membrane Dynamics with Line-Scan FCS. *Biophys. J.* **2009**, 96 (5), 1999–2008.

(61) Kabbani, A. M.; Raghunathan, K.; Lencer, W. I.; Kenworthy, A. K.; Kelly, C. V. Structured Clustering of the Glycosphingolipid GM1 Is Required for Membrane Curvature Induced by Cholera Toxin. *Proc. Natl. Acad. Sci. U. S. A.* **2020**, 117 (26), 14978–14986.

(62) Sezgin, E.; Levental, I.; Grzybek, M.; Schwarzmann, G.; Mueller, V.; Honigsmann, A.; Belov, V. N.; Eggeling, C.; Coskun, Ü.; Simons, K.; Schwille, P. Partitioning, Diffusion, and Ligand Binding of Raft Lipid Analogs in Model and Cellular Plasma Membranes. *Biochim. Biophys. Acta, Biomembr.* **2012**, 1818 (7), 1777–1784.

(63) Saeedimane, M.; Montanino, A.; Kleiven, S.; Villa, A. Role of Lipid Composition on the Structural and Mechanical Features of Axonal Membranes: A Molecular Simulation Study. *Sci. Rep.* **2019**, 9 (1), 1–12.

(64) Lin, W. C.; Blanchette, C. D.; Ratto, T. V.; Longo, M. L. Lipid Asymmetry in DLPC/DSPC-Supported Lipid Bilayers: A Combined AFM and Fluorescence Microscopy Study. *Biophys. J.* **2006**, 90 (1), 228–237.

(65) García-Sáez, A. J.; Chiantia, S.; Schwille, P. Effect of Line Tension on the Lateral Organization of Lipid Membranes. *J. Biol. Chem.* **2007**, 282 (46), 33537–33544.

(66) Calero, C.; Franzese, G. Membranes with Different Hydration Levels: The Interface between Bound and Unbound Hydration Water. *J. Mol. Liq.* **2019**, 273, 488–496.

(67) Hetzer, M.; Heinz, S.; Grage, S.; Bayerl, T. M. Asymmetric Molecular Friction in Supported Phospholipid Bilayers Revealed by NMR Measurements of Lipid Diffusion. *Langmuir* **1998**, 14 (5), 982–984.

(68) Zhang, L.; Granick, S. Lipid Diffusion Compared in Outer and Inner Leaflets of Planar Supported Bilayers. *J. Chem. Phys.* **2005**, 123, 211104.

(69) Visco, I.; Chiantia, S.; Schwille, P. Asymmetric Supported Lipid Bilayer Formation via Methyl- $\beta$ -Cyclodextrin Mediated Lipid Exchange: Influence of Asymmetry on Lipid Dynamics and Phase Behavior. *Langmuir* **2014**, 30, 7475–7484.

(70) Mazères, S.; Schram, V.; Tocanne, J. F.; Lopez, A. 7-Nitrobenz-2-Oxa-1,3-Diazole-4-Yl-Labeled Phospholipids in Lipid Membranes: Differences in Fluorescence Behavior. *Biophys. J.* **1996**, 71 (1), 327–335.

(71) Fery-Forgues, S.; Fayet, J. P.; Lopez, A. Drastic Changes in the Fluorescence Properties of NBD Probes with the Polarity of the Medium: Involvement of a TICT State? *J. Photochem. Photobiol., A* **1993**, 3, 229–243.

(72) Bhide, S. Y.; Berkowitz, M. L. Structure and Dynamics of Water at the Interface with Phospholipid Bilayers. *J. Chem. Phys.* **2005**, 123 (22), 224702.

(73) Hristova, K.; White, S. H. Determination of the Hydrocarbon Core Structure of Fluid Dioleoylphosphocholine (DOPC) Bilayers by x-Ray Diffraction Using Specific Bromination of the Double-Bonds: Effect of Hydration. *Biophys. J.* **1998**, 74 (5), 2419–2433.

(74) Calero, C.; Stanley, H. E.; Franzese, G. Structural Interpretation of the Large Slowdown of Water Dynamics at Stacked Phospholipid Membranes for Decreasing Hydration Level: All-Atom Molecular Dynamics. *Materials* **2016**, 9 (5), 319.

(75) Almeida, P. F. F.; Thompson, T. E. Lateral Diffusion in the Liquid Phases of Dimyristoylphosphatidylcholine/Cholesterol Lipid Bilayers: A Free Volume Analysis. *Biochemistry* **1992**, 31 (29), 6739–6747.

(76) LeNeveu, D. M.; Rand, R. P. Measurement and Modification of Forces between Lecithin Bilayers. *Biophys. J.* **1977**, 18 (2), 209–230.

(77) Bag, N.; Yap, D. H. X.; Wohland, T. Temperature Dependence of Diffusion in Model and Live Cell Membranes Characterized by Imaging Fluorescence Correlation Spectroscopy. *Biochim. Biophys. Acta, Biomembr.* **2014**, 1838 (3), 802–813.

(78) Baumgart, T.; Offenhäuser, A. Lateral Diffusion in Substrate-Supported Lipid Monolayers as a Function of Ambient Relative Humidity. *Biophys. J.* **2002**, 83 (3), 1489–1500.

(79) Pfeiffer, H.; Binder, H.; Klose, G.; Heremans, K. Hydration Pressure and Phase Transitions of Phospholipids: II. Thermotropic Approach. *Biochim. Biophys. Acta, Biomembr.* **2003**, 1609 (2), 148–152.

(80) Gennaro, A.; Deschaume, O.; Pfeiffer, H.; Bartic, C.; Wagner, P.; Wübbenhorst, M. Understanding the Dehydration Stress in Lipid Vesicles by a Combined Quartz Crystal Microbalance and Dielectric Spectroscopy Study. *Phys. Status Solidi A* **2020**, 217 (13), 1900986.

## Supplementary Information for

# Hydration layer of only few molecules controls lipid mobility in biomimetic membranes

Madhurima Chattopadhyay,<sup>1\*</sup> Emilia Krok,<sup>1</sup> Hanna Orlikowska,<sup>1</sup> Petra Schwille,<sup>2</sup> Henri G. Franquelim,<sup>2</sup> and Lukasz Piatkowski<sup>1\*</sup>

<sup>1</sup>*Faculty of Materials Engineering and Technical Physics, Poznan University of Technology, Piotrowo 3, 60-965 Poznań, Poland*

<sup>2</sup>*Department of Cellular and Molecular Biophysics, Max Planck Institute of Biochemistry, Am Klopferspitz 18, 82152 Martinsried, Germany*

### Table of contents:

Supplementary figures S1 – S11.

**Figure S1**

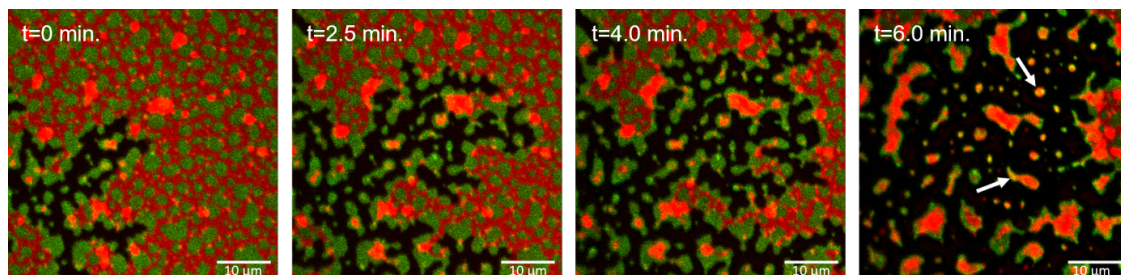


Fig. S1. Consecutive fluorescence images of the same area of SLB exposed abruptly to ambient RH. Desorption of water causes shrinking of the remnant water layer and induces delamination of the lipids from the mica substrate (black). During drying, the water layer wavefront passes over the surface and causes detachment of the  $L_d$  phase (red).  $L_o$  phase (green), which has a stronger affinity to the mica substrate, stays unperturbed for a longer time. With time both phases pill off the solid support. Dried SLB (rightmost image) contains aggregates composed of both phases (yellow spots, marked with white arrows).

**Figure S2**

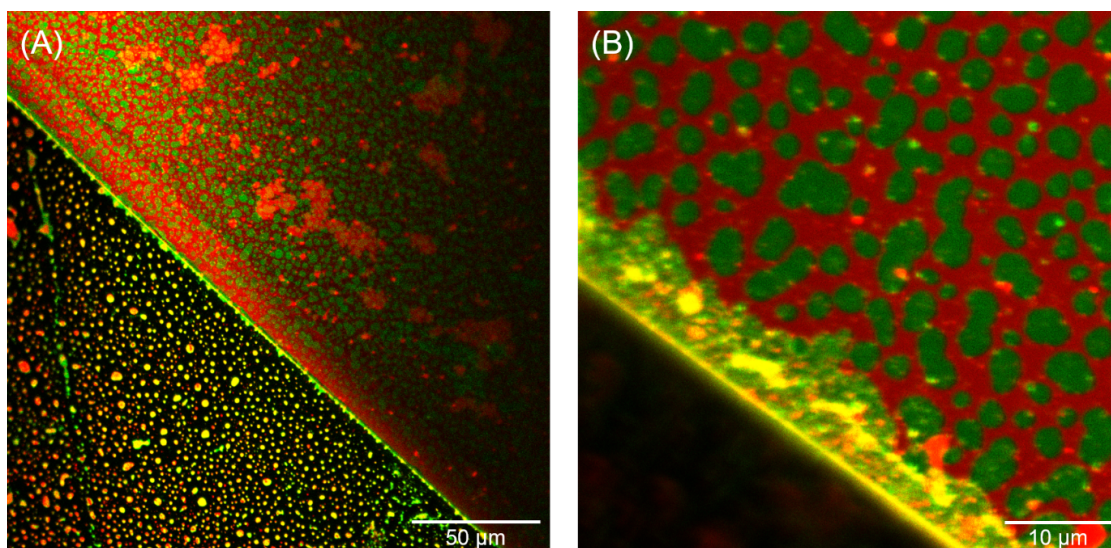
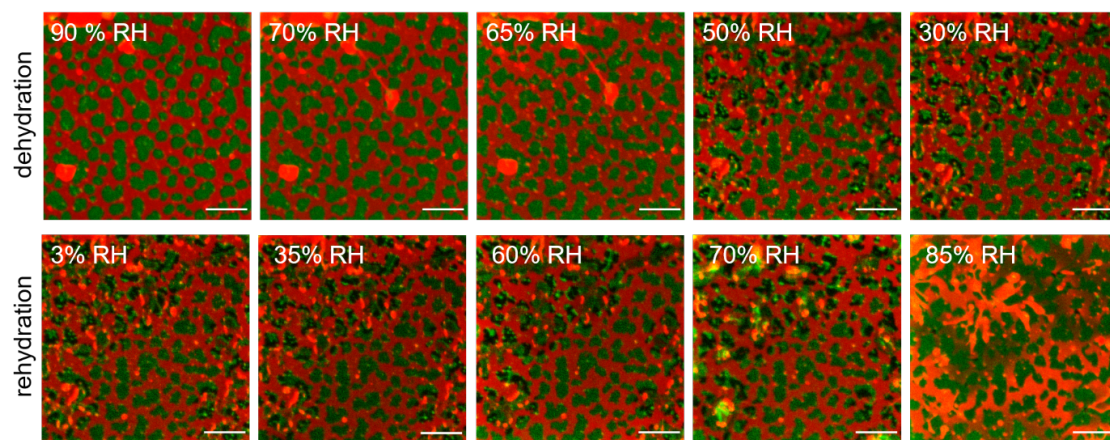


Fig. S2. The presence of defects of the solid support (mica cleaving-induced defects) can influence membrane stability upon rapid dehydration. Mica terraces stop the drying water front and act as an obstruction preventing the membrane from delamination. (A) Membrane curls up in the bottom-left part of the image, forming vesicles and aggregates (orange and yellow), and remains unperturbed in the upper-right part section of the image, (B) Close-up image of the border between the two regions. During dehydration, the dragged lipids were deposited by the moving water front along with the defect. In case of rapid dehydration, the membrane curls up in the absence of the mica terraces, which act as mechanical obstruction. In stark contrast, during controlled dehydration membrane remains unperturbed irrespective of the presence of the mica terrace as shown in Figure S3 and S4.



**Figure S3**

**Area 1**



**Area 2**

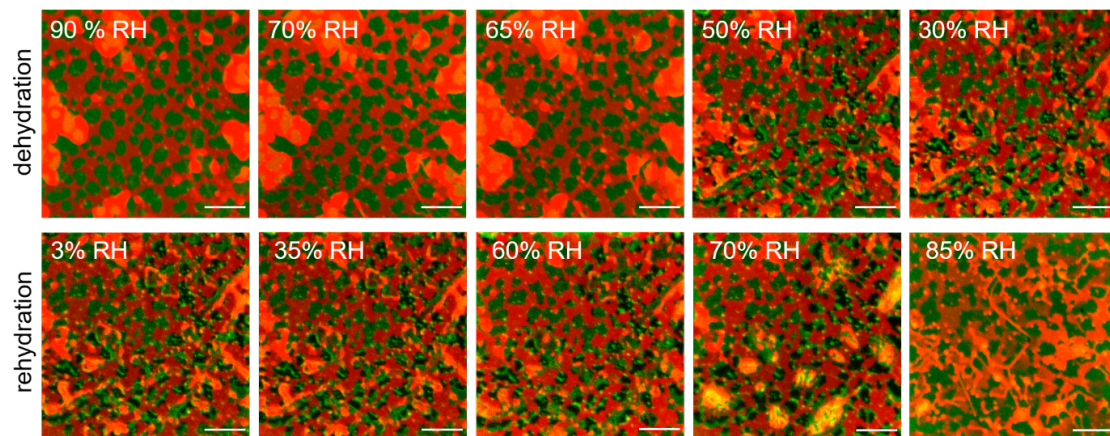


Fig. S3. Consecutive fluorescence images of two different areas (area 1 and area 2) of SLB during dehydration (top row) and rehydration (bottom row). At the humidity of around 50% RH and lower, in some areas of the membrane, local aggregation of the GM1-CTxB occurs, which is visible as the formation of darker and brighter spots within the  $L_o$  domains. At about 50% RH aggregates (orange and yellow) accumulated on top of the membrane break into smaller ones. During rehydration,  $L_o$  domains regain homogeneous CTxB distribution (and hence homogeneous fluorescence signal) at about 85% RH. The scale bar is 10  $\mu$ m.

**Figure S4**

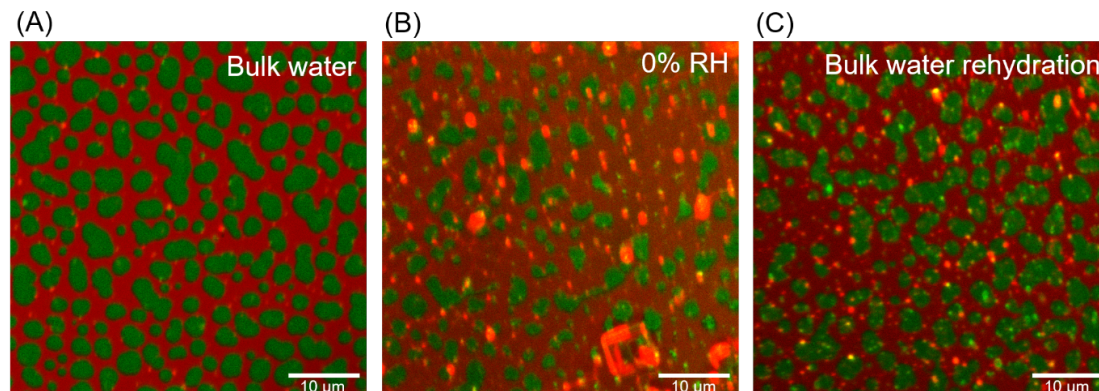


Fig. S4. Confocal images of the same sample recorded at different hydration conditions: (A) right after preparation, full hydration with bulk water, (B) slowly dehydrated by decreasing the humidity level and kept at 0% RH, (C) slowly rehydrated and refilled with bulk water. Membrane structure remains unaffected after a complete cycle of de(re)hydration.

**Figure S5**

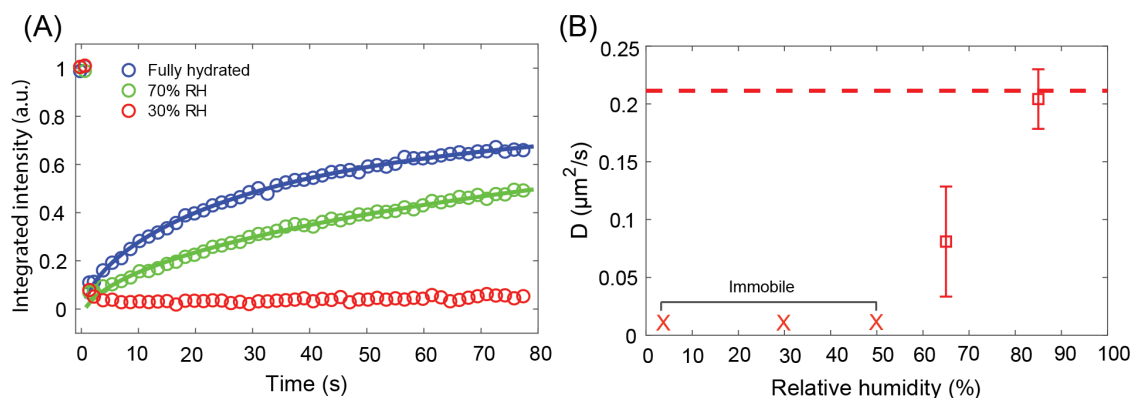
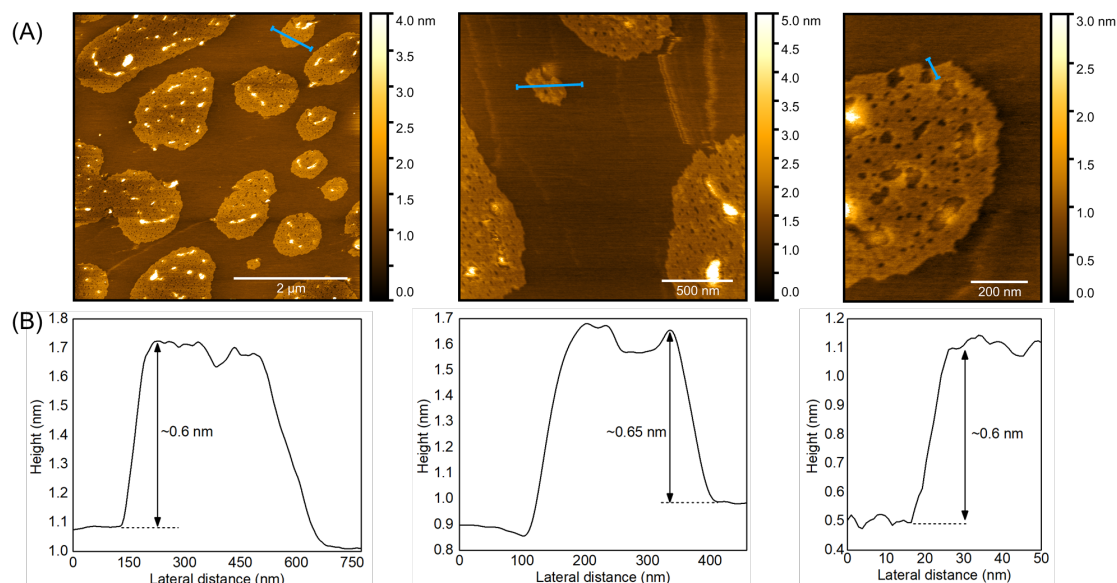


Fig. S5. FRAP traces and diffusion coefficient of the  $L_o$  phase labeled with TopFluor cholesterol as a function of membrane hydration. The single component membrane was composed of only SM and cholesterol with the same ratio as in the phase separated membranes (1:1 molar ratio). (A) FRAP traces of the fully hydrated SLB and SLB equilibrated at 70% and 30% relative humidity. (B) The diffusion coefficient for the  $L_o$  phase for SLB at different relative humidity during dehydration. The red dashed line corresponds to the diffusion coefficient of the  $L_o$  phase at full hydration conditions (bulk water hydration). FRAP traces for lipid membrane at 50%, 30% and 3% RH could not be reliably fitted due to the lack of fluorescence recovery. Values of diffusion coefficient for these hydration conditions are indicated here as immobile (red X). Notably, the changes of the diffusion coefficient as a function of hydration exhibit the same trend as those presented for the  $L_d$  phase (see Fig. 3B), indicating that both phases respond to the dehydration process in a similar manner.

**Figure S6**



**Fig. S6.** AFM images of dehydrated SLB. (A) Topography scans confirming intact membrane with continuous  $L_d$  phase at dehydrated condition. Presence of nanoscopic depressions with a depth of  $\sim 0.5$ - $0.7$  nm is noticed in  $L_o$  phase domains. Given the same height difference as between the  $L_o$  and  $L_d$  phases, these depressions correspond to  $L_d$  nanodomains trapped in the  $L_o$  phase. A similar effect was observed for ceramide-rich membranes, where due to lower line tension of the  $L_o$  phase,  $L_d$  nanodomains participated in the  $L_o$  domains<sup>1</sup>. Elevated features with the height of  $\sim 6$  nm (from the average surface height of  $L_o$  domains) correspond to the GM1-CTxB complexes. Scale bars are  $2\ \mu\text{m}$ ,  $0.5\ \mu\text{m}$  and  $0.2\ \mu\text{m}$  for the left, middle and rightmost image, respectively. (B) Cross-sections profiles highlighting the height difference between the  $L_d$  and  $L_o$  phase (marked by blue lines in panel A).



**Figure S7**

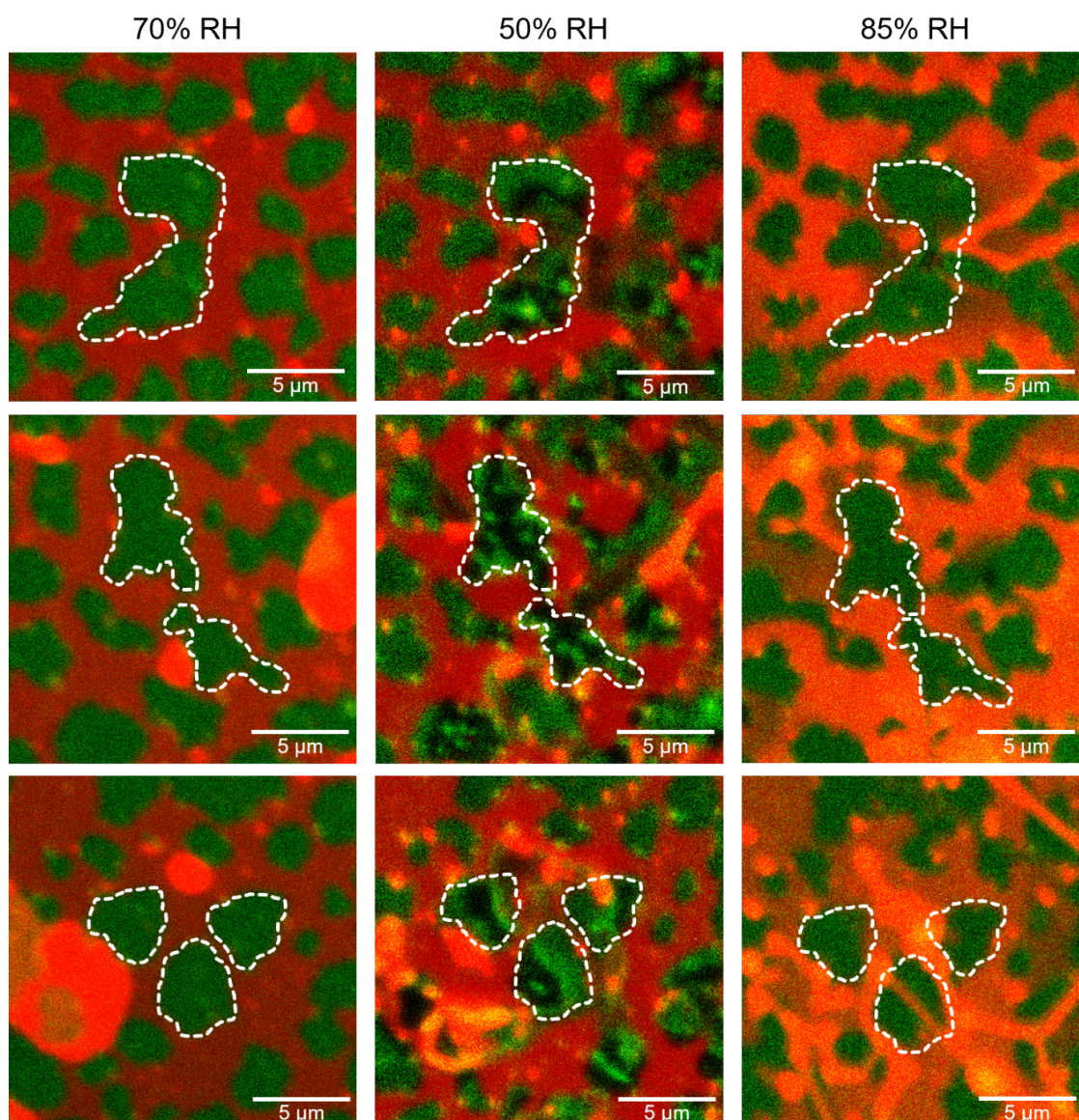


Fig. S7. SLB consisting of  $L_d$  (red) and  $L_o$  (green) phase exposed to the relative humidity of 70% and 50% (during dehydration) and 85% (during rehydration). The white, dashed lines mark the outlines of the domains. The shape and area of the domains during the dehydration and rehydration processes remain largely the same. The GM1-CTxB complexes aggregate at around 50% RH but upon rehydration redistribute again evenly within the whole domain.



Figure S8

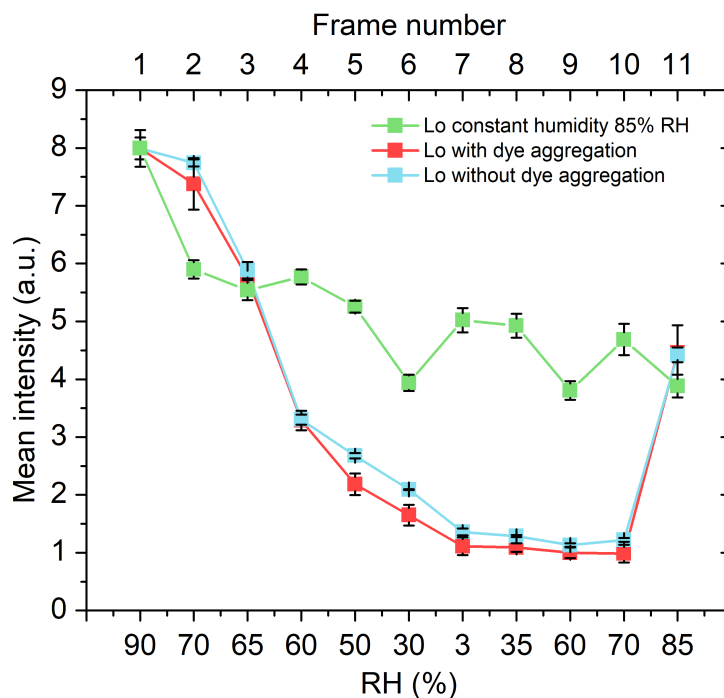


Fig. S8. Changes in the mean intensity of the  $L_o$  domains with de(re)hydration. Green trace reflects the native fluorescence bleaching of the Alexa Fluor 488 dye caused by the consecutive imaging of the SLB exposed to the constant humidity of 85% RH. The mean intensity is plotted as a function of frame number (top x-scale). Red trace shows the changes in the fluorescence intensity of the domain showing aggregation of the GM1-CTxB complexes during dehydration and rehydration. Light blue trace represents the changes in the domain intensity for a domain that did not show any aggregation of the GM1-CTxB complex. The overall fluorescence intensity for the domains with and without the aggregation changes in the same manner but it shows a more rapid intensity decrease than for the sample kept in constant humidity. Upon rehydration, at 75-85% RH, the fluorescence of the domain is restored. The final mean intensity of the fluorescence after taking 11 images at constant humidity is the same as after the whole de-/rehydration cycle. Evidently, the strong decrease in fluorescence of the Alexa Fluor 488 dye is due to the lower quantum efficiency of the dye at lower hydration and not solely due to photobleaching of the dye. Lipid domains were analyzed using ImageJ software by measuring the mean intensity from the chosen  $L_o$  domains (three showing GM1-CTxB aggregation and three with homogeneous GM1-CTxB distribution). Intensities were normalized with respect to their initial value.

**Figure S9**

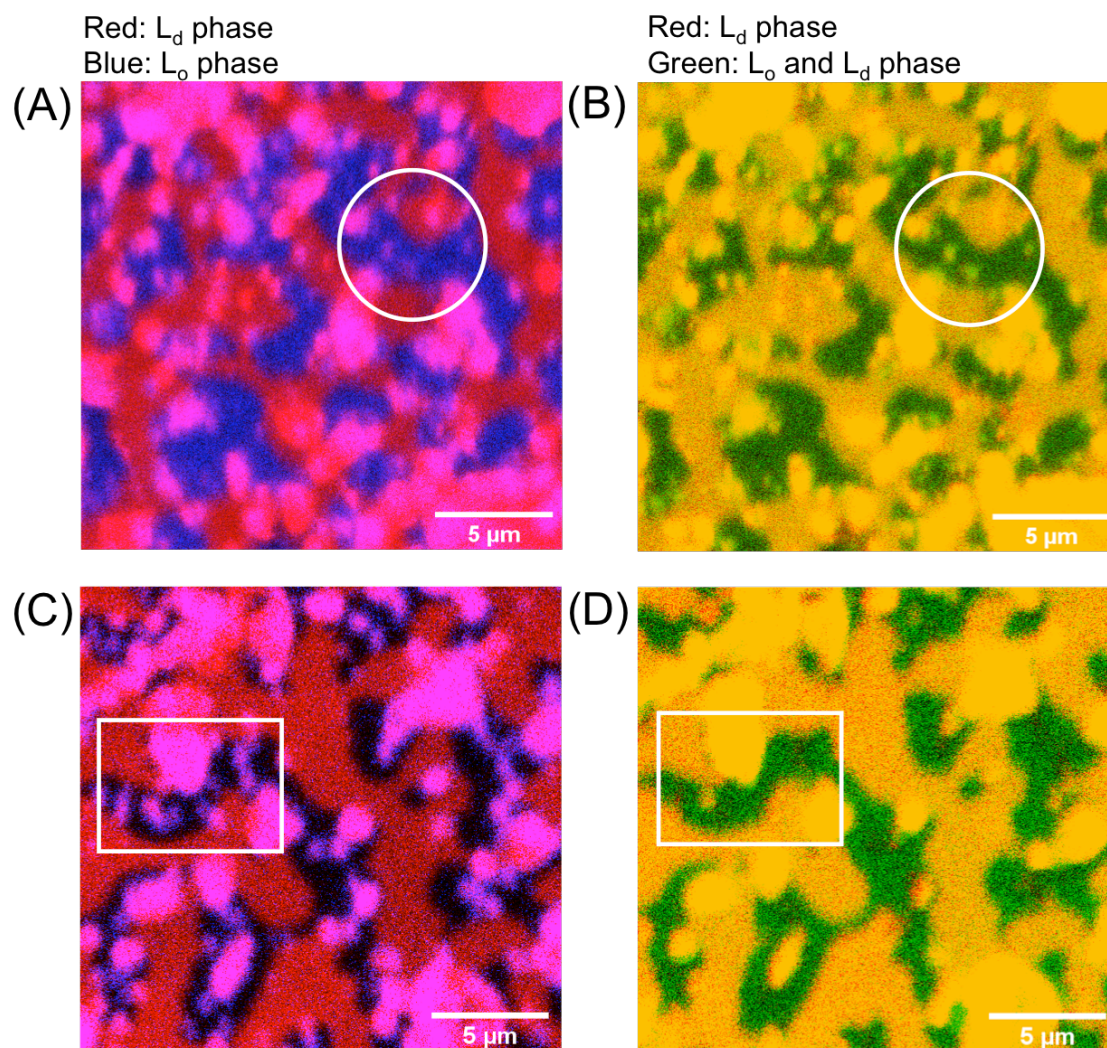


Fig. S9 Confocal images of two areas of SLB equilibrated at low relative humidity (~30% RH), where L<sub>o</sub> domains show homogeneous (top row, A-B) and inhomogeneous (bottom row, C-D) distribution of the GM1-CTxB. (A, C) L<sub>d</sub> phase is labeled with Atto-633-DOPE (red) and L<sub>o</sub> phase is labeled with CTxB-Alexa594 (blue). (B, D) L<sub>d</sub> phase is labeled with Atto-633-DOPE (red), while cholesterol, which partitions in both L<sub>d</sub> and L<sub>o</sub> phase is labeled with the TopFluor dye (green). L<sub>d</sub> phase appear yellow in panels B and D, as it overlaps homogeneously with the green signal assigned to the cholesterol label. It is clear that, while in some areas GM1-CTxB tends to aggregate leaving dark (no fluorescence) spots within the L<sub>o</sub> domains (panel C, white rectangle), the structure of the L<sub>o</sub> domains themselves remains intact. This is evident from the unperturbed, homogeneous distribution of the cholesterol-TopFluor (panels B, D).

**Figure S10**

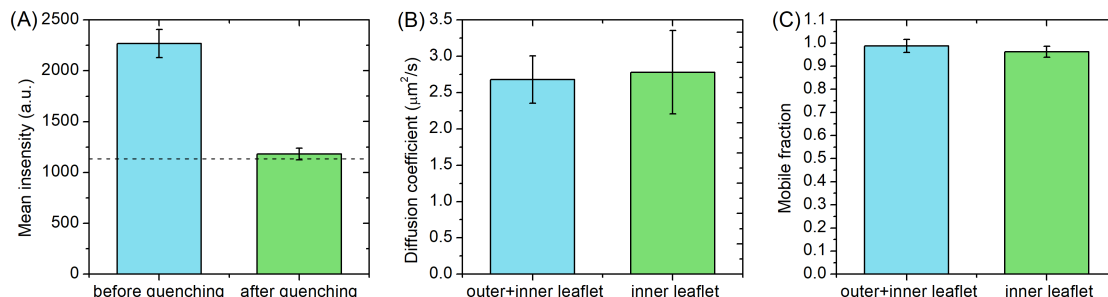


Fig. S10 Analysis of the mobility of outer and inner leaflet at fully hydrated condition. (A) Mean fluorescence intensity averaged over 10 confocal images for the bilayer (blue bar, indicated here as “before quenching”), and for the inner leaflet only (green bar, described as “after quenching”), obtained after the dithionite quenching of the NBD-labeled lipids. The dashed, black line indicates 50% level of the mean fluorescence intensity before quenching. The mean intensity shows a 2-fold decrease (green bar) upon addition of sodium dithionite. (B) Diffusion coefficient of  $L_d$  phase for both outer (upper) and inner leaflet (lower/support facing) and for inner leaflet only, averaged over 6 FRAP traces. (C) Mobile fraction of  $L_d$  phase for both leaflets (blue) and for inner leaflet only (green) - values were averaged over 6 FRAP traces. These observations confirm that both outer and inner leaflets behave in similar way for our system at fully hydrated condition.

**Figure S11**

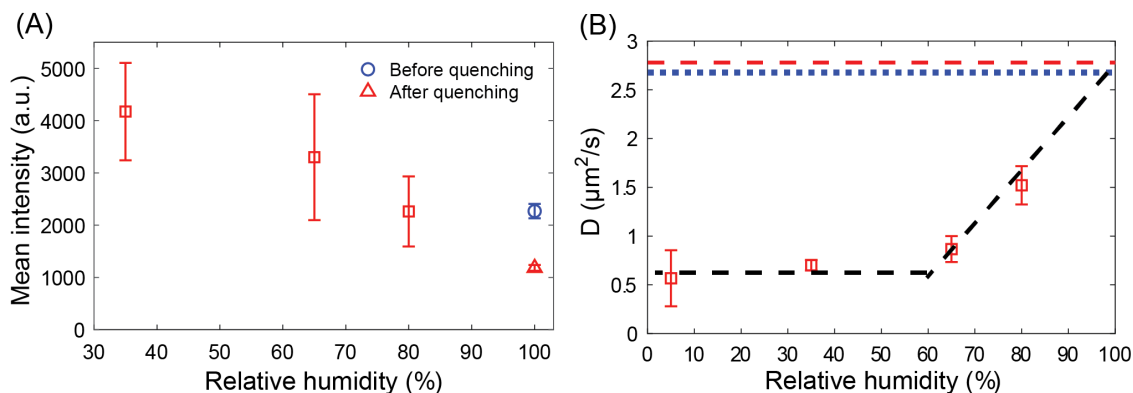


Fig. S11 Mean intensity of SLB with quenched upper leaflet and mobility of the lower leaflet as a function of hydration. (A) The mean intensity of the SLB decreases by a factor of two upon dithionite addition (as described in S10). Upon dehydration mean intensity of SLB with quenched upper leaflet increases as the quantum yield of NBD dye increases at dehydrated conditions<sup>2,3</sup>. (B) The diffusion coefficient of the inner leaflet as a function of hydration condition.  $D$  was averaged over 6 FRAP traces at each hydration level. The blue dashed line shows the average diffusion coefficient for the bilayer at fully hydrated condition. The red dashed line corresponds to the average diffusion coefficient at full hydration for the inner leaflet only. Change in diffusion coefficient for the lower leaflet during dehydration follows the same trend as for full bilayer.

**References:**

- (1) Kol, M.; Williams, B.; Toombs-Ruane, H.; Franquelim, H. G.; Korneev, S.; Schroeer, C.; Schwille, P.; Trauner, D.; Holthuis, J. C.; Frank, J. A. Optical Manipulation of Sphingolipid Biosynthesis Using Photoswitchable Ceramides. *Elife* **2019**, *8*.
- (2) Mazères, S.; Schram, V.; Tocanne, J. F.; Lopez, A. 7-Nitrobenz-2-Oxa-1,3-Diazole-4-Yl-Labeled Phospholipids in Lipid Membranes: Differences in Fluorescence Behavior. *Biophys. J.* **1996**, *71*, 327–335.
- (3) Fery-Forgues, S.; Fayet, J. P.; Lopez, A. Drastic Changes in the Fluorescence Properties of NBD Probes with the Polarity of the Medium: Involvement of a TICT State? *J. Photochem. Photobiol. A Chem.* **1993**, *70*, 229–243.

## Chapter 8

# Sensing hydration of biomimetic cell membranes

Transient, local dehydration is one of the crucial steps in various biological processes such as the adsorption of macromolecules, membrane fusion events, viral entry, neurotransmission, fertilization or exocytosis, just to give a few examples. A certain amount of hydration force has to be overcome during the fusion of two membranes, where the two separate lipid layers come in contact, expelling the hydration layer from the lipid layers interface. Consequently, quantification of the local hydration state in terms of the number of water molecules per lipid for the intermediate

steps is very crucial for the molecular-level understanding of such biological processes. In Publication 2, I studied the hydration dependence of the lipid mobility of single phase (single component) PC lipid (14:1 PC). Using FRAP technique, I showed that similarly to phase-separated membranes, the diffusion coefficient for PC lipids in single component membranes decreases with dehydration down to 50% RH and then remains stable at very low values. With an increase in hydration level,  $D$  also increases back following the same trajectory. With the repetition of dehydration and rehydration cycles for a few times, I established that changes of the  $D$  value are completely reversible and repeatable. This confirms that there is a strong correlation between the lateral diffusion of lipids and the availability of water molecules per lipid and that the lipid-lipid interactions are instantaneously responsive to the changes of the hydration properties of their direct surrounding. Given the correlation between the number of water molecules present per lipid molecule and the hydration (read RH) level of the membrane, precise measurement of the diffusion coefficient forms a basis for an unprecedented method for sensing the local hydration state of biomembranes with a precision down to about 2-3 water molecules per lipid. This methodology of hydration sensing provides a basis for determining a complete, step-wise map of hydration structure and interpretation of (de)hydration-mediated processes in lipid membranes. Importantly, the approach of hydration sensing through lateral diffusion is not limited only to FRAP technique, but can be easily extended to other diffusivity-oriented measurement techniques such as FCS or SPT. The above results and the perspective of the hydration sensing approach were published in the Biosensors journal (publication 2), which is attached below for detailed reading. Moreover, together with my co-workers, I filed two patent applications (pending) related to the hydration sensing methodology.

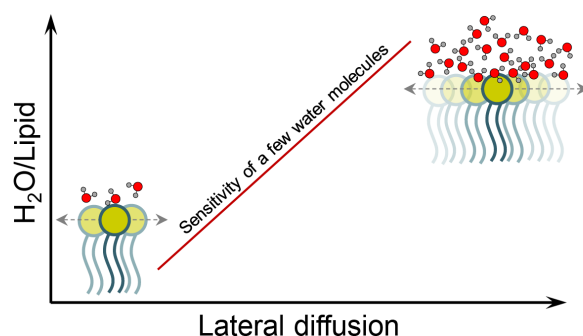


Figure 8.1: Schematic representation of hydration sensing approach of lipids in lipid membranes.





## Article

## Sensing Hydration of Biomimetic Cell Membranes

Madhurima Chattopadhyay <sup>\*,†</sup>, Hanna Orlikowska <sup>†</sup> , Emilia Krok and Lukasz Piatkowski <sup>\*</sup>

Faculty of Materials Engineering and Technical Physics, Institute of Physics, Division of Molecular Physics, Poznan University of Technology, Piotrowo 3, 60-965 Poznan, Poland; hanna.orlikowska@put.poznan.pl (H.O.); emilia.krok@put.poznan.pl (E.K.)

<sup>\*</sup> Correspondence: madhurima.chattopadhyay@put.poznan.pl (M.C.); lukasz.j.piatkowski@put.poznan.pl (L.P.)

<sup>†</sup> These authors contributed equally to this work.

**Abstract:** Biological membranes play a vital role in cell functioning, providing structural integrity, controlling signal transduction, and controlling the transport of various chemical species. Owing to the complex nature of biomembranes, the self-assembly of lipids in aqueous media has been utilized to develop model systems mimicking the lipid bilayer structure, paving the way to elucidate the mechanisms underlying various biological processes, as well as to develop a number of biomedical and technical applications. The hydration properties of lipid bilayers are crucial for their activity in various cellular processes. Of particular interest is the local membrane dehydration, which occurs in membrane fusion events, including neurotransmission, fertilization, and viral entry. The lack of universal technique to evaluate the local hydration state of the membrane components hampers understanding of the molecular-level mechanisms of these processes. Here, we present a new approach to quantify the hydration state of lipid bilayers. It takes advantage of the change in the lateral diffusion of lipids that depends on the number of water molecules hydrating them. Using fluorescence recovery after photobleaching technique, we applied this approach to planar single and multicomponent supported lipid bilayers. The method enables the determination of the hydration level of a biomimetic membrane down to a few water molecules per lipid.

**Keywords:** hydration; lipid mobility; lateral diffusion; FRAP; model biomembrane; solid supported lipid bilayer; biological water; hydration sensing



**Citation:** Chattopadhyay, M.; Orlikowska, H.; Krok, E.; Piatkowski, L. Sensing Hydration of Biomimetic Cell Membranes. *Biosensors* **2021**, *11*, 241. <https://doi.org/10.3390/bios11070241>

Received: 31 May 2021

Accepted: 6 July 2021

Published: 16 July 2021

**Publisher's Note:** MDPI stays neutral with regard to jurisdictional claims in published maps and institutional affiliations.



**Copyright:** © 2021 by the authors. Licensee MDPI, Basel, Switzerland. This article is an open access article distributed under the terms and conditions of the Creative Commons Attribution (CC BY) license (<https://creativecommons.org/licenses/by/4.0/>).

## 1. Introduction

Phospholipid membranes are indispensable architectural components of cells, subcellular compartments, and nanometer-sized biological objects such as exosomes or viruses [1]. The basic role of biological membranes is to define boundaries and enable compartmentalization of different parts of the cell, thus fulfilling a fundamental condition for the existence of life [2]. Besides providing structural integrity, biological membranes carry out a variety of other important functions, including but not limited to, mediating and modulating the transport of ions and sugars, regulating the permeability of nonelectrolytes, and facilitating signal transduction and metabolic reactions [3,4].

Lipids, due to their amphiphilic nature, spontaneously self-assemble in the aqueous environment. This efficient self-organization has been widely used to mimic the essential lipid bilayer structures of biological systems in both basic and applied research. Bilayers in the form of black lipid membranes, vesicles (free-standing or tethered to supports), and planar supported bilayers (interacting directly with a solid substrate or tethered to the substrate) are commonly used as biomimetic membranes [5]. Such model systems, on the one hand, preserve the essential characteristic of the lipid bilayer and, on the other hand, simplify the biological membrane system so that the roles of the individual membrane components, as well as their organization and dynamics, can be effectively explored. Consequently, the use of biomimetic membranes, often integrated with functional proteins, has proven to be a powerful tool used in drug screening [6–8] and delivery

systems [9,10], artificial cell design [11], nanoreactors [12,13], biosensors [14–16], and the most commercially developed water purification applications [17–19], to name just a few spectacular examples from the very long list reported in the literature.

Essential to the activity of biological and biomimetic membranes are their hydration properties, in which water molecules form partially ordered structures due to dipole interactions and hydrogen bonding with the membrane [20–22]. Of particular interest, yet remaining elusive, is the local, temporary membrane dehydration, which is believed to be one of the crucial steps in various biological processes such as adsorption of biomacromolecules or membrane fusion events. Membrane fusion constitutes a central mechanism in phenomena involving subcellular compartmentalization, cell growth, hormone secretion, neurotransmission, fertilization, viral entry, and exocytosis [1,23]. A certain amount of hydration barrier has to be overcome to initiate the hydrophobic interactions between the two fusing bilayers. To understand the molecular-level mechanism of these cellular processes, information about the local hydration state (i.e., the number of water molecules hydrating a lipid headgroup) of the membrane components at each intermediate step is very important.

For the investigation of phospholipid membrane hydration, different experimental methods have been applied. Among the most widely used, one can mention nuclear magnetic resonance spectroscopy [24], X-ray [25] and neutron [26] diffraction, dielectric relaxation spectroscopy [27,28], quartz crystal microbalance measurements [29], linear and nonlinear infrared spectroscopy [30,31], and various fluorescence microscopy approaches [32–34], often combined with the theoretical simulations [22,35]. In particular, fluorescence methods are convenient tools for studying lipid membranes due to the existence of the ever-expanding palette of fluorescent probes and techniques that allow for data collection over a wide range of spatial and temporal scales. Fluorescence studies aimed at understanding the local hydration state of the lipid membrane rely on dedicated fluorophores, whose spectroscopic and photophysical properties depend on the microenvironment (so-called environment-sensitive probes), and in particular, on the polarity of the immediate environment in which they are located [33]. As such, various fluorescence-based techniques have flourished such as fluorescent solvent relaxation [36–38], general polarization [39], and red edge excitation shift [40,41]. Although these techniques provide important information about the lipid bilayer hydration, they pose two major inconveniences, namely the need to know the precise probe location and the challenging process of data correlation, both crucial for drawing valuable conclusions [42,43]. Consequently, it is clear that a novel experimental approach towards molecular-level sensing of local hydration conditions of lipid membranes is needed.

Here, we present a new approach to gain insight into the hydration state of the lipid membranes. It is based on measuring the change in the lateral diffusion coefficient of lipids forming a bilayer, which is dependent on the number of water molecules hydrating the lipids. We illustrate and validate the method using fluorescence recovery after photobleaching (FRAP) technique applied to a planar solid-supported lipid bilayer (SLB). Our approach exhibits sensitivity at the quasi-single molecule level, enabling the determination of the hydration level of a biomimetic membrane down to a few water molecules per lipid. This new approach has the potential to reveal the local heterogeneity in hydration of biomimetic and biological lipid membranes, and thus sheds light on the processes incorporating changes in membrane hydration, such as membrane fusion.

## 2. Materials and Methods

### 2.1. Materials

1,2-dimyristoleoyl-sn-glycero-3-phosphocholine (DMoPC), egg yolk sphingomyelin (SM), and cholesterol were purchased from Avanti Polar Lipids (Alabaster, AL, USA). 1,2-dioleoyl-sn-glycero-3-phosphoethanolamine (DOPE) labeled with Atto 633, sodium chloride (NaCl), and chloroform (HPLC grade) were purchased from Merck KGaA (Darmstadt, Germany). 4-(2-hydroxyethyl)piperazine-1-ethanesulphonic acid (HEPES PUFFERAN®)

was obtained from Carl Roth GmbH&Co KG (Karlsruhe, Germany). Calcium chloride ( $\text{CaCl}_2$ ) was purchased from P.P.H. STANLAB sp. j., Lublin, Poland. Optical adhesive glue Norland 68 was purchased from Thorlabs Sweden AB (Mölnådal, Sweden). All the materials were used without further purification. The ultrapure water ( $\text{ddH}_2\text{O}$ ) was obtained by using Milli-Q reference water purification system from Merck KGaA (Darmstadt, Germany).

## 2.2. Methods

### 2.2.1. SLB Preparation

SLBs were prepared by a widely used vesicle deposition method [44] with required modification. For single component SLBs, 10 mM solution of DMOPC was prepared in chloroform along with 0.1 mol% of DOPE-Atto 633. DMOPC, egg SM, and cholesterol were mixed in 1:1:1 molar ratio with an overall 10 mM lipid concentration, along with 0.1 mol% of Atto-633-DOPE, for the preparation of phase-separated SLBs. The chloroform was evaporated by dry nitrogen gas depositing a thin film of lipid at the bottom of the glass vial followed by vacuum desiccation for a minimum of 2 h. After complete evaporation of the organic solvent, a 10 mM suspension of DMOPC multilamellar vesicles (MLVs) was prepared by dissolving the lipid film in a suitable amount of 10 mM HEPES with 150 mM NaCl buffer, adjusted to pH 7.4. The solution was vigorously vortexed and heated to 60 °C to obtain a homogeneous suspension of MLVs. Aliquots of 1 mM lipid concentration were prepared by diluting the solution 10 times with the previously mentioned buffer solution and stored at −20 °C in sterilized glass vials for further use. In order to obtain small unilamellar vesicles (SUVs) from MLVs, the aliquoted lipid solution was bath-sonicated for at least 10 min until the solution became clear. A thin sheet of freshly cleaved mica was glued to a coverslip using UV-activated glue Norland 68. A half-cut Eppendorf tube was attached and sealed with silicone adhesive on top of the coverslip. At room temperature, 100 µL of 1 mM SUVs solution was deposited on mica followed by immediate addition of 0.2 µL of 0.1 M  $\text{CaCl}_2$  in a buffer. After 30 s, 400 µL of HEPES-NaCl buffer (pH adjusted to 7.4) was added to the sample to prevent drying out of the SLB. The sample was incubated for 30 min at room temperature and then rinsed multiple times with a total of 20 mL of buffer solution. To obtain a fully hydrated sample, the Eppendorf tube sample reservoir was completely filled with buffer, closed with another coverslip, and sealed by silicone adhesive.

### 2.2.2. SLBs Hydration State Control

Precise control over the hydration state of the sample was achieved using a home-built humidity control set-up. Nitrogen gas of desired relative humidity (RH) was purged inside the open half-cut Eppendorf tube of the sample. The relative humidity of the nitrogen gas was regulated by mixing wet (~90% RH) and dry (2%–3% RH) nitrogen with a suitable ratio. The flows of wet and dry  $\text{N}_2$  gas were individually adjusted using two manual valves while monitoring the readings shown in the two flowmeters connected to the wet and dry  $\text{N}_2$  flow paths. A third flowmeter along with a manual valve were used to keep the final flow of  $\text{N}_2$  gas constant at ~1.2 L/min throughout the experiment. An electronic hygrometer (0%–95% RH range and 1% precision) was employed to record the RH and temperature of the final flow purged towards the sample, and it also created a feedback loop for adjusting the amount of wet and dry  $\text{N}_2$  gas. The silicone seal of the fully hydrated sample was cut and the buffer was pipetted out completely followed by immediate purging of  $\text{N}_2$  gas of 90% RH. FRAP measurements were taken for SLBs equilibrated to 90%, 70%, 50%, 30%, and 0% RH at constant temperature. The dehydration and rehydration were performed in steps of ~20% RH with change rate of 2%–3% RH/min. The sample was rehydrated in a similar manner that is by purging  $\text{N}_2$  gas and increasing its RH. Finally the sample was again filled with buffer and sealed to obtain bulk rehydration of the sample.



### 2.2.3. FRAP Experiments

Zeiss LSM 710 (Carl Zeiss, Jena, Germany) microscope with 40 $\times$ , 1.3 NA oil immersion objective was used for confocal imaging and FRAP experiments. Atto-633 was excited by a laser with a 633 nm wavelength. Laser power was adjusted to a minimum to avoid excessive overall photobleaching of the sample during measurements. For FRAP experiments, a selected circular spot of 10  $\mu\text{m}$  diameter within a 50  $\mu\text{m}$   $\times$  50  $\mu\text{m}$  area was instantaneously bleached with maximum laser power in every measurement. In the experiment 100 consecutive fluorescence images of the same area were recorded with 0.5 s intervals. The data were analyzed using MATLAB software and the diffusion coefficient was determined considering free Brownian lateral diffusion of lipid molecules in the membrane, by fitting the fluorescence recovery curve using modified Soumpasis Formula (1) [45]:

$$F(t) = b + a \cdot f(t), \quad (1)$$

where  $a$  is the amplitude of the recovery function,  $b$  is the remaining fluorescence after bleaching, and  $f(t)$  is the Soumpasis function. The FRAP traces were normalized taking the overall fluorescence intensity signal of the image except the bleached spot as the reference. FRAP experiments were performed on one representative single component and one phase-separated SLB throughout complete dehydration-rehydration cycles. A minimum of 5 FRAP measurements at various areas of the samples were recorded at a particular RH for each sample.

## 3. Results

### 3.1. Measurement and Analysis of Diffusion Coefficient of Lipids at Different Hydration Conditions

In this study, lateral diffusion of DMOPC in single component SLB as well as in phase-separated DMOPC/egg SM/cholesterol 1:1:1 SLB was investigated by FRAP experiments at different hydration conditions, starting from fully hydrated to membrane equilibrated to ~0% RH. In order to achieve the desired hydration state, the SLBs, immediately after removal of bulk water from the sample, were carefully equilibrated to the atmosphere of a nitrogen gas of specific relative humidity using our home-built hydration control unit. SLBs dehydrated by this method can withstand multiple dehydration-rehydration cycles without experiencing major structural damage [46].

The representative confocal images, selected from the FRAP measurement series of single component SLB at pre-bleached, bleached, and recovered (completely or partially) conditions are shown in Figure 1. Clearly, remarkable differences in bleaching depth and recovery of fluorescence intensity within the bleached spot are observed. FRAP experiments are based on measuring the recovery of fluorescence intensity in the bleached area that is caused by lateral Brownian motion due to the reorganization of bleached and non-bleached lipid molecules [45]. The dehydrated membrane showed higher bleaching depth and slower fluorescence intensity recovery (Figure 1b) than a fully hydrated one (Figure 1a). Thus, it can be concluded that there is a vivid decline in lateral mobility of lipids in the absence of full hydration of membrane constituents. This observation is clearly reflected in the FRAP traces for fully hydrated and dehydrated (~30% RH) membranes, as shown in Figure 2a,c, for single component and phase-separated SLBs, respectively. In the case of fully hydrated membranes, the fluorescence intensity recovers up to  $95 \pm 2\%$  of the initial intensity within ~50 s after bleaching, whereas more than 50% fluorescence recovery is scarcely achieved for dried SLBs within the same time frame. For a detailed investigation of the dependence of the lateral diffusion ( $D$ ) of lipids on hydration conditions, diffusion coefficients of DMOPC were measured for single component and phase-separated SLBs at various relative humidity levels, starting from fully hydrated to ~0% RH via 85%, 65%, 45%, and 30% RH. The SLBs were rehydrated subsequently by increasing RH levels in steps up to ~85%, and they were finally rehydrated fully with the addition of bulk water. Figure 2b,d depicts the diffusion coefficients of DMOPC during a complete dehydration and rehydration cycle for single component and phase-separated SLBs, respectively, averaged

over at least five FRAP traces from various spots of the sample at a particular RH level. It should be duly noted that the absolute mobility of liquid-disordered ( $L_d$ ) phase lipids in phase-separated membranes is significantly lower than in pure  $L_d$  phase, single component membranes, as part of  $L_o$  lipids and cholesterol partition into the  $L_d$  phase, thus increasing the order and viscosity [47].

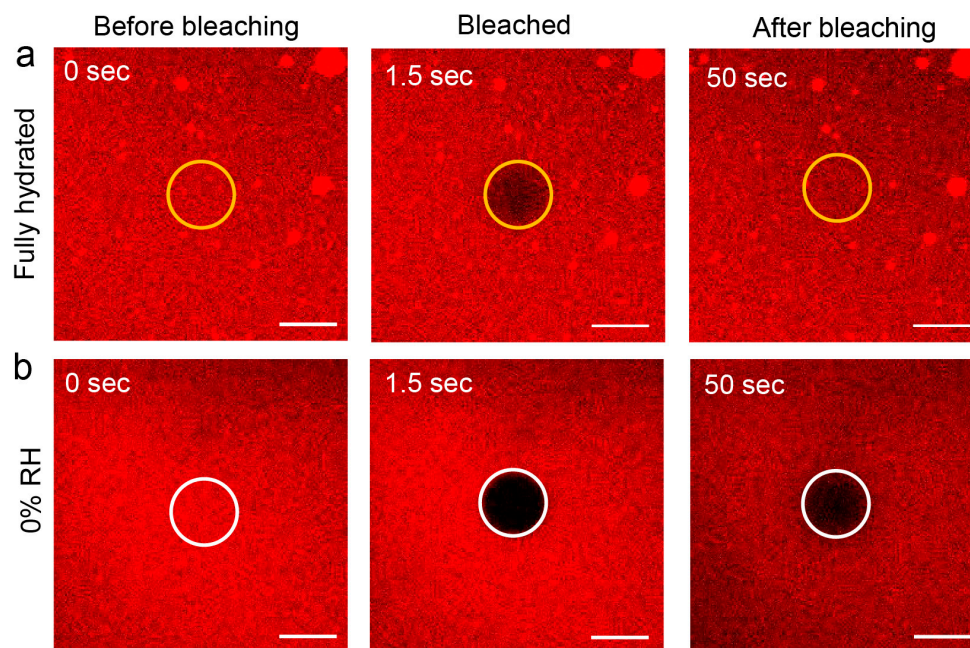


**Figure 1.** Representative confocal images from the FRAP experiment for a fully hydrated, single component SLB (a) and SLB exposed to 0% RH (b). The areas marked by yellow (a) and white (b) circles denote the spot of 10  $\mu\text{m}$  diameter that was bleached during FRAP measurements. In case of fully hydrated sample (a), the bleached area completely regained its fluorescence within 50 s, while for sample exposed to 0% RH (b), the spot remained largely bleached after 50 s. The scale bars correspond to 10  $\mu\text{m}$ .

At the fully hydrated condition, the diffusion coefficients of DMoPC in a single component and phase-separated SLBs were found to be  $5.35 \pm 0.79 \mu\text{m}^2/\text{s}$  and  $1.66 \pm 0.22 \mu\text{m}^2/\text{s}$ , respectively. A roughly 3.5-fold higher  $D$  explains the shallower bleaching of fully hydrated single component SLB compared to the phase-separated one (see Figure 2a,c). In spite of the difference in absolute values of diffusion coefficients of lipids for both systems, the change of lateral diffusion followed an analogous trend with dehydration and subsequent rehydration. A strong correlation between the lipid mobility and the relative humidity of the sample environment was observed. The  $D$  of DMoPC in the single component SLB steadily dropped down from  $4.75 \pm 1.14 \mu\text{m}^2/\text{s}$  to  $0.25 \pm 0.18 \mu\text{m}^2/\text{s}$  as the hydration of the atmosphere was lowered from  $\sim 85\%$  RH to  $\sim 0\%$  RH. Likewise, in phase-separated SLBs, a sharp downfall of  $D$  was noticed from  $1.52 \pm 0.08 \mu\text{m}^2/\text{s}$  at  $\sim 85\%$  RH to  $0.04 \pm 0.01 \mu\text{m}^2/\text{s}$  at  $\sim 0\%$  RH. This firmly indicates that water molecules attached to the polar head group of the lipid molecules play a key role in modulating the lateral movement of lipids. Interestingly, with consecutive rehydration, lipid mobility increased back following the same trend as during dehydration, with relatively lower absolute values of  $D$ . However, with bulk rehydration, the lipids regained their natural mobility, which is the same as for fully hydrated conditions measured before de- and rehydration. Thus, from fully hydrated to fully rehydrated conditions,  $D$  changes reversibly with change in native hydration state of the membrane. The strong dependence of  $D$  on the membranes' hydration state can be associated with a reversible change in the local hydration structure around the lipid head group caused by de(re)hydration [46]. Furthermore, it is clearly

evident from Figure 2b,d that the most dramatic change of  $D$  values took place in the range of 100–50% RH; lowering the relative humidity below this range hardly affected the lateral diffusion of lipids. This breaking point at ~50% RH can be correlated with the breaking of clathrate cage structure around the phosphocholine group of DMOPC molecule [46]. We note that at the salt concentrations used in the buffer for experiments (10 mM HEPES and 150 mM NaCl), lipid diffusion remained unaffected by the change in ionic strength [48].

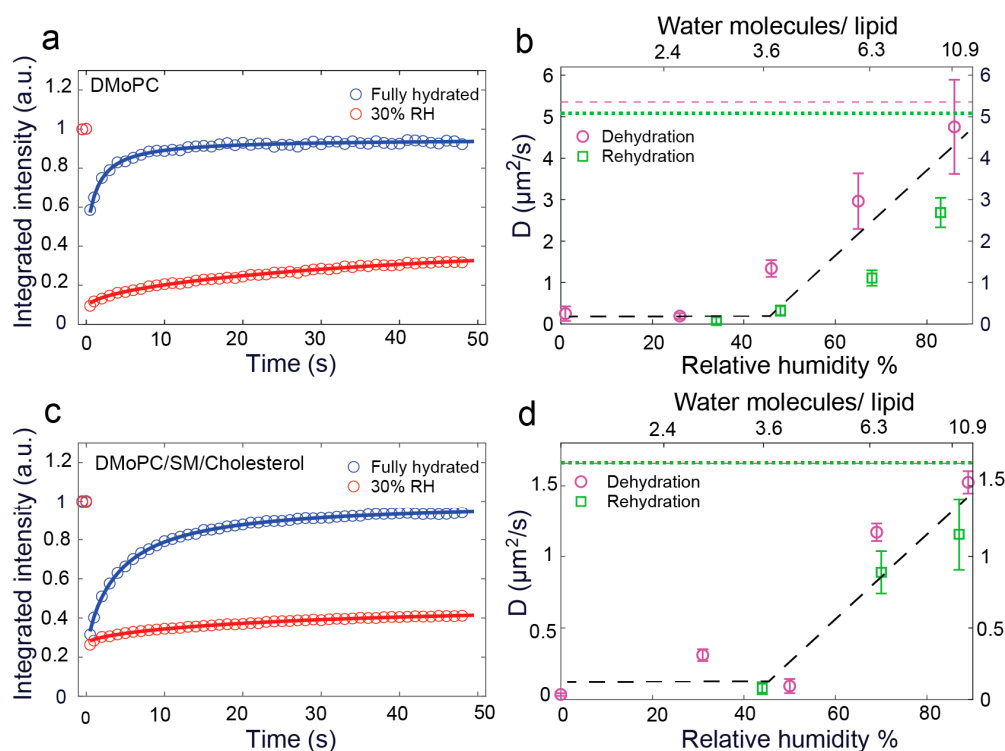


**Figure 2.** FRAP traces of fully hydrated and dehydrated down to 30% RH SLBs for a single component (a) and phase-separated (c) membrane. Panels (b,d) show the dependence of diffusion coefficient with RH for a single component and phase-separated SLB, respectively. The magenta dashed and green dotted lines are the average values of  $D$  at the fully hydrated condition and fully rehydrated condition, respectively. The black dashed line is a guide to the eye to highlight the trend in  $D$  with de(re)hydration.

The presented results reveal that the lateral diffusion of lipids in the  $L_d$  phase of the zwitterionic lipid bilayer is particularly sensitive towards the hydration state of the membrane, or more precisely, of the lipid itself. Moreover, the dependence of  $D$  on the hydration of the membrane constituents uniformly applies to phosphatidylcholines (PC) in a completely liquid-disordered environment as well as in phase-separated membranes, irrespective of the presence of  $L_o$  domains slowing down the overall mobility.

### 3.2. Hydration Sensing

Our results reveal a significant dependence of the diffusion coefficient of lipids on their local hydration state. Thus, it gives the possibility to be exploited as a technique to quantify the hydration level of the membrane by using  $D$  as a hydration indicator. In previous X-ray diffraction [49] and infrared spectroscopy [30] studies, the RH of the membrane environment has been correlated with the number of water molecules present in the hydration shell of a single lipid molecule, specifically in its head group region. Approximately 10.5, 6.3, 3.6, and 2.4 water molecules, averaged from the results of the above-mentioned experimental studies, were found per PC lipid when stacked lipid membranes were exposed to an atmosphere with 95%, 75%, 50%, and 25% RH, respectively. Marrying these findings

with our results, the number of water molecules per lipid head group corresponding to a particular RH can be correlated with  $D$ . Consequently, the precise determination of the lipids' diffusion coefficient can give insights into the local hydration state of the membrane. The changes in the lipids' mobility can be used as a local hydration sensor not only in biomimetic membranes, but also in native cell membranes. The general concept of our approach is depicted in Figure 3. It should be noted here that while extrapolating the above experimental results for membranes equilibrated with 0% RH, one would expect the membranes to be free of water. However, previous molecular dynamics simulations revealed, even after drastic drying, up to 3–4 water molecules per lipid remain strongly hydrogen bonded to the carbonyl and/or phosphate group [22,35]. Hence, for membranes equilibrated to  $RH < 25\%$ , one can state that there are not more than four water molecules associated with the lipids.

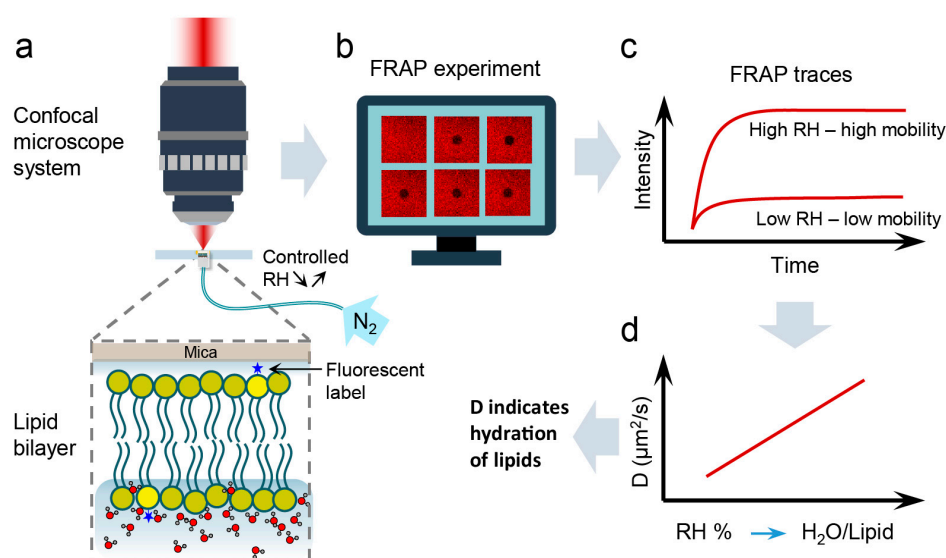


**Figure 3.** Schematic diagram of the hydration sensing concept. (a) Once the bulk water is removed, sample is inserted into the microscope system and subjected to a controlled dehydration/rehydration process using nitrogen gas of known humidity. (b) At each hydration state, FRAP measurements are performed. (c) From FRAP traces acquired for a particular humidity, the diffusion coefficient ( $D$ ) of lipids is calculated. (d) The diffusion coefficient is then presented as a function of relative humidity (RH) of the sample environment, which in turn can be directly related to the number of water molecules hydrating a single lipid molecule. Thus, using this calibration plot, the hydration of the lipid membrane can be determined from the measured lipid lateral diffusion coefficient.

### 3.3. Validation of Hydration Sensing Approach

The reversibility, repeatability, and response time of the sensor are crucial criteria to validate a sensing technique. To check these parameters, a single component DMOPC SLB was exposed to high (80%) and low (5%) RH alternatively several times. The RH was instantaneously adjusted from 80% to 5% by closing the N<sub>2</sub> flow through the water reservoir and only letting dry N<sub>2</sub> flow over the membrane. A humidity sensor attached to the flow tube close to the outlet was used to continuously monitor the RH of N<sub>2</sub> gas. The set RH (5% or 80%) was reached typically within 1 min. Subsequently, the RH was kept constant for the next four minutes after each consecutive RH alteration, and two FRAP measurements were performed. Figure 4 shows the change of  $D$  over time upon sudden increase or decrease in RH in several dehydration-rehydration cycles. Clearly, the successive de(re)hydration cycles do not leave a permanent effect on the lateral diffusion of lipids, instead, a variation of  $D$  is absolutely reversible and repeatable. We note that the measured  $D$  at high/low RH appeared to be lower/higher than the average  $D$  values at these two hydration levels, as shown in Figure 2b. This results from the fact that the

RH of the purged nitrogen gas was swapped quickly (75% RH change in 1 min), and the FRAP measurements were started immediately before the SLB was fully equilibrated to the particular RH provided. This is also evident from the fact that the second FRAP trace always yields higher (for 80% RH) and lower (for 5% RH)  $D$ , while the membrane still undergoes equilibration. Generally, in our experiments, we noticed that the equilibration time at a particular RH was around 10 min. Nevertheless, the prompt change of  $D$ , shown in Figure 4, within 1 min of changing RH is sufficient to unambiguously indicate a significant change in the hydration state of the system. This confirms that a quick response in  $D$  is expected as soon as the hydration state is altered.

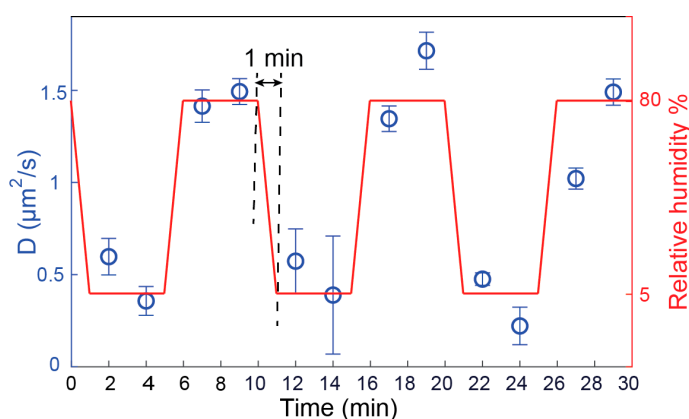


**Figure 4.** Diffusion coefficients of single component DMoPC SLB exposed to a successive switching between high (80%) and low (5%) RH over time. Each data point corresponds to the diffusion coefficient derived from a single FRAP trace. The confidence bounds of the fits of the FRAP traces were used to form the error bars for the data points. One minute time was taken to alter the RH from 80% to 5%. In the following four minutes, two FRAP measurements were performed before re-altering the RH.

#### 4. Discussion

##### 4.1. Applicability and Measurement Criteria

Transient, local dehydration of membranes is one of the most important intermediate steps in numerous biological processes, for example, endo- and exocytosis, fertilization, viral entry, biogenesis of muscle tissue [50], etc. The central mechanism of these processes constitutes membrane fusion. The lipid layers merge, overcoming a specific hydration barrier. This results from the removal of water molecules from lipid head groups when the hydrophobic tails come into contact with the water-caged hydrophilic head groups of the two lipid layers [51]. A molecular-level understanding of such processes requires quantification of the local hydration state in terms of the number of water molecules attached per lipid in each intermediate step of the process. Our hydration sensing methodology forms a solid base for developing a complete stepwise map of hydration structures of lipid molecules in the course of membrane fusion or any other process that involves local dehydration of the membrane. Here, we verified the hydration sensing approach for DMoPC as a representative PC lipid, being one of the most abundant group of lipids found in biological cell membranes. As water molecules present in the clathrate cage around phosphocholine head group are related to lipid mobility, it is expected for other PC lipids to show dependence of the diffusion on hydration. It is important to note that the observed correlation between the diffusion coefficient and hydration state of the membrane is equally valid for a single component membrane as well as for more complex, multicomponent lipid bilayers that exhibit phase separation and formation of domains.

A few criteria of measurement conditions should be considered for an effective and fruitful hydration sensing. Apart from the hydration level, several additional parameters affect lipid dynamics in a membrane. The presence of saturated and unsaturated lipids,



cholesterol, membrane proteins, and phase separation in membranes influence the absolute values of the diffusion coefficients of lipids. In presence of various ions in the medium, the complex formation of an ion binding with more than one lipid may slow down the mobility of lipids and weaken the polarization of water molecules in the interior of the membranes [48]. Moreover, physical factors such as temperature variation also affect the diffusion of lipids. In order to obtain a clear picture of the hydration state of lipids in a membrane, lipid diffusion should be measured keeping all other parameters constant. In complex biological membranes, where a variety of parameters modulates lipid dynamics, the presented approach still enables comparative studies of hydration structure and hydration heterogeneity between various membrane sites. The high sensitivity of this methodology (few water molecules per lipid) allows for the qualitative determination of the hydration state.

#### 4.2. Perspectives

From the technical standpoint, it must be emphasized that our approach is not limited to using the FRAP technique. In fact, it could be easily transferred to any method that enables quantitative analysis of lipid diffusion, such as, for instance, fluorescence correlation spectroscopy (FCS). Although both FRAP and FCS techniques meet the temporal resolution needed to resolve membrane dynamics, their spatial resolution, when performed with conventional confocal microscopes, is diffraction limited [52]. Consequently, the heterogeneity of diffusion, and thus the heterogeneity of hydration that can occur at the nanoscale, may be overlooked due to the inherent ensemble averaging across the entire illumination area [53,54]. One of the strategies to breach the diffraction limit barrier is a coupling of the well-established FCS approach with super-resolution imaging technique such as stimulated emission depletion (STED) nanoscopy [52,55,56]. STED-FCS has been successfully applied to model biomembranes for studying nanoscale lipid dynamical heterogeneities induced by pore-forming proteins [56], as well as to the plasma membrane of living cells to discern nanoscale molecular diffusion modes [52]. An alternative approach is marrying the aforementioned FCS with near-field scanning optical microscopy, capable of confining the illumination light at the nanoscale [54,57]. High spatial resolution has also been achieved with a single-molecule FRAP (smFRAP) approach, which was employed to determine the distribution and translocation rates of inner and outer nuclear membrane proteins in live cells in real-time conditions [58]. An alternative solution is to trace the motion of individual particles attached to the lipids of interest using the single-particle tracking (SPT) technique [59]. Although conventional SPT yields a limited temporal resolution (often in the millisecond range), solutions have already emerged to improve it by combining SPT with interferometric scattering microscopy (iSCAT) techniques. Using the SPT-iSCAT approach, microsecond temporal resolution with simultaneous sub-1 nm spatial precision of lipid localization has been achieved [60–62].

Clearly, the possibilities are tremendous. Synthesizing the evidence from our studies with single-molecule approaches could truly provide capabilities to sense biomimetic and biological membrane hydration at the single-molecule level. Adsorption of large biomolecules (such as proteins) onto the membrane often disturbs the hydration layer locally in the vicinity of the binding site [63]. Using single-molecule approach, it is feasible to sense hydration changes even in the case of single biomolecule–membrane interactions.

For using lipid diffusion as a hydration marker, two distinct approaches can be undertaken. One of these approaches is to provide an absolute number of water molecules per lipid in a membrane looking at the diffusion coefficient of the very lipid. However, as the exact number of water molecules per lipid varies depending on the lipid structure and its surroundings, the number of water molecules per lipid at different relative humidity levels should be determined precisely for that specific system. Additionally, to gain information on the number of water molecules correlated with diffusion coefficient of lipids accurately, calibration for complete dehydration and rehydrated cycle is essential. On the other hand, for a system that is homogeneous in terms of diffusion-affecting

parameters other than hydration state, by local probing of lipid diffusion in different sites of interest, a qualitative comparison of the hydration structure and state can be revealed. In this scenario, the method becomes self-referential and the requirement for calibration is eliminated.

## 5. Conclusions

We developed a novel approach for sensing the hydration state of lipids and hydration heterogeneity within lipid membranes, based on the strong correlation between lateral mobility of phospholipids with the number of water molecules forming the hydration shell around lipids' polar head groups. Hence, the diffusion coefficient of a lipid can be considered as a measure of its hydration state at a molecular level. The change in lateral diffusion coefficients of lipids with the number of water molecules hydrating a lipid is fully reversible and repeatable. For a comparative study of hydration heterogeneity of different sites within the membrane, the methodology is self-sufficient and self-referential. Finally, the presented approach can readily be equipped with a single-molecule hydration sensing capabilities if the diffusion coefficient is measured with single-molecule sensitivity approaches such as SPT or FCS. Thus, the approach for hydration sensing possesses an enormous potential for quantitative, molecular-level studies of the (de)hydration-mediated processes in lipid membranes.

## 6. Patents

Chattopadhyay, M.; Krok, E.; Orlikowska, H.; Piatkowski, L. Method for Measuring the Local Hydration of Lipid Layers of Biomimetic and Biological Systems. Patent Application (Poland), P.437600 and P.437601, 16.04.2021.

**Author Contributions:** Conceptualization, M.C. and L.P.; methodology, M.C., E.K., and L.P.; validation, L.P.; formal analysis, M.C.; investigation, M.C. and E.K.; writing—original draft preparation, M.C. and H.O.; writing—review and editing, M.C., H.O., E.K., and L.P.; supervision, L.P.; funding acquisition, L.P. and H.O.; patent application writing, H.O. and L.P. All authors have read and agreed to the published version of the manuscript.

**Funding:** This research was funded by Foundation for Polish Science (First TEAM grant POIR.04.04.00-00-5D32/18-00), EMBO Installation Grant 2019, and National Science Centre (Poland) 2020/37/B/ST4/01785. This work was also financed from the budget funds allocated for science in the years 2019–2023 as a research project under the “Diamond Grant” program (decision: 0042/DIA/2019/48).

**Institutional Review Board Statement:** Not applicable.

**Informed Consent Statement:** Not applicable.

**Data Availability Statement:** All data underlying the study are available from the authors.

**Acknowledgments:** The authors gratefully thank Petra Schwillie and Henri G. Franquelim for their suggestions and useful discussion.

**Conflicts of Interest:** The authors declare no conflict of interest. The funders had no role in the design of the study; in the collection, analyses, or interpretation of data; in the writing of the manuscript, or in the decision to publish the results.

## References

1. Aeffer, S.; Reusch, T.; Weinhausen, B.; Salditt, T. Energetics of Stalk Intermediates in Membrane Fusion Are Controlled by Lipid Composition. *Proc. Natl. Acad. Sci. USA* **2012**, *109*, 1609–1618. [\[CrossRef\]](#)
2. Subczynski, W.K.; Pasenkiewicz-Gierula, M.; Widomska, J.; Mainali, L.; Raguz, M. High Cholesterol/Low Cholesterol: Effects in Biological Membranes: A Review. *Cell Biochem. Biophys.* **2017**, *75*, 369–385. [\[CrossRef\]](#)
3. Jackman, J.A.; Cho, N.J. Supported Lipid Bilayer Formation: Beyond Vesicle Fusion. *Langmuir* **2020**, *36*, 1387–1400. [\[CrossRef\]](#)
4. Richter, R.P.; Bérat, R.; Brisson, A.R. Formation of Solid-Supported Lipid Bilayers: An Integrated View. *Langmuir* **2006**, *22*, 3497–3505. [\[CrossRef\]](#)
5. Chan, Y.H.M.; Boxer, S.G. Model Membrane Systems and Their Applications. *Curr. Opin. Chem. Biol.* **2007**, *11*, 581–587. [\[CrossRef\]](#)
6. Nieciecka, D.; Królikowska, A.; Kryszewski, P. Probing the Interactions of Mitoxantrone with Biomimetic Membranes with Electrochemical and Spectroscopic Techniques. *Electrochim. Acta* **2015**, *165*, 430–442. [\[CrossRef\]](#)

7. Khadka, N.K.; Cheng, X.; Ho, C.S.; Katsaras, J.; Pan, J. Interactions of the Anticancer Drug Tamoxifen with Lipid Membranes. *Biophys. J.* **2015**, *108*, 2492–2501. [\[CrossRef\]](#)
8. Bilginer, R.; Arslan Yildiz, A. Biomimetic Model Membranes as Drug Screening Platform. In *Biomimetic Lipid Membranes: Fundamentals, Applications, and Commercialization*; Springer International Publishing: Cham, Switzerland, 2019; pp. 225–247.
9. Wang, H.; Liu, Y.; He, R.; Xu, D.; Zang, J.; Weeranoppanant, N.; Dong, H.; Li, Y. Cell Membrane Biomimetic Nanoparticles for Inflammation and Cancer Targeting in Drug Delivery. *Biomater. Sci.* **2020**, *8*, 552–568. [\[CrossRef\]](#) [\[PubMed\]](#)
10. Zhang, M.; Cheng, S.; Jin, Y.; Zhang, N.; Wang, Y. Membrane Engineering of Cell Membrane Biomimetic Nanoparticles for Nanoscale Therapeutics. *Clin. Transl. Med.* **2021**, *11*, e292. [\[CrossRef\]](#) [\[PubMed\]](#)
11. Hindley, J.W.; Law, R.V.; Ces, O. Membrane Functionalization in Artificial Cell Engineering. *SN Appl. Sci.* **2020**, *2*, 1–10. [\[CrossRef\]](#)
12. Zhang, L.; Wang, Z.; Zhang, Y.; Cao, F.; Dong, K.; Ren, J.; Qu, X. Erythrocyte Membrane Cloaked Metal-Organic Framework Nanoparticle as Biomimetic Nanoreactor for Starvation-Activated Colon Cancer Therapy. *ACS Nano* **2018**, *12*, 10201–10211. [\[CrossRef\]](#)
13. Liu, W.; Wu, J.; Ji, X.; Ma, Y.; Liu, L.; Zong, X.; Yang, H.; Dai, J.; Chen, X.; Xue, W. Advanced Biomimetic Nanoreactor for Specifically Killing Tumor Cells through Multi-Enzyme Cascade. *Theranostics* **2020**, *10*, 6245–6260. [\[CrossRef\]](#) [\[PubMed\]](#)
14. Andersson, J.; Knoll, W. Tethered Lipid Membranes as Platforms for Biophysical Studies and Advanced Biosensors. In *Biomimetic Lipid Membranes: Fundamentals, Applications, and Commercialization*; Springer International Publishing: Cham, Switzerland, 2019; pp. 183–191.
15. Alvarez-Malmagro, J.; García-Molina, G.; De Lacey, A.L. Electrochemical Biosensors Based on Membrane-Bound Enzymes in Biomimetic Configurations. *Sensors* **2020**, *20*, 3393. [\[CrossRef\]](#) [\[PubMed\]](#)
16. Ito, Y.; Osaki, T.; Kamiya, K.; Yamada, T.; Miki, N.; Takeuchi, S. Rapid and Resilient Detection of Toxin Pore Formation Using a Lipid Bilayer Array. *Small* **2020**, *16*, 2005550. [\[CrossRef\]](#) [\[PubMed\]](#)
17. Li, Y.; Qi, S.; Tian, M.; Widjajanti, W.; Wang, R. Fabrication of Aquaporin-Based Biomimetic Membrane for Seawater Desalination. *Desalination* **2019**, *467*, 103–112. [\[CrossRef\]](#)
18. Di Vincenzo, M.; Tiraferri, A.; Musteata, V.E.; Chisca, S.; Sougrat, R.; Huang, L.B.; Nunes, S.P.; Barboiu, M. Biomimetic Artificial Water Channel Membranes for Enhanced Desalination. *Nat. Nanotechnol.* **2021**, *16*, 190–196. [\[CrossRef\]](#) [\[PubMed\]](#)
19. Abaie, E.; Xu, L.; Shen, Y.X. Bioinspired and Biomimetic Membranes for Water Purification and Chemical Separation: A Review. *Front. Environ. Sci. Eng.* **2021**, *15*, 124. [\[CrossRef\]](#)
20. Fukuma, T.; Higgins, M.J.; Jarvis, S.P. Direct Imaging of Individual Intrinsic Hydration Layers on Lipid Bilayers at Ångstrom Resolution. *Biophys. J.* **2007**, *92*, 3603–3609. [\[CrossRef\]](#)
21. Pasenkiewicz-Gierula, M.; Baczynski, K.; Markiewicz, M.; Murzyn, K. Computer Modelling Studies of the Bilayer/Water Interface. *Biochim. Biophys. Acta Biomembr.* **2016**, *1858*, 2305–2321. [\[CrossRef\]](#)
22. Disalvo, E.A.; Lairion, F.; Martini, F.; Tymczyszyn, E.; Frias, M.; Almaleck, H.; Gordillo, G.J. Structural and Functional Properties of Hydration and Confined Water in Membrane Interfaces. *Biochim. Biophys. Acta Biomembr.* **2008**, *1778*, 2655–2670. [\[CrossRef\]](#)
23. Tian, Z.; Gong, J.; Crowe, M.; Lei, M.; Li, D.; Ji, B.; Diao, J. Biochemical Studies of Membrane Fusion at the Single-Particle Level. *Prog. Lipid Res.* **2019**, *73*, 92–100. [\[CrossRef\]](#) [\[PubMed\]](#)
24. Sparrman, T.; Westlund, P.O. An NMR Line Shape and Relaxation Analysis of Heavy Water Powder Spectra of the L $\alpha$ , L $\beta'$  and P $\beta'$  Phases in the DPPC/Water System. *Phys. Chem. Chem. Phys.* **2003**, *5*, 2114–2121. [\[CrossRef\]](#)
25. Tristram-Nagle, S.; Nagle, J.F. Lipid Bilayers: Thermodynamics, Structure, Fluctuations, and Interactions. *Chem. Phys. Lipids* **2004**, *127*, 3–14. [\[CrossRef\]](#)
26. Rheinstädter, M.C.; Ollinger, C.; Fragneto, G.; Demmel, F.; Salditt, T. Collective Dynamics of Lipid Membranes Studied by Inelastic Neutron Scattering. *Phys. Rev. Lett.* **2004**, *93*, 108107. [\[CrossRef\]](#)
27. Berntsen, P.; Svanberg, C.; Swenson, J. Interplay between Hydration Water and Headgroup Dynamics in Lipid Bilayers. *J. Phys. Chem. B* **2011**, *115*, 1825–1832. [\[CrossRef\]](#)
28. Tielrooij, K.J.; Paparo, D.; Piatkowski, L.; Bakker, H.J.; Bonn, M. Dielectric Relaxation Dynamics of Water in Model Membranes Probed by Terahertz Spectroscopy. *Biophys. J.* **2009**, *97*, 2484–2492. [\[CrossRef\]](#)
29. Gennaro, A.; Deschaume, O.; Pfeiffer, H.; Bartic, C.; Wagner, P.; Wübbenhorst, M. Understanding the Dehydration Stress in Lipid Vesicles by a Combined Quartz Crystal Microbalance and Dielectric Spectroscopy Study. *Phys. Status Solidi* **2020**, *217*, 1900986. [\[CrossRef\]](#)
30. Piatkowski, L.; De Heij, J.; Bakker, H.J. Probing the Distribution of Water Molecules Hydrating Lipid Membranes with Ultrafast Förster Vibrational Energy Transfer. *J. Phys. Chem. B* **2013**, *117*, 1367–1377. [\[CrossRef\]](#)
31. Volkov, V.V.; Palmer, D.J.; Righini, R. Distinct Water Species Confined at the Interface of a Phospholipid Membrane. *Phys. Rev. Lett.* **2007**, *99*, 078302. [\[CrossRef\]](#)
32. Demchenko, A.P.; Mély, Y.; Duportail, G.; Klymchenko, A.S. Monitoring Biophysical Properties of Lipid Membranes by Environment-Sensitive Fluorescent Probes. *Biophys. J.* **2009**, *96*, 3461–3470. [\[CrossRef\]](#)
33. Watanabe, N.; Suga, K.; Slotte, J.P.; Nyholm, T.K.M.; Umakoshi, H. Lipid-Surrounding Water Molecules Probed by Time-Resolved Emission Spectra of Laurdan. *Langmuir* **2019**, *35*, 46. [\[CrossRef\]](#)
34. Jurkiewicz, P.; Olżyńska, A.; Langner, M.; Hof, M. Headgroup hydration and mobility of DOTAP/DOPC bilayers: A fluorescence solvent relaxation study. *Langmuir* **2006**, *22*, 8741–8749. [\[CrossRef\]](#) [\[PubMed\]](#)



35. Calero, C.; Franzese, G. Membranes with Different Hydration Levels: The Interface between Bound and Unbound Hydration Water. *J. Mol. Liq.* **2019**, *273*, 488–496. [\[CrossRef\]](#)
36. Hutterer, R.; Hof, M. Dynamics in Diether Lipid Bilayers and Interdigitated Bilayer Structures Studied by Time-Resolved Emission Spectra, Decay Time and Anisotropy Profiles. *J. Fluoresc.* **2001**, *11*, 227–236. [\[CrossRef\]](#)
37. Sýkora, J.; Kapusta, P.; Fidler, V.; Hof, M. On What Time Scale Does Solvent Relaxation in Phospholipid Bilayers Happen? *Langmuir* **2002**, *18*, 571–574. [\[CrossRef\]](#)
38. Jurkiewicz, P.; Cwiklik, L.; Jungwirth, P.; Hof, M. Lipid Hydration and Mobility: An Interplay between Fluorescence Solvent Relaxation Experiments and Molecular Dynamics Simulations. *Biochimie* **2012**, *94*, 26–32. [\[CrossRef\]](#)
39. Parasassi, T.; De Stasio, G.; d’Ubaldo, A.; Gratton, E. Phase Fluctuation in Phospholipid Membranes Revealed by Laurdan Fluorescence. *Biophys. J.* **1990**, *57*, 1179–1186. [\[CrossRef\]](#)
40. Mukherjee, S.; Chattopadhyay, A. Wavelength-Selective Fluorescence as a Novel Tool to Study Organization and Dynamics in Complex Biological Systems. *J. Fluoresc.* **1995**, *5*, 237–246. [\[CrossRef\]](#)
41. Chattopadhyay, A. Exploring Membrane Organization and Dynamics by the Wavelength-Selective Fluorescence Approach. *Chem. Phys. Lipids* **2003**, *122*, 3–17. [\[CrossRef\]](#)
42. Barucha-Kraszewska, J.; Kraszewski, S.; Jurkiewicz, P.; Ramseyer, C.; Hof, M. Numerical Studies of the Membrane Fluorescent Dyes Dynamics in Ground and Excited States. *Biochim. Biophys. Acta Biomembr.* **2010**, *1798*, 1724–1734. [\[CrossRef\]](#) [\[PubMed\]](#)
43. Jurkiewicz, P.; Sýkora, J.; Olżyńska, A.; Humpolíčková, J.; Hof, M. Solvent Relaxation in Phospholipid Bilayers: Principles and Recent Applications. *J. Fluoresc.* **2005**, *15*, 883–894. [\[CrossRef\]](#)
44. Matysik, A.; Kraut, R.S. Preparation of Mica Supported Lipid Bilayers for High Resolution Optical Microscopy Imaging. *J. Vis. Exp.* **2014**, *88*, 52054. [\[CrossRef\]](#)
45. Soumpasis, D.M. Theoretical Analysis of Fluorescence Photobleaching Recovery Experiments. *Biophys. J.* **1983**, *41*, 95–97. [\[CrossRef\]](#)
46. Chattopadhyay, M.; Krok, E.; Orlikowska, H.; Schwille, P.; Franquelim, H.G.; Piatkowski, L. Hydration Layer of Only Few Molecules Controls Lipid Mobility in Biomimetic Membranes. *bioRxiv* **2021**. [\[CrossRef\]](#)
47. Honigsmann, A.; Mueller, V.; Hell, S.W.; Eggeling, C. STED Microscopy Detects and Quantifies Liquid Phase Separation in Lipid Membranes Using a New Far-Red Emitting Fluorescent Phosphoglycerolipid Analogue. *Faraday Discuss.* **2012**, *161*, 77–89. [\[CrossRef\]](#)
48. Böckmann, R.A.; Hac, A.; Heimburg, T.; Grubmüller, H. Effect of Sodium Chloride on a Lipid Bilayer. *Biophys. J.* **2003**, *85*, 1647–1655. [\[CrossRef\]](#)
49. Hristova, K.; White, S.H. Determination of the Hydrocarbon Core Structure of Fluid Dioleoylphosphocholine (DOPC) Bilayers by X-ray Diffraction Using Specific Bromination of the Double-Bonds: Effect of Hydration. *Biophys. J.* **1998**, *74*, 2419–2433. [\[CrossRef\]](#)
50. Leikin, S.L.; Kozlov, M.M.; Chernomordik, L.V.; Markin, V.S.; Chizmadzhev, Y.A. Membrane Fusion: Overcoming of the Hydration Barrier and Local Restructuring. *J. Theor. Biol.* **1987**, *129*, 411–425. [\[CrossRef\]](#)
51. Wilschut, J.; Hoekstra, D. Membrane Fusion: Lipid Vesicles as a Model System. *Chem. Phys. Lipids* **1986**, *40*, 145–166. [\[CrossRef\]](#)
52. Schneider, F.; Waithe, D.; Galiani, S.; Bernardino De La Serna, J.; Sezgin, E.; Eggeling, C. Nanoscale Spatiotemporal Diffusion Modes Measured by Simultaneous Confocal and Stimulated Emission Depletion Nanoscopy Imaging. *Nano Lett.* **2018**, *18*, 4233–4240. [\[CrossRef\]](#) [\[PubMed\]](#)
53. Manzo, C.; Van Zanten, T.S.; Garcia-Parajo, M.F. Nanoscale Fluorescence Correlation Spectroscopy on Intact Living Cell Membranes with NSOM Probes. *Biophys. J.* **2011**, *100*, L8. [\[CrossRef\]](#)
54. Sezgin, E.; Schneider, F.; Galiani, S.; Urbančič, I.; Waithe, D.; Lagerholm, B.C.; Eggeling, C. Measuring Nanoscale Diffusion Dynamics in Cellular Membranes with Super-Resolution STED-FCS. *Nat. Protoc.* **2019**, *14*, 1054–1083. [\[CrossRef\]](#)
55. Eggeling, C. Super-Resolution Optical Microscopy of Lipid Plasma Membrane Dynamics. *Essays Biochem.* **2015**, *57*, 69–80.
56. Sarangi, N.K.; Roobala, C.; Basu, J.K. Unraveling Complex Nanoscale Lipid Dynamics in Simple Model Biomembranes: Insights from Fluorescence Correlation Spectroscopy in Super-Resolution Stimulated Emission Depletion Mode. *Methods* **2018**, *140–141*, 198–211. [\[CrossRef\]](#)
57. Regmi, R.; Winkler, P.M.; Flauraud, V.; Borgman, K.J.E.; Manzo, C.; Brugger, J.; Rigneault, H.; Wenger, J.; García-Parajo, M.F. Planar Optical Nanoantennas Resolve Cholesterol-Dependent Nanoscale Heterogeneities in the Plasma Membrane of Living Cells. *Nano Lett.* **2017**, *17*, 6295–6302. [\[CrossRef\]](#)
58. Mudumbi, K.C.; Schirmer, E.C.; Yang, W. Single-Point Single-Molecule FRAP Distinguishes Inner and Outer Nuclear Membrane Protein Distribution. *Nat. Commun.* **2016**, *7*, 1–6. [\[CrossRef\]](#)
59. Manzo, C.; Garcia-Parajo, M.F. A Review of Progress in Single Particle Tracking: From Methods to Biophysical Insights. *Rep. Prog. Phys.* **2015**, *78*, 124601. [\[CrossRef\]](#) [\[PubMed\]](#)
60. Wu, H.M.; Lin, Y.H.; Yen, T.C.; Hsieh, C.L. Nanoscopic Substructures of Raft-Mimetic Liquid-Ordered Membrane Domains Revealed by High-Speed Single-Particle Tracking. *Sci. Rep.* **2016**, *6*, 1–10.
61. Spillane, K.M.; Ortega-Arroyo, J.; De Wit, G.; Eggeling, C.; Ewers, H.; Wallace, M.I.; Kukura, P. High-Speed Single-Particle Tracking of Gm1 in Model Membranes Reveals Anomalous Diffusion Due to Interleaflet Coupling and Molecular Pinning. *Nano Lett.* **2014**, *14*, 5390–5397. [\[CrossRef\]](#)

62. Hsieh, C.L.; Spindler, S.; Ehrig, J.; Sandoghdar, V. Tracking Single Particles on Supported Lipid Membranes: Multimobility Diffusion and Nanoscopic Confinement. *J. Phys. Chem. B* **2014**, *118*, 1545–1554. [[CrossRef](#)]
63. Pohl, P.; Saparov, S.M.; Pohl, E.E.; Evtodienko, V.Y.; Agapov, I.I.; Tonevitsky, A.G. Dehydration of Model Membranes Induced by Lectins from *Ricinus Communis* and *Viscum Album*. *Biophys. J.* **1998**, *75*, 2868–2876. [[CrossRef](#)]

# Chapter 9

## Cooperativity between sodium ions and water molecules facilitates lipid mobility in model cell membranes

An aqueous buffer solution containing various ions is present around the cellular membranes, often with an ion concentration gradient across the membrane. It is well-established that these ions modulate the local and global properties of membranes, including their hydration properties[104]. At the same time, interactions of interfacial water with lipids in biomembranes play a vital role in modulating the structure and dynamics of the membrane [212]. Hence understanding the 3-fold interplay between

water-lipids-ions is crucial to elucidate its influence on the lipid diffusion. In Publication 3, I investigated the effect of various biologically relevant monovalent and divalent cations ( $\text{Na}^+$ ,  $\text{K}^+$ ,  $\text{Mg}^{2+}$  and  $\text{Ca}^{2+}$ ) on the lateral diffusion of PC lipids in phase-separated membranes at varying hydration conditions. I performed a systemic studies on the structural organization and lipid dynamics in phase-separated membranes using confocal imaging and FRAP experiments. I found that with increase in NaCl concentration, the average  $L_o$  domain area and the total  $L_o$  phase area increase, which is a manifestation of an enhanced phase separation. At fully hydrated condition, the presence and changes to concentration of  $\text{Na}^+$  ions have little or no effect on the  $D$  values of the PC lipids. But intriguingly, after removal of the bulk water, lipid mobility is retained only in the presence of a certain amount of NaCl. However, even with increasing concentration of NaCl, the lipid mobility could not be maintained below 50% RH, indicating that  $\text{Na}^+$  ions and water molecules work in a concerted manner to facilitate the lateral diffusion of lipids at water scarcity conditions.  $\text{Na}^+$  ions strengthen the water hydration shell structure around the phosphocholine headgroup of PC lipids, which in turn supports lipid mobility.  $\text{K}^+$  ions also show the similar effect. Interestingly,  $\text{Ca}^{2+}$  and  $\text{Mg}^{2+}$  ions are unable to maintain lipid mobility at perturbed hydration conditions.  $\text{Ca}^{2+}$  ions bind to more than one lipid oxygen and replace the water molecules in the lipid headgroup region. Thus they destabilize the hydration shell around the lipid headgroup causing very low mobility in the absence of bulk water.  $\text{Mg}^{2+}$  ions having a high energy barrier to bind with lipid oxygen, neither

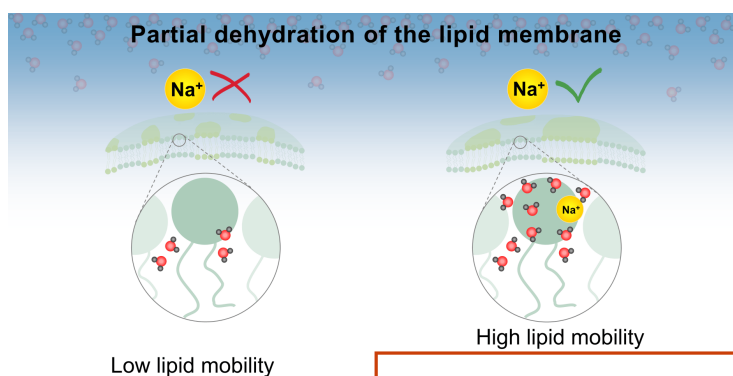


Figure 9.1: A schematic illustration summarizing the key results of publication 3.

stabilize or destabilize the lipid hydration layer. I concluded that the ion-specific dependence of lipid mobility at lower hydration conditions results from the competition between lipid binding affinity and the hydration energy of the ions. For a detailed description of the above results, the full-length, peer-reviewed article (Publication 3) and the associated supplementary information, published in the Chemical Science journal are attached below.

EDGE ARTICLE



Cite this: *Chem. Sci.*, 2023, 14, 4002

All publication charges for this article have been paid for by the Royal Society of Chemistry

Received 12th December 2022  
Accepted 21st March 2023

DOI: 10.1039/d2sc06836b

rsc.li/chemical-science

## Cooperativity between sodium ions and water molecules facilitates lipid mobility in model cell membranes†

Madhurima Chattopadhyay,<sup>1</sup> Emilia Krok,<sup>2</sup> Hanna Orlikowska-Rzeznik<sup>2</sup> and Lukasz Piatkowski<sup>1\*</sup>

Cellular membranes are surrounded by an aqueous buffer solution containing various ions, which influence the hydration layer of the lipid head groups. At the same time, water molecules hydrating the lipids play a major role in facilitating the organisation and dynamics of membrane lipids. Employing fluorescence microscopy imaging and fluorescence recovery after photobleaching measurements, we demonstrate that the cooperativity between water and sodium ( $\text{Na}^+$ ) ions is crucial to maintain lipid mobility upon the removal of the outer hydration layer of the lipid membrane. Under similar hydration conditions, lipid diffusion ceases in the absence of  $\text{Na}^+$  ions. We find that  $\text{Na}^+$  ions (and similarly  $\text{K}^+$  ions) strengthen the water clathrate cage around the lipid phosphocholine headgroup and thus prevent its breaking upon removal of bulk water. Intriguingly,  $\text{Ca}^{2+}$  and  $\text{Mg}^{2+}$  do not show this effect. In this article, we provide a detailed molecular-level picture of ion specific dependence of lipid mobility and membrane hydration properties.

## Introduction

Biological membranes are self-assembled structures composed of various lipids embedded with proteins. They act as dynamic barriers separating intra- and extra-cellular matrices and encapsulate various subcellular organelles. A large variety of lipids in terms of chain length, chain saturation, headgroup structure, and charge is present in biomembranes. The structural lipid heterogeneity, in particular the length mismatch between the hydrophobic tails of the lipids, promotes the formation of lipid domains in response to their unfavourable interactions with the membrane aqueous hydration layer – the so-called “hydrophobic mismatch”. Saturated lipids, such as sphingomyelin (SM) along with cholesterol form more compact liquid ordered ( $L_o$ ) phase domains in the sea of more fluid liquid disordered phase ( $L_d$ ) composed predominantly of unsaturated lipids.<sup>1</sup> The  $L_o$  domains are believed to be platforms for various important biological processes like the attachment of proteins, cell signalling, ion channel regulation, pathogen entry, and many more.<sup>2</sup> The extent of phase separation in membranes is modulated not only by lipid composition and structure, but also by various other physicochemical

factors, such as temperature, pH, and the ionic strength of the environment.<sup>3</sup> The latter in particular is an important factor known to alter various structural as well as functional properties of membranes. The interactions between lipids and ions modulate the local and global properties of the lipid bilayer such as thickness, packing, phase transition temperature, acyl chain ordering, headgroup tilt or swelling,<sup>4–7</sup> but also take part in the regulation of ion channels, and signal transduction.<sup>4,8,9</sup> Several molecular dynamics (MD) simulations have claimed that various ions have also a profound effect on the dynamics of the lipids in the membrane.<sup>10,11</sup> A number of ions, predominantly  $\text{Na}^+$ ,  $\text{K}^+$ ,  $\text{Ca}^{2+}$ ,  $\text{Mg}^{2+}$ , and  $\text{Cl}^-$ , are found at the membrane interface with different intracellular and extracellular concentrations. The asymmetric distribution of lipids with different charge characters, as well as the different concentrations of various ions across the membrane, generate a suitable membrane potential for biochemical reactions.<sup>12,13</sup>

Ions are known to affect the structure and dynamics of the hydration layer of lipid headgroups. The presence of  $\text{Na}^+$  and  $\text{Ca}^{2+}$  ions significantly influences the hydration and orientation of the phosphate group of DPPC lipids.<sup>14</sup> Song *et al.* showed that slowing down of water molecules present within 10 Å of the hydrophilic surface of lipid vesicles was modulated by the presence of different ions following the order of the well-known Hofmeister series.<sup>15</sup> At the same time, water molecules hydrating the lipids play a major role in determining membrane structure, organization, and lipid dynamics.<sup>16</sup> Intriguingly, recent MD simulations showed that hydrogen-bonded water network directly hydrating the membrane exhibits both

Institute of Physics, Poznan University of Technology, Piotrowo 3, 60-965 Poznan, Poland. E-mail: madhurima.chattopadhyay@put.poznan.pl; lukasz.j.piatkowski@put.poznan.pl

† Electronic supplementary information (ESI) available: Experimental procedures and supplementary notes and figures. See DOI: <https://doi.org/10.1039/d2sc06836b>

structural and dynamical heterogeneity.<sup>17,18</sup> Clearly, both in native as well as in biomimetic membrane systems water-lipids-ions interactions are strongly interdependent. Hence numerous endeavors were made to elucidate the exact nature of the effect of a particular ion on lipid-water interactions and the resulting alterations of the lipid bilayer properties. Yet, the existing studies are mostly limited to molecular dynamics simulations, except few experimental works,<sup>7,14</sup> which mainly addressed the effect of salts on the lipid-water interplay in the excess of water. While most common biological conditions indeed involve full hydration, nature exhibits several phenomena of “anhydrobiosis”, where living organisms, such as tardigrades, nematodes, yeasts, bdelloid rotifer, seeds or pollens survive complete dehydration.<sup>19–21</sup> In addition, many biochemical processes, such as cell fusion or adsorption of macromolecules, involve both local variations of ion concentration as well as local and transient membrane dehydration.<sup>22–24</sup>

Clearly, it is very important to obtain an explicit picture of how ions affect lipid-water interactions at the molecular level under different membrane hydration conditions. To date, however, the understanding of lipid-ion interplay in the presence and absence of water has remained rather poor due to the unavailability of suitable membrane hydration modulation technique. Exploiting the recently developed protocol of preparation of desiccation-tolerant membranes,<sup>16</sup> the present work pioneers the experimental study of ion-water-lipid interactions under low hydration conditions.

Herein, using fluorescence imaging and fluorescence recovery after photobleaching (FRAP) experiments we showed how  $\text{Na}^+$  and  $\text{Ca}^{2+}$  ions affect the structure and lipid dynamics of phase-separated solid supported lipid bilayers (SLBs) at fully hydrated and dehydrated conditions. We addressed not only how a specific ion influences the lipid-water interactions but also focused on how the entire process of lipid dehydration modulates diffusion of phospholipids (14 : 1 PC) in membranes at various hydration conditions as well as with varying concentrations of  $\text{Na}^+$  ions. We discovered that  $\text{Na}^+$  ions play a crucial role in retaining the water hydration layer around the phosphocholine moiety in membranes subjected to dehydration. Surprisingly,  $\text{Ca}^{2+}$  cation, although comparable in size with  $\text{Na}^+$ , does not exhibit hydration structure-promoting capabilities. This behavior of  $\text{Na}^+$  and  $\text{Ca}^{2+}$  ions is confronted with the activity of  $\text{K}^+$  and  $\text{Mg}^{2+}$  ions. As such our findings highlight the unique characteristic of  $\text{Na}^+$  ion-lipid interactions based on its specific charge density, binding affinity, and hydration energy. Our study provides molecular-level insights into a scarcely studied but important topic of the specificity of the ionic composition of membrane local environment modulating the hydration properties and lipid diffusion within the membrane.

## Results and discussion

### Impact of $\text{Na}^+$ ions on the structure of SLBs

To understand how the ion-lipid-water interactions relate to the structure and lipid dynamics in biomimetic cell

membranes, SLBs were reconstructed from 14 : 1 PC, egg SM and cholesterol and characterized with fluorescence imaging and FRAP experiments. At room temperature, the prepared lipid membranes undergo a prominent phase separation due to the considerable difference in 14 : 1 PC and SM hydrophobic chain lengths and packing. Unsaturated 14 : 1 PC forms  $\text{L}_d$  phase, saturated SM forms  $\text{L}_o$  domains, while cholesterol partitions in both phases, with a strong preference for the  $\text{L}_o$  phase. The membranes were prepared either in Milli-Q water or in a buffer with the addition of 5 mM up to 1.5 M of NaCl. As the pH of the buffer has a prominent effect on the phase separation in lipid membranes,<sup>25</sup> 10 mM HEPES buffer was used to keep the pH of the medium constant at pH = 5.2, equal to that of Milli-Q water (see Experimental section in ESI†). Representative confocal images of the phase-separated SLBs prepared in Milli-Q water as well as in buffers of different composition are shown in Fig. 1A. Qualitatively, the size of  $\text{L}_o$  domains (black patches) for SLB prepared in Milli-Q water (sample #1) is the same as for the SLB prepared in 10 mM HEPES buffer (sample #2). Similarly, the domain size of SLB prepared in 150 mM NaCl solution (sample #5) is very similar to that prepared in 10 mM HEPES–150 mM NaCl buffer (sample #6). These observations indicate that HEPES salt itself does not have a noticeable effect on the phase separation of lipids in the reconstructed SLBs. At the same time, the average domain size in SLBs hydrated with buffer containing NaCl (sample #6) is significantly higher than for the SLBs hydrated without the addition of NaCl (sample #2). Quantitative analysis confirms the strong dependence of the phase separation architecture on the NaCl content – the average domain area and the total  $\text{L}_o$  phase area % (percentage of the total image area covered by the  $\text{L}_o$  phase) increase significantly with an increase in NaCl concentration (Fig. 1B and C). The average size of domains for SLBs prepared in Milli-Q and in 10 mM HEPES–1.5 M NaCl buffer are  $0.45 \pm 0.15 \mu\text{m}^2$  and  $3.79 \pm 0.36 \mu\text{m}^2$  respectively, showing over an eightfold increase. Similarly, the percentage of area occupied by the  $\text{L}_o$  phase domains increases with an increase in NaCl concentration (Fig. 1C). Between SLBs prepared in Milli-Q and in 10 mM HEPES–1.5 M NaCl buffer the area occupied by the  $\text{L}_o$  phase increases over 3 times.

To further corroborate that the increase in average domain area is caused solely by the addition of NaCl, we prepared SLB in Milli-Q water and imaged it before and after replacing the water by 10 mM HEPES–150 mM NaCl buffer (Fig. S1A†). Directly upon buffer replacement, the domain size did not increase considerably, but when imaging after ~20 hours, significantly (nearly 4 times) bigger domains were present. The difference in domain area (~4×) is fully consistent with domain area variation observed in membranes prepared directly in Milli-Q water and in HEPES/NaCl buffer (sample #1 vs. sample #6, Fig. 1B). For the reference sample, which was kept in Milli-Q water, the domains grew merely 1.5 times over the same time span. Likewise, the area occupied by the  $\text{L}_o$  domains increased by ~68% upon buffer change, whereas for the reference SLB it remained unchanged (Fig. S1B†). The two quantities, the average domain area and the percentage of the total area occupied by the  $\text{L}_o$



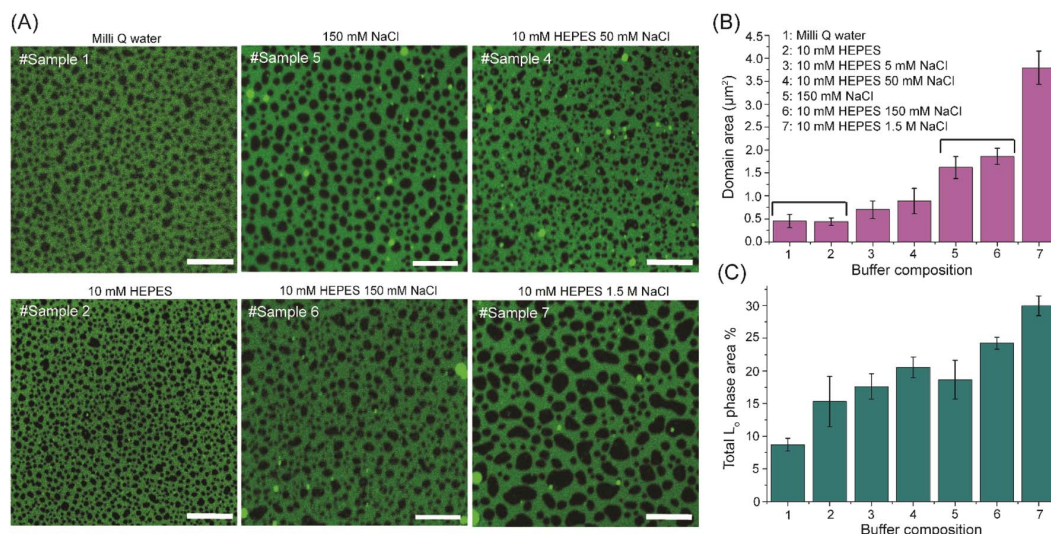


**Fig. 1** (A) Fluorescence images of phase-separated SLBs (L<sub>d</sub> phase – green; L<sub>o</sub> domains – black) prepared in Milli-Q water and HEPES buffer with various NaCl concentrations. Scale bar represents 10 μm. Dependence of the L<sub>o</sub> phase domain size (B) and percentage of area occupied by the L<sub>o</sub> phase (C) on the buffer composition. The error bars reflect standard deviations calculated from 10 images (50 × 50 micrometers) from each of at least three samples with a specific buffer composition.

phase, are very much related, but a comparison of the two can provide more information about the system. The total area % occupied by the L<sub>o</sub> phase may increase from merging of the small lipid clusters (below the diffraction limit) into bigger, resolvable entities. Likewise, the average domain area also increases when domains merge into bigger ones and/or with the inflow of unresolvable SM entities dissolved within the L<sub>d</sub> phase. However, increase of the average domain area does not necessarily guarantee the increase of the total L<sub>o</sub> phase area. If only the average domain area increases, but not the total L<sub>o</sub> area %, only merging of L<sub>o</sub> domains takes place. On the other hand, if only total L<sub>o</sub> phase area increases but the average domain size remains the same, formation of new, resolvable domains would be the dominant process.

With an increase in NaCl concentration, both the average domain area and percentage of the area occupied by the L<sub>o</sub> phase increase, which unambiguously confirms the presence of unresolvable L<sub>o</sub> phase entities within the L<sub>d</sub> phase, which upon addition of NaCl and enhancement of phase separation, cluster and merge into bigger (resolvable) domains. In contrast, at lower salt concentration, saturated and unsaturated lipids have stronger tendency to be mixed *i.e.* more SM entities remain unresolvable. At the experimental pH (~5.2), HEPES acts as a monoanionic species. Hence the solution around SLBs contains Na<sup>+</sup>, Cl<sup>-</sup> and HEPES<sup>-</sup> ions. MD simulations showed that Cl<sup>-</sup> hardly penetrates into the bilayer due to its larger size compared to Na<sup>+</sup>. Instead, Cl<sup>-</sup> ions remain mostly in the water phase and weakly interact with the choline group of PC lipids.<sup>26</sup> Analogously, HEPES<sup>-</sup> is also expected to be prevalent in the aqueous phase without much interaction with the membrane. This is consistent with our observation of no significant difference in domain size for SLBs prepared in the presence and

absence of HEPES for a constant NaCl concentration (Fig. 1, samples #1 vs. #2 and #5 vs. #6). Evidently, Na<sup>+</sup> ions are the key players that influence the degree of phase separation in SLBs.

With the increase in NaCl concentration, we observed that the extent of phase separation increases, which can be explained by more favourable PC-PC and/or SM-SM interactions and less favourable PC-SM interactions. Due to the densely packed structure of the L<sub>o</sub> phase, Na<sup>+</sup> ions preferentially interact (in terms of intercalation between the lipid headgroups) with the L<sub>d</sub> phase.<sup>26,27</sup> Hence, it is reasonable to assume that the PC-PC interactions are affected much more than the SM-SM interactions upon increase in Na<sup>+</sup> concentration. Both, PC and SM have choline moieties and consequently their headgroup hydration properties should be rather similar. However, PC and SM have distinct structural difference in their hydrophobic chain saturation – the two hydrocarbon chains of SM are saturated, whereas 14:1 PC has unsaturated hydrocarbon chains. The lipid tail saturation is one of the main determinants of the packing and order of the membrane. Consequently, SM forms densely packed, highly ordered and thicker L<sub>o</sub> phase with preferential partitioning of cholesterol, and PC forms more fluid L<sub>d</sub> phase with looser packing. This inter-phase height mismatch, enhanced by the intrinsic hydrocarbon chain length difference between SM and 14:1 PC (16 vs. 14 carbons), leads to the exposure of part of SM hydrophobic tail to water and results in energetically unfavourable interactions at the boundary zone between PC and SM molecules. This hydrophobic mismatch affects the local hydration properties between the interfacing PC and SM molecules, but it also likely influences how Na<sup>+</sup> ions interact with these two lipids. In case PC-SM interactions would be strongly affected by the addition of NaCl, we would expect to see a change in

circularity parameter of the domains. However, we do not observe any changes to the  $L_o$  phase domains shape and circularity as a function of salt concentration (Fig. S2†). Therefore we conclude that the PC–PC interactions are the ones that are most sensitive to the presence of  $\text{Na}^+$  ions. This is understandable – when  $\text{Na}^+$  ions bind to PC lipids, first the electrostatic repulsion between the headgroups is screened by the  $\text{Na}^+$  ions and second, the van der Waals interactions between hydrophobic tails increase,<sup>28,29</sup> altogether making the PC–PC interactions more favourable. Our observations are consistent with the general understanding that the increase in NaCl concentration leads to a decrease of the area per lipid, both in case of saturated and unsaturated lipids. This conclusion comes from experimental<sup>10,30,31</sup> and theoretical works,<sup>10,31–35</sup> for saturated,<sup>36</sup> partially saturated,<sup>32,33</sup> and unsaturated lipids.<sup>31,35,37</sup> Using molecular dynamics simulations Böckmann *et al.* showed that the area per POPC (unsaturated lipid) decreases from  $0.655 \pm 0.011 \text{ nm}^2$  in the absence of NaCl to  $0.625 \pm 0.011 \text{ nm}^2$  at 50 mM, and finally to  $0.606 \pm 0.009 \text{ nm}^2$  at 220 mM of NaCl,<sup>10</sup> consistent with other works on POPC membranes.<sup>32,33</sup> A similar trend was observed for unsaturated DOPC lipid bilayers.<sup>35,37</sup> These findings were corroborated experimentally using small angle X-ray diffraction (SAXD)<sup>30</sup> and heat capacity measurements<sup>10</sup> on POPC bilayer, as well as more recent fluorescence correlation spectroscopy measurements on DOPC membranes.<sup>31</sup> In parallel, thickening of the POPC bilayer by 1.1 Å and 2.2 Å was observed with the addition of 50 mM and 220 mM NaCl respectively.<sup>36</sup> These observations are generally attributed to the reduction of electrostatic repulsion between the lipid head groups, which leads to more favourable interactions between the PC lipids (PC–PC affinity increases) and consequently to the enhancement in phase separation. The decrease in area per lipid and thickening of the membrane is associated with the tighter packing of lipids within the  $L_d$  phase and potentially could lead to a displacement of cholesterol molecules and to a change in cholesterol partitioning. To verify this hypothesis we performed additional experiment using fluorescently labeled cholesterol (TopFluor cholesterol) as a function of NaCl concentration (see Fig. S3A and B† for representative confocal images). We found that there is a small decrease, on the order of ~8–10% (see Fig. S3C†), in partitioning of cholesterol in the  $L_d$  phase when increasing NaCl content. The observed decrease in cholesterol partitioning is fully consistent with the decrease in area per lipid and thickening of the membrane and thus somewhat tighter packing of lipids within the  $L_d$  phase with increasing NaCl content in the membrane hydration buffer.

It is clear that in water-rich conditions  $\text{Na}^+$  ions modulate phase separation in lipid bilayers. The question arises whether  $\text{Na}^+$  ions have the same ability when hydration conditions are altered. To this end, SLBs with varying NaCl concentration were imaged after removing bulk buffer and equilibrating them to relative humidity (RH) of 85% (see Experimental section in ESI†). In such conditions only a single hydration layer around lipid headgroups is present, comprising of about 12 water molecules coordinated by a single PC lipid.<sup>16,38,39</sup> No structural changes were observed for the SLBs prepared in buffer solutions

of different salt concentrations apart from domain size variation similar to that observed for fully hydrated membranes (Fig. S4†). We note, however, that mechanical stability was lower for dehydrated membranes prepared in buffer with low  $\text{Na}^+$  content (see ESI, Note 1†).

### Impact of $\text{Na}^+$ ions on the dynamics of lipids in SLBs

Given that structure of membranes and affinity for phase separation is strongly altered by the presence of  $\text{Na}^+$  it is expected that it may also have a prominent effect on the lateral dynamics of lipids within the membrane. In earlier FCS studies on fully hydrated, single phase POPC bilayers slowing down of lipid mobility was observed with increasing NaCl concentration.<sup>10</sup> On the other hand, MD simulations of lipid–ion interactions in POPE bilayers suggested that presence of cations leads to the decrease in membrane fluidity, likely due to the ion-induced lipid dehydration.<sup>11</sup> Despite a few studies investigating the role of ions affecting lipid mobility at fully hydrated conditions, the influence of ions on lipid mobility at lower hydration conditions has so far remained unexplored. We thus examined the dynamics of the  $L_d$  phase lipids both in fully hydrated and in dehydrated phase-separated membranes. Exemplary FRAP traces are shown in Fig. 2A. For fully hydrated membrane, the diffusion coefficient ( $D$ ) remained similar within the error bars (confirmed by the statistical analysis –  $t$ -test) – it varied in the range of  $2.3\text{--}2.8 \mu\text{m}^2 \text{ s}^{-1}$  for SLBs prepared in Milli-Q water to 10 mM HEPES–150 mM NaCl buffer. Only for 1.5 M NaCl  $D$  was reduced by about 30% of the average value for other buffer compositions, which could be explained by  $\text{Na}^+$ –lipids complexations in the presence of excess NaCl.<sup>10</sup> The mobile fraction was high (>90%) and did not change with NaCl concentration (Fig. 2C, magenta squares).

While for fully hydrated membranes in the presence of  $\text{Na}^+$  ions lipid mobility is hardly affected, for dehydrated membranes the picture is drastically different. The membranes prepared in different buffers were exposed to and carefully equilibrated with the environment of high relative humidity (~85%). Remarkably, in the absence of  $\text{Na}^+$  ions lipids become nearly immobile,  $D$  reaches very low value of  $<0.2 \mu\text{m}^2 \text{ s}^{-1}$  (Fig. 2B, green circles). Similarly,  $L_d$  lipids exhibit very little mobility in the membrane exposed to buffer containing low (5 mM) concentration of NaCl. However, for the membranes exposed to higher NaCl concentrations ( $\geq 20 \text{ mM}$ ), lipid mobility is significantly higher reaching value of about  $1.5 \mu\text{m}^2 \text{ s}^{-1}$  (vs.  $\sim 2.5 \mu\text{m}^2 \text{ s}^{-1}$  observed in fully hydrated membranes). A similar trend is observed for the mobile fractions (Fig. 2C, green circles). For the membranes containing little or no NaCl, mobile fractions (MF) are considerably lower (MF ~ 45%) than for the membranes containing more NaCl (MF > 80%). Here we recall that PC lipids exposed to high RH, close to 100%, are hydrated with a single hydration shell containing about 12 water molecules.<sup>29,30,36</sup> For the membranes equilibrated with the RH of 85%, this hydration shell starts to be affected and becomes unstable.<sup>16</sup> Based on the changes of  $D$ , it is evident that as soon as bulk hydration is removed and the first hydration shell starts



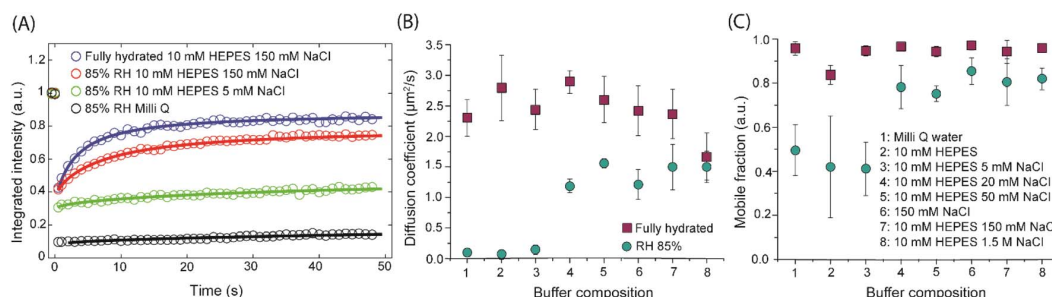


**Fig. 2** (A) FRAP traces for membrane in full hydration state and for membranes equilibrated to 85% RH. Diffusion coefficient (B) and mobile fraction (C) of  $L_d$  phase lipids at fully hydrated condition and at 85% RH condition for SLBs prepared in HEPES buffers of different NaCl concentrations. Each data point is an average of at least 10 values obtained from each of minimum two samples. The error bars denote the standard deviation of an average value.

to disintegrate, the presence of  $\text{Na}^+$  ions is crucial for the lipids to maintain their mobility.

To underpin the key role of  $\text{Na}^+$  in promoting the lipid mobility after bulk dehydration, an SLB prepared in 10 mM HEPES buffer was dehydrated to 85% RH followed by 6 h of purging of wet  $\text{N}_2$  gas through a buffer solution containing

150 mM NaCl. The wet  $\text{N}_2$  gas contains tiny droplets of the buffer, which over time blend with the hydration layer of the membrane. While initially lipids in the SLB exhibited no mobility, after 6 h of purging with the  $\text{N}_2$  rich in buffer aerosol, a clear difference in the fluorescence recovery (Fig. 3A) was observed with an increase of  $D$  from  $0.03 \pm 0.03 \mu\text{m}^2 \text{s}^{-1}$  to  $0.24 \pm 0.07 \mu\text{m}^2 \text{s}^{-1}$ . It may seem that the sole presence of  $\text{Na}^+$  ions is sufficient for the lipids to maintain their lateral mobility in water scarcity conditions. To verify such a possibility we determined the diffusion coefficients at varying membrane hydration levels for SLBs prepared in HEPES buffer with an addition of 50 mM, 150 mM and 1.5 M of NaCl. Fig. 3B shows the extracted diffusion coefficients as a function of membrane hydration level. Interestingly, the change of  $D$  follows the same trend, irrespective of the salt concentration.  $D$  drops abruptly at the initial stages of dehydration and then below approximately 50% RH it remains largely unchanged. The gradual disintegration of the lipid hydration shell leads to a sharp decline in the lateral diffusion coefficient of PC lipids, underlining that the presence of the hydration shell is absolutely necessary for the lipids to maintain their mobility at mild dehydration conditions, in agreement with our previous work.<sup>16</sup> However, this experiment unambiguously shows that  $\text{Na}^+$  ions alone cannot facilitate lipid mobility once dehydration progresses. Instead,  $\text{Na}^+$  ions and water molecules need to work in tandem to support lipid mobility when the membrane is subjected to mild dehydration.

To clear up the molecular picture and to find an explanation for the extraordinary ability of  $\text{Na}^+$  ions to shape lipid mobility after dehydration, it is important to understand how various ions bind to PC lipids. Based on the different MD simulation studies, it is generally accepted that  $\text{Na}^+$  ions can penetrate bilayer interfacial region and localize in the vicinity of the phosphate and carbonyl oxygens of the PC headgroup.<sup>35,40</sup> Consequently,  $\text{Na}^+$  as well as phosphate and/or carbonyl oxygens become partially dehydrated. According to the free energy of ion binding calculations, the most stable state for  $\text{Na}^+$  in the vicinity of a fully hydrated lipid bilayer, is to be fully hydrated in bulk water with a hydration coordination number of 5.<sup>41</sup> However,  $\text{Na}^+$  can also attach to 4 water molecules and one lipid oxygen with energy higher by only 1–2  $\text{kcal mol}^{-1}$  (Fig. 4B).

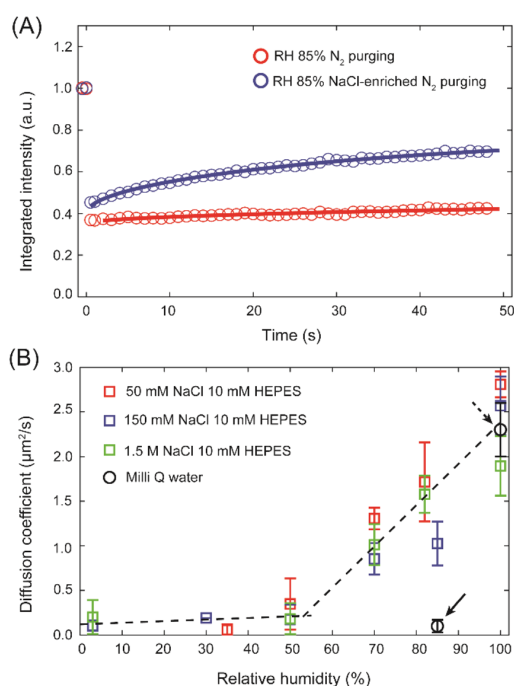


**Fig. 3** (A) FRAP traces for partially dehydrated SLB prepared in HEPES buffer and subsequently purged with wet  $\text{N}_2$  gas enriched with NaCl. (B) Diffusion coefficients of  $L_d$  phase lipids at different hydration conditions for SLBs prepared in HEPES buffer with the addition of 50 mM (red), 150 mM (blue) and 1.5 M of NaCl (green). Each data point is an average of at least 6 FRAP traces at different areas of one sample for each buffer composition. The error bars represent the standard deviation of the data. The  $D$  values for SLB prepared in Milli-Q water at fully hydrated condition and at 85% RH (highlighted by black arrows) are shown by black circles for comparison.

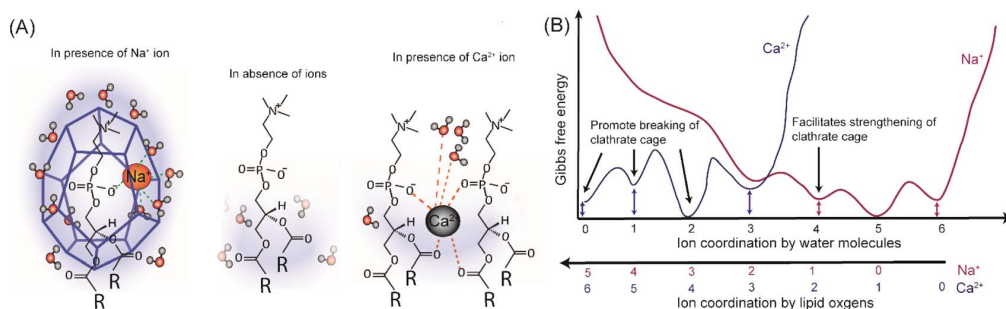


**Fig. 4** (A) Illustrative pictures of the hydration structures of PC headgroups equilibrated to 85% RH after removal of bulk water in the absence of ions as well as in the presence of Na<sup>+</sup> and Ca<sup>2+</sup> ions, (B) comparative, simplified schematic diagram of free energies of ion hydration for different coordination scenarios (by water molecules and lipid oxygens) for Na<sup>+</sup> and Ca<sup>2+</sup> ion. The scheme is based on the MD simulations data of free energies for Na<sup>+</sup> and Ca<sup>2+</sup> ions at various lipid and water coordination by Yang *et al.*<sup>41</sup>

Thus, there is little energetic penalty for the Na<sup>+</sup> ions to be (at least partially) dehydrated. Considering other local minima of ion binding free energy, Na<sup>+</sup> ions bound to lipid bilayer can coordinate up to 5–6 oxygen atoms, 1–3 from phosphate/carbonyl oxygen atoms from same or neighbouring lipid molecules and the rest (2–4) of the coordination is filled by water molecules. In fully hydrated conditions, the binding of the Na<sup>+</sup> ions with PC is in a dynamic equilibrium with a maximum residence time of 10<sup>−4</sup> s at the polar group.<sup>42</sup> This could explain the fact that at fully hydrated condition, water plays the main role in shaping the lipid mobility with a little or no change in *D* upon a moderate increase in Na<sup>+</sup> concentration. On the other hand, upon removal of the bulk water due to the unavailability of excess water the binding probability of Na<sup>+</sup> to the lipids and the residence time of Na<sup>+</sup> at the bilayer interface will increase. In order to keep the free energy of binding lowest, Na<sup>+</sup> ion bound to phosphate oxygen (O<sub>P</sub>) will preferably coordinate 2–5 water molecules to fulfill its coordination instead of binding with other lipid oxygens. Further membrane dehydration leads to increased coordination of Na<sup>+</sup> by lipids' oxygens.

It is widely accepted that for zwitterionic PC lipids, the first hydration shell around the phosphocholine moiety, contains ~6–7 water molecules.<sup>16</sup> This hydration shell is often referred to as water clathrate cage/structure. However, given its highly dynamic nature it should be viewed rather as a fluid hydration shell. This hydration layer is held in place through O<sub>P</sub>–H<sub>2</sub>O H-bonds and van der Waals interactions.<sup>29</sup> The water molecules attached to O<sub>P</sub>-bound Na<sup>+</sup> ion, being polarized and slower,<sup>43</sup> also bind to other water molecules through H-bonds. Thus, with the introduction of coulombic interactions between O<sub>P</sub>–Na<sup>+</sup>–H<sub>2</sub>O, together with the O<sub>P</sub>–H<sub>2</sub>O and H<sub>2</sub>O–H<sub>2</sub>O hydrogen bonds, the PC–Na<sup>+</sup>–water clathrate complex becomes stronger than simple PC–water clathrate complex. In other words, sodium ions strengthen and stabilise the hydration structure around the PC moiety, preventing immediate disintegration of this hydration shell upon bulk dehydration (Fig. 4A). As the membrane becomes dehydrated further, coulombic interactions between lipids, Na<sup>+</sup> ions and water molecules fail in stabilising the hydration layer leading to a sharp decline in lipid mobility. The same trajectory of changes in *D*, regardless of Na<sup>+</sup>

concentration, highlights that the role of Na<sup>+</sup> ions is only related to holding the adequate number of water molecules around the phosphocholine group, but not controlling the lipid mobility directly. Consequently, Na<sup>+</sup> ions themselves do not promote lipid mobility at very low hydration conditions (≤50% RH). Hence, it has to be emphasized that it is not just Na<sup>+</sup> ions that maintain lipid mobility after the removal of bulk water but the perfect balance between sodium and hydration play the key role. Both sodium and water molecules complement each other to promote lipid mobility after the removal of the outer hydration layer of the lipids. On the other hand, in the absence of Na<sup>+</sup> ions, the hydration structure, bound by only weak van der Waals interactions and H-bonds, falls apart already after the removal of bulk water, resulting in very low lipid mobility at 85% RH (Fig. 4A).

#### Impact of Ca<sup>2+</sup>, Mg<sup>2+</sup> and K<sup>+</sup> ions on the dynamics of lipids in SLBs

An additional reason for high mobility at ~85% RH could be that the presence of ions polarizes the water around the lipid headgroups, which in turn shields the electrostatic repulsion between adjacent lipids better. Naturally, in that case, divalent ions, due to higher charge density, should be more efficient in supporting lipid mobility after dehydration. To verify this possibility, we measured the lateral diffusion of lipids at fully hydrated and dehydrated conditions for SLBs prepared in 10 mM HEPES buffer containing 150 mM of CaCl<sub>2</sub>. Ca<sup>2+</sup> is a divalent ion but has a very similar ionic radius to Na<sup>+</sup>. The average domain size in the SLB prepared in buffer containing 150 mM of CaCl<sub>2</sub> was 0.82 ± 0.13 μm<sup>2</sup>, which is smaller (approximately by a factor of 2) than the average domain size in SLB prepared with 150 mM of NaCl (Fig. S5†).

The *D* value at fully hydrated condition was found to be 1.18 ± 0.22 μm<sup>2</sup> s<sup>−1</sup>, which is around half of the *D* observed for the same concentration of Na<sup>+</sup> ions. Consistently, the mobile fraction was also slightly lower (~85%) than that in the presence of NaCl. Strikingly, after the removal of bulk water, lipid mobility was almost ceased already at 85% RH (*D* = 0.11 ± 0.08 μm<sup>2</sup> s<sup>−1</sup>, ~10 times drop), similar to the SLB hydrated with Milli-Q water (Fig. 5). This indicates that Ca<sup>2+</sup> ions are unable to contribute to

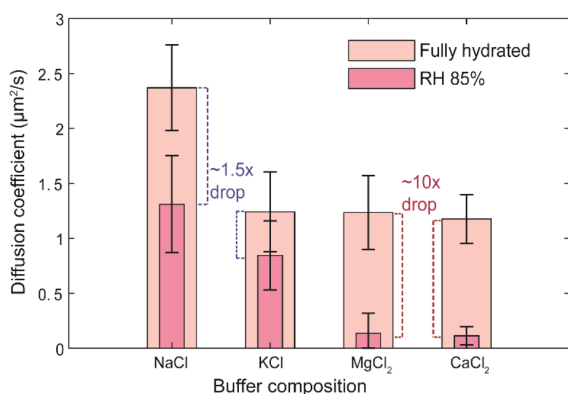


Fig. 5 Comparison of  $D$  values of  $L_d$  phase lipids for 10 mM HEPES buffer containing 150 mM of NaCl, KCl, MgCl<sub>2</sub> and CaCl<sub>2</sub> for fully hydrated SLBs and equilibrated to 85% RH. Each bar represent the average  $D$  value over at least 6 FRAP traces acquired from each of minimum three samples for each buffer and hydration conditions. The error bars denote the standard deviations of the obtained  $D$  values.

the stabilisation of the hydration layer around lipid headgroups. Previous studies showed that the binding constant of Ca<sup>2+</sup> to the membrane is much higher than for Na<sup>+</sup> and that Ca<sup>2+</sup> preferentially binds to the lipid oxygens rather than to water molecules, leading to dehydration of the phosphate region.<sup>44</sup> Similar conclusions have been reached in infrared studies on bulk lipid paste in different hydration conditions and containing various ions.<sup>44</sup> Recent MD simulations showed that the lowest free energy state for Ca<sup>2+</sup> is when it binds to 4 lipid oxygen and 2 water molecules to have its coordination number of 6 filled (see Fig. 4B).<sup>41</sup> The other energy minima, 2–4 kcal mol<sup>−1</sup> higher in energy than the global minimum, correspond to binding with 3–5 lipid oxygens with total coordination number 4–6, leaving the number of water molecules attached to Ca<sup>2+</sup> close to 0. This in return leads to destabilisation of the complex hydration structure, which can no longer anchor to the phosphate oxygens. Hence, it is of no surprise that in the presence of Ca<sup>2+</sup> ions the hydration shell disintegrates immediately after bulk water removal causing very low lipid mobility already at 85% RH. Moreover, preferential binding of Ca<sup>2+</sup> to phosphate and carbonyl oxygens of lipids promotes the formation of Ca<sup>2+</sup> complex with more than one lipid,<sup>7,45,46</sup> which also explains the lower (approximately 2-fold) diffusion coefficient in the presence of 150 mM of Ca<sup>2+</sup>, already in full hydration conditions. Last but not least, the divergent action of CaCl<sub>2</sub> with respect to NaCl also confirms that Cl<sup>−</sup> has no noticeable effect on the dynamics of the membrane constituents, in agreement with the MD simulation, which showed that Cl<sup>−</sup> being larger in size mostly resides in the bulk water.<sup>40</sup>

Evidently, strengthening of lipid hydration structure in the presence of Na<sup>+</sup> is not related directly to the size or charge of the cation, but it is the hydration energy and the lipid binding energy of these ions that play the key role here. To further corroborate this conclusion we measured  $D$  of  $L_d$  lipids in membranes hydrated with the buffer containing another two

biologically relevant ions K<sup>+</sup> and Mg<sup>2+</sup> (10 mM HEPES–150 mM KCl and 10 mM HEPES–10 mM MgCl<sub>2</sub>), but for which very different hydration energies have been reported (for representative confocal images of these membranes see Fig. S5†). K<sup>+</sup> ions have similar hydration energy and lipid binding affinity as Na<sup>+</sup> ions,<sup>41</sup> thus one could expect that the lipid diffusion could also be promoted by the presence of K<sup>+</sup>. On contrary, for Mg<sup>2+</sup>, which has very high energy barrier (>25 kcal) to bind with a single lipid oxygen in transition from the fully hydrated state (in comparison to only 1–2 kcal energy barrier in case of Na<sup>+</sup> and K<sup>+</sup>), one would expect similar behavior as for Ca<sup>2+</sup> or for the membrane with no salt present in the buffer, that is low lipid mobility in the absence of bulk water. The experimental data fully confirm these expectations – after the removal of bulk water in the presence of K<sup>+</sup> lipid mobility was mere ~1.5 times lower, whereas for Mg<sup>2+</sup> over 10 times lower diffusion coefficient was measured (Fig. 5). Clearly, K<sup>+</sup> has similar effect on the lipid mobility upon membrane dehydration as Na<sup>+</sup>, whereas the activity of Mg<sup>2+</sup> resembles that of Ca<sup>2+</sup>. It should be noted that though in the presence of divalent cations Ca<sup>2+</sup> and Mg<sup>2+</sup> lipid diffusion drops down to a very low value upon removal of bulk water, the underlying mechanism of action is likely different. Mg<sup>2+</sup> does not bind to the membrane lipids, thus it neither stabilize nor disrupt the lipid hydration shell. On the other hand, Ca<sup>2+</sup> having stronger lipid oxygen binding affinity than to water molecules, it destabilizes the lipid hydration structure. Altogether our observations confirm the importance of the free energy difference between the lipid-bound states and fully water-coordinated state of the investigated cations in determining the ability to support lipid mobility at reduced hydration conditions. We note here, that at fully hydrated conditions, lipid mobility was found to be consistently smaller in the presence of KCl, MgCl<sub>2</sub> and CaCl<sub>2</sub> (~1.3 μm<sup>2</sup> s<sup>−1</sup>) compared to NaCl (2.3 μm<sup>2</sup> s<sup>−1</sup>), however the origin of this difference is unclear.

Furthermore, it is interesting to address how  $L_o$  phase lipid mobility is affected in the presence of various cations. Therefore we determined the mobility of lipids in single ( $L_o$ ) phase SLBs composed of 1:1 SM/cholesterol and with the addition of fluorescent lipid analogue NBD-DPPE. The experiments were performed in the presence of 10 mM HEPES–150 mM NaCl and 10 mM HEPES–150 mM CaCl<sub>2</sub> since Na<sup>+</sup> and Ca<sup>2+</sup> showed very different effect on the lipid mobility in case of the  $L_d$  phase. At fully hydrated conditions, both for Na<sup>+</sup> and Ca<sup>2+</sup> present in the buffer the  $D$  values were very similar (~0.18 μm<sup>2</sup> s<sup>−1</sup>) and fully consistent with the typical values obtained for the  $L_o$  phase lipids.<sup>16,47</sup> After removal of bulk water, unlike what was observed for the  $L_d$  phase, in the presence of NaCl lipid diffusion ceases indicating that even Na<sup>+</sup> can not assist in maintaining lipid mobility in the  $L_o$  phase. The relative (full hydration vs. 85% RH) large decrease (~9-fold) in diffusion coefficient is very similar for both Na<sup>+</sup> and Ca<sup>2+</sup> (Fig. S6†). This experimental observation is understandable and corroborates the MD simulation finding – the Na<sup>+</sup> ion binding to the more densely packed  $L_o$  phase is much less probable than it is to the loosely packed  $L_d$  phase.<sup>26</sup>

## Conclusions

In summary, we demonstrated that the cooperativity between water and specific ions (sodium and potassium) is an essential factor that controls lipid mobility in membranes under water depletion conditions.  $\text{Na}^+$  ions reveal their importance already in fully hydrated membranes, in which the extent of phase separation increases significantly with an increase of  $\text{Na}^+$  concentration. At the same time, in these conditions,  $\text{Na}^+$  ions have hardly any effect on the mobility of lipids. In stark contrast, the true capabilities of  $\text{Na}^+$  ions are revealed upon membrane dehydration, when they actively penetrate the inter-lipid headgroup region. There, both  $\text{Na}^+$  and  $\text{K}^+$  ions act to *stabilise* the hydration shell structure around the lipid headgroups, thereby facilitating lipid diffusion. However, we emphasize that the ability of these cations to promote lipid dynamics after membrane dehydration does not nullify the principal role of water in supporting lipid mobility. At very low hydration conditions, where not enough water molecules are present to form the hydration layer,  $\text{Na}^+$  and  $\text{K}^+$  ions alone fail to retain lipid mobility even at high concentration. Clearly, it is a cooperative effect, in which down to a certain dehydration level water and  $\text{Na}^+/\text{K}^+$  ions work in a concerted manner in promoting lipid diffusion. The uniqueness of these monovalent cations is evident when compared to the activity of divalent  $\text{Ca}^{2+}$  or  $\text{Mg}^{2+}$  cations.  $\text{Ca}^{2+}$  despite having similar ionic radius to  $\text{Na}^+$ , has the tendency to *destabilise* the hydration structure around the lipid headgroups due to its greater binding affinity to lipid oxygens than to remnant water molecules.  $\text{Mg}^{2+}$  ions on the other hand prefer to be fully hydrated by water and need to overcome a very high energy barrier in order to bind to the lipids. Consequently, in the presence of  $\text{Ca}^{2+}$  or  $\text{Mg}^{2+}$  lipid mobility drops to very low values upon membrane dehydration. We can thus conclude that while  $\text{Na}^+$  and  $\text{K}^+$  promote fluidity of the membrane when its hydration layer is perturbed,  $\text{Ca}^{2+}$  or  $\text{Mg}^{2+}$  rather lead to gelification (in terms of mobility) of the membrane. Importantly, confronting the activity of the studied cations it is evident that it is not the charge or the ability to polarise the local environment but purely the competition between ion hydration and ion binding to lipid oxygens that cause such a divergent activity of various cations.

This work unveils the important and unique role of specific cations in modulating the membrane structure as well as lipid dynamics and emphasizes the importance of local ion composition and concentration for membrane biophysical homeostasis. Numerous reports underpin the importance of ions in various biological cell fusion events such as during viral entry, neurotransmission or fertilisation, processes where two merging lipid bilayers undergo transient membrane dehydration.<sup>24</sup> Specifically, it has been proposed that the presence of NaCl promotes fusion of *E. coli* membranes and the local aggregation of the bacterial potassium channel KcsA.<sup>48</sup> This was ascribed to  $\text{Na}^+$ -induced lowering of hydration repulsive forces and modulation of the local water structure. Recently it was reported that the infection by bunyavirus depends on the local ion composition. It was shown that viral spike-membrane

interactions are enhanced in the presence of locally elevated  $\text{K}^+$  concentration.<sup>49</sup> On the other hand, the presence of  $\text{Ca}^{2+}$  ions is known to be one of the important factors in neurotransmission events, where also transient dehydration occurs during membrane fusion.<sup>50</sup> It is thus feasible that depending on the particular mechanism underlying the fusion process it may involve either maintenance or a local decrease in membrane fluidity.

Our findings have also important implications for biological systems where water activity can be very low such as in cytoplasm moieties for instance Golgi apparatus or the intracellular leaflet of the membrane, which interacts strongly with the cortical actin. Another example, where low hydration is accompanied by high ion concentrations is the case of amphibian oocytes, where the cytoplasm contains approximately half of the water content compared to the nucleus, whereas the  $\text{Na}^+$  concentration is 5–10 times higher than in the cytoplasm.<sup>51</sup>

Thus overall, the presented results provide important implications and new molecular-level perspective for reviewing biochemical processes involving biomembranes subjected to transient dehydration. Yet, the challenge remains in being able to monitor locally hydration, ion composition, and lipid membrane properties in living cells.

## Data availability

All relevant data supporting this article have been included in the main text and the ESI.† All original data generated during this work are available from the corresponding authors upon request.

## Author contributions

MC: conceptualization, methodology, investigation, formal analysis, validation, visualization, writing – original draft, writing – review and editing; EK: methodology, writing – review and editing; HOR: methodology, writing – review and editing; LP: supervision, conceptualization, validation, funding acquisition, writing – review and editing.

## Conflicts of interest

There are no conflicts of interest to declare.

## Acknowledgements

L.P. acknowledges the financial support from the EMBO Installation Grant (IG 4147). M.C. and E.K. acknowledge the financial support from the First TEAM Grant No. POIR.04.04.00-00-5D32/18-00, provided by the Foundation for Polish Science (FNP). H.O.R. acknowledges financial support from the National Science Centre (Poland), grant number 2020/37/B/ST4/01785.



## Notes and references

- 1 S. J. Singer and G. L. Nicolson, The Fluid Mosaic Model of the Structure of Cell Membranes, *Science*, 1972, **175**, 720–731.
- 2 W. H. Binder, V. Barragan and F. M. Menger, Domains and Rafts in Lipid Membranes, *Angew. Chem., Int. Ed.*, 2003, **42**, 5802–5827.
- 3 R. Ohtani, Y. Anegawa, H. Watanabe, Y. Tajima, M. Kinoshita, N. Matsumori, K. Kawano, S. Yanaka, K. Kato, M. Nakamura, M. Ohba and S. Hayami, Metal Complex Lipids for Fluid–Fluid Phase Separation in Coassembled Phospholipid Membranes, *Angew. Chem., Int. Ed.*, 2021, **60**, 13603–13608.
- 4 R. J. Alsop, R. Maria Schober and M. C. Rheinstädter, Swelling of Phospholipid Membranes by Divalent Metal Ions Depends on the Location of the Ions in the Bilayers, *Soft Matter*, 2016, **12**, 6737–6748.
- 5 H. Trauble and H. Eibl, Electrostatic Effects on Lipid Phase Transitions: Membrane Structure and Ionic Environment, *Proc. Natl. Acad. Sci. U. S. A.*, 1974, **71**, 214–219.
- 6 J. N. Sachs, H. Nanda, H. I. Petrache and T. B. Woolf, Changes in Phosphatidylcholine Headgroup Tilt and Water Order Induced by Monovalent Salts: Molecular Dynamics Simulations, *Biophys. J.*, 2004, **86**, 3772–3782.
- 7 M. Sovago, G. W. H. Worpel, M. Smits, M. Müller and M. Bonn, Calcium-Induced Phospholipid Ordering Depends on Surface Pressure, *J. Am. Chem. Soc.*, 2007, **129**, 11079–11084.
- 8 P. Lauger, Mechanisms of Biological Ion Transport-Carriers, Channels, and Pumps in Artificial Lipid Membranes, *Angew. Chem., Int. Ed.*, 1985, **24**, 905–923.
- 9 A. Raasakka, N. C. Jones, S. V. Hoffmann and P. Kursula, Ionic Strength and Calcium Regulate Membrane Interactions of Myelin Basic Protein and the Cytoplasmic Domain of Myelin Protein Zero, *Biochem. Biophys. Res. Commun.*, 2019, **511**, 7–12.
- 10 R. A. Böckmann, A. Hac, T. Heimburg and H. Grubmüller, Effect of Sodium Chloride on a Lipid Bilayer, *Biophys. J.*, 2003, **85**, 1647–1655.
- 11 R. Kagawa, Y. Hirano, M. Taiji, K. Yasuoka and M. Yasui, Dynamic Interactions of Cations, Water and Lipids and Influence on Membrane Fluidity, *J. Membr. Sci.*, 2013, **435**, 130–136.
- 12 A. A. Gurtovenko and I. Vattulainen, Lipid Transmembrane Asymmetry and Intrinsic Membrane Potential: Two Sides of the Same Coin, *J. Am. Chem. Soc.*, 2007, **129**, 5358–5359.
- 13 A. L. Hodgkin and P. Horowicz, The Influence of Potassium and Chloride Ions on the Membrane Potential of Single Muscle Fibers, *J. Physiol.*, 1959, **148**, 127–160.
- 14 N. N. Casillas-Ituarte, X. Chen, H. Castada and H. C. Allen, Na<sup>+</sup> and Ca<sup>2+</sup> Effect on the Hydration and Orientation of the Phosphate Group of DPPC at Air - Water and Air - Hydrated Silica Interfaces, *J. Phys. Chem. B*, 2010, **114**, 9485–9495.
- 15 J. Song, J. Franck, P. Pincus, M. W. Kim and S. Han, Specific Ions Modulate Diffusion Dynamics of Hydration Water on Lipid Membrane Surfaces, *J. Am. Chem. Soc.*, 2014, **136**, 2642–2649.
- 16 M. Chattopadhyay, E. Krok, H. Orlikowska, P. Schwillie, H. G. Franquelim and L. Piatkowski, Hydration Layer of Only a Few Molecules Controls Lipid Mobility in Biomimetic Membranes, *J. Am. Chem. Soc.*, 2021, **143**, 14551–14562.
- 17 C. Calero and G. Franzese, Membranes with Different Hydration Levels: The Interface between Bound and Unbound Hydration Water, *J. Mol. Liq.*, 2019, **273**, 488–496.
- 18 C. Calero, H. E. Stanley and G. Franzese, Structural Interpretation of the Large Slowdown of Water Dynamics at Stacked Phospholipid Membranes for Decreasing Hydration Level: All-Atom Molecular Dynamics, *Materials*, 2016, **9**, 319.
- 19 K. A. C. Madin and J. H. Crowe, Anhydrobiosis in Nematodes: Carbohydrate and Lipid Metabolism during Dehydration, *J. Exp. Zool.*, 1975, **193**, 335–342.
- 20 J. H. Crowe, L. M. Crowe and D. Chapman, Preservation of Membranes in Anhydrobiotic Organisms: The Role of Trehalose, *Science*, 1984, **223**, 701–703.
- 21 R. Marotta, F. Leasi, A. Uggetti, C. Ricci and G. Melone, Dry and Survive: Morphological Changes during Anhydrobiosis in a Bdelloid Rotifer, *J. Struct. Biol.*, 2010, **171**, 11–17.
- 22 J. Wilschut, N. DiizgiineS, R. Fraley and D. Papahadjopoulos, Studies on the Mechanism of Membrane Fusion: Kinetics of Calcium Ion Induced Fusion of Phosphatidylserine Vesicles Followed by a New Assay for Mixing of Aqueous Vesicle Contents, *Biochemistry*, 1980, **19**, 6011–6021.
- 23 A. Portis, C. Newton, W. Pangborn and D. Papahadjopoulos, Studies on the Mechanism of Membrane Fusion: Evidence for an Intermembrane Ca<sup>2+</sup>-Phospholipid Complex, Synergism with Mg<sup>2+</sup>, and Inhibition by Spectrin, *Biochemistry*, 1979, **18**, 780–790.
- 24 S. Aeffer, T. Reusch, B. Weinhausen and T. Salditt, Energetics of Stalk Intermediates in Membrane Fusion Are Controlled by Lipid Composition, *Proc. Natl. Acad. Sci. U. S. A.*, 2012, **109**, E1609–E1618.
- 25 E. Krok, A. Batura, M. Chattopadhyay, H. Orlikowska and L. Piatkowski, Lateral Organization of Biomimetic Cell Membranes in Varying PH Conditions, *J. Mol. Liq.*, 2022, **345**, 117907.
- 26 M. Stępniewski, A. Bunker, M. Pasenkiewicz-Gierula, M. Karttunen and T. Róg, Effects of the Lipid Bilayer Phase State on the Water Membrane Interface, *J. Phys. Chem. B*, 2010, **114**, 11784–11792.
- 27 A. Magarkar, V. Dhawan, P. Kallinteri, T. Viitala, M. Elmowafy, T. Róg and A. Bunker, Cholesterol Level Affects Surface Charge of Lipid Membranes in Saline Solution, *Sci. Rep.*, 2014, **4**, 5005.
- 28 R. Friedman, Membrane–Ion Interactions, *J. Membr. Biol.*, 2018, **251**, 453–460.
- 29 C. C. Logisz and J. S. Hovis, Effect of Salt Concentration on Membrane Lysis Pressure, *Biochim. Biophys. Acta, Biomembr.*, 2005, **1717**, 104–108.

- 30 G. Pabst, A. Hodzic, J. Štrancar, S. Danner, M. Rappolt and P. Laggner, Rigidification of Neutral Lipid Bilayers in the Presence of Salts, *Biophys. J.*, 2007, **93**, 2688–2696.
- 31 M. Jan Akhunzada, F. D'Autilia, B. Chandramouli, N. Bhattacharjee, A. Catte, R. Di Rienzo, F. Cardarelli and G. Brancato, Interplay between Lipid Lateral Diffusion, Dye Concentration and Membrane Permeability Unveiled by a Combined Spectroscopic and Computational Study of a Model Lipid Bilayer, *Sci. Rep.*, 2019, **9**, 1508.
- 32 P. Jurkiewicz, L. Cwiklik, A. Vojtišková, P. Jungwirth and M. Hof, Structure, Dynamics, and Hydration of POPC/POPS Bilayers Suspended in NaCl, KCl, and CsCl Solutions, *Biochim. Biophys. Acta, Biomembr.*, 2012, **1818**, 609–616.
- 33 A. A. Gurtovenko and I. Vattulainen, Effect of NaCl and KCl on Phosphatidylcholine and Phosphatidylethanolamine Lipid Membranes: Insight from Atomic-Scale Simulations for Understanding Salt-Induced Effects in the Plasma Membrane, *J. Phys. Chem. B*, 2008, **112**, 1953–1962.
- 34 A. Cordoní, O. Edholm and J. J. Perez, Effect of Ions on a Dipalmitoyl Phosphatidylcholine Bilayer. A Molecular Dynamics Simulation Study, *J. Phys. Chem. B*, 2008, **112**, 1397–1408.
- 35 R. Vácha, S. W. I. Siu, M. Petrov, R. A. Böckmann, J. Barucha-Kraszewska, P. Jurkiewicz, M. Hof, M. L. Berkowitz and P. Jungwirth, Effects of Alkali Cations and Halide Anions on the DOPC Lipid Membrane, *J. Phys. Chem. A*, 2009, **113**, 7235–7243.
- 36 S. A. Pandit, D. Bostick and M. L. Berkowitz, Molecular Dynamics Simulation of a Dipalmitoylphosphatidylcholine Bilayer with NaCl, *Biophys. J.*, 2003, **84**, 3743–3750.
- 37 L. F. Pineda De Castro, M. Dopson and R. Friedman, Biological Membranes in Extreme Conditions: Anionic Tetraether Lipid Membranes and Their Interactions with Sodium and Potassium, *J. Phys. Chem. B*, 2016, **120**, 10628–10634.
- 38 L. Piatkowski, J. De Heij and H. J. Bakker, Probing the Distribution of Water Molecules Hydrating Lipid Membranes with Ultrafast Förster Vibrational Energy Transfer, *J. Phys. Chem. B*, 2013, **117**, 1367–1377.
- 39 K. Hristova and S. H. White, Determination of the Hydrocarbon Core Structure of Fluid Dioleoylphosphocholine (DOPC) Bilayers by x-Ray Diffraction Using Specific Bromination of the Double Bonds: Effect of Hydration, *Biophys. J.*, 1998, **74**, 2419–2433.
- 40 M. Pasenkiewicz-Gierula, K. Baczynski, M. Markiewicz and K. Murzyn, Computer Modelling Studies of the Bilayer/Water Interface, *Biochim. Biophys. Acta, Biomembr.*, 2016, **1858**, 2305–2321.
- 41 J. Yang, C. Calero, M. Bonomi and J. Martí, Specific Ion Binding at Phospholipid Membrane Surfaces, *J. Chem. Theory Comput.*, 2015, **11**, 4495–4499.
- 42 H. Akutsut and J. Seelig, Interaction of Metal Ions with Phosphatidylcholine Bilayer Membranes, *Biochemistry*, 1981, **20**, 7366–7373.
- 43 K. J. Tielrooij, N. Garcia-Araez, M. Bonn and H. J. Bakker, Cooperativity in Ion Hydration, *Science*, 2010, **328**, 1006–1009.
- 44 H. Binder and O. Zschö, The Effect of Metal Cations on the Phase Behavior and Hydration Characteristics of Phospholipid Membranes, *Chem. Phys. Lipids*, 2002, **115**, 39–61.
- 45 A. Melcrová, S. Pokorna, S. Pullanchery, M. Kohagen, P. Jurkiewicz, M. Hof, P. Jungwirth, P. S. Cremer and L. Cwiklik, The Complex Nature of Calcium Cation Interactions with Phospholipid Bilayers, *Sci. Rep.*, 2016, **6**, 1–12.
- 46 R. A. Böckmann and H. Grubmüller, Multistep Binding of Divalent Cations to Phospholipid Bilayers: A Molecular Dynamics Study, *Angew. Chem., Int. Ed.*, 2004, **43**, 1021–1024.
- 47 N. Kahya, D. Scherfeld, K. Bacia, B. Poolman and P. Schwille, Probing Lipid Mobility of Raft-Exhibiting Model Membranes by Fluorescence Correlation Spectroscopy, *J. Biol. Chem.*, 2003, **278**, 28109–28115.
- 48 M. Raja and E. Vales, Effects of Sodium Chloride on Membrane Fusion and on the Formation of Aggregates of Potassium Channel KcsA in Escherichia Coli Membrane, *Biophys. Chem.*, 2009, **142**, 46–54.
- 49 E. K. Punch, S. Hover, H. T. W. Blest, J. Fuller, R. Hewson, J. Fontana, J. Mankouri and J. N. Barr, Potassium Is a Trigger for Conformational Change in the Fusion Spike of an Enveloped RNA Virus, *J. Biol. Chem.*, 2018, **293**, 9937–9944.
- 50 J. Rizo, Molecular Mechanisms Underlying Neurotransmitter Release, *Annu. Rev. Biophys.*, 2022, **51**, 377–408.
- 51 T. J. Century, I. R. Fenichel and S. B. Horowitz, The Concentrations of Water, Sodium and Potassium in the Nucleus and Cytoplasm of Amphibian Oocytes, *J. Cell Sci.*, 1970, **7**, 5–13.

Electronic Supplementary Material (ESI) for Chemical Science.  
This journal is © The Royal Society of Chemistry 2023

## Supplementary information

### Cooperativity between sodium ions and water molecules facilitates lipid mobility in model cell membranes

Madhurima Chattopadhyay\*, Emilia Krok, Hanna Orlikowska-Rzeznik and Lukasz Piatkowski\*

Institute of Physics, Poznan University of Technology, Piotrowo 3, 60-965 Poznan, Poland

Email: [madhurima.chattopadhyay@put.poznan.pl](mailto:madhurima.chattopadhyay@put.poznan.pl);

[lukasz.j.piatkowski@put.poznan.pl](mailto:lukasz.j.piatkowski@put.poznan.pl)

#### Experimental procedures

**Materials:** 1,2-Dimyristoleoyl-sn-glycero-3-phosphocholine (14:1 PC), egg yolk sphingomyelin (SM), and cholesterol were purchased from Avanti Polar Lipids, Alabaster, AL, USA. 1,2-dioleoyl-snglycero-3-phosphoethanolamine labeled with Atto 633 (DOPE-Atto 633), 4-(2-hydroxyethyl)piperazine-1-ethanesulfonic acid (HEPES), sodium chloride (NaCl), calcium chloride (CaCl<sub>2</sub>), Magnesium chloride (MgCl<sub>2</sub>), potassium chloride (KCl), 1,2-dioleoyl-sn-glycero-3-phosphoethanolamine-N-(7-nitro-2-1,3-benzoxadiazol-4-yl)-ammonium salt (18:1 NBD DOPE), 1,2-dipalmitoyl-sn-glycero-3-phosphoethanolamine-N-(7-nitro-2-1,3-benzoxadiazol-4-yl)-ammonium salt (16:0 NBD DPPE), TopFluor cholesterol and chloroform (HPLC grade) were purchased from Merck KGaA, Darmstadt, Germany. All the materials were used without further purification.

**Vesicle Preparation:** Vesicle deposition method following a formerly established protocol with suitable adaptations was used to prepare SLBs<sup>1</sup>. 14:1 PC, SM, and cholesterol were mixed at a molar ratio 1:1:1 with an appropriate fluorescent label (0.5 mol% of NBD-PE or 0.1 mol% of TopFluor cholesterol) in chloroform solution. The chloroform was evaporated by blowing nitrogen gas and to ensure complete removal of the solvent, the dried thin film of lipids deposited on the bottom of the vial was desiccated under vacuum for at least 2 h. The lipids were dissolved in an appropriate buffer solution (pH adjusted to 7.4) to form multilamellar vesicles (MLVs) of overall 10 mM lipid concentration and were heated to 60 °C on a hot plate and vortexed for a few cycles to obtain a completely homogeneous aqueous solution of lipids. The MLV suspension was distributed as aliquots into sterilized glass vials and those were stored at -20 °C for further use.

**Preparation of SLBs of varying salt concentration:** HEPES buffers of varying Na<sup>+</sup> ion concentrations were prepared by adding suitable amounts of NaCl salt with HEPES in fresh Milli Q water. Buffer solutions containing 5 mM, 20 mM, 50 mM, 150 mM and 1.5 M NaCl with 10 mM HEPES were used to investigate the effect of sodium ions on SLBs. Additionally, fresh Milli Q water, 10 mM HEPES buffer, 150 mM NaCl solution in fresh Milli Q water as well as 10 mM HEPES buffer solutions with 150 mM CaCl<sub>2</sub>, MgCl<sub>2</sub> and KCl were also used. The pH of the buffer solutions was around 5.2 naturally after dissolving HEPES to fresh Milli Q water. The pH was not adjusted to the biological pH range (pH ~7.4) to refrain from altering the sodium ion concentration by adding excess NaOH. Another reason was to keep the pH comparable to the pH of Milli Q water, which came down to around 5.5 soon after the collection due to absorption of atmospheric CO<sub>2</sub>. The frozen 10 mM MLV aliquots were thawed and diluted 10 times (final concentration of lipids 1 mM) using a suitable water/ buffer solution with desired salt concentration. These cloudy MLV suspensions were bath-sonicated for 10 mins to generate a clear solution of small unilamellar vesicles (SUVs). A half-cut Eppendorf tube was placed on a coverslip with a freshly cleaved mica sheet glued on it by UV-activated glue (Norland 68) and was sealed with silicone. At room temperature, 100 µL of SUVs solution in the desired buffer was deposited on the mica followed by immediate addition of 2 µL of 0.1 M CaCl<sub>2</sub> solution. 400 µL of Milli Q water or buffer solution of desired salt concentration was added to it after around 30 sec and then the sample was incubated for 30 minutes. The bilayer was rinsed with total of 20 mL of specific buffer solution to eliminate excess unburst vesicles. The Eppendorf tube reservoir was fully filled with desired buffer solution and sealed with a glass coverslip and silicone to prepare a fully hydrated sample.

**Preparation of SLBs of different hydration states:** The SLBs were dehydrated by the removal of bulk water/buffer solution using pipette and immediate purging with nitrogen gas using our home-built humidity control setup by the method of slow and gradual decrease of the relative humidity<sup>2</sup>. SLBs were equilibrated for about 10 mins to 85%, 70%, 50%, 30% and 3% RH before FRAP measurements were performed.

**Fluorescence Microscopy and FRAP:** Fluorescence imaging and FRAP experiments were performed on SLBs in buffer with varying salt concentrations using an upright Zeiss LSM 710 (Carl Zeiss, Jena, Germany) microscope with 100x, 1.3 NA oil immersion objective. Fluorescent dyes NBD-DOPE, NBD-DPPE and TopFluor cholesterol were excited by laser of wavelength 488 nm. Confocal imaging and FRAP experiments were performed on at least three samples of each salt concentration at fully hydrated condition to obtain the average domain size and diffusion coefficient. Minimum 10 different, 50x50  $\mu\text{m}$  areas were imaged for each sample for domain size determination. The original confocal images were converted to 8-bit black and white binary images. Domains were identified by adjusting the threshold of contrast, and the domain sizes were obtained using the ImageJ software<sup>3</sup>.

FRAP experiments were performed on at least 6 different, 50  $\mu\text{m}$   $\times$  50  $\mu\text{m}$  areas of each hydrated and dehydrated sample by bleaching a circular spot of 10  $\mu\text{m}$  diameter. Diffusion coefficients of lipids were quantified by fitting the fluorescence recovery curves assuming free Brownian lateral diffusion of lipid molecules in the membrane using modified Soumpasis formula<sup>4</sup>:

$$f(t) = a \cdot e^{\frac{2\tau_D}{t}} \left( I_0\left(\frac{2\tau_D}{t}\right) + I_1\left(\frac{2\tau_D}{t}\right) \right) \quad (1)$$

where

$$\tau_D = \frac{w^2}{4D} \quad (2)$$

where  $a$  is an amplitude of the fitted recovery curve,  $b$  is the fluorescence intensity remaining after photobleaching,  $w$  is the radius of the bleached area, and  $I_0(t)$  and  $I_1(t)$  are modified Bessel functions. Intensity of the bleached spot was normalized with respect to the reference intensity signal of the whole image excluding a circular area around the bleached spot with radius  $2w$ .

### Results and Discussion

#### Supplementary Note 1

Preparation of SLBs in buffer conditions depleted in ions and control over their hydration state do not pose major difficulties. At the same time it should be noted that membrane preservation after dehydration appeared to be more difficult for SLBs with lower salt concentrations. Often, in large area of the sample, a dense layer of aggregates was observed on top of the membrane and membrane coverage of the solid support (mica) was lower. This suggests decreased mechanical stability of the membrane in the absence (or low content) of ions. This observation is consistent with previous atomic force microscopy, transmission IR and force spectroscopy studies, which showed that presence of ions leads to an increase of the mechanical strength of SLBs. This has been ascribed to the decrease in intermolecular distances due to screening of polar head groups and enhancement of the order of hydrocarbon tails in presence of various cations<sup>5,6</sup>.



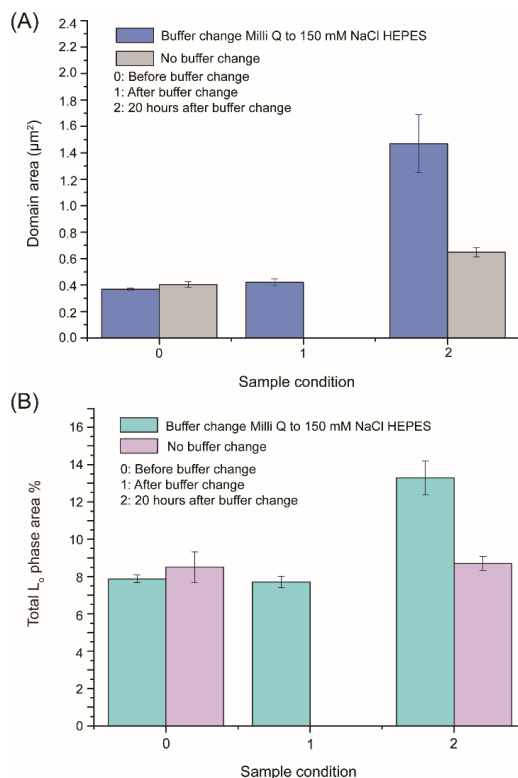


**Figure S1.** Average domain area (A) and total  $L_0$  phase area % i.e. percentage of area of the  $L_0$  phase with respect to the area of the entire image (B) before (0), immediately after (1) and 20 hours after (2) replacing Milli Q water with 10 mM HEPES 150 mM NaCl buffer (blue and cyan in panel A and B, respectively) in comparison to control experiments with no buffer change (grey and purple in panel A and B, respectively). Clearly, upon buffer exchange, the average domain area and total  $L_0$  phase area % increase, whereas SLBs left in Milli Q water did not show any significant change of the average domain area or the total  $L_0$  phase area %.

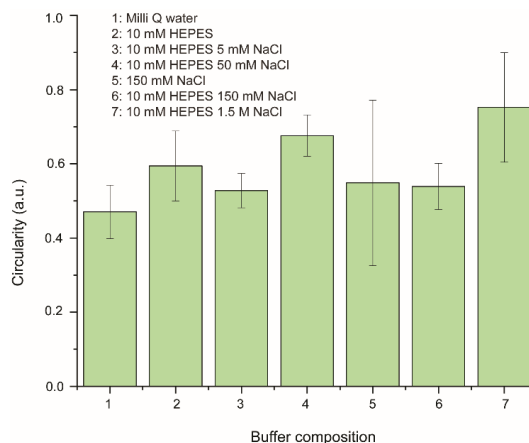


**Figure S2.** Circularity parameter, which is indicative of line tension along the domain boundary, as a function of SLB buffer composition. The domain circularity was determined using FIJI (ImageJ) software from minimum 10 confocal images from each of at least three SLBs prepared at each buffer composition<sup>1</sup>. The error bars stand for the standard deviations calculated

## CHAPTER 9. COOPERATIVITY BETWEEN SODIUM IONS AND WATER MOLECULES FACILITATES LIPID MOBILITY IN MODEL CELL MEMBRANES

from the circularity values for all images at a particular buffer composition. No significant changes were observed when changing buffer composition, indicating that the PC-SM interactions do not get significantly affected by the addition of NaCl salt.

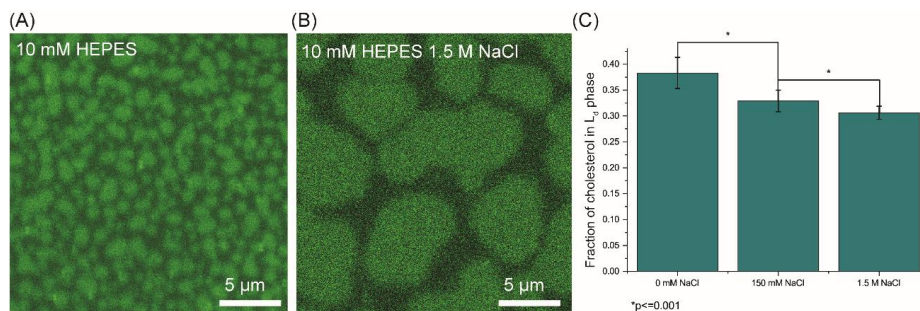


**Figure S3.** Phase separated SLBs with fluorescently labeled cholesterol analog (TopFluor cholesterol) were imaged in 10 mM HEPES buffer containing 0 mM, 150 mM and 1.5 M of NaCl. The fraction of cholesterol in the  $L_d$  phase was calculated as  $I_{L_d}/(I_{L_d} + I_{L_o})$ , where  $I_{L_d}$  and  $I_{L_o}$  are the intensity in  $L_d$  and  $L_o$  phase, respectively. Minimum 5  $L_d$  and 5  $L_o$  phase areas from at least 5 images for each buffer composition were analysed using FIJI (Imagej) software<sup>3</sup>. The error bars represent the standard deviation of the calculated fractions. Statistical analysis (t- test) confirms that the calculated  $L_d$  fractions for different buffer compositions are significantly different.

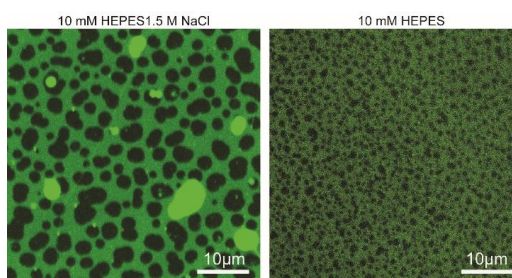


**Figure S4.** Confocal images of SLBs prepared in 10 mM HEPES buffer with 1.5 M NaCl (left) and without NaCl (right) after removal of bulk water and equilibration to 85% relative humidity (RH). The  $L_o$  domain size is bigger at higher NaCl concentration. No other structural changes were observed after removal of bulk water, except the variation in domain size, analogously to fully hydrated membranes in different buffer conditions.

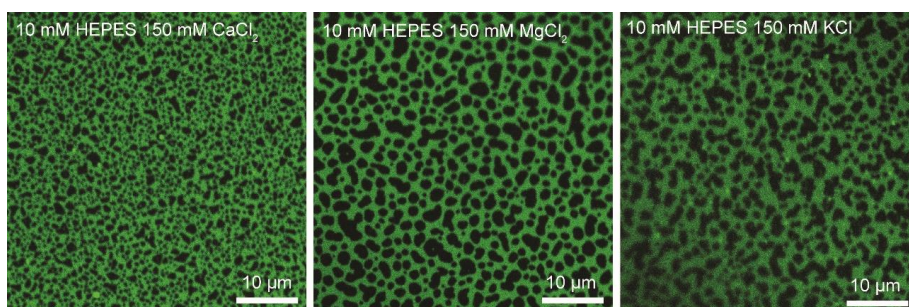


**Figure S5.** Representative fluorescence image of the fully hydrated, phase-separated SLBs prepared in the presence of 10 mM HEPES 150 mM  $\text{CaCl}_2$ , 10 mM HEPES 150 mM  $\text{MgCl}_2$  and 10 mM HEPES 150 mM KCl buffer.

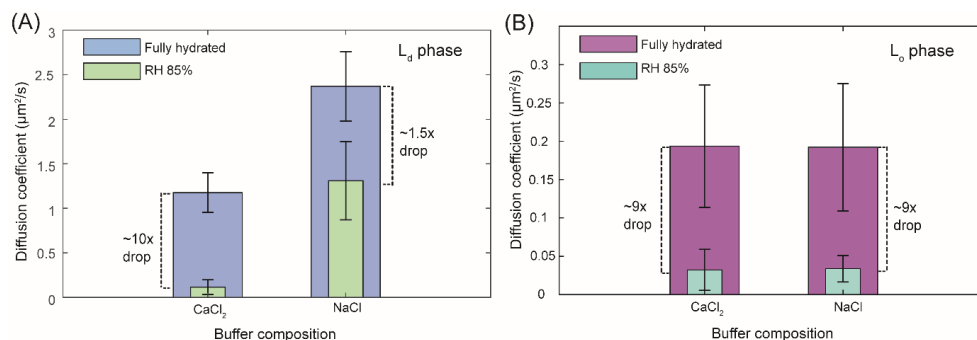


**Figure S6.** The average diffusion coefficient ( $D$ ) values for 1:1 egg SM/cholesterol  $L_0$  phase SLBs in the presence of 10 mM HEPES buffer with addition of 150 mM NaCl or 150 mM CaCl<sub>2</sub> (B) in comparison to the  $L_d$  phase (A) at fully hydrated condition and at 85% RH.

## References

- (1) Matysik, A.; Kraut, R. S. Preparation of Mica Supported Lipid Bilayers for High Resolution Optical Microscopy Imaging. *J. Vis. Exp.* **2014**, No. 88, e52054.
- (2) Chattopadhyay, M.; Krok, E.; Orlikowska, H.; Schwille, P.; Franquelim, H. G.; Piatkowski, L. Hydration Layer of Only a Few Molecules Controls Lipid Mobility in Biomimetic Membranes. *J. Am. Chem. Soc.* **2021**, *143*, 14551–14562.
- (3) Schindelin, J.; Arganda-Carreras, I.; Frise, E.; Kaynig, V.; Longair, M.; Pietzsch, T.; Preibisch, S.; Rueden, C.; Saalfeld, S.; Schmid, B.; Tinevez, J. Y.; White, D. J.; Hartenstein, V.; Eliceiri, K.; Tomancak, P.; Cardona, A. Fiji: An Open-Source Platform for Biological-Image Analysis. *Nat. Methods* **2012**, *9*, 676–682.
- (4) Soumpasis, D. M. Theoretical Analysis of Fluorescence Photobleaching Recovery Experiments. *Biophys. J.* **1983**, *41*, 95–97.
- (5) Garcia-Manyes, S.; Oncins, G.; Sanz, F. Effect of Ion-Binding and Chemical Phospholipid Structure on the Nanomechanics of Lipid Bilayers Studied by Force Spectroscopy. *Biophys. J.* **2005**, *89*, 1812–1826.
- (6) Redondo-Morata, L.; Giannotti, M. I.; Sanz, F. Structural Impact of Cations on Lipid Bilayer Models: Nanomechanical Properties by AFM-Force Spectroscopy. <http://dx.doi.org/10.3109/09687688.2013.868940> **2014**, *31*, 17–28.



# Chapter 10

## Phospholipids undergo anomalous sub-diffusion at reduced hydration conditions in model membranes

### 10.1 Abstract

Lipid diffusion plays a central role in shaping the structural reorganization of the cell membrane, maintaining lipid homeostasis, and helping in cellular transport and signalling. Lateral mobility of phospholipids in membranes was shown to be highly dependent on their local hydration level. Moreover, the activation energy of diffusion increases at reduced hydration conditions, suggesting that the underlying mechanism of diffusion changes upon membrane dehydration. Using two variants of fluorescence correlation spectroscopy (point FCS and scanning FCS) and two benchmark dyes, I show that after the removal of bulk water, the mechanism of the lipid diffusion in the phase-separated biomimetic cell membrane is altered and lipids undergo anomalous sub-diffusion instead of free Brownian motion. I propose that dehydration leads to the formation of temporarily immobile lipid pockets in the membrane that underline the anomaly of lipid diffusion. Thus, these results provide important insights into the mechanism of lipid diffusion in membranes undergoing local and transient dehydration, which is an important intermediate step of various biological processes, e.g. neurotransmission, fertilization or viral entry.

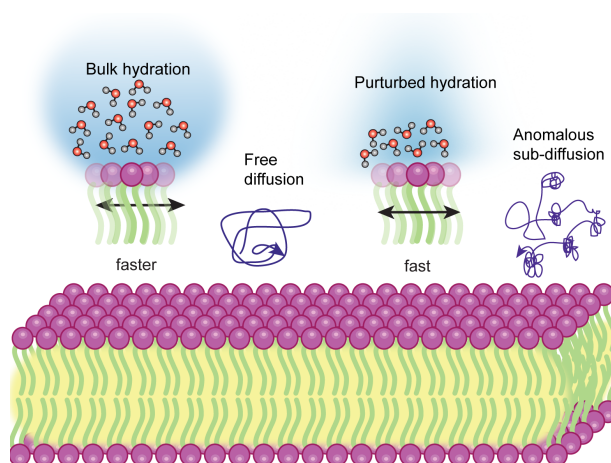


Figure 10.1: A schematic representation of the main findings from the experiments presented in this chapter.

### 10.2 Introduction

Lateral diffusion of lipids is a fundamental process that leads to continuous reorganization of cell membrane components and modulates membranes' structural flexibility. Due to its immense importance in, for example, cell signalling, membrane trafficking and structural reorganization, lipid dynamics has been broadly studied in cellular as well as model membrane systems[134, 135]. Lipid dynamics can be affected by various physico-chemical parameters - lipid composition, fluidity, viscosity, presence of nano-hindrance and

compartmentalization, to mention a few[137]. It has been reported that the diffusion coefficients of lipids and proteins in cells are significantly lower than those observed in a model system[148, 146]. Moreover, the lateral diffusion of membrane constituents in cellular systems does not always show free diffusion, but often time-dependent mean square displacement (MSD) is observed, where MSD is proportional to  $t^\alpha$ , with  $\alpha < 1$ [152, 153]. Such diffusion processes are termed as anomalous sub-diffusion and  $\alpha$  is the anomaly parameter. The general reason of this anomaly of lipid diffusivity is believed to be the highly complex microenvironment that lipids experience in the plasma membrane. The presence of slow-moving obstacles, impermeable domains, transient immobilization, interaction with the cytoskeleton, compartmentalization etc. are commonly attributed to the anomaly of lipid dynamics, although all the possible influencing factors are still not clear[213, 150, 151].

To investigate the lateral diffusion of lipids fluorescence-based optical microscopy techniques, such as FCS, FRAP and SPT are typically deployed, as discussed in chapter 5[214]. FCS and SPT are particularly useful for recognizing and understanding the anomalous sub-diffusion of lipids and proteins. Information about both  $D$  and  $\alpha$  can be obtained by constant monitoring of the fluorescence fluctuations of particles in the microscope observation volume or over a line of a few micrometers in length, for point FCS and scanning FCS (s-FCS), respectively, followed by appropriate modelling of the auto-correlation curves. In case of SPT, the labelled fluorophore is monitored over time at a single molecule level, providing detailed information about the time dependence of the moving particle. Both of these techniques can precisely distinguish Brownian and non-Brownian (anomalous sub-diffusion) motions in cellular as well as in model membrane systems[181, 215, 216].

Biomimetic model membrane systems, such as SLBs, have been widely exploited to study the anomalous diffusion behavior of lipids and to understand its plausible origins[215, 217, 143, 218]. FCS combined with stimulated emission depletion microscopy (STED-FCS) revealed that in phase-separated SLBs on mica lipids in both  $L_o$  and  $L_d$  phase move freely, whereas in SLBs on glass, they showed anomalous sub-diffusion[186]. Moreover, introducing heterogeneities in a form of different lipid phases with varying lipid composition or membrane associated proteins, has been observed to cause anomaly in lipid lateral diffusion[151, 215, 219]. Similar results were obtained from molecular dynamics (MD) simulations. Anomalous sub-diffusion of lipid binding Pleckstrin homology (PH) domains was reported in phosphatidyl-inositol phosphate (PIP) containing lipid bilayer[138]. Systematic MD simulation studies on membranes of varying lipid composition showed that lipid sub-diffusion is dependent on lipid chemistry, phase and the presence of cholesterol in the membrane[220]. Using Monte Carlo simulations Nicolau et al. demonstrated the expected extent of anomaly caused by the interactions with fixed obstacles, rafts, and collisions with picket fence posts[150]. Simulations involving varying number and size of immobile obstructions and different percolation thresholds have been performed and showed the enhancement of hindered diffusion with an increase of the number and decrease in the size of the obstructions[221]. However, in spite of extensive research on anomalous diffusion in membranes caused by various compositional and mechanical factors, the effect of physicochemical parameters, such as viscosity, temperature and in particular hydration has remained unexplored.

Among many physicochemical parameters affecting lipid diffusion, water molecules present near the polar head group of lipids play a crucial role in modulating the lateral diffusion of lipids[212]. Intriguingly, many biochemical processes, such as cells fusion or adsorption of macromolecules, are associated with the local and transient dehydration of the membrane. Therefore, given its biological significance, it is crucial to gain knowl-

edge of the precise diffusion behavior of membrane components under scarcely hydrated conditions. Regrettably, studying the effects of local (de)hydration on the mobility of membrane components has so far been hampered by the lack of methodology for preparing lipid membranes with a well-defined hydration conditions. In this work, employing our recently devised strategy of slow and gradual dehydration of SLBs, I investigated the characteristics of lateral diffusion of phospholipids in SLBs on mica substrate under lower hydration conditions. For this purpose, I used two variants of FCS technique - point FCS and s-FCS, to verify the consistency of the results and two benchmark fluorescent dyes Atto-633 and Abberior STAR RED (ASR) to ensure that the results are independent of the fluorophores used. As already discussed, FCS is an excellent tool to discern free diffusion from anomalous sub-diffusion both in model membranes and in cellular systems. Atto and abberior dyes were also proved to be perfect choices for reliable FCS experiments for their photostability and high quantum yield[186]. With careful analysis of FCS curves, I revealed that the phospholipids undergo a transition to anomalous sub-diffusion in the absence of bulk water, and exhibit free diffusion after rehydration with bulk water. I speculate that such anomaly is caused by the formation of transient nano-hindrance at lower hydration conditions. This study provides deeper understanding of the lipid diffusion behavior in membranes with perturbed hydration states, relevant to the biological phenomena involving membranes' fusion events.

## 10.3 Experimental section

### 10.3.1 Materials

1,2-Dimyristoleoyl-sn-glycero-3-phosphocholine (14:1 PC), egg yolk sphingomyelin (egg SM), and cholesterol were purchased from Avanti Polar Lipids, Alabaster, AL, USA. 1,2-dioleoyl-snglycero-3-phosphoethanolamine labeled with Atto 633 (DOPE-Atto 633), Alexa 488 fluorescent dye, 4-(2-hydroxyethyl)piperazine-1-ethanesulfonic acid (HEPES), sodium chloride (NaCl) and chloroform (HPLC grade) were purchased from Merck KGaA, Darmstadt, Germany. 1,2-dipalmitoyl-sn-glycero-3-phosphoethanolamine (DPPE) conjugated with the Abberior STAR RED fluorescent dye (ASR-PE) was bought from Abberior GmbH, Göttingen, Germany. All the materials were used without further purification.

### 10.3.2 SLB preparation

Previously documented vesicle deposition method with the required adaptations was used to prepare SLBs on mica substrate[222]. Chloroform solutions of 14:1 PC, egg SM, and cholesterol at 1:1:1 molar ratio with 0.002 mol% of ASR-PE and 0.01 mol% of Atto-DOPE were mixed separately followed by evaporation of the chloroform by blowing nitrogen gas for at least 50 mins to guarantee complete removal of the solvent. The dried thin film of lipids deposited on the bottom of the vial was dissolved in aqueous buffer (10 mM HEPES and 150 mM NaCl buffer solution, pH adjusted to 7.4) to form multilamellar vesicles (MLVs) of 10 mM lipid concentration. The MLVs suspension was vortexed well to produce a completely homogeneous aqueous solution of lipids, diluted 10 times to obtain 1 mM final lipid concentration and then distributed as aliquots into sterilized glass vials that were stored at  $-20^{\circ}$  C for further use. The MLVs suspensions were bath sonicated for 10 minutes at maximum power to produce a solution of small unilamellar vesicles (SUVs). Freshly cleaved mica was adhered to the #1.5 coverslip by UV-activated adhesive Norland



68 and a quarter-cut Eppendorf tube was attached on top of it as a water reservoir using silicone glue. 100  $\mu\text{L}$  of SUVs solution was deposited on the mica followed by the addition of 2  $\mu\text{L}$  of 0.1 M  $\text{CaCl}_2$  solution and 400  $\mu\text{L}$  of the buffer. The sample was incubated for 30 mins and then rinsed well with 10 ml of the buffer to remove unfused vesicles.

### 10.3.3 Preparation of SLBs with lower hydration conditions

To obtain SLBs with lower hydration, the bulk part of the buffer was removed from the top of the SLB with a pipette and the sample was immediately purged with  $\text{N}_2$  gas of high ( $>90\%$ ) relative humidity (RH). The RH of the  $\text{N}_2$  gas was monitored and controlled using our home-build humidity control set-up[212] and gradually decreased to 80% and 70% RH, followed by increasing back to 85% RH. SLBs were equilibrated for about 10 mins to a particular RH% before taking the measurements. Finally, 200  $\mu\text{L}$  of the buffer was added on top of the SLB to obtain ‘bulk rehydration’ of the membrane.

### 10.3.4 Point and scanning FCS data acquisition and analysis

Fluorescence imaging and FCS measurements were performed on SLBs of varying hydration conditions using an inverted LSM 780 (Carl Zeiss, Jena, Germany) microscope with 40X 1.2 NA water immersion objective with correction collar. Fluorescent dyes Atto633 and ASR were excited by He-Ne laser of wavelength 633 nm and Argon laser (488 nm) was used for Alexa 488 dye. For both point FCS and s-FCS experiments, the pinhole was set to be 1 airy unit. The pinhole and objective correction collar adjustments were performed routinely before all FCS experiments. Calibration of the confocal volume and the structural parameter was routinely performed using a 5 nM aqueous solution of standard calibration dye Alexa 488 before the FCS measurements on SLBs based on the formula  $\tau_D = \frac{\omega^2}{4D}$ , where  $\tau_D$  is the diffusion time and  $\omega$  is the confocal volume. The obtained  $\tau_D$  of Alexa 488 and its  $D$  value in aqueous solution (known from literature) are used later to calculate the  $D$  value of the sample. Point FCS measurements were taken using the FCS module in Zen software (Carl Zeiss, Jena, Germany). Each point FCS measurement was taken for a duration of 5-10 s with 5 times repetition in a particular spot, at low laser power (2-5 microwatts). For each hydration level, point FCS measurements were recorded at minimum 6 different areas of the sample. The s-FCS experiments were performed in line scan mode by continuously imaging a 2.8  $\mu\text{m}$  line 100,000 times with the highest scanning speed attained by the microscope. The line was imaged with 36 pixels and 5.64  $\mu\text{sec}$  pixel dwell, resulting in 1032 Hz scanning frequency and a total measurement time of 96 s. All s-FCS measurements were done in photon counting mode. The point FCS correlated data were fitted by FoCusPoint software[223]. The s-FCS data were analysed in FoCusScan software[224], where correlation carpets were generated after reprocessing the fluorescence fluctuations data with binning 5 and local averaging (10 s) method of photobleaching correction. The extracted correlation curves from a single carpet were averaged and then fitted using a suitable auto correlation function model[224]. The diffusion time for lipids obtained from the FCS data fitting was converted to diffusion coefficient using

$$D = \frac{430 \cdot \tau_{D_{A-488}}}{\tau_{D_{\text{sample}}}} \quad (10.1)$$

where the diffusion coefficient of Alexa dye is 430  $\mu\text{m}^2/\text{s}$ [225],  $\tau_{D_{A-488}}$  is the diffusion time of Alexa-488 dye in an aqueous solution, routinely measured during calibration procedure prior to FCS experiments and  $\tau_{D_{\text{sample}}}$  is the diffusion time of the lipids in the sample.

## 10.4 Results

In this study, deploying point and scanning FCS, I investigated the nature of lipid dynamics at varying hydration conditions in phase-separated SLBs of an equimolar mixture of 14:1 PC, egg SM and cholesterol. Two standard dyes for FCS measurements, Atto-633 and ASR, conjugated with lipid analogs DOPE and DPPE, respectively, were chosen for separate experiments to eliminate the possible influence of the fluorophore characteristics on the lipid diffusion mechanism. In this context, it should also be noted that ASR dye is more hydrophilic in nature compared to Atto-633 dye[186], which might result in differences in their behavior for experiments involving dehydration. Due to the differences in hydrophobic chain saturation and length, the so-called hydrophobic mismatch, 14:1 PC forms highly fluid  $L_d$  phase and egg SM forms compact  $L_o$  phase with higher cholesterol content. Atto-633 being conjugated with unsaturated lipid DOPE partitions selectively to the  $L_d$  phase. Although linked to a saturated lipid, given the difficulties of the large fluorophore entering compact  $L_o$  phase ASR-DPPE also gravitates toward the fluid and less constricted  $L_d$  phase[62]. Since after dehydration the mobility in the  $L_o$  phase drops to extremely low values[212], hampering the accurate determination of the diffusion coefficient using FCS, the lipid diffusion in the  $L_d$  phase was specifically investigated in this work.

Point FCS and s-FCS experiments were performed on SLBs at fully hydrated condition and SLBs equilibrated to 90%, 80%, 70% RH during dehydration trajectory, to 85% RH during rehydration and then finally SLBs experiencing bulk rehydration. The structure of the SLBs remained unaffected on a micrometer scale (Figure 10.2) upon removal of bulk water following our slow and gradual dehydration protocol[212]. As discussed in chapter

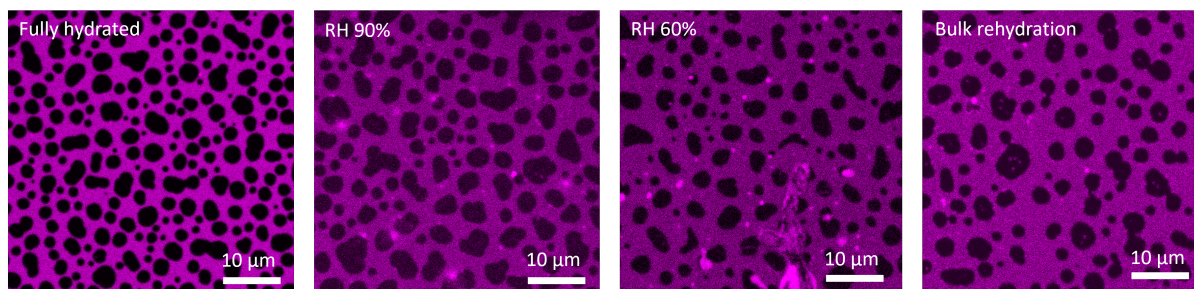


Figure 10.2: (A) Confocal images of SLBs at varying hydration conditions.

5, FCS is highly sensitive to photobleaching of the fluorescent probes. After removal of the bulk water both Atto-633 and ASR dyes showed significant photobleaching, though ASR was subject to higher photobleaching than Atto-633. For Atto-633 reliable point and scanning FCS curves could be obtained down to 70% RH. Below 70% RH, the curves took shape indicative of huge photobleaching (Figure 10.3A-B), hindering the reliable analysis of the FCS data. In contrast, for ASR dye, no credible point FCS curves could be obtained after removal of bulk water due to high photobleaching during the experiment (Figure 10.3C). However, s-FCS being comparatively less sensitive to photobleaching, allowed me to obtain reasonably good quality FCS curves for membranes with ASR down to 70% RH, provided that appropriate photobleaching corrections were used for analysis. The increase in photobleaching of the dyes upon dehydration could be caused by the slower diffusion of lipids resulting in longer residence time within excitation spot. Moreover, a change in the photophysical properties of these dyes is suspected upon dehydration due to a change of the

polarity of their environment, an effect that needs further investigation. The photostability and high quantum yield of ASR dye in aqueous solution is well studied and it has been observed to be significantly more photostable than Atto dye[186]. But given the highly hydrophilic nature of the ASR, in comparison with moderately hydrophilic Atto-633, it is understandable that the photostability of ASR is more sensitive to changes in its hydration than Atto-633.

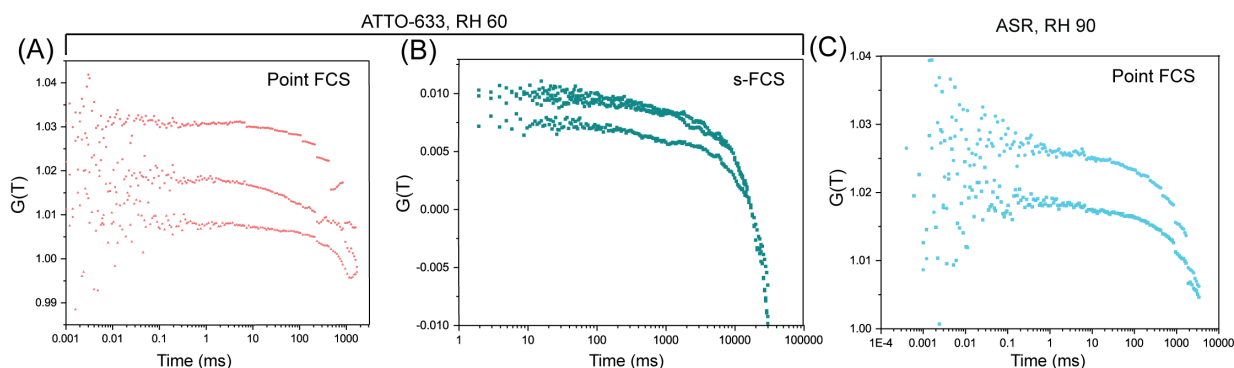


Figure 10.3: Representative point FCS (A) and s-FCS (B) curves for SLBs with Atto-633-DOPE at lower hydration conditions (<70% RH). For Atto-633, extensive photobleaching hinders the acquisition of good-quality FCS curves below 70% RH. (C) Representative point FCS curves for SLBs with ASR-DPPE at 90% RH. For ASR dye, photobleaching becomes prevalent just after the removal of bulk water inhibiting the acquisition of reliable point FCS curves.

### 10.4.1 Point FCS measurements

FCS is based on the temporal fluorescence fluctuations at the observation spot/volume of the microscope, caused by the movement of the fluorophores attached to the target molecules (Figure 10.4A). In other words, the lateral diffusion is calculated based on the similarity of the fluorescence intensity fluctuations over time. Point FCS measurements were performed on 6 SLBs doped with Atto-633-DOPE, among which for 3 samples data were taken for all the above mentioned RH levels and the other 3 samples were measured only at fully hydrated conditions and 90% or 80% RH. Figure 10.4B depicts non-averaged, normalized FCS curves for a single SLB containing Atto-633-DOPE at fully hydrated condition (red), at 90% (blue) and 80% (green) RH during dehydration, and finally bulk rehydration (magenta). The FCS curves shift to the longer diffusion time (to the right, highlighted by blue arrow) with dehydration and return back to the shorter diffusion time range (to the left) with rehydration, reconfirming the hydration-dependence of the lateral diffusion of lipids, in agreement to our previous work[212]. Intriguingly, not only the diffusion time, but a clear change of the shape of the FCS curve upon dehydration is observed (highlighted by orange arrow), which is reversible with bulk rehydration. The change of the shape of the autocorrelation curves gives first indication that the nature of the diffusion of the lipids at perturbed hydration conditions is different than in fully hydrated membrane. The obtained FCS curves for fully hydrated SLBs could be fitted well with single component free diffusion model (Figure 10.4C). However, the FCS curves for SLB after removal of bulk water could not be described well with a single free diffusion model (Figure 10.4C). Consequently, for the FCS curves obtained for SLBs at reduced hydration states we attempted to fit the data with two models, considering i) single component anomalous diffusion and ii) two component free diffusion. In the 1<sup>st</sup> model, instead of keeping alpha

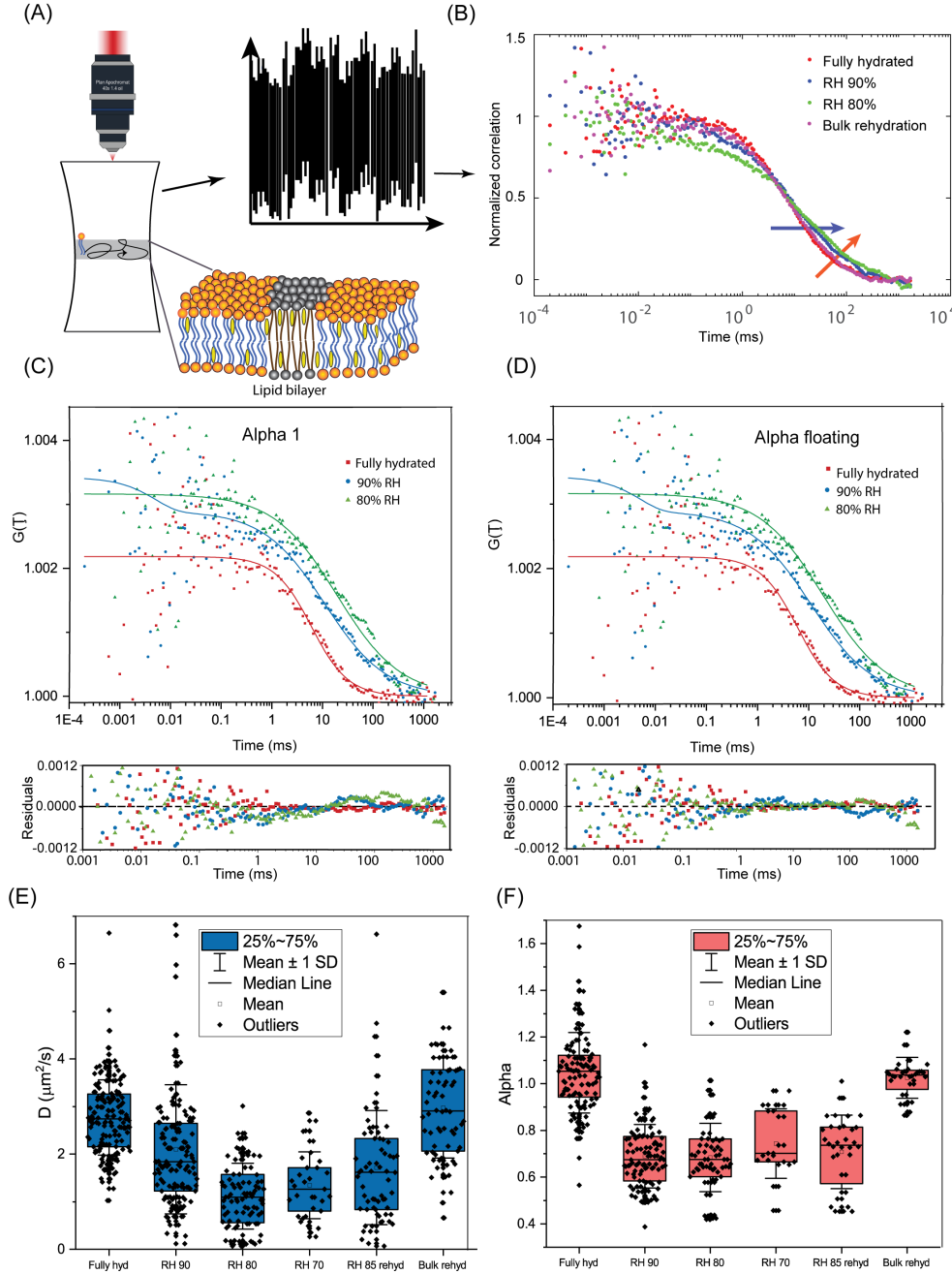


Figure 10.4: (A) Schematic representation of the point FCS experiment on SLB. (B) Normalized autocorrelation curves obtained from point FCS measurements on SLBs doped with Atto-633-DOPE at fully hydrated condition (red), RH 90% (blue), RH 80% (green) and bulk rehydration (magenta). Blue and orange arrows indicate the shift and shape change of the FCS curves upon dehydration, respectively. (C)-(D) FCS autocorrelation curves and fitting residuals for SLBs at fully hydrated (red) condition and equilibrated to RH 90% (blue) and RH 80% (green) fitted with  $\alpha=1$  (C) and floating values of  $\alpha$  (D) respectively.  $D$  (E) and  $\alpha$  (F) values for  $L_d$  phase lipids at varying hydration conditions.

constant at 1,  $\alpha$  parameter is released, which accounts for the time-dependence of the  $D$  value. And in the 2<sup>nd</sup> model two separate populations of freely diffusing particles are considered and their fractions are released, while  $\alpha$  is kept constant at 1. Both free  $\alpha$  (Figure 10.4D) and two component free diffusion (Figure 10.5) models mathematically fitted the FCS curves well. Hence the next step was to check the credibility of the obtained  $D$  values

in a physical sense. The  $D$  values obtained from the two component free diffusion model did not fall within the generally accepted range of lipid diffusion times in either gel or in fluid phase[186]. The fast component ( $\sim 25\%$  fraction of total lipids) was shown to be 7-10 times faster than the standard lipid diffusion in the  $L_d$  phase, and the slower component ( $\sim 75\%$  fraction) was 5–10 times slower. Moreover, such a huge increase in  $D$  value of the first component upon dehydration is physically impossible. Hence, the possibility of two free diffusion was discarded. On the other hand,  $D$  values obtained by fitting the FCS

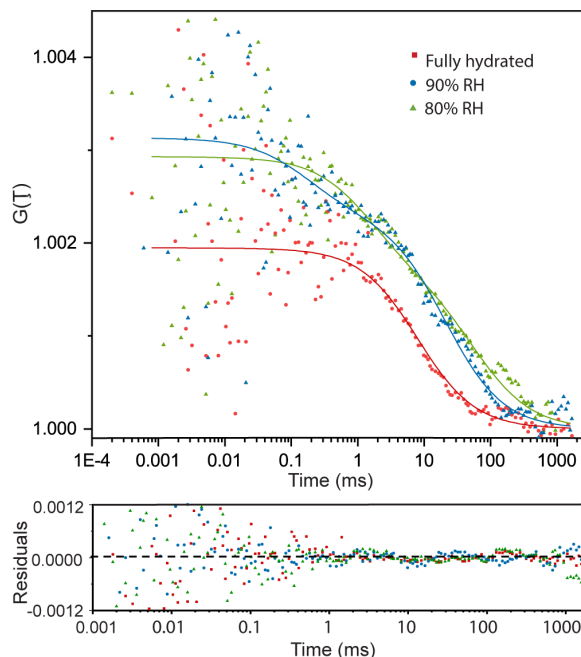


Figure 10.5: Results of the fitting with two component free diffusion model and residuals of representative point FCS curves for lipids in SLBs at fully hydrated condition, at 90% RH and 80% RH.

curves with floating  $\alpha$  parameter were physically understandable and matched with our previous results from FRAP measurements[212, 226]. Therefore fitting with floating  $\alpha$  parameter was chosen. With careful analysis of the FCS curves, a two-fold drop in  $D$  values was observed from  $2.77 \pm 0.79 \mu\text{m}^2/\text{s}$  (fully hydrated) to  $1.35 \pm 0.70 \mu\text{m}^2/\text{s}$  (70% RH) and then  $D$  increased back with rehydration ( $2.97 \pm 1.05 \mu\text{m}^2/\text{s}$  for bulk rehydration) (Figure 10.4E). The relative change of  $D$  values is in complete accordance with our previous FRAP results[212, 226]. Noticeably, the  $\alpha$  parameter was found to be very close to 1 for fully hydrated SLBs ( $1.05 \pm 0.17$ ) (Figure 10.4F), indicating free Brownian diffusion of lipids. Interestingly, upon removal of bulk water,  $\alpha$  decreased to  $0.69 \pm 0.14$  at 90% RH (Figure 10.4F). Upon further dehydration to 70% RH ( $0.74 \pm 0.15$ ) followed by rehydration to 85% RH ( $0.71 \pm 0.16$ )  $\alpha$  remained largely constant within the error bar. Again after bulk rehydration, it came back to  $1.03 \pm 0.09$ . The observed significant (yet reversible) lowering of  $\alpha$  strongly indicates that lipids undertake anomalous sub-diffusion in the absence of bulk water layer. To rule out the fluorophore bias in these experiments, the same point FCS measurements were attempted using ASR-DPPE fluorescent probe, but reliable data could not be obtained due to huge photobleaching of the fluorophore, as discussed above.

## 10.4.2 Scanning FCS measurements

Scanning FCS is an impressive method that has been previously used to distinguish free diffusion and hindered diffusion[227]. In this technique, instead of recording fluorescence fluctuations at a single point, fluorescence intensity of a selected line is collected systematically multiple times and the auto-correlation carpet with several auto-correlation curves is generated correlating fluorescence fluctuations at each pixel of the line (Figure 10.6A-B). Then the diffusion time information is extracted by fitting these correlation curves similarly as in the case of point FCS data. Thus, insights into the spatial heterogeneity as well as a significant statistical average of the mobility data are collected, while making a little compromise on the temporal resolution.

Crucially, in the context of these particular experiments, since in scanning FCS a single observation spot is not continuously illuminated with the laser excitation light, the effect of photobleaching is less pronounced. Hence, in order to validate our findings from point FCS, s-FCS measurements were performed on 3 SLBs with Atto-633-DOPE and one SLB with ASR-DPPE. Thanks to comparatively lower photobleaching of ASR-PE during s-FCS, much more reliable correlation data could be obtained in this case. To tackle the noise of the data upon dehydration, for both dyes, the correlation curves from a single correlation carpets were averaged into a single curve. Though by such averaging the spatial information about the diffusion is lost, the averaging was done considering the fact that the spatial heterogeneity was not prominent in the correlation carpets. Representative correlation carpets for a fully hydrated SLB and SLB equilibrated to 80% RH, containing ASR-DPPE dye, are presented in Figure 10.6B. The averaged and normalized, auto-correlation curves for  $L_d$  lipids in SLBs with ASR-DPPE dye at fully hydrated, 90% RH and 80% RH conditions are shown in Figure 10.6C. The FCS curves shift to the right with decrease in RH% indicating lowering of the diffusion coefficient value. Moreover, clearly, a noticeable change in the shape of the correlation curves, similar to point FCS data, is observed upon SLB dehydration, validating the point FCS results. Analogously to the point FCS curve fitting, the correlation curves were fitted with both floating  $\alpha$  (anomalous diffusion) and two component free diffusion models. However, the fitting of the two component free diffusion model was abandoned due to similar reason as in case of point FCS - the  $D$  values obtained were not consistent and often out of the physically acceptable range of  $D$  values for lipids. The same correlation curves, shown in Figure 10.6C, fitted with  $\alpha$  fixed at 1 and  $\alpha$  floating are shown in Figure 10.6D-E, respectively. Similarly, for SLBs with Atto-633-DOPE dye, fitting of three representative auto-correlation curves, each averaged over single carpet, with  $\alpha = 1$  and  $\alpha$  floating are presented in Figure 10.6E-F. From the fits and their residuals, it is evident that at fully hydrated condition free diffusion model ( $\alpha$  fixed at 1) fits well to the experimental data, but the fitting is not satisfactory at 90% RH and 80% RH levels. At the same time letting  $\alpha$  free significantly improves the fit quality for the lower hydration conditions. Thus FCS curves fits for both dyes confirm the appearance of anomalous sub-diffusion at perturbed hydration conditions. The diffusion coefficient and  $\alpha$  values for Atto-633-DOPE and ASR-DPPE dyes as a function of the SLB hydration state are plotted in Figure 10.7A-B and 10.7C-D, respectively. The  $D$  values are numerically lower than the values obtained from point FCS measurements, but they follow the same trend with dehydration and rehydration as for point FCS results, irrespective of the dye used. Moreover,  $\alpha$  was also found to be around 1 ( $0.97 \pm 0.12$ ) at fully hydrated condition ( $0.87 \pm 0.11$  after bulk rehydration) and lower at lower hydration conditions ( $0.85 \pm 0.12$  at 80% RH). I would like to note here, that the numerical values obtained from the data analysis are largely dependent on the photobleaching corrections performed on the raw



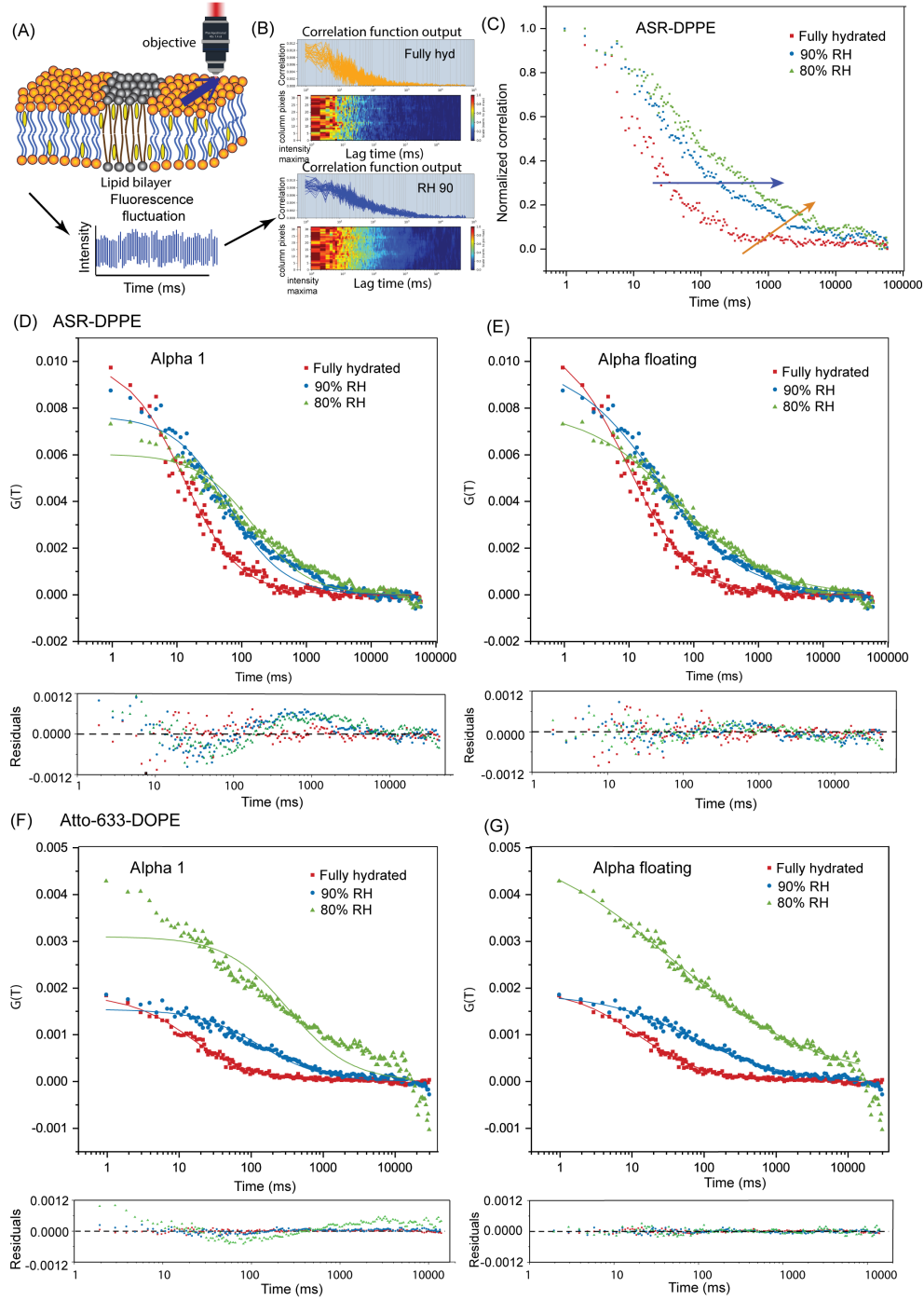


Figure 10.6: (A)-(C) Schematic representation of scanning FCS on SLB; (B) Representative correlation carpets for SLBs doped with ASR-DPPE at fully hydrated condition and at 90% RH; (C) Normalized correlation curves, each averaged from single correlation carpets at fully hydrated condition (red), RH 90% (blue) and RH 80% (green). Blue and orange arrows indicate the shift and shape change of the FCS curves upon dehydration respectively. (D)-(E) s-FCS curves for SLBs with ASR-DPPE at fully hydrated (red) condition and equilibrated to RH 90% (blue) and RH 80% (green) fitted with  $\alpha=1$  (D) and floating values of  $\alpha$  (E); (F)-(G) s-FCS curves for SLBs with Atto-633-DOPE at fully hydrated condition (red) and equilibrated to RH 90% (blue) and RH 80% (green) fitted with  $\alpha=1$  (F) and floating values of  $\alpha$  (G).



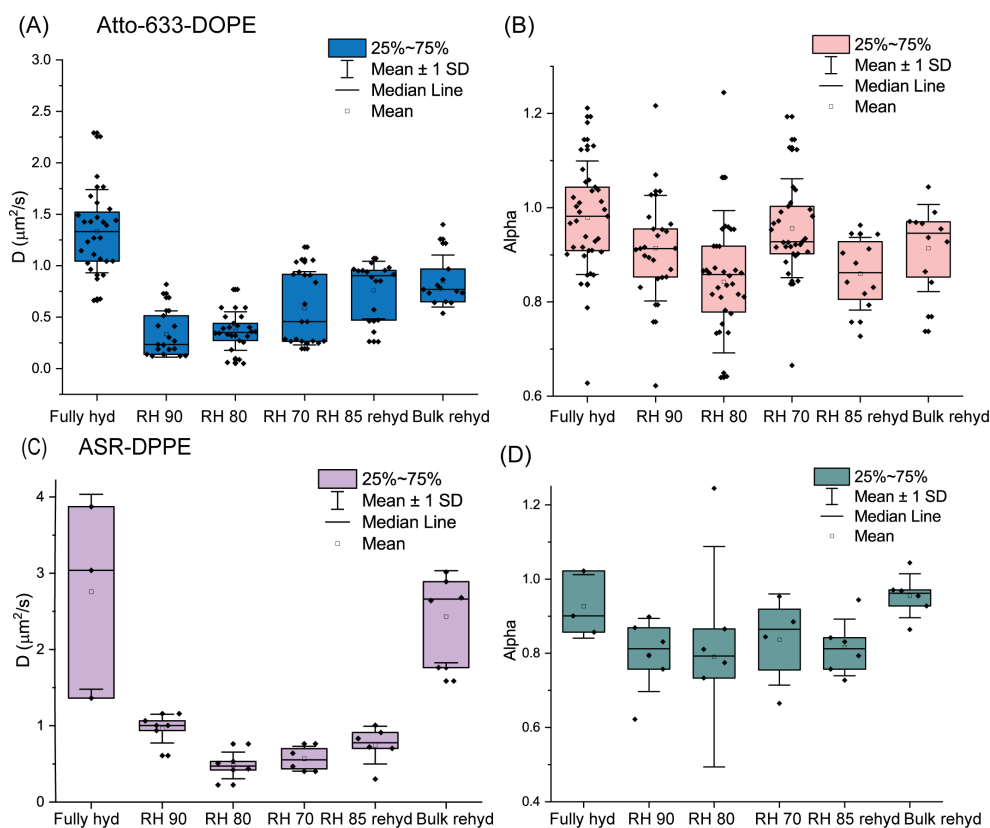


Figure 10.7:  $D$  (A) and  $\alpha$  (B) values obtained from s-FCS measurements for  $L_d$  phase lipids at SLBs with Atto-633-DOPE at varying hydration conditions.  $D$  (C) and  $\alpha$  (D) values obtained from s-FCS measurements for  $L_d$  phase lipids at SLBs with ASR-DPPE at varying hydration conditions.

data. The data analysis procedure is still being improved to obtain more reliable results, free from any bias caused by the photobleaching correction method. Hence the absolute values of these results are subject to slight changes upon further analysis. However, in spite of these difficulties in the analysis, the scanning FCS results completely support the findings from the point FCS measurements.

## 10.5 Discussion

The similar trend in  $D$  values acquired from point and s-FCS data for different SLB hydration states agree well with the trend of the lateral diffusion found in my previously reported FRAP measurements, validating the FCS data at lower hydration conditions[212, 226, 228]. Both point FCS and s-FCS data confirm that in the presence of bulk water on top of the SLB,  $L_d$  phase lipids undergo free diffusion on mica substrate. On the other hand, upon dehydration, anomaly parameter  $\alpha$  drops significantly for both point and s-FCS, strongly indicating that PC lipids undergo anomalous sub-diffusion in the absence of bulk water. Moreover, the changes of  $\alpha$  parameter are completely reversible, that is  $\alpha$  reaches back to the value of 1 upon bulk rehydration. Now, concerns may surface as to whether these lower values of  $\alpha$  are the actual representation of the nature of lipid diffusion or whether they are a result of the experimental artifacts or properties of the fluorescent dyes at lower hydration levels. Despite the relatively poor quality and signal-to-noise ratio of the FCS data under dehydrated conditions, the strong reproducibility

and reversibility of the results with de(re)hydration for point and s-FCS and for the two benchmark dyes Atto-633 and ASR provide strong arguments in favor of the conclusion that the lower values of  $\alpha$  represent the true diffusion information of the lipids in SLBs with reduced hydration. Additionally, our previous experiments reported that the activation energy of diffusion increases with dehydration, which is strongly indicative of the change of the diffusion mechanism[212]. This further demonstrates the veracity of the anomalous sub-diffusion results.

Anomalous diffusion is mostly observed in the presence of some mobile or immobile obstruction traps, domains and alike features[151]. Upon removal of water, the emergence of nanoholes in the membrane, which could prevent lipids from diffusing freely, would be the first place to look for the cause of the anomalous diffusion behavior of the lipids. However, using atomic force microscopy, we established that no nanoscopic holes emerge in the  $L_d$  phase during dehydration[212, 229], which rules out the hypothesis that the anomaly is related to structural defects (holes or nanodomains) acting as excluded area for the diffusion. Hence, it has to be some other membrane feature causing transiently mobile or immobile hindrance or trap for the lipid movement. In previous study, I have also demonstrated that the mobile fraction of lipids decreases with dehydration, i.e. at a particular time, higher number of lipid molecules become transiently immobile[212]. At full hydration, the PC lipid headgroups are surrounded by 10-12 water molecules per lipid, among which around 6 water molecules form a clathrate-like shell structure around the phosphocholine group, as choline group can not form hydrogen bonds. Some of these water molecules, loosely bound with van der Waals interactions slowly start to desorb as the hydration level decreases from 90% RH, leaving gradually more and more lipids without shielding water layer around their headgroups. Missing the water molecules around, electrostatic repulsion emerges between the lipid headgroups, which increases the energy requirement for the diffusion step. This could lead to either transient immobilization of those lipids or they become completely immobile. If these lipids become immobile, the other lipids will find them as obstructions causing anomalous diffusivity pattern.

However, in reality, the water clathrate cage around the lipid headgroups is not exactly a concrete or discrete cage structure, rather the water molecules form an exchangeable water shell around the headgroups. Upon dehydration, the hydration shell of some of the lipids undergo a momentary perturbation. Again this transient disturbance in hydration shell is released when water molecules come in from the hydration layer of neighboring lipids, making the hydration shell of those neighboring lipids water deficit. Such transient water-deficit condition of lipid headgroups passes on from one lipid to another by the exchange of water molecules in their hydration shells. The lipids with compromised water availability around the headgroup, and/or their neighboring lipids stop for a while when they feel electrostatic repulsion. Now it is very obvious to rationalize that their diffusion pattern would be far from free diffusion. Additionally, these momentarily immobilized lipid pockets can act as nano-hindrance for the other mobile lipids, leading to severe anomalous behavior.

Previous research on the phase transition temperature, height mismatch between the  $L_o$  and  $L_d$  phase and fluorescence spectra of the  $L_d$  phase lipids at dehydrated conditions indicate a liquid-disordered to gel phase transition[12, 14, 15, 229]. If the fluid lipids would gradually transform into gel phase, the two component free diffusion model with  $D$  values matching the fluid and gel phase diffusion would describe the diffusion data, with a gradual increase in fraction of lipids with gel-phase-like diffusion coefficient values. However, my experimental data clearly shows that this is not the case. Rather single

component anomalous sub-diffusion was found to better describe the lipid dynamics after dehydration. Therefore, our data suggest that more and more lipids undergoing phase transition from fluid to gel phase is not the most prominent change in lipid diffusion behavior upon dehydration. Rather it indicates that all  $L_d$  phase lipid molecules behave as a single population undergoing anomalous sub-diffusion. Losing their screening water molecules around the headgroups, the lipids momentarily stiffen and gellify, which act as hindrances to the other still mobile lipid molecules, leading to anomalous diffusion. And, since these transient halts are temporary, and are passes on from one lipid to another, all the  $L_d$  phase lipids behave as a single population.

It is noticeable that  $\alpha$  drops down to  $\sim 0.7$  already after removal of bulk water and remains more or less constant afterwards, though the diffusion coefficient decreases steadily as the hydration level decreases. If we assume that with dehydration, more and more lipids feel the electrostatic repulsion around the head groups which act as obstacles, the  $\alpha$  could also gradually decrease as the mobile fraction goes down. Generally, the anomaly parameter decreases with an increase in obstacle concentration at longer measurement time scale, until the percolation threshold of anomaly is reached, when the diffusion becomes anomalous at all time scales[230]. Hence, constant  $\alpha$  suggests that as soon as bulk water is removed, the number of obstacles i.e. transiently immobile lipid pockets already reaches the percolation threshold of anomalous diffusion, and naturally with further dehydration, even if the number of immobilized lipid pockets increases,  $\alpha$  does not decrease anymore.

To look for the reason of anomalous sub-diffusion of scarcely hydrated lipids, another possibility that can not be neglected is the chance of altered interaction of the lipids with the mica substrate at reduced hydration conditions. Though it is presumed that a thin layer of water is present between the lower leaflet and mica, the interactions of the lower leaflet lipids with the substrate are not well understood. However, Honigman et al. showed free diffusion of PC lipids on mica in fully hydrated conditions whereas on acid-cleaned glass surface the same lipids undergo anomalous sub-diffusion[186]. Both point and scanning FCS experiments with two fluorescent dyes reconfirm that at fully hydrated conditions, the diffusion is free on mica. At lower hydration conditions, the interaction between PC lipids and mica might change, but in that case anomalous diffusion of lipids in lower leaflet would be more prominent, and the diffusion coefficient should be lower for the lipids in the lower leaflet. My previous study of lipid diffusion in a lipid bilayer with fluorescence quenched upper leaflet showed that mobility of the lower leaflet follows the same trend as the whole bilayer during dehydration[212]. This hints that the anomaly in lipid diffusion is not, at least solely, an effect of changes in the lipid-mica interactions upon dehydration.

After establishing the presence of anomalous sub-diffusion of lipids at scarcely hydrated membrane, the next step is to find out the type of the anomaly of lipid dynamics. Spot variation FCS, in other words, STED-FCS has been used previously to discern various types of anomalous sub-diffusion such as hop diffusion or transient immobilization[162, 157, 160]. A detailed understanding of the type of anomalous behavior of the lipid diffusion could be extracted from STED-FCS measurements on dehydrated membranes. Hence, STED-FCS experiments were planned, but could not be performed due to low photostability of the chosen dyes at reduced hydration conditions. In STED-FCS, very high laser power is used to vary the observation spot size. Hence, the strong photobleaching of ASR and Atto-633 dyes upon dehydration makes the experiment extremely challenging. Consequently, the quest for finding a suitable dye, that is photostable at lower hydration conditions and when exposed to high laser power, goes on.

## 10.6 Conclusion

Using point FCS and s-FCS measurements with two benchmark fluorescent dyes, I showed that PC lipids in SLBs on mica substrate undergo moderate to severe anomalous sub-diffusion at reduced hydration conditions, in contrast to free diffusion at fully hydrated conditions for the same system. This anomaly of lateral diffusion of lipids, I postulate, is caused by the dehydration-induced transiently immobile lipid pockets that act as nano-hindrance to moving lipids causing obstructed diffusion pattern. Transient dehydration is an important intermediate step for any cell fusion based biological phenomena, neurotransmission, fertilization or viral entry, to mention a few. Hence, the detailed molecular level understanding of the lipid dynamics at dehydrated conditions is crucial to unravel the mechanisms underlying such biological events. This study offers a new insight into the lipid diffusion pattern of PC lipids in dehydrated membranes. Moreover, it contributes to the field of in vitro research and to the quest for determining the diverse causes of anomalous diffusion in biological systems. Further research on these systems with a suitable fluorescent dye, employing spot-variation FCS/STED-FCS, in my opinion, will shed additional light on the precise nature of the anomaly observed in the diffusion of scarcely hydrated lipids.

## Note

It should be noted that the presented discussion and conclusions are based on the preliminary analysis of the obtained FCS data. The data, especially the s-FCS data are still to be analysed further aiming to improve the photobleaching correction and to obtain more reliable results. Though, after improvement of the data analysis process, the absolute values of  $D$  and  $\alpha$  may slightly change, I am convinced that the main conclusions are still valid.

# Chapter 11

## Conclusions and outlook

### 11.1 Conclusions

To summarize, in this thesis, I present several experimental works elucidating the role of biological water on the lateral diffusion of lipids in biomimetic cell membranes, which I believe, are important contribution to the biomimetic biophysics field. In the course of my doctoral studies, together with my group members I have developed a new method of preserving lipid membranes at dehydrated condition without any external chemical or mechanical modification, which led to the understanding of lipid behavior at lower hydration conditions. I discovered that lateral diffusion of PC lipids is highly responsive to membrane water content and that the water molecules forming the hydration shell structure around the phosphocholine moiety facilitate lipid diffusion by screening the inter-lipid electrostatic repulsion between neighboring lipid headgroups (chapter 7). Moreover, I demonstrated that the preservation of this diffusion-defining hydration shell is highly dependent on the presence of biologically relevant ions (chapter 9).  $\text{Na}^+$  and  $\text{K}^+$  ions support mobility at reduced hydration condition by stabilizing the hydration shell. In contrast, in the presence of  $\text{Mg}^{2+}$  and  $\text{Ca}^{2+}$  ions, lipid mobility ceases after the removal of bulk water. Furthermore, I have exhibited that the free diffusion of PC lipids in phase-separated SLBs on mica is replaced by anomalous sub-diffusion at lower hydration conditions (chapter 10, manuscript in preparation). Moreover, I proposed a novel approach of molecular-level hydration sensing in biomembranes using lateral diffusion of lipids as a measure of local hydration (chapter 8), an approach that has a tremendous potential to be utilized in studying step-wise mechanisms of various biological and cellular processes like cell fusion, viral entry, fertilization, neurotransmission, exocytosis; processes that involve local and transient membrane dehydration.

The works presented in this thesis show a pioneering approach to elucidate the role of biological water and lipid-ion-water interplay in lipid diffusion in biomimetic membranes and contribute significantly to the fields of membrane biology and biophysical chemistry. The showcased works provide new, molecular-level insights into the role of water in determining membrane properties, in particular lipid dynamics and overall phase-separation architecture in biomimetic membranes. Furthermore, they provide a detailed molecular-scale picture of the de/rehydration process involving the evolution of the lipid hydration structure in the presence and absence of various ions as well as activation energy of diffusion of PC lipids in biomimetic cell membranes. Our successful dehydration method of SLBs does not require any additional chemical modifications of the lipid structure or external physical or mechanical confinement of the lipid membranes. Hence this method offers a great opportunity to study lipid membranes in well-defined hydration conditions without altering their native behavior. Thus this approach opens up a doorway to a wide range of experiments on biomimetic membranes addressing various physical properties and structural parameters at lower hydration conditions, for instance, changes in hydrophobic mismatch, line tension or lipid-protein/lipid-lipid interactions. Addressing these proper-

ties of cell membranes has been so far elusive as any dehydration attempts have resulted either in the curling up of membranes during dehydration or the membrane structure had to be modified. Thus, clearly, research covered in this doctoral thesis not only provides molecular insight into the physical chemistry of lipid-water-ion interactions but possesses far-reaching biological and technological implications.

## 11.2 Outlook

As discussed above, the work presented in this thesis is only the tip of the iceberg – a number of follow-up studies await to be explored in order to gain deeper understanding of the role of biological water in modulating lipid dynamics and consequently the cell membrane properties. To mention some specific directions for future research, the first question that comes to mind is – how the lipids with a different type of the head group (and hence different hydration shell structure) would react, in terms of lateral diffusion, at reduced hydration conditions? It would be very interesting to investigate the mobility of positively and negatively charged lipids such as DOTAP, DOPE, DOPG, DOPS, which do not have a water clathrate cage structure around their headgroups. Instead, these lipids being both donors and acceptors of H-bonds, form strong H-bonds with water molecules and adjacent lipids. Hence, it is tempting to speculate that dehydration of a membrane composed of those lipids may not have as dramatic effect on their lateral diffusion as in the case of PC lipids. Otherwise, one could also expect a more linear and gradual decline in lipid mobility. This would also validate my results pointing at the central role of the water molecules comprising the water shell structure in facilitating lipid diffusion. Yet the challenge lies in preparing single-component SLBs with the above mentioned lipids, as their structural curvature inhibits the formation of stable SLBs[157].

Another interesting follow-up study could focus on the differentiation between the effect of de/rehydration on the two leaflets of the bilayer separately. In publication 1 (supporting information), by irreversible fluorescence quenching of the fluorescent dye in the upper leaflet, I showed that during dehydration lipid diffusion in both lower and upper leaflet is affected similarly. But additionally, preliminary results indicate that the lipid diffusion in the lower leaflet does not increase back to its initial value after rehydration (Figure 11.1B). Further investigations are required to confirm this observation. This experiment would provide answers to the question if the thin layer of water between mica support and the lower leaflet of the bilayer is permanently removed upon dehydration altering the interactions between mica and the lower lipid leaflet.

Additionally, measuring lipid diffusion in the presence of  $\text{H}_2\text{O}$  vs  $\text{D}_2\text{O}$  could be interesting as another follow-up study. These experiments could indicate the role of H-bonded water molecules in modulating lipid diffusion as, on average, the H-bond strength is higher in case of  $\text{D}_2\text{O}$ . Moreover, spot variation FCS (STED-FCS) experiments on dehydrated SLBs could provide information about the exact nature of anomalous diffusion of lipids and information about the lipid dynamics at the  $\text{L}_\text{o}$ - $\text{L}_\text{d}$  boundary zone under varying hydration conditions, as discussed in chapter 10. How dehydration affects the mobility of cholesterol in the presence and absence of various ions would be an interesting question to address as well.

It is clear that having the possibility to alter membrane hydration state allows to address a number of interesting research questions regarding the structural and dynamical properties of lipid membranes. Thus the methodology and investigations presented in this thesis build an important initial step towards many interesting follow-up studies for deeper

understanding of the effect of hydration on physico-chemical properties of lipid membranes.

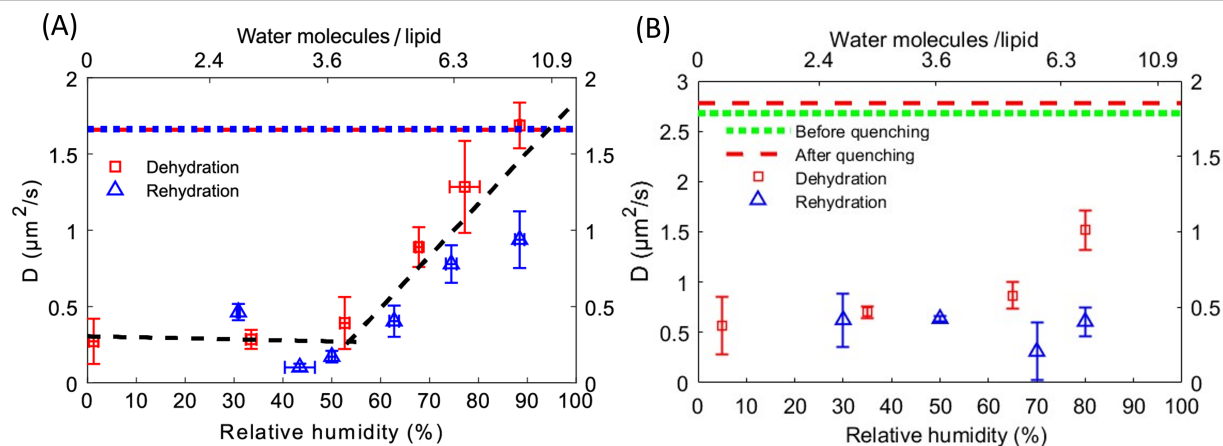


Figure 11.1: A) Changes in  $D$  as a function of hydration for both leaflets of the lipid bilayer (from Publication 1), B) Preliminary results showing  $D$  as a function of hydration of the lower leaflet, after irreversibly quenching the dye from upper leaflet of the bilayer.





# Bibliography

- [1] C. Calero, H. E. Stanley, and G. Franzese, “Structural interpretation of the large slowdown of water dynamics at stacked phospholipid membranes for decreasing hydration level: All-atom molecular dynamics,” *Materials*, vol. 9, no. 5, p. 319, 2016.
- [2] B. Bagchi, *Water in Biological and Chemical Processes: From Structure and Dynamics to Function*. Cambridge University Press, 2013.
- [3] F. Martelli, C. Calero, and G. Franzese, “Redefining the concept of hydration water near soft interfaces,” *Biointerphases*, vol. 16, p. 020801, 2021.
- [4] J. M. Harp, L. Coates, B. Sullivan, and M. Egli, “Water structure around a left-handed Z-DNA fragment analyzed by cryo neutron crystallography,” *Nucleic Acids Research*, vol. 49, no. 8, pp. 4782–4792, 2021.
- [5] H. Khesbak, O. Savchuk, S. Tsushima, and K. Fahmy, “The role of water H-bond imbalances in B-DNA substate transitions and peptide recognition revealed by time-resolved FTIR spectroscopy,” *Journal of the American Chemical Society*, vol. 133, no. 15, pp. 5834–5842, 2011.
- [6] E. A. Disalvo, F. Lairion, F. Martini, E. Tymczyszyn, M. Frías, H. Almaleck, and G. J. Gordillo, “Structural and functional properties of hydration and confined water in membrane interfaces,” *Biochimica et Biophysica Acta (BBA) - Biomembranes*, vol. 1778, no. 12, pp. 2655–2670, 2008.
- [7] D. M. LeNeveu and R. P. Rand, “Measurement and modification of forces between lecithin bilayers,” *Biophysical Journal*, vol. 18, no. 2, pp. 209–230, 1977.
- [8] K. J. Tielrooij, D. Paparo, L. Piatkowski, H. J. Bakker, and M. Bonn, “Dielectric relaxation dynamics of water in model membranes probed by terahertz spectroscopy,” *Biophysical Journal*, vol. 97, no. 9, pp. 2484–2492, 2009.
- [9] C. Calero and G. Franzese, “Membranes with different hydration levels: The interface between bound and unbound hydration water,” *Journal of Molecular Liquids*, vol. 273, pp. 488–496, 2019.
- [10] L. Piatkowski, J. de Heij, and H. J. Bakker, “Probing the distribution of water molecules hydrating lipid membranes with ultrafast förster vibrational energy transfer,” *The Journal of Physical Chemistry B*, vol. 117, no. 5, pp. 1367–1377, 2013.
- [11] L. Beranová, J. Humpolíčková, J. Sýkora, A. Benda, L. Cwiklik, P. Jurkiewicz, G. Gröbner, and M. Hof, “Effect of heavy water on phospholipid membranes: experimental confirmation of molecular dynamics simulations,” *Physical Chemistry Chemical Physics*, vol. 14, no. 42, pp. 14516–14522, 2012.
- [12] H. Orlikowska-Rzeznik, E. Krok, M. Chattopadhyay, A. Lester, and L. Piatkowski, “Laurdan Discerns Lipid Membrane Hydration and Cholesterol Content,” *The Journal of Physical Chemistry B*, vol. 127, no. 15, pp. 3382–3391, 2023.

- [13] S. Malik and A. Debnath, “Dehydration induced dynamical heterogeneity and ordering mechanism of lipid bilayers,” *Journal of Chemical Physics*, vol. 154, no. 17, 2021.
- [14] A. Gennaro, O. Deschaume, H. Pfeiffer, C. Bartic, P. Wagner, and M. Wübbenhorst, “Understanding the Dehydration Stress in Lipid Vesicles by a Combined Quartz Crystal Microbalance and Dielectric Spectroscopy Study,” *physica status solidi (a)*, vol. 217, no. 13, p. 1900986, 2020.
- [15] H. Pfeiffer, H. Binder, G. Klose, and K. Heremans, “Hydration pressure and phase transitions of phospholipids: Ii. thermotropic approach,” *Biochimica et Biophysica Acta (BBA) - Biomembranes*, vol. 1609, no. 2, pp. 148–152, 2003.
- [16] T. Baumgart and A. Offenhäusser, “Lateral diffusion in substrate-supported lipid monolayers as a function of ambient relative humidity,” *Biophysical Journal*, vol. 83, no. 3, pp. 1489–1500, 2002.
- [17] J. C. Wright, “Cryptobiosis 300 Years on from van Leuwenhoek: What Have We Learned about Tardigrades?,” *Zoologischer Anzeiger - A Journal of Comparative Zoology*, vol. 240, no. 3-4, pp. 563–582, 2001.
- [18] R. Marotta, F. Leasi, A. Uggetti, C. Ricci, and G. Melone, “Dry and survive: Morphological changes during anhydrobiosis in a bdelloid rotifer,” *Journal of Structural Biology*, vol. 171, no. 1, pp. 11–17, 2010.
- [19] S. E. Abusharkh, C. Erkut, J. Oertel, T. V. Kurzchalia, and K. Fahmy, “The role of phospholipid headgroup composition and trehalose in the desiccation tolerance of *caenorhabditis elegans*,” *Langmuir*, vol. 30, no. 43, pp. 12897–12906, 2014.
- [20] Y. A. Chizmadzhev, “Membrane Fusion,” *Biologicheskije Membrany*, vol. 29, no. 1-2, pp. 379–399, 2016.
- [21] M. Pasenkiewicz-Gierula, K. Baczynski, M. Markiewicz, and K. Murzyn, “Computer modelling studies of the bilayer/water interface,” *Biochimica et Biophysica Acta (BBA) - Biomembranes*, vol. 1858, no. 10, pp. 2305–2321, 2016.
- [22] E. Fahy, S. Subramaniam, H. A. Brown, C. K. Glass, A. H. Merrill, R. C. Murphy, C. R. Raetz, D. W. Russell, Y. Seyama, W. Shaw, T. Shimizu, F. Spener, G. Van Meer, M. S. VanNieuwenhze, S. H. White, J. L. Witztum, and E. A. Dennis, “A comprehensive classification system for lipids,” *Journal of lipid research*, vol. 46, no. 5, pp. 839–861, 2005.
- [23] E. Fahy, S. Subramaniam, R. C. Murphy, M. Nishijima, C. R. H. Raetz, T. Shimizu, F. Spener, G. van Meer, M. J. O. Wakelam, and E. A. Dennis, “Update of the LIPID MAPS comprehensive classification system for lipids,” *Journal of lipid research*, vol. 50 Suppl, pp. 9–14, 4 2009.
- [24] B. Alberts, A. Johnson, J. Lewis, M. Raff, K. Roberts, and P. Walter, *The Lipid Bilayer*. Garland Science, 2002.
- [25] H. Petrache, “Lipid Bilayer Structure,” in *Comprehensive Biophysics*, vol. 5, pp. 3–15, Elsevier, 2012.

- [26] K. Keegstra, M. Werner-Washburne, K. Cline, and J. Andrews, “The chloroplast envelope: Is it homologous with the double membranes of mitochondria and gram-negative bacteria?,” *Journal of Cellular Biochemistry*, vol. 24, no. 1, pp. 55–68, 1984.
- [27] J. Schumann, “Molecular Mechanism of Cellular Membranes for Signal Transduction,” *Membranes*, vol. 12, no. 8, p. 748, 2022.
- [28] A. N. Bondar and S. Keller, “Lipid Membranes and Reactions at Lipid Interfaces: Theory, Experiments, and Applications,” *Journal of Membrane Biology*, vol. 251, no. 3, pp. 295–298, 2018.
- [29] S. J. Singer and G. L. Nicolson, “The fluid mosaic model of the structure of cell membranes,” *Science*, vol. 175, no. 4023, pp. 720–731, 1972.
- [30] K. Simons and E. Ikonen, “Functional rafts in cell membranes,” *Nature*, vol. 387, no. 6633, pp. 569–572, 1997.
- [31] L. Rajendran and K. Simons, “Lipid rafts and membrane dynamics,” *Journal of Cell Science*, vol. 118, no. 6, pp. 1099–1102, 2005.
- [32] E. L. Elson, E. Fried, J. E. Dolbow, and G. M. Genin, “Phase Separation in Biological Membranes: Integration of Theory and Experiment,” *Annual Review of Biophysics*, vol. 39, no. 1, pp. 207–226, 2010.
- [33] K. Jacobson, O. G. Mouritsen, and R. G. Anderson, “Lipid rafts: at a crossroad between cell biology and physics,” *Nature Cell Biology*, vol. 9, no. 1, pp. 7–14, 2007.
- [34] E. Klotzsch and G. J. Schütz, “A critical survey of methods to detect plasma membrane rafts,” *Philosophical Transactions of the Royal Society B: Biological Sciences*, vol. 368, pp. 1–16, 2 2013.
- [35] G. M’Baye, Y. Mély, G. Duportail, and A. S. Klymchenko, “Liquid ordered and gel phases of lipid bilayers: Fluorescent probes reveal close fluidity but different hydration,” *Biophysical Journal*, vol. 95, no. 3, pp. 1217–1225, 2008.
- [36] L. K. Tamm and H. M. McConnell, “Supported phospholipid bilayers,” *Biophysical Journal*, vol. 47, no. 1, pp. 105–113, 1985.
- [37] R. P. Richter and A. R. Brisson, “Following the formation of supported lipid bilayers on Mica: A study combining AFM, QCM-D, and ellipsometry,” *Biophysical Journal*, vol. 88, no. 5, pp. 3422–3433, 2005.
- [38] R. P. Richter, R. Bérat, and A. R. Brisson, “Formation of solid-supported lipid bilayers: An integrated view,” *Langmuir*, vol. 22, no. 8, pp. 3497–3505, 2006.
- [39] A. R. Ferhan, B. K. Yoon, S. Park, T. N. Sut, H. Chin, J. H. Park, J. A. Jackman, and N. J. Cho, “Solvent-assisted preparation of supported lipid bilayers,” *Nature Protocols*, vol. 14, no. 7, pp. 2091–2118, 2019.
- [40] J. A. Jackman and N. J. Cho, “Supported Lipid Bilayer Formation: Beyond Vesicle Fusion,” *Langmuir*, vol. 36, no. 6, pp. 1387–1400, 2020.

- [41] A. C. Simonsen and L. A. Bagatolli, "Structure of spin-coated lipid films and domain formation in supported membranes formed by hydration," *Langmuir*, vol. 20, no. 22, pp. 9720–9728, 2004.
- [42] J. Nissen, S. Gritsch, G. Wiegand, and J. O. Rädler, "Wetting of phospholipid membranes on hydrophilic surfaces - Concepts towards self-healing membranes," *European Physical Journal B*, vol. 10, no. 2, pp. 335–344, 1999.
- [43] J. Kurniawan, J. F. Ventrici De Souza, A. T. Dang, G. Y. Liu, and T. L. Kuhl, "Preparation and Characterization of Solid-Supported Lipid Bilayers Formed by Langmuir-Blodgett Deposition: A Tutorial," *Langmuir*, vol. 34, no. 51, pp. 15622–15639, 2018.
- [44] J. A. Frank, H. G. Franquelim, P. Schwille, and D. Trauner, "Optical Control of Lipid Rafts with Photoswitchable Ceramides," *Journal of the American Chemical Society*, vol. 138, no. 39, pp. 12981–12986, 2016.
- [45] L. Picas, F. Rico, and S. Scheuring, "Direct measurement of the mechanical properties of lipid phases in supported bilayers," *Biophysical Journal*, vol. 102, no. 1, pp. L01–L03, 2012.
- [46] A. J. García-Sáez, S. Chiantia, and P. Schwille, "Effect of line tension on the lateral organization of lipid membranes," *Journal of Biological Chemistry*, vol. 282, no. 46, pp. 33537–33544, 2007.
- [47] J. Sarkis and V. Vié, "Biomimetic Models to Investigate Membrane Biophysics Affecting Lipid-Protein Interaction," *Frontiers in Bioengineering and Biotechnology*, vol. 8, p. 270, 2020.
- [48] A. Alessandrini and P. Facci, "Nanoscale mechanical properties of lipid bilayers and their relevance in biomembrane organization and function," *Micron*, vol. 43, no. 12, pp. 1212–1223, 2012.
- [49] N. Bag, D. H. X. Yap, and T. Wohland, "Temperature dependence of diffusion in model and live cell membranes characterized by imaging fluorescence correlation spectroscopy," *Biochimica et Biophysica Acta (BBA) - Biomembranes*, vol. 1838, no. 3, pp. 802–813, 2014.
- [50] P. Urban, S. D. Pritzl, M. F. Ober, C. F. Dirscherl, C. Pernpeintner, D. B. Konrad, J. A. Frank, D. Trauner, B. Nickel, and T. Lohmueller, "A Lipid Photoswitch Controls Fluidity in Supported Bilayer Membranes," *Langmuir*, vol. 36, no. 10, pp. 2629–2634, 2020.
- [51] C. Larsson, M. Rodahl, and F. Höök, "Characterization of DNA immobilization and subsequent hybridization on a 2D arrangement of streptavidin on a biotin-modified lipid bilayer supported on SiO<sub>2</sub>," *Analytical Chemistry*, vol. 75, no. 19, pp. 5080–5087, 2003.
- [52] E. Sackmann, "Supported membranes: Scientific and practical applications," *Science*, vol. 271, no. 5245, pp. 43–48, 1996.
- [53] A. Meister and A. Blume, "(Cryo)Transmission Electron Microscopy of Phospholipid Model Membranes Interacting with Amphiphilic and Polyphilic Molecules," *Polymers*, vol. 9, no. 10, p. 521, 2017.

- [54] E. I. Goksu, J. M. Vanegas, C. D. Blanchette, W. C. Lin, and M. L. Longo, “AFM for structure and dynamics of biomembranes,” *Biochimica et Biophysica Acta (BBA) - Biomembranes*, vol. 1788, no. 1, pp. 254–266, 2009.
- [55] S. Matsunaga, H. Shimizu, T. Yamada, T. Kobayashi, and M. Kawai, “In Situ STM and Vibrational Study of Nanometer-Scale Reorganization of a Phospholipid Monolayer Accompanied by Potential-Driven Headgroup Digestion,” *Langmuir*, vol. 33, pp. 13157–13167, 11 2017.
- [56] A. Simon, C. Gounou, S. Tan, L. Tiefenauer, M. Di Berardino, and A. R. Brisson, “Free-standing lipid films stabilized by Annexin-A5,” *Biochimica et Biophysica Acta (BBA) - Biomembranes*, vol. 1828, no. 11, pp. 2739–2744, 2013.
- [57] W. Miyashita, D. Saeki, and H. Matsuyama, “Formation of supported lipid bilayers on porous polymeric substrates induced by hydrophobic interaction,” *Colloids and Surfaces A: Physicochemical and Engineering Aspects*, vol. 538, pp. 297–303, 2018.
- [58] M. L. Wagner and L. K. Tamm, “Tethered polymer-supported planar lipid bilayers for reconstitution of integral membrane proteins: Silane-polyethyleneglycol-lipid as a cushion and covalent linker,” *Biophysical Journal*, vol. 79, no. 3, pp. 1400–1414, 2000.
- [59] Z. Boban, I. Mardešić, W. K. Subczynski, and M. Raguz, “Giant Unilamellar Vesicle Electroformation: What to Use, What to Avoid, and How to Quantify the Results,” *Membranes*, vol. 11, no. 11, 2021.
- [60] C. O. Gurdap, L. Wedemann, T. Sych, and E. Sezgin, “Influence of the extracellular domain size on the dynamic behavior of membrane proteins,” *Biophysical Journal*, vol. 121, no. 20, pp. 3826–3836, 2022.
- [61] J. Wilschut and D. Hoekstra, “Membrane fusion: Lipid vesicles as a model system,” *Chemistry and Physics of Lipids*, vol. 40, no. 2-4, pp. 145–166, 1986.
- [62] T. Sych, C. O. Gurdap, L. Wedemann, and E. Sezgin, “How Does Liquid-Liquid Phase Separation in Model Membranes Reflect Cell Membrane Heterogeneity?,” *Membranes*, vol. 11, no. 5, p. 323, 2021.
- [63] J. Ries, S. Chiantia, and P. Schwille, “Accurate determination of membrane dynamics with line-scan FCS,” *Biophysical Journal*, vol. 96, no. 5, pp. 1999–2008, 2009.
- [64] T. Bhatia, P. Husen, J. Brewer, L. A. Bagatolli, P. L. Hansen, J. H. Ipsen, and O. G. Mouritsen, “Preparing giant unilamellar vesicles (GUVs) of complex lipid mixtures on demand: Mixing small unilamellar vesicles of compositionally heterogeneous mixtures,” *Biochimica et Biophysica Acta (BBA) - Biomembranes*, vol. 1848, no. 12, pp. 3175–3180, 2015.
- [65] T. J. Crites, M. Maddox, K. Padhan, J. Muller, C. Eigsti, and R. Varma, “Supported Lipid Bilayer Technology for the Study of Cellular Interfaces,” *Current protocols in cell biology*, vol. 68, no. 1, p. 24.5.1, 2015.
- [66] M. Letrou, S. Cribier, N. Rodriguez, and J. Heuvingh, “Studying membrane fusion using supported lipid bilayers on superparamagnetic beads,” *Biochimica et Biophysica Acta (BBA) - Biomembranes*, vol. 1865, no. 1, p. 184070, 2023.

- [67] E. R. Tyndall and F. Tian, "Spherical Nanoparticle Supported Lipid Bilayers: a Tool for Modeling Protein Interactions with Curved Membranes," *Methods in molecular biology*, vol. 1688, p. 99, 2018.
- [68] J. Schlegel, B. Porebski, L. Andronico, L. Hanke, S. Edwards, H. Brismar, B. Murrell, G. M. McInerney, O. Fernandez-Capetillo, and E. Sezgin, "A multiparametric and high-throughput platform for host-virus binding screens.," *Nano letters*, vol. 23, no. 9, pp. 3701–3707, 2023.
- [69] Z. Gerstle, R. Desai, and S. L. Veatch, "Giant Plasma Membrane Vesicles: An Experimental Tool for Probing the Effects of Drugs and Other Conditions on Membrane Domain Stability," *Methods in enzymology*, vol. 603, pp. 129–150, 2018.
- [70] E. Sezgin, "Giant plasma membrane vesicles to study plasma membrane structure and dynamics," *Biochimica et Biophysica Acta (BBA) - Biomembranes*, vol. 1864, no. 4, p. 183857, 2022.
- [71] R. Dharan, S. Goren, S. K. Cheppali, P. Shendrik, G. Brand, A. Vaknin, L. Yu, M. M. Kozlov, and R. Sorkin, "Transmembrane proteins tetraspanin 4 and CD9 sense membrane curvature," *Proceedings of the National Academy of Sciences of the United States of America*, vol. 119, no. 43, p. e2208993119, 2022.
- [72] S. Zemljic Jokhadar, U. Klancnik, M. Grundner, T. Svelc Kebe, S. Vrhovec Hartman, M. Liović, and J. Derganc, "GPMVs in variable physiological conditions: could they be used for therapy delivery?," *BMC biophysics*, vol. 11, no. 1, p. 1, 2018.
- [73] C. Luo, X. Hu, R. Peng, H. Huang, Q. Liu, and W. Tan, "Biomimetic Carriers Based on Giant Membrane Vesicles for Targeted Drug Delivery and Photodynamic/Photothermal Synergistic Therapy," *ACS Applied Materials and Interfaces*, vol. 11, no. 47, pp. 43811–43819, 2019.
- [74] J. L. Symons, K. J. Cho, J. T. Chang, G. Du, M. N. Waxham, J. F. Hancock, I. Levental, and K. R. Levental, "Lipidomic atlas of mammalian cell membranes reveals hierarchical variation induced by culture conditions, subcellular membranes, and cell lineages," *Soft Matter*, vol. 17, no. 2, pp. 288–297, 2021.
- [75] L. Zartner, M. Garni, I. Craciun, T. Einfalt, and C. G. Palivan, "How Can Giant Plasma Membrane Vesicles Serve as a Cellular Model for Controlled Transfer of Nanoparticles?," *Biomacromolecules*, vol. 22, no. 1, pp. 106–115, 2021.
- [76] D. Zhong, S. K. Pal, and A. H. Zewail, "Biological water: A critique," *Chemical Physics Letters*, vol. 503, no. 1-3, pp. 1–11, 2011.
- [77] V. Bianco and G. Franzese, "Contribution of Water to Pressure and Cold Denaturation of Proteins," *Physical Review Letters*, vol. 115, no. 10, p. 108101, 2015.
- [78] D. March, V. Bianco, and G. Franzese, "Protein Unfolding and Aggregation near a Hydrophobic Interface," *Polymers*, vol. 13, no. 1, p. 156, 2021.
- [79] V. Bianco, G. Franzese, and I. Coluzza, "In Silico Evidence That Protein Unfolding is a Precursor of Protein Aggregation," *ChemPhysChem*, vol. 21, no. 5, pp. 377–384, 2020.



- [80] P. Jungwirth, “Biological Water or Rather Water in Biology?,” *Journal of Physical Chemistry Letters*, vol. 6, no. 13, pp. 2449–2451, 2015.
- [81] R. Zhang, T. A. Cross, X. Peng, and R. Fu, “Surprising Rigidity of Functionally Important Water Molecules Buried in the Lipid Headgroup Region,” *Journal of the American Chemical Society*, vol. 144, no. 17, pp. 7881–7888, 2022.
- [82] M. Pasenkiewicz-Gierula, K. Baczynski, M. Markiewicz, and K. Murzyn, “Computer modelling studies of the bilayer/water interface,” *Biochimica et Biophysica Acta (BBA) - Biomembranes*, vol. 1858, no. 10, pp. 2305–2321, 2016.
- [83] S. Y. Bhide and M. L. Berkowitz, “Structure and dynamics of water at the interface with phospholipid bilayers,” *Journal of Chemical Physics*, vol. 123, no. 22, p. 224702, 2005.
- [84] S. Re, W. Nishima, T. Tahara, and Y. Sugita, “Mosaic of water orientation structures at a neutral zwitterionic lipid/water interface revealed by molecular dynamics simulations,” *Journal of Physical Chemistry Letters*, vol. 5, no. 24, pp. 4343–4348, 2014.
- [85] S. Pal, N. Samanta, D. Das Mahanta, R. K. Mitra, and A. Chattopadhyay, “Effect of Phospholipid Headgroup Charge on the Structure and Dynamics of Water at the Membrane Interface: A Terahertz Spectroscopic Study,” *Journal of Physical Chemistry B*, vol. 122, no. 19, pp. 5066–5074, 2018.
- [86] K. Åman, E. Lindahl, O. Edholm, P. Håkansson, and P. O. Westlund, “Structure and Dynamics of Interfacial Water in an  $L\alpha$  Phase Lipid Bilayer from Molecular Dynamics Simulations,” *Biophysical Journal*, vol. 84, no. 1, pp. 102–115, 2003.
- [87] C. F. Lopez, S. O. Nielsen, M. L. Klein, and P. B. Moore, “Hydrogen bonding structure and dynamics of water at the dimyristoylphosphatidylcholine lipid bilayer surface from a molecular dynamics simulation,” *Journal of Physical Chemistry B*, vol. 108, pp. 6603–6610, 5 2004.
- [88] S. Simon and T. McIntosh, “[38] depth of water penetration into lipid bilayers,” in *Biomembranes Part O: Protons and Water: Structure and Translocation*, vol. 127 of *Methods in Enzymology*, pp. 511–521, Academic Press, 1986.
- [89] J. F. Nagle, R. Zhang, S. Tristram-Nagle, W. Sun, H. I. Petrache, and R. M. Suter, “X-ray structure determination of fully hydrated L alpha phase dipalmitoylphosphatidylcholine bilayers,” *Biophysical journal*, vol. 70, no. 3, pp. 1419–1431, 1996.
- [90] K. Hristova and S. H. White, “Determination of the hydrocarbon core structure of fluid dioleoylphosphocholine (DOPC) bilayers by x-ray diffraction using specific bromination of the double-bonds: Effect of hydration,” *Biophysical Journal*, vol. 74, no. 5, pp. 2419–2433, 1998.
- [91] T. Róg, K. Murzyn, J. Milhaud, M. Karttunen, and M. Pasenkiewicz-Gierula, “Water Isotope Effect on the Phosphatidylcholine Bilayer Properties: A Molecular Dynamics Simulation Study,” *Journal of Physical Chemistry B*, vol. 113, no. 8, pp. 2378–2387, 2009.

- [92] P. Murray-Rust, P. Murray-Rust, and J. P. Glusker, "Directional Hydrogen Bonding to  $sp^2$ - and  $sp^3$ -Hybridized Oxygen Atoms and Its Relevance to Ligand-Macromolecule Interactions," *Journal of the American Chemical Society*, vol. 106, no. 4, pp. 1018–1025, 1984.
- [93] K. Murzyn, T. Róg, and M. Pasenkiewicz-Gierula, "Phosphatidylethanolamine-Phosphatidylglycerol Bilayer as a Model of the Inner Bacterial Membrane," *Biophysical Journal*, vol. 88, no. 2, pp. 1091–1103, 2005.
- [94] K. Murzyn, T. Róg, G. Jezierski, Y. Takaoka, and M. Pasenkiewicz-Gierula, "Effects of Phospholipid Unsaturation on the Membrane/Water Interface: A Molecular Simulation Study," *Biophysical Journal*, vol. 81, no. 1, pp. 170–183, 2001.
- [95] H. Martinez-Seara, T. Róg, M. Pasenkiewicz-Gierula, I. Vattulainen, M. Karttunen, and R. Reigada, "Effect of Double Bond Position on Lipid Bilayer Properties: Insight through Atomistic Simulations," *Journal of Physical Chemistry B*, vol. 111, no. 38, pp. 11162–11168, 2007.
- [96] H. Martinez-Seara, T. Róg, M. Pasenkiewicz-Gierula, I. Vattulainen, M. Karttunen, and R. Reigada, "Interplay of Unsaturated Phospholipids and Cholesterol in Membranes: Effect of the Double-Bond Position," *Biophysical Journal*, vol. 95, no. 7, pp. 3295–3305, 2008.
- [97] T. Dingjan and A. H. Futerman, "The role of the 'sphingoid motif' in shaping the molecular interactions of sphingolipids in biomembranes," *Biochimica et Biophysica Acta (BBA) - Biomembranes*, vol. 1863, no. 11, p. 183701, 2021.
- [98] M. I. Oh, C. I. Oh, and D. F. Weaver, "Effect of Cholesterol on the Structure of Networked Water at the Surface of a Model Lipid Membrane," *Journal of Physical Chemistry B*, vol. 124, no. 18, pp. 3686–3694, 2020.
- [99] C.-Y. Cheng, L. L. C. Olijve, R. Kausik, and S. Han, "Cholesterol enhances surface water diffusion of phospholipid bilayers," *The Journal of chemical physics*, vol. 141, no. 22, p. 22D513, 2014.
- [100] M. Dolores Elola and J. Rodriguez, "Influence of Cholesterol on the Dynamics of Hydration in Phospholipid Bilayers," *The Journal of Physical Chemistry B*, vol. 122, pp. 5897–5907, 5 2018.
- [101] S. A. Pandit, D. Bostick, and M. L. Berkowitz, "Molecular Dynamics Simulation of a Dipalmitoylphosphatidylcholine Bilayer with NaCl," *Biophysical Journal*, vol. 84, no. 6, pp. 3743–3750, 2003.
- [102] R. A. Böckmann, A. Hac, T. Heimburg, and H. Grubmüller, "Effect of sodium chloride on a lipid bilayer," *Biophysical Journal*, vol. 85, no. 3, pp. 1647–1655, 2003.
- [103] M. Stepniewski, A. Bunker, M. Pasenkiewicz-Gierula, M. Karttunen, and T. Róg, "Effects of the lipid bilayer phase state on the water membrane interface," *Journal of Physical Chemistry B*, vol. 114, no. 36, pp. 11784–11792, 2010.
- [104] N. N. Casillas-Ituarte, X. Chen, H. Castada, and H. C. Allen, "Na<sup>+</sup> and Ca<sup>2+</sup> Effect on the Hydration and Orientation of the Phosphate Group of DPPC at Air-Water and

- Air-Hydrated Silica Interfaces,” *Journal of Physical Chemistry B*, vol. 114, no. 29, pp. 9485–9495, 2010.
- [105] D. Uhríková, N. Kučerka, J. Teixeira, V. Gordeliy, and P. Balgavý, “Structural changes in dipalmitoylphosphatidylcholine bilayer promoted by  $\text{Ca}^{2+}$  ions: a small-angle neutron scattering study,” *Chemistry and physics of lipids*, vol. 155, no. 2, pp. 80–89, 2008.
- [106] A. Das, C. Adhikari, and A. Chakraborty, “Interaction of Different Divalent Metal Ions with Lipid Bilayer: Impact on the Encapsulation of Doxorubicin by Lipid Bilayer and Lipoplex Mediated Deintercalation,” *Journal of Physical Chemistry B*, vol. 121, no. 8, pp. 1854–1865, 2017.
- [107] R. A. Böckmann and H. Grubmüller, “Multistep binding of divalent cations to phospholipid bilayers: A molecular dynamics study,” *Angewandte Chemie - International Edition*, vol. 43, no. 8, pp. 1021–1024, 2004.
- [108] H. Binder and O. Zschörnig, “The effect of metal cations on the phase behavior and hydration characteristics of phospholipid membranes,” *Chemistry and Physics of Lipids*, vol. 115, pp. 39–61, 5 2002.
- [109] M. B. França, A. D. Panek, and E. C. Eleutherio, “Oxidative stress and its effects during dehydration,” *Comparative Biochemistry and Physiology Part A: Molecular & Integrative Physiology*, vol. 146, no. 4, pp. 621–631, 2007.
- [110] F. Schliess and D. Häussinger, “The cellular hydration state: A critical determinant for cell death and survival,” *Biological Chemistry*, vol. 383, pp. 577–583, 4 2002.
- [111] A. Rapoport, “Anhydrobiosis and dehydration of yeasts,” in *Biotechnology of Yeasts and Filamentous Fungi*, pp. 87–116, Springer International Publishing, 2017.
- [112] J. H. Crowe, L. M. Crowe, and D. Chapman, “Preservation of Membranes in Anhydrobiotic Organisms: The Role of Trehalose,” *Science*, vol. 223, no. 4637, pp. 701–703, 1984.
- [113] K. A. Madin and J. H. Crowe, “Anhydrobiosis in nematodes: Carbohydrate and lipid metabolism during dehydration,” *Journal of Experimental Zoology*, vol. 193, no. 3, pp. 335–342, 1975.
- [114] E. C. Eleutheria, P. S. de Araujo, and A. D. Panek, “Role of the trehalose carrier in dehydration resistance of *saccharomyces cerevisiae*,” *Biochimica et Biophysica Acta (BBA) - General Subjects*, vol. 1156, no. 3, 1993.
- [115] J. Lapinski and A. Tunnacliffe, “Anhydrobiosis without trehalose in bdelloid rotifers,” *FEBS Letters*, vol. 553, no. 3, pp. 387–390, 2003.
- [116] K. Goyal, L. J. Walton, and A. Tunnacliffe, “LEA proteins prevent protein aggregation due to water stress,” *Biochemical Journal*, vol. 388, no. 1, pp. 151–157, 2005.
- [117] J. Rizo, “Molecular Mechanisms Underlying Neurotransmitter Release,” *Annual Review of Biophysics*, vol. 51, pp. 377–408, 2022.
-

- [118] S. Aeffer, T. Reusch, B. Weinhausen, and T. Salditt, "Energetics of stalk intermediates in membrane fusion are controlled by lipid composition," *Proceedings of the National Academy of Sciences of the United States of America*, vol. 109, no. 25, p. 9678, 2012.
- [119] A. M. Sendek, M. F. Poyton, A. J. Baxter, T. Yang, and P. S. Cremer, "Supported Lipid Bilayers with Phosphatidylethanolamine as the Major Component," *Langmuir*, vol. 33, no. 46, pp. 13423–13429, 2017.
- [120] M. A. Holden, S. Y. Jung, T. Yang, E. T. Castellana, and P. S. Cremer, "Creating fluid and air-stable solid supported lipid bilayers," *Journal of the American Chemical Society*, vol. 126, no. 21, pp. 6512–6513, 2004.
- [121] D. Chapman, "Biomembranes and New Hemocompatible Materials," *Langmuir*, vol. 9, no. 1, pp. 39–45, 1993.
- [122] C.-t. Han and L. Chao, "Creating Air-Stable Supported Lipid Bilayers by Physical Confinement Induced by Phospholipase A 2," *ACS Applied Materials and Interfaces*, vol. 6, pp. 6378–6383, 2014.
- [123] Y. Deng, Y. Wang, B. Holtz, J. Li, N. Traaseth, G. Veglia, B. J. Stottrup, R. Elde, and D. Pei, "Fluidic and Air-Stable Supported Lipid Bilayer and Cell-Mimicking Microarrays," *Journal of American Chemical Society*, no. 12, pp. 6267–6271, 2008.
- [124] B. P. Oberts and G. J. Blanchard, "Formation of Air-Stable Supported Lipid Monolayers and Bilayers," *Langmuir*, vol. 1322, no. 11, pp. 2962–2970, 2009.
- [125] R. M. Fabre and D. R. Talham, "Stable Supported Lipid Bilayers on Zirconium Phosphonate Surfaces," *Langmuir*, vol. 25, no. 9, pp. 12644–12652, 2009.
- [126] Y. Fang, A. G. Frutos, and J. Lahiri, "Membrane Protein Microarrays," *Journal of American Chemical Society*, vol. 124, no. 11, pp. 2394–2395, 2002.
- [127] M. Halter, Y. Nogata, O. Dannenberger, T. Sasaki, and V. Vogel, "Engineered Lipids That Cross-Link the Inner and Outer Leaflets of Lipid Bilayers," *Langmuir*, no. 14, pp. 2416–2423, 2004.
- [128] J. C. Conboy, S. Liu, D. F. O. Brien, and S. S. Saavedra, "Planar Supported Bilayer Polymers Formed from Bis-Diene Lipids by Langmuir - Blodgett Deposition and UV Irradiation," *Biomacromolecules*, vol. 4, no. 3, pp. 841–849, 2003.
- [129] F. Albertorio, A. J. Diaz, T. Yang, V. A. Chapa, S. Kataoka, E. T. Castellana, and P. S. Cremer, "Fluid and air-stable lipopolymer membranes for biosensor applications," *Langmuir*, vol. 21, no. 16, pp. 7476–7482, 2005.
- [130] S. Chiantia, N. Kahya, and P. Schwille, "Dehydration Damage of Domain-Exhibiting Supported Bilayers : An AFM Study on the Protective Effects of Disaccharides and Other Stabilizing Substances," *Langmuir*, vol. 21, no. 14, pp. 6317–6323, 2005.
- [131] Y. Dong, K. S. Phillips, and Q. Cheng, "Immunosensing of Staphylococcus enterotoxin B (SEB) in milk with PDMS microfluidic systems using reinforced supported bilayer membranes (r-SBMs)," *Lab on a Chip*, vol. 6, no. 5, pp. 675–681, 2006.

- [132] J. H. Lorent, K. R. Levental, L. Ganesan, G. Rivera-Longsworth, E. Sezgin, M. Doktorova, E. Lyman, and I. Levental, “Plasma membranes are asymmetric in lipid unsaturation, packing and protein shape,” *Nature Chemical Biology*, vol. 16, no. 6, pp. 644–652, 2020.
- [133] R. A. Chaurio, C. Janko, L. E. Muñoz, B. Frey, M. Herrmann, and U. S. Gaipf, “Phospholipids: Key Players in Apoptosis and Immune Regulation,” *Molecules*, vol. 14, no. 12, pp. 4892–4914, 2009.
- [134] V. Haucke and G. Di Paolo, “Lipids and lipid modifications in the regulation of membrane traffic,” *Current opinion in cell biology*, vol. 19, no. 4, p. 426, 2007.
- [135] H. Sunshine and M. L. Iruela-Arispe, “Membrane Lipids and Cell Signaling,” *Current opinion in lipidology*, vol. 28, no. 5, p. 408, 2017.
- [136] P. G. Saffman and M. Delbrück, “Brownian motion in biological membranes,” *Proceedings of the National Academy of Sciences*, vol. 72, no. 8, pp. 3111–3113, 1975.
- [137] R. Machán and M. Hof, “Lipid diffusion in planar membranes investigated by fluorescence correlation spectroscopy,” *Biochimica et Biophysica Acta (BBA) - Biomembranes*, vol. 1798, no. 7, pp. 1377–1391, 2010.
- [138] E. Yamamoto, A. C. Kalli, T. Akimoto, K. Yasuoka, and M. S. P. Sansom, “Anomalous Dynamics of a Lipid Recognition Protein on a Membrane Surface,” *Scientific Reports*, vol. 5, no. 1, p. 18245, 2015.
- [139] L. Ebersberger, T. Schindler, S. A. Kirsch, K. Pluhackova, A. Schambony, T. Seydel, R. A. Böckmann, and T. Unruh, “Lipid Dynamics in Membranes Slowed Down by Transmembrane Proteins,” *Frontiers in Cell and Developmental Biology*, vol. 8, p. 1120, 2020.
- [140] J. E. Goose and M. S. Sansom, “Reduced lateral mobility of lipids and proteins in crowded membranes,” *PLoS computational biology*, vol. 9, no. 4, p. e1003033, 2013.
- [141] M. Sovago, G. W. Worpel, M. Smits, M. Müller, and M. Bonn, “Calcium-induced phospholipid ordering depends on surface pressure,” *Journal of the American Chemical Society*, vol. 129, no. 36, pp. 11079–11084, 2007.
- [142] A. Melcrová, S. Pokorna, S. Pullanchery, M. Kohagen, P. Jurkiewicz, M. Hof, P. Jungwirth, P. S. Cremer, and L. Cwiklik, “The complex nature of calcium cation interactions with phospholipid bilayers,” *Scientific Reports*, vol. 6, pp. 1–12, 12 2016.
- [143] T. V. Ratto and M. L. Longo, “Obstructed Diffusion in Phase-Separated Supported Lipid Bilayers : A Combined Atomic Force Microscopy and Fluorescence Recovery after Photobleaching Approach,” *Biophysical Journal*, vol. 83, no. 6, pp. 3380–3392, 2002.
- [144] P. F. Almeida and T. E. Thompson, “Lateral Diffusion in the Liquid Phases of Dimyristoylphosphatidylcholine/Cholesterol Lipid Bilayers : A Free Volume Analysis,” *Biochemistry*, vol. 31, no. 29, pp. 6739–6747, 1992.

- [145] M. A. Deverall, E. Gindl, E. K. Sinner, H. Besir, J. Ruehe, M. J. Saxton, and C. A. Naumann, "Membrane Lateral Mobility Obstructed by Polymer-Tethered Lipids Studied at the Single Molecule Level," *Biophysical Journal*, vol. 88, no. 3, pp. 1875–1886, 2005.
- [146] N. L. Thompson and D. Axelrod, "Reduced lateral mobility of a fluorescent lipid probe in cholesterol-depleted erythrocyte membrane," *Biochimica et Biophysica Acta (BBA) - Biomembranes*, vol. 597, no. 1, pp. 155–165, 1980.
- [147] T. Fujiwara, K. Ritchie, H. Murakoshi, K. Jacobson, and A. Kusumi, "Phospholipids undergo hop diffusion in compartmentalized cell membrane," *Journal of Cell Biology*, vol. 157, no. 6, pp. 1071–1081, 2002.
- [148] M. Przybylo, J. Sýkora, J. Humpolíčová, A. Benda, A. Zan, and M. Hof, "Lipid diffusion in giant unilamellar vesicles is more than 2 times faster than in supported phospholipid bilayers under identical conditions," *Langmuir*, vol. 22, no. 22, pp. 9096–9099, 2006.
- [149] M. J. Saxton, "A Biological Interpretation of Transient Anomalous Subdiffusion. I. Qualitative Model," *Biophysical Journal*, vol. 92, no. 4, pp. 1178–1191, 2007.
- [150] D. V. Nicolau, J. F. Hancock, and K. Burrage, "Sources of anomalous diffusion on cell membranes: A Monte Carlo study," *Biophysical Journal*, vol. 92, no. 6, pp. 1975–1987, 2007.
- [151] H. L. Coker, M. R. Cheetham, D. R. Kattnig, Y. J. Wang, S. Garcia-Manyes, and M. I. Wallace, "Controlling Anomalous Diffusion in Lipid Membranes," *Biophysical Journal*, vol. 116, no. 6, pp. 1085–1094, 2019.
- [152] A. Kusumi, Y. Sako, and M. Yamamoto, "Confined lateral diffusion of membrane receptors as studied by single particle tracking (nanovid microscopy). Effects of calcium-induced differentiation in cultured epithelial cells," *Biophysical Journal*, vol. 65, no. 5, pp. 2021–2040, 1993.
- [153] K. Ritchie, X. Y. Shan, J. Kondo, K. Iwasawa, T. Fujiwara, and A. Kusumi, "Detection of Non-Brownian Diffusion in the Cell Membrane in Single Molecule Tracking," *Biophysical Journal*, vol. 88, no. 3, pp. 2266–2277, 2005.
- [154] E. Sezgin, "Super-resolution optical microscopy for studying membrane structure and dynamics," *Journal of Physics: Condensed Matter*, vol. 29, no. 27, p. 273001, 2017.
- [155] A. Kusumi, C. Nakada, K. Ritchie, K. Murase, K. Suzuki, H. Murakoshi, R. S. Kasai, J. Kondo, and T. Fujiwara, "Paradigm Shift of the Plasma Membrane Concept from the Two-Dimensional Continuum Fluid to the Partitioned Fluid: High-Speed Single-Molecule Tracking of Membrane Molecules," *Annual Review of Biophysics and Biomolecular Structure*, vol. 34, no. 1, pp. 351–378, 2005.
- [156] K. Murase, T. Fujiwara, Y. Umemura, K. Suzuki, R. Iino, H. Yamashita, M. Saito, H. Murakoshi, K. Ritchie, and A. Kusumi, "Ultrafine membrane compartments for molecular diffusion as revealed by single molecule techniques," *Biophysical Journal*, vol. 86, no. 6, pp. 4075–4093, 2004.

- [157] C. Eggeling, C. Ringemann, R. Medda, G. Schwarzmann, K. Sandhoff, S. Polyakova, V. N. Belov, B. Hein, C. Von Middendorff, A. Schönle, and S. W. Hell, “Direct observation of the nanoscale dynamics of membrane lipids in a living cell,” *Nature*, vol. 457, no. 7233, pp. 1159–1162, 2009.
- [158] T. K. Fujiwara, K. Iwasawa, Z. Kalay, T. A. Tsunoyama, Y. Watanabe, Y. M. Umemura, H. Murakoshi, K. G. Suzuki, Y. L. Nemoto, N. Morone, and A. Kusumi, “Confined diffusion of transmembrane proteins and lipids induced by the same actin meshwork lining the plasma membrane,” *Molecular Biology of the Cell*, vol. 27, no. 7, p. 1101, 2016.
- [159] M. P. Clausen and B. C. Lagerholm, “Visualization of plasma membrane compartmentalization by high-speed quantum dot tracking,” *Nano Letters*, vol. 13, no. 6, pp. 2332–2337, 2013.
- [160] D. M. Andrade, M. P. Clausen, J. Keller, V. Mueller, C. Wu, J. E. Bear, S. W. Hell, B. C. Lagerholm, and C. Eggeling, “Cortical actin networks induce spatio-temporal confinement of phospholipids in the plasma membrane – a minimally invasive investigation by STED-FCS,” *Scientific Reports*, vol. 5, no. 1, pp. 1–12, 2015.
- [161] C. Ringemann, B. Harke, C. Von Middendorff, R. Medda, A. Honigsmann, R. Wagner, M. Leutenegger, A. Schönle, S. W. Hell, and C. Eggeling, “Exploring single-molecule dynamics with fluorescence nanoscopy,” *New Journal of Physics*, vol. 11, no. 10, p. 103054, 2009.
- [162] M. P. Clausen, E. Sezgin, J. Bernardino de la Serna, D. Waithe, B. C. Lagerholm, and C. Eggeling, “A straightforward approach for gated STED-FCS to investigate lipid membrane dynamics,” *Methods*, vol. 88, pp. 67–75, 2015.
- [163] F. Schneider, D. Waithe, M. P. Clausen, S. Galiani, T. Koller, G. Ozhan, C. Eggeling, and E. Sezgin, “Diffusion of lipids and GPI-anchored proteins in actin-free plasma membrane vesicles measured by STED-FCS,” *Molecular Biology of the Cell*, vol. 28, no. 11, pp. 1507–1518, 2017.
- [164] R. Schwarzer, I. Levental, A. Gramatica, S. Scolari, V. Buschmann, M. Veit, and A. Herrmann, “The cholesterol-binding motif of the HIV-1 glycoprotein gp41 regulates lateral sorting and oligomerization,” *Cellular microbiology*, vol. 16, no. 10, pp. 1565–1581, 2014.
- [165] F. X. Contreras, A. M. Ernst, P. Haberkant, P. Björkholm, E. Lindahl, B. Gönen, C. Tischer, A. Elofsson, G. Von Heijne, C. Thiele, R. Pepperkok, F. Wieland, and B. Brügger, “Molecular recognition of a single sphingolipid species by a protein’s transmembrane domain,” *Nature*, vol. 481, no. 7382, pp. 525–529, 2012.
- [166] U. Kuhad, G. Goel, P. K. Maurya, and R. C. Kuhad, “Sukshmjeevanu in Vedas: The Forgotten Past of Microbiology in Indian Vedic Knowledge,” *Indian Journal of Microbiology*, vol. 61, no. 1, p. 108, 2021.
- [167] S. Padhy, “Vedic Indians were Aware of the Microbial Biodiversity, Demanding ‘Kannva’ as the Father of Microbiology,” *Journal of Biodiversity*, vol. 7, no. 2, pp. 101–103, 2016.



- [168] H. Gest, “The discovery of microorganisms by Robert Hooke and Antoni van Leeuwenhoek, Fellows of The Royal Society,” *Notes and Records of the Royal Society of London*, vol. 58, no. 2, pp. 187–201, 2004.
- [169] B. Valeur and M. N. Berberan-Santos, “A brief history of fluorescence and phosphorescence before the emergence of quantum theory,” *Journal of Chemical Education*, vol. 88, pp. 731–738, 6 2011.
- [170] E. Sezgin, *Continuously variable lipid packing as the principle of functional membrane heterogeneity*. PhD thesis, Technical University Dresden, 2012.
- [171] M. M., “Microscopy apparatus,” *U.S. patent 3,0130467*, 1961.
- [172] M. Minsky, “Memoir on inventing the confocal scanning microscope,” *Scanning*, vol. 10, no. 4, pp. 128–138, 1988.
- [173] J. L. Nadeau, *Introduction to Experimental Biophysics : Biological Methods for Physical Scientists*. CRC press, 2nd ed., 2017.
- [174] D. M. Soumpasis, “Theoretical analysis of fluorescence photobleaching recovery experiments,” *Biophysical Journal*, vol. 41, no. 1, pp. 95–97, 1983.
- [175] B. L. Sprague, R. L. Pego, D. A. Stavreva, and J. G. McNally, “Analysis of binding reactions by fluorescence recovery after photobleaching,” *Biophysical Journal*, vol. 86, no. 6, pp. 3473–3495, 2004.
- [176] B. L. Sprague and J. G. McNally, “FRAP analysis of binding: Proper and fitting,” *Trends in Cell Biology*, vol. 15, no. 2, pp. 84–91, 2005.
- [177] M. J. Saxton, “Anomalous subdiffusion in fluorescence photobleaching recovery: a Monte Carlo study,” *Biophysical Journal*, vol. 81, no. 4, p. 2226, 2001.
- [178] A. Tannert, S. Tannert, S. Burgold, and M. Schaefer, “Convolution-based one and two component FRAP analysis: theory and application,” *European biophysics journal : EBJ*, vol. 38, no. 5, pp. 649–661, 2009.
- [179] E. Sezgin and P. Schwille, “Fluorescence Techniques to Study Lipid Dynamics,” *Cold Spring Harbor Perspectives in Biology*, vol. 3, no. 11, p. a009803, 2011.
- [180] L. S. Nicholson, N. Gervasi, T. Falières, A. Leroy, D. Miremont, D. Zala, and C. Hanus, “Whole-Cell Photobleaching Reveals Time-Dependent Compartmentalization of Soluble Proteins by the Axon Initial Segment,” *Frontiers in Cellular Neuroscience*, vol. 14, p. 180, 2020.
- [181] P. Schwille, J. Korlach, and W. W. Webb, “Fluorescence correlation spectroscopy with single-molecule sensitivity on cell and model membranes,” *Cytometry*, vol. 36, no. 3, pp. 176–182, 1999.
- [182] E. L. Elson, “Fluorescence Correlation Spectroscopy: Past, Present, Future,” *Biophysical Journal*, vol. 101, no. 12, pp. 2855–2870, 2011.
- [183] E. L. Elson and D. Magde, “Fluorescence correlation spectroscopy. I. Conceptual basis and theory,” *Biopolymers*, vol. 13, no. 1, pp. 1–27, 1974.

- [184] M. Ehrenberg and R. Rigler, "Rotational brownian motion and fluorescence intensify fluctuations," *Chemical Physics*, vol. 4, no. 3, pp. 390–401, 1974.
- [185] L. Onsager, "Reciprocal Relations in Irreversible Processes. I.," *Physical Review*, vol. 37, no. 4, p. 405, 1931.
- [186] A. Honigsmann, V. Mueller, S. W. Hell, and C. Eggeling, "STED microscopy detects and quantifies liquid phase separation in lipid membranes using a new far-red emitting fluorescent phosphoglycerolipid analogue," *Faraday Discuss.*, vol. 161, no. 0, pp. 77–89, 2013.
- [187] M. Weiss, M. Elsner, F. Kartberg, and T. Nilsson, "Anomalous Subdiffusion Is a Measure for Cytoplasmic Crowding in Living Cells," *Biophysical Journal*, vol. 87, no. 5, pp. 3518–3524, 2004.
- [188] A. Lubelski and J. Klafter, "Fluorescence Correlation Spectroscopy: The Case of Subdiffusion," *Biophysical Journal*, vol. 96, no. 6, p. 2055, 2009.
- [189] F. Schneider, D. Waithe, S. Galiani, J. Bernardino De La Serna, E. Sezgin, and C. Eggeling, "Nanoscale Spatiotemporal Diffusion Modes Measured by Simultaneous Confocal and Stimulated Emission Depletion Nanoscopy Imaging," *Nano Letters*, vol. 18, no. 7, pp. 4233–4240, 2018.
- [190] K. Bacia, S. A. Kim, and P. Schwille, "Fluorescence cross-correlation spectroscopy in living cells," *Nature Methods*, vol. 3, no. 2, pp. 83–89, 2006.
- [191] O. Shimomura, F. H. Johnson, and Y. Saiga, "Extraction, Purification and Properties of Aequorin, a Bioluminescent Protein from the Luminous Hydromedusan, *Aequorea*," *Journal of Cellular and Comparative Physiology*, vol. 59, no. 3, pp. 223–239, 1962.
- [192] M. Chalfie, Y. Tu, G. Euskirchen, W. W. Ward, and D. C. Prasher, "Green fluorescent protein as a marker for gene expression.," *Science*, vol. 263, no. 5148, pp. 802–805, 1994.
- [193] A. Gaebler, R. Milan, L. Straub, D. Hoelper, L. Kuerschner, and C. Thiele, "Alkyne lipids as substrates for click chemistry-based in vitro enzymatic assays," *Journal of Lipid Research*, vol. 54, no. 8, pp. 2282–2290, 2013.
- [194] A. B. Neef and C. Schultz, "Selective Fluorescence Labeling of Lipids in Living Cells," *Angewandte Chemie International Edition*, vol. 48, no. 8, pp. 1498–1500, 2009.
- [195] D. Liang, K. Wu, R. Tei, T. W. Bumpus, J. Ye, and J. M. Baskin, "A real-time click chemistry imaging approach reveals stimulus-specific subcellular locations of phospholipase D activity," *Proceedings of the National Academy of Sciences of the United States of America*, vol. 116, pp. 15453–15462, 7 2019.
- [196] A. S. Klymchenko and R. Kreder, "Fluorescent Probes for Lipid Rafts: From Model Membranes to Living Cells," *Chemistry & Biology*, vol. 21, no. 1, pp. 97–113, 2014.
- [197] T. Baumgart, A. T. Hammond, P. Sengupta, S. T. Hess, D. A. Holowka, B. A. Baird, and W. W. Webb, "Large-scale fluid/fluid phase separation of proteins and lipids in giant plasma membrane vesicles," *Proceedings of the National Academy of Sciences of the United States of America*, vol. 104, no. 9, pp. 3165–3170, 2007.

- [198] P. Sengupta, A. Hammond, D. Holowka, and B. Baird, “Structural determinants for partitioning of lipids and proteins between coexisting fluid phases in giant plasma membrane vesicles,” *Biochimica et Biophysica Acta (BBA) - Biomembranes*, vol. 1778, no. 1, pp. 20–32, 2008.
- [199] E. Sezgin, I. Levental, M. Grzybek, G. Schwarzmann, V. Mueller, A. Honigsmann, V. N. Belov, C. Eggeling, U. Coskun, K. Simons, and P. Schwille, “Partitioning, diffusion, and ligand binding of raft lipid analogs in model and cellular plasma membranes,” *Biochimica et Biophysica Acta (BBA) - Biomembranes*, vol. 1818, no. 7, pp. 1777–1784, 2012.
- [200] N. Kahya, D. Scherfeld, K. Bacia, B. Poolman, and P. Schwille, “Probing lipid mobility of raft-exhibiting model membranes by fluorescence correlation spectroscopy,” *Journal of Biological Chemistry*, vol. 278, no. 30, pp. 28109–28115, 2003.
- [201] M. Amaro, F. Reina, M. Hof, C. Eggeling, and E. Sezgin, “Laurdan and Di-4-ANEPPDHQ probe different properties of the membrane,” *Journal of Physics D: Applied Physics*, vol. 50, no. 13, p. 134004, 2017.
- [202] A. S. Klymchenko, “Solvatochromic fluorescent dyes as universal tools for biological research,” *L’Actualité Chimique*, vol. 359, pp. 20–26, 2012.
- [203] G. Gunther, L. Malacrida, D. M. Jameson, E. Gratton, and S. A. Sánchez, “LAURDAN since Weber: The Quest for Visualizing Membrane Heterogeneity,” *Accounts of chemical research*, vol. 54, no. 4, p. 976, 2021.
- [204] T. Parasassi, G. De Stasio, A. d’Ubaldo, and E. Gratton, “Phase fluctuation in phospholipid membranes revealed by Laurdan fluorescence,” *Biophysical Journal*, vol. 57, no. 6, pp. 1179–1186, 1990.
- [205] G. Weber and F. J. Farris, “Synthesis and Spectral Properties of a Hydrophobic Fluorescent Probe: 6-Propionyl-2-(dimethylamino)naphthalene,” *Biochemistry*, vol. 18, no. 14, pp. 3075–3078, 1979.
- [206] F. Ragaller, L. Andronico, J. Sykora, W. Kulig, T. Rog, Y. B. Urem, Abhinav, D. I. Danylchuk, M. Hof, A. Klymchenko, M. Amaro, I. Vattulainen, and E. Sezgin, “Dissecting the mechanisms of environment sensitivity of smart probes for quantitative assessment of membrane properties,” *Open Biology*, vol. 12, no. 9, p. 220175, 2022.
- [207] M. Weber, H. von der Emde, M. Leutenegger, P. Gunkel, S. Sambandan, T. A. Khan, J. Keller-Findeisen, V. C. Cordes, and S. W. Hell, “MINSTED nanoscopy enters the Ångström localization range,” *Nature Biotechnology*, vol. 41, no. 4, pp. 569–576, 2022.
- [208] M. Weber, M. Leutenegger, S. Stoldt, S. Jakobs, T. S. Mihaila, A. N. Butkevich, and S. W. Hell, “MINSTED fluorescence localization and nanoscopy,” *Nature Photonics*, vol. 15, no. 5, pp. 361–366, 2021.
- [209] K. C. Gwosch, J. K. Pape, F. Balzarotti, P. Hoess, J. Ellenberg, J. Ries, and S. W. Hell, “MINFLUX nanoscopy delivers 3D multicolor nanometer resolution in cells,” *Nature Methods*, vol. 17, no. 2, pp. 217–224, 2020.

- [210] R. Schmidt, T. Weihs, C. A. Wurm, I. Jansen, J. Rehman, S. J. Sahl, and S. W. Hell, “MINFLUX nanometer-scale 3D imaging and microsecond-range tracking on a common fluorescence microscope,” *Nature Communications*, vol. 12, no. 1, pp. 1–12, 2021.
- [211] S. Hell, “Minflux and minsted provide moleculescale resolution in fluorescence microscopy,” *FEBS Open Bio*, vol. 12, no. 1, 2022. PL-12-1, Presentation at the Biochemistry Global Summit, Lisbon.
- [212] M. Chattopadhyay, E. Krok, H. Orlikowska, P. Schwille, H. G. Franquelim, and L. Piatkowski, “Hydration layer of only a few molecules controls lipid mobility in biomimetic membranes,” *Journal of the American Chemical Society*, vol. 143, no. 36, pp. 14551–14562, 2021.
- [213] M. J. Saxton, “A Biological Interpretation of Transient Anomalous Subdiffusion. I. Qualitative Model,” *Biophysical Journal*, vol. 92, no. 4, pp. 1178–1191, 2007.
- [214] Y. Chen, B. C. Lagerholm, B. Yang, and K. Jacobson, “Methods to measure the lateral diffusion of membrane lipids and proteins,” *Methods*, vol. 39, no. 2, pp. 147–153, 2006.
- [215] M. R. Horton, F. Höfling, J. O. Rädler, and T. Franosch, “Development of anomalous diffusion among crowding proteins,” *Soft Matter*, vol. 6, no. 12, pp. 2648–2656, 2010.
- [216] C. L. Hsieh, S. Spindler, J. Ehrig, and V. Sandoghdar, “Tracking single particles on supported lipid membranes: Multimobility diffusion and nanoscopic confinement,” *Journal of Physical Chemistry B*, vol. 118, no. 6, pp. 1545–1554, 2014.
- [217] G. J. Schuitz, H. Schindler, and T. Schmidt, “Single-Molecule Microscopy on Model Membranes Reveals Anomalous Diffusion,” *Biophysical Journal*, vol. 73, pp. 1073–1080, 1997.
- [218] K. M. Spillane, J. Ortega-Arroyo, G. De Wit, C. Eggeling, H. Ewers, M. I. Wallace, and P. Kukura, “High-speed single-particle tracking of gm1 in model membranes reveals anomalous diffusion due to interleaflet coupling and molecular pinning,” *Nano Letters*, vol. 14, no. 9, pp. 5390–5397, 2014.
- [219] T. V. Ratto and M. L. Longo, “Anomalous Subdiffusion in Heterogeneous Lipid Bilayers,” *Langmuir*, vol. 19, no. 5, pp. 1788–1793, 2002.
- [220] J.-H. Jeon, H. M.-S. Monne, M. Javanainen, and R. Metzler, “Anomalous Diffusion of Phospholipids and Cholesterols in a Lipid Bilayer and its Origins,” *Physical Review Letters*, vol. 109, no. 18, p. 188103, 2012.
- [221] A. Arnold, M. Paris, and M. Auger, “Anomalous Diffusion in a Gel-Fluid Lipid Environment: A Combined Solid-State NMR and Obstructed Random-Walk Perspective,” *Biophysical Journal*, vol. 87, no. 4, pp. 2456–2469, 2004.
- [222] A. Matysik and R. S. Kraut, “Preparation of Mica Supported Lipid Bilayers for High Resolution Optical Microscopy Imaging,” *Journal of Visualized Experiments*, no. 88, p. 52054, 2014.

- [223] D. Waithe, M. P. Clausen, E. Sezgin, and C. Eggeling, “FoCuS-point: software for STED fluorescence correlation and time-gated single photon counting,” *Bioinformatics*, vol. 32, no. 6, pp. 958–960, 2016.
- [224] D. Waithe, F. Schneider, J. Chojnacki, M. P. Clausen, D. Shrestha, J. B. de la Serna, and C. Eggeling, “Optimized processing and analysis of conventional confocal microscopy generated scanning FCS data,” *Methods*, vol. 140-141, pp. 62–73, 2018.
- [225] Z. Petrášek and P. Schwille, “Precise measurement of diffusion coefficients using scanning fluorescence correlation spectroscopy,” *Biophysical Journal*, vol. 94, no. 4, pp. 1437–1448, 2008.
- [226] M. Chattopadhyay, E. Krok, H. Orlikowska-Rzeznik, and L. Piatkowski, “Cooperativity between sodium ions and water molecules facilitates lipid mobility in model cell membranes,” *Chemical Science*, vol. 14, no. 15, pp. 4002–4011, 2023.
- [227] F. Schneider, D. Waithe, B. C. Lagerholm, D. Shrestha, E. Sezgin, C. Eggeling, and M. Fritzsche, “Statistical Analysis of Scanning Fluorescence Correlation Spectroscopy Data Differentiates Free from Hindered Diffusion,” *ACS Nano*, vol. 12, pp. 8540–8546, 8 2018.
- [228] M. Chattopadhyay, H. Orlikowska, E. Krok, and L. Piatkowski, “Sensing Hydration of Biomimetic Cell Membranes,” *Biosensors*, vol. 11, no. 7, p. 241, 2021.
- [229] E. Krok, H. G. Franquelim, M. Chattopadhyay, H. Orlikowska-Rzeznik, P. Schwille, and L. Piatkowski, “Nanoscale structural response of biomimetic cell membranes to controlled dehydration.” unpublished work.
- [230] M. J. Saxton, “Wanted: A Positive Control for Anomalous Subdiffusion,” *Biophysical Journal*, vol. 103, no. 12, pp. 2411–2422, 2012.

# Chapter 12

## Scientific achievements

### 12.1 Publications

#### 12.1.1 Articles

1. Hanna Orlikowska-Rzeznik\*, Emilia Krok, **Madhurima Chattopadhyay** and Lukasz Piatkowski\*, *Laurdan discerns lipid membrane hydration and cholesterol content*, **Journal of Physical Chemistry B**, 2023, volume 127, issue 15, page 3382-3391, **IF 3.466**
2. **Madhurima Chattopadhyay\***, Emilia Krok, Hanna Orlikowska-Rzeznik and Lukasz Piatkowski\*, *Cooperativity between sodium ions and water molecules facilitates lipid mobility in model cell membranes*, **Chemical Science**, 2023, issue 14, page 4002-4011, **IF 9.969**
3. Emilia Krok\*, Agnieszka Batura, **Madhurima Chattopadhyay**, Hanna Orlikowska and Lukasz Piatkowski\*, *Lateral organization of biomimetic cell membranes in varying pH conditions*, **Journal of Molecular Liquids**, 2022, volume 345, page 117907, **IF: 6.633**
4. **Madhurima Chattopadhyay\***, Emilia Krok, Hanna Orlikowska, Petra Schwillle, Henri G. Franquelim and Lukasz Piatkowski\*, *Hydration layer of only few molecules controls lipid mobility in biomimetic membranes*, **Journal of the American Chemical Society**, 2021, volume 143, issue 36, page 14551-14562, **IF: 16.383**
5. **Madhurima Chattopadhyay\*#**, Hanna Orlikowska<sup>#</sup>, Emilia Krok and Lukasz Piatkowski\*, *Sensing hydration of biomimetic cell membranes*, **Biosensors**, 2021, volume 11, issue 7, page 241, **IF: 5.743**

#### 12.1.2 Conference papers

1. **Madhurima Chattopadhyay\***, Emilia Krok, Hanna Orlikowska-Rzeznik and Lukasz Piatkowski\*, *Sodium ions support lipid mobility in dehydrated biomembranes*, **FEBS Open Bio**, 2022 volume 12, issue 270, P-04.2-009, **IF: 2.792**
2. Lukasz Piatkowski\*, **Madhurima Chattopadhyay\***, Emilia Krok, Hanna Orlikowska-Rzeznik and Agnieszka Lester, *How the absence of just a few water molecules affects the structure and dynamics of cell membranes*, **FEBS Open Bio**, 2022 volume 12, page 268, P-04.2-005, **IF: 2.792**
3. Emilia Krok\*, **Madhurima Chattopadhyay**, Hanna Orlikowska, Lukasz Piatkowski\*, *Decreased hydration causes nanoscale structural rearrangement within biomimetic cell*

*membranes,*

FEBS Open Bio, 2022, volume 12, issue 1, ShT-04.2-1, **IF: 2.792**

4. Agnieszka Lester\*, Emilia Krok, **Madhurima Chattopadhyay**, Lukasz Piatkowski\*,  
*Engineering cell membranes—the effect of pH on the formation, structure, and mobility of biomimetic cell membranes,*  
FEBS Open Bio, 2022, volume 12, page 269-270, P-04.2-008, **IF: 2.792**
5. Hanna Orlikowska-Rzeznik\*, Emilia Krok, **Madhurima Chattopadhyay**, Agnieszka Lester, Lukasz Piatkowski\*, *Direct effect of biomimetic cell membrane hydration on Laurdan fluorescence,*  
FEBS Open Bio, 2022 volume 12, page 269, P-04.2-007, **IF: 2.792**

\*corresponding author(s)

#Co-first authors

## 12.2 Patent applications

1. **Madhurima Chattopadhyay**, Emilia Krok, Hanna Orlikowska, Lukasz Piatkowski,  
*Method for measuring the local hydration of lipid layers of biomimetic and biological systems,*  
patent application (Poland), P.437600, 2021
2. **Madhurima Chattopadhyay**, Emilia Krok, Hanna Orlikowska, Lukasz Piatkowski,  
*Method for measuring the local hydration of lipid layers of biomimetic and biological systems,*  
patent application (Poland), P.437601, 2021.
3. Emilia Krok, Agnieszka Batura, Hanna Orlikowska, **Madhurima Chattopadhyay**,  
Lukasz Piatkowski,  
*The method of formation of solid supported lipid membranes with controlled size of laterally separated domains,*  
patent application (Poland), PL438733, 2021

## 12.3 Participation in conferences

### Talks:

1. Hydration layer of few molecules controls lateral diffusion of lipids in biomembranes,  
National Science Day Seminar, organized by the Indian Photobiology Society, Kolkata,  
India, 03-05 March 2023
2. Hydration layer of few molecules controls lateral diffusion of lipids in biomembranes,  
Chemistry World conference, 13-14 June 2022, **invited talk**
3. Hydration layer of few molecules controls lateral diffusion of lipids in biomembranes,  
FEBS advanced course: Functional Imaging of Cellular Dynamics, Van Leeuwenhoek  
Centre for Advanced Microscopy (LCAM) and the University of Amsterdam, The  
Netherlands, 12-18 June 2022



4. Lateral diffusion of lipids senses local hydration in biomembranes, Molecular biosensing: from theory to practice”, International symposium organized by University of Jena, Germany, 17-19 November 2021
5. Water facilitating lateral diffusion in biomembrane, Young Scientists’ Conference Biology, Chemistry, Environment – the Perspective of Young Scientists/ Konferencja Młodych Naukowców nt. Biologia, Chemia i Środowisko - Spojrzenie Młodych Naukowców), Krakow, Poland, 24-25 April 2021
6. The Effect of Environmental Conditions on the Structure and Dynamics of Biomimetic Cell Membrane, 11th National Conference Young Scientists in Poland - Research and Development/XI Ogólnokrajowa Konferencja Młodzi Naukowcy w Polsce - Badania i Rozwój, Poznan (Poland), 30 March 2020

### **Poster presentations:**

1. Cooperative effect of Na<sup>+</sup> ions and water support lipid mobility at sparsely hydrated biomembranes, #RSCPoster Twitter conference 28 February - 01 March 31, 2023
2. Sodium ions support lipid mobility in dehydrated biomembranes, IUBMB-FEBS-PABMB Biochemistry Global Summit, Lisbon, Portugal, 09-14 July 2022
3. Water and Na<sup>+</sup> collectively control the lateral diffusion of lipids in dehydrated biomembranes, FEBS advanced course: Functional Imaging of Cellular Dynamics, Van Leeuwenhoek Centre for Advanced Microscopy (LCAM) and the University of Amsterdam, The Netherlands, 12-18 June 2022
4. Sodium ions support lipid mobility after membrane dehydration, #RSCPoster Twitter conference 01-02 March, 2022
5. Lipid diffusion indicates local hydration in biomembranes, Systems Chemistry Virtual Symposium, Strasbourg, France, 7-9 July 2021
6. Water facilitates lateral diffusion in biomembranes, Time-Resolved Vibrational Spectroscopy (TRVS) International Conference, Michigan, USA, 13-18 June 2021
7. Lipid mobility as a hydration sensing tool in SLBs, Young Scientists’ Conference Biology, Chemistry, Environment – the Perspective of Young Scientists/ Konferencja Młodych Naukowców nt. Biologia, Chemia i Środowisko - Spojrzenie Młodych Naukowców), Krakow, Poland, 24-25 April 2021
8. Lipid mobility as hydration sensing tool in SLBs, Chemical Systems Meeting - NanoGee conference, Spain 22-23 March 2021
9. Effect of hydration on structure and dynamics of biomimetic cell membranes, System chemistry Symposium “Life-like emergent behavior in complex molecules and ensembles”, International symposium organized by City University of New York, USA, 18-20 May 2020

10. Lipid mobility as hydration sensing tool in SLBs,  
Chemical Science conference, ChemSci2020: Leaders in the Field Symposium, International Symposium organized by IISER Kolkata, India, 07-10 September 2020
11. The Effect of Environmental Conditions on the Structure and Dynamics of Biomimetic Cell Membrane,  
The 11th National Conference Young Scientists in Poland - Research and Development/XI Ogólnokrajowa Konferencja Młodzi Naukowcy w Polsce - Badania i Rozwój, Poznan, Poland, 30 March 2020

## 12.4 Participation in courses

1. **FEBS Advanced Course – Functional Imaging of Cellular Dynamics** at the University of Amsterdam, the Netherlands, 12-19 June 2022
2. Course for reviewers **ACS Reviewer Lab** organized by American Chemical Society, 26 June 2021
3. **Summer School in Protocell Models: Coacervates and Vesicles organized by Max Planck Institute of Molecular Cell Biology and Genetics**, Dresden, Germany, 05-08 April 2021
4. **FSK3533 New Super-resolution, Light-sheet, STED-FCS and FRET-FCS methods** from Scilifelab, Stockholm, Sweden, 31 May-04 April 2021
5. Online workshop **Good practices in the writing of scientific articles**, organized by National Institute of Geriatrics, Rheumatology and Rehabilitation, TERMEDIA Publishing House, Warsaw, 18-19 November 2020
6. **Academic English - Practical course**, organized by Academia Internacjonalizacji, Poland, 10 April 2020
7. **22nd Neutron Scattering Lab Course** conducted by JCNS-1, 03-14 September 2018, Forschungszentrum Juelich and MLZ Garching, Germany

## 12.5 Research internships

1. Research internship on project “Elucidating the interplay between biological water and nanoscale lipid dynamics in cellular membranes” at **SciLifeLab, Karolinska Institute, Stockholm, Sweden** at the group of Dr. Erdinc Sezgin, funded by **EMBO Scientific Exchange Grant** (August - October 2022)
2. Research internship on “Conformational Analysis and Study of Photochemical Changes of some Biologically Significant Molecules Using Ion Mobility Mass Spectroscopy” at the **Indian Association for the Cultivation of Science, Kolkata, India** with Prof. Tapas Chakraborty Group (January - April 2019)
3. Summer internship project on "Stability Analysis of a FRET-Based Glucose Sensor Protein" at **Forschungszentrum Juelich, Juelich, Germany** with Dr. Andreas Stadler, funded by **BIOSOFT Guest Student Program** (July - September 2018)

## 12.6 Grants

### Mobility grants:

1. European Molecular Biology Organization (EMBO) **Scientific Exchange Grant** for a three months foreign research internship **EMBO-SEG**, grant number: 9439, *Elucidating the interplay between biological water and nanoscale lipid dynamics in cellular membranes*, principal investigator: M.Sc. Madhurima Chattopadhyay
2. **Erasmus+ Staff Mobility Teaching grant** for 5 days 10 hours teaching at the Department of Physics, IIT (ISM) Dhanbad, India, under the framework of Staff Training Assignments (STA), project KA 107 2019, grantee: M.Sc. Madhurima Chattopadhyay

### Co-investigator in research grants:

1. **First Team grant**, Foundation for Polish Science, grant number: POIR.04.04.00-00-5D32/18-00, *HYDRA – Elucidating the role of hydration heterogeneity and hydrophobic mismatch in biomimetic cell membranes organization*, principal investigator: Dr. hab. Eng. Lukasz Piatkowski (prof. PUT)
2. **Installation Grant**, European Molecular Biology Organization (**EMBO IG**), grant number: IG 4147, *Biological water: the role of hydration in cell membrane organization*, principal investigator: Dr. hab. Eng. Lukasz Piatkowski (prof. PUT)
3. Projekt w ramach wydzielonych z subwencji Wydziału Inżynierii Materiałowej i Fizyki Technicznej środków na prowadzenie badań naukowych lub prac rozwojowych oraz zadań z nimi związanych, służących rozwojowi młodych naukowców finansowanych w wewnętrznym trybie konkursowym w 2020 roku (**SBAD-MK**), grant number: 0512/SBAD-/6209, *Badanie wpływu cząsteczek wody na formowanie dwuwarstw lipidowych na podłożu stałym oraz określenie ilościowe ich nawodnienia przy pomocy mikrowa-gi kwarcowej*, principal investigator: M.Sc. Eng. Hanna-Orlikowska Rzeznik
4. Projekt w ramach wydzielonych z subwencji Wydziału Inżynierii Materiałowej i Fizyki Technicznej środków na prowadzenie badań naukowych lub prac rozwojowych oraz zadań z nimi związanych, służących rozwojowi młodych naukowców finansowanych w wewnętrznym trybie konkursowym w 2022 roku (**SBAD-MK**), grant number: 0512/SBAD-/6212, *Biomimetyczne błony komórkowe w warunkach ekstremalnego odwodnienia – analiza nanoskopowych zmian strukturalnych*, principal investigator: M.Sc. Eng. Emilia Krok

## 12.7 Awards and distinctions

1. **EBSA Student Bursary award** for participation in EBSA congress 2023 in Stockholm, Sweden, covering all costs of accommodation and congress registration fees

2. **Best oral presentation award** at the National Science Day Seminar 2023 organized by the Indian Photobiology Society, 03-05 March 2023
3. **Scholarship** from INPUTDOC project in the frame of the STER program "Internationalization of the doctoral students" co-financed by NAWA for scientific achievements being the result of international cooperation, December-May 2023
4. **The Rector's Award as a team** of the Poznan University of Technology for outstanding scientific achievements, October 2022
5. **Molecular Biology Organization Scientific Exchange Grant (EMBO-SEG)** for a three months foreign research internship on "elucidating the interplay between biological water and nanoscale lipid dynamics in cellular membranes" at Dr. Erdinc Sezgin's laboratory at Karolinska Institute, Stockholm, Sweden, August-October 2022
6. **Erasmus+ stuff mobility teaching grant** for teaching at IIT (ISM) Dhanbad, India, July 2022
7. **Front cover** of the *Journal of American Chemical Society*, Volume 143, Issue 36, 2021
8. **Best poster presentation award** at Young Scientists' Conference Biology, Chemistry, Environment – the Perspective of Young Scientists (Konferencja Młodych Naukowców nt. Biologia, Chemia i Środowisko - Spojrzenie Młodych Naukowców), Krakow, Poland, 24-25 April 2021, for the poster presentation titled "Lipid mobility as a hydration sensing tool in SLBs"

## 12.8 Scientific outreach

1. **Organization and hosting of an online, bimonthly seminar series**, namely, "Ph.D. students forum" for creating a platform to discuss research and mental health challenges faced by graduate students, since January 2023
2. Participation in **European Researchers' Night** at SciLifeLab, Karolinska Institutet, 30 September 2022
3. Erasmus+ stuff mobility program – 5 days, 8 hours teaching for M.Sc. and PhD students at the Department of Physics, IIT (ISM) Dhanbad, India, 18-22 July 2022
4. **Invited live webinar** for high school students on **Prospects/scopes of higher studies and research in chemistry in India and abroad** organized by ASED Kolkata Association for Science and Environmental Development, 31st July 2021

# Acknowledgements

It says “life does not need to be long, but great.” My four years of PhD life have not been too long, but I must say it has been so great and meaningful. Today at the end of my PhD journey I realize that this time has not only generated my doctoral thesis but also evolved me into an improved version. Only my name will be written on the title page of the thesis, but here I take the opportunity to thank the people without whom this doctoral thesis would not exist.

First of all, I sincerely thank Lukasz (Dr. hab. Lukasz Piatkowski), my doctoral Supervisor, for all his invaluable guidance, support, mentoring and encouragement. You were brave to give a chance to an unknown foreign student to pursue her dreams and accept her as one of your first PhD students. Thanks for believing in me. Thanks for my first day in Poland, when you showed up at the airport with little Szymon to pick me up after my long travel and hosted me at your flat as I missed the train to Poznan. I have learnt so many things from you – how to look from a different angle on a problem and turn it into an advantage, how to come up with research ideas, scientific writing, and speaking skills, how many more can I mention! Thanks for all those scientific discussions that enriched my thoughts, and shaped me into a better scientist. Not only scientifically, but also you played a role of a caring big brother for me in this foreign land. So many times I have been amazed by your fatherly protecting and caring nature. You made me laugh with your dark humor, I felt amused by your love for Indian food. Words can not fully express my gratitude and respect for you.

I am deeply indebted to my dear fellow PhD students and friends Emilia, Hanna and Agnieszka who have eventually become like my sisters. I can not thank Emilia enough for her active help and support in handling all my Polish documents and accompanying me to places where communication in Polish was needed. Those experiments together taught me a lot – her never-giving-up attitude, enthusiasm and excellent managing and organization skills left a deep impact on me. She never let me spend a single Christmas and Easter alone in this foreign land and always warmly hosted me in her family to share the joyful festive times. I wholeheartedly thank Hanna for all our joint research endeavors from the very beginning of our PhD days, support and our meaningful discussions – research related and beyond. Thanks to both Hanna and Emilia from whom I learned and improved my scientific drawing and various software skills. I thank Agnieszka for all her help in the lab and beyond, and the excellent cakes she baked on each occasion and also without any occasion. My heartfelt thanks to all of you who made our lab a deeply bonded family to me. I am so lucky to have you all, you gave me a feeling of "home away from home" in Poland.

I thank our whole Institute of Physics, especially Andrzej, Michał, Karol, Kamil, Alicja, Paulina, Semir, Marta, Marek and Damian for their help and support. I never heard ‘no’ from them whenever I needed some help in the lab. Thanks for all the corridor chats and for making our department so friendly and welcoming. I will cherish our departmental barbeques near Warta and on our campus every summer. Thanks to Karol for making me taste traditional Polish foods that will stay in my memory and taste buds.

I thank Przemek (Dr. Przemysław Głowacki) for his help and guidance during teaching laboratory courses for Bachelors students.

I am extremely grateful to Erdinc (Dr. Erdinc Sezgin) for giving me a chance to join

his lab for a research internship in the course of my PhD and I express my sincere thanks and appreciation to Taras (Dr. Taras Sych) and Erdinc for guiding and supporting me during the internship.

I would like to express my deepest gratitude to the Dean of our faculty, Prof. Mirosław Szybowicz, former Dean Prof. Ryszard Czajka, Head of the institute Prof. Arkadiusz Ptak and the Head of Doctoral school Prof. Alina Dudkowiak for their sincere help during my PhD studies here.

I thank Foundation for Polish Science (FNP), European Molecular Biology Organization (EMBO) and the PUT doctoral school for the research funding during my doctoral studies.

Today, near the completion of my PhD, I must also mention their names, whose continuous support and encouragement have brought me here, given me an unstoppable inspiration to go ahead towards my aim. I am immensely thankful to my school-level teachers Mrs. Sonali Sen Biswas, Mr. Debdulal Mandal, Mr. Niharkanti Sardar, and college-level teacher Dr. Nabakumar Bera (who made me fall in love with physical chemistry) for their extraordinary in-depth teaching, character-building lessons, love, care and motivation. I also thank my all other school, college, university and research-level teachers and mentors for making the base for me to become an aspiring PhD student.

I thank my uncle Dr. Tapan Chatterji, a motivated researcher, who had always been my role model from my childhood for his support and encouragement in my studies and research.

I sincerely thank Arghyadeep Basu for his constant love and care and for helping and supporting me during all the ups and downs of my PhD journey. With him, I have practiced all my research presentations and always received his useful comments.

I also express my deep love and appreciation to my sister Arunima Chattopadhyay, who owns a special soft corner in my heart. I can not thank her enough for her constant love, care, friendship, company and mental support.

Finally, thanking is far from enough to express my gratitude to my parents for their ever-lasting love, care, sincere efforts and encouragement for my studies, for the way they brought me up seeding a deep sense of curiosity and desire for knowledge in me, for sending me abroad to pursue PhD studies sacrificing the company of their beloved daughter. As said by the famous writer Kahlil Gibran, parents are the bows from which children fly forward - the more the bows stretch, the farther the arrow flies. Without the strong support and encouragement of my parents, I would not be in a place to write a doctoral thesis. I dedicate this thesis to my dear parents Mrs. Ranjana Chattopadhyay and Mr. Swapan Kumar Chattopadhyay, along with my doctoral supervisor, Lukasz Piatkowski.

## Declarations of the co-authors



Poznan, Date: 20.05.2023

Dr. hab. Eng. Lukasz Piatkowski (Prof. PUT)

Poznan University of Technology

Poznan, Poland

I declare that according to the CRediT author statement, in the following publications:

1. Hydration layer of only few molecules controls lipid mobility in biomimetic membranes, Madhurima Chattopadhyay\*, Emilia Krok, Hanna Orlikowska, Petra Schwille, Henri G. Franquelim, and Lukasz Piatkowski\*,  
*Journal of the American Chemical Society*, volume 143, issue 36, page 14551–14562, 2021,
2. Cooperativity between sodium ions and water molecules facilitates lipid mobility in model cell membranes, Madhurima Chattopadhyay\*, Emilia Krok, Hanna Orlikowska-Rzeznik, and Lukasz Piatkowski\*,  
*Chemical Science*, 2023, DOI: 10.1039/D2SC06836B,
3. Sensing hydration of biomimetic cell membranes, Madhurima Chattopadhyay\*, Hanna Orlikowska, Emilia Krok and Lukasz Piatkowski\*,  
*Biosensors*, volume 11, issue 7, page 241, 2021,

my contribution was in software (1), validation (1-3), supervision (1-3), co-conceptualization (1-3) project administration (1-3), writing - review and editing (1-3) and funding acquisition (1-3).

I agree to submit the above work by Madhurima Chattopadhyay, as a part of her PhD dissertation in the form of a collection of published and thematically related scientific articles.



.....  
Co-author's signature

Poznan, Date: 12.05.2023

M.Sc. Eng. Emilia Krok  
Poznan University of Technology  
Poznan, Poland

I declare that according to the CRediT author statement, in the following publications:

1. Hydration layer of only few molecules controls lipid mobility in biomimetic membranes, Madhurima Chattopadhyay\*, Emilia Krok, Hanna Orlikowska, Petra Schwille, Henri G. Franquelim, and Lukasz Piatkowski\*, *Journal of the American Chemical Society*, volume 143, issue 36, page 14551–14562, 2021,
2. Cooperativity between sodium ions and water molecules facilitates lipid mobility in model cell membranes, Madhurima Chattopadhyay\*, Emilia Krok, Hanna Orlikowska-Rzeznik, and Lukasz Piatkowski\*, *Chemical Science*, 2023, DOI: 10.1039/D2SC06836B,
3. Sensing hydration of biomimetic cell membranes, Madhurima Chattopadhyay\*, Hanna Orlikowska, Emilia Krok and Lukasz Piatkowski\*, *Biosensors*, volume 11, issue 7, page 241, 2021,

my contribution was in methodology (1-3), formal analysis (1), visualization (1) and writing - review and editing (1-3).

I agree to submit the above work by Madhurima Chattopadhyay, as a part of her PhD dissertation in the form of a collection of published and thematically related scientific articles.

  
.....  
Co-author's signature

Poznan, Date: 10.05.2023

M.Sc. Eng. Hanna Orlikowska-Rzeznik  
Poznan University of Technology  
Poznan, Poland

I declare that according to the CRediT author statement, in the following publications:

1. Hydration layer of only few molecules controls lipid mobility in biomimetic membranes, Madhurima Chattopadhyay\*, Emilia Krok, Hanna Orlikowska, Petra Schwille, Henri G. Franquelim, and Lukasz Piatkowski\*, *Journal of the American Chemical Society*, volume 143, issue 36, page 14551–14562, 2021,
2. Cooperativity between sodium ions and water molecules facilitates lipid mobility in model cell membranes, Madhurima Chattopadhyay\*, Emilia Krok, Hanna Orlikowska-Rzeznik, and Lukasz Piatkowski\*, *Chemical Science*, 2023, DOI: 10.1039/D2SC06836B,
3. Sensing hydration of biomimetic cell membranes, Madhurima Chattopadhyay\*, Hanna Orlikowska, Emilia Krok and Lukasz Piatkowski\*, *Biosensors*, volume 11, issue 7, page 241, 2021,

my contribution was in methodology (1), visualization (2-3) and writing - review and editing (1-2) and co-writing original draft (3).

I agree to submit the above work by Madhurima Chattopadhyay, as a part of her PhD dissertation in the form of a collection of published and thematically related scientific articles.



Co-author's signature



UNIVERSITÄT  
LEIPZIG

Leipzig University, Molecular Nanophotonics Department, 04103 Leipzig

Faculty of Physics and  
Earth Sciences,  
**Peter Debye Institute for  
Soft Matter Physics**

Dr. Henri Franquelim

---

**Declaration for Ms. Madhurima Chattopadhyay**

Leipzig, May 29, 2023

I declare that in the publication:

Hydration layer of only few molecules controls lipid mobility in biomimetic membranes,

Madhurima Chattopadhyay\*, Emilia Krok, Hanna Orlikowska, Petra Schwille, Henri G. Franquelim, and Lukasz Piatkowski\*,

*Journal of the American Chemical Society*, volume 143, issue 36, pages 14551–14562, 2021

my contribution was sharing SLB preparation protocol, reading manuscript and giving feedback on it.

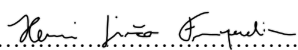
**Leipzig University**

**Interfaculty Centre for  
Bioactive Matter  
(b-ACT<sup>matter</sup>)**

Junior Research Group  
Biomimetic Nanotechnology

I agree to submit the above work by Madhurima Chattopadhyay, as a part of her PhD dissertation in the form of a collection of published and thematically related scientific articles.

Deutscher Platz 5  
(BBZ)  
04103 Leipzig  
Germany

.....  
  
Co-author's signature  
(Dr. Henri G. Franquelim)

**Telefon**  
+49 341 97- 31365

**Fax**  
+49 341 97-32598

**E-Mail**  
henri.franquelim@uni-leipzig.de

**Web**  
<https://research.uni-leipzig.de/bact/technology-labs/biomimetic-nanotechnology//>

Martinsried, Date: 10.05.2023


Prof. Dr. Petra Schwille  
Director  
Max Planck Institute of Biochemistry  
Martinsried, Germany

I declare that in the publication:

Hydration layer of only few molecules controls lipid mobility in biomimetic membranes,  
Madhurima Chattopadhyay\*, Emilia Krok, Hanna Orlikowska, Petra Schwille, Henri G. Franquelim, and  
Lukasz Piatkowski\*,  
*Journal of the American Chemical Society*, volume 143, issue 36, page 14551–14562, 2021

my contribution was final proofreading and giving feedback.

I agree to submit the above work by Madhurima Chattopadhyay, as a part of her PhD dissertation in  
the form of a collection of published and thematically related scientific articles.

  
.....  
Co-author's signature